Judith Binder, Dipl.-Ing., BSc

Synthesis, Characterization and Reactivity of novel Arylsilanes - steps towards new materials

DOCTORAL THESIS

to achieve the university degree of

Doktorin der technischen Wissenschaften

submitted to

Graz University of Technology

Supervisor

Univ.-Prof. Dipl.-Chem. Dr.rer.nat. Frank Uhlig

Institute of Inorganic Chemistry

Graz, June 2015

Abstract

A series of novel and previously published organo(chloro)silanes, R_nSiCl_{4-n}/R_nSiH_{4-n} (R = benzyl, fluorenyl, *p*-tolyl *p*-*n*-butylphenyl, *p*-biphenyl, *m*-tolyl, *o*-tolyl, 2,4-xylyl, 2,6-xylyl, *p*-biphenyl, 1-naphthyl, 9-anthracenyl), were synthesized and characterized using ^{1}H-, ^{13}C- and ^{29}Si-NMR spectroscopy. Effects of substituent bulk on both experimental and calculated ^{29}Si-NMR shifts are compared and discussed. In addition, single crystal X-ray diffraction was employed to elucidate the molecular structure of all solid organo(chloro)silanes. These compounds display non-covalent intermolecular interactions in the form of edge to face, π–π stacking and CH_3···π interactions. Dependency of substituent type on the nature of interactions present was highlighted and discussed. The obtained organosilanes were investigated regarding their reactivity towards thermolysis, oligomerization, selective chlorination as well as irradiation with UV and DXRL techniques.

Content

List of Abbreviations

THF	tetrahydrofuran
LAH	lithium aluminum hydride
Et_2O	diethyl ether
UV	ultra violet
Vis	visible
t	*tert*
o	*ortho*
p	*para*
m	*meta*
J	coupling constant
$SiCl_4$	silicon tetrachloride
HCl	hydrochloric acid
H_2SO_4	sulfuric acid
BuLi	butyllithium
TGA	thermogravimetric analysis
DSC	differential scanning calorimetry
Cp	cyclopentadienyl
MS	mass spectroscopy
SEM	scanning electron microscope
EDX	energy dispersive X-ray analysis
DXRL	deep x-ray lithography
ATR-IR	attenuated total reflection - infrared spectroscopy
NMR	nuclear magnetic resonance
ppm	parts per million
DEPT	distortionless enhancement by polarization transfer
MALDI	matrix-assisted laser desorption/ionization
DI	direct insertion
EI	electron impact ionization
TOF	time of flight
GC	gas chromatography

1 Introduction and objective

Silicon and organosilicon compounds have found broad technical applications and have become indispensable materials in many industrial fields. They are widely encountered in commercial products such as sealants, adhesives, and coatings made from silicones. Organosilicon halides are one of the most important groups of functional organosilanes, and through a vast variety of substitution reactions are versatile precursors to diverse organosilicon derivatives.[1] The corresponding hydrogen rich organosilanes have many attractive properties, including air and moisture stability as well as low toxicity. The silicon atom is more electropositive than carbon, therefore certain chemistry occurs more readily at silicon than carbon, providing access to different types of products. Organosilanes have manifold uses, ranging from the preparation of composite materials like ceramics *via* coupling reactions followed by thermolysis,[2] protecting groups in organic chemistry,[3,4] to surface modification agents for a whole host of applications in various industries.[5] Furthermore, the high chemical stability of organosilanes make them ideal for use as nucleophilic partners in transition-metal-catalyzed cross-coupling with organic halides.[6] Both organosilicon halides and hydrogen rich organosilanes are precursors for inorganic silicon polymers, which show many promising properties for opto-electronic devices.[7] Vapor deposition of gaseous silanes to form silicon thin films is a widely used technique in the production of advanced electronic devices.[8] However in the instance of solid organosilanes the thermolytic degradation might lead to solvent-processable silicon or silicon-carbon composite material that could be used in solar cell technology or in electric devices like transistors.

Despite these wide-areas of applications and recent interests in organo(chloro)silane chemistry, there is a considerable lack of experimental data, especially for aryl substituted silanes. For instance, ^{29}Si-NMR spectroscopy was established in the early sixties,[9] but did not become conventional until the eighties. Consequently, despite many compounds being presented in literature, ^{29}Si-NMR shifts are only partially reported and there is no information on effects of the bulkiness of the aryl substituent on NMR behavior. In addition, only a few crystal structures of chlorosilanes[10-13] and hydrogen-rich organosilanes[14-20] have been published thus far, therefore there is little information on how the substituent affects the solid state structures of these compounds. In particular, the presence of stabilizing factors in the form of non-covalent secondary interactions including π–π stacking, edge to face or $CH_3\cdots\pi$ interactions attributed to the nature of the aromatic substituents in the solid state has not been reported. However,

understanding and utilization of all non-covalent interactions including π-π stacking is of fundamental importance for the further development of supramolecular chemistry and prediction of crystal structures.

For this reason, novel and previously published organosilicon chlorides and hydrides have been synthesized in which the silicon atom is bonded to either a sp^3 carbon, or bonded directly to the sp^2 carbon of an aromatic system with increasing steric demand of the substituent. ^{29}Si-NMR spectroscopy and the effect of substituent bulk on shifts were examined for all novel species and for published compounds where ^{29}Si-NMR data had not been reported. The solid state structures of presented compounds display intermolecular interactions and are highlighted and discussed.

The present work aimed to give a comprehensive overview about the spectroscopic as well as solid state structures and interactions of various aryl silanes, to allow a better understanding of these compounds, which would also allow tailoring of properties. The obtained organosilanes were investigated regarding their reactivity to reveal novel applications.

2 Literature

2.1 Organo(chloro)silanes

The chemistry of Group IV elements is dominated by silicon. Silicon is the eighth most abundant element in the universe and the second most abundant element in the earth's crust after oxygen.[21,22] Elemental silicon is available in various degrees of purity and the production, purification and chemical processes of silicon are well described in literature.[23] It exhibits an essential role in various industrial applications and has a large impact on the modern world economy. Silicon is used in the production of electrical steels[24], aluminum-alloys[25] and in fine chemical industries. A great deal of modern technology depends on highly purified silicon that is used in semiconductor electronics such as integrated circuits representing the basis of most computers.

Organosilanes are compounds containing a silicon-carbon bond. The chemistry of these compounds is basically similar to organic compounds, with some major distinctions, due to the more electropositive nature of the silicon atom (Figure 1) First, the nucleophilic substitution at silicon is more facile than at carbon. Also bond energies with electronegative elements like oxygen, fluorine and chlorine are greater. Silicon-carbon bonds stabilize carbanions in the *α*-position and carbocations in the *β*-position. Furthermore, the Si-H bond is polarized with Si^{+} and H^{-}, which leads to *anti*-Markovnikov additions to olefins under catalytic conditions and the ability to transfer hydride under limited conditions.

Figure 1: Bond polarization and electronegativities χ for C-H and Si-H

The greatest quantities of organosilanes are methyl substituted. They are produced on an industrial scale in the Müller Rochow synthesis (Figure 2). Chlorosilanes are often intermediates in the production of organosilanes and can be reacted with Grignard reagents or alkali metal organics to give organic substitution. A different route is the hydrosilylation of an olefin catalyzed by chloroplatinic acid or di-*t*-butyl peroxide (see Figure 2).

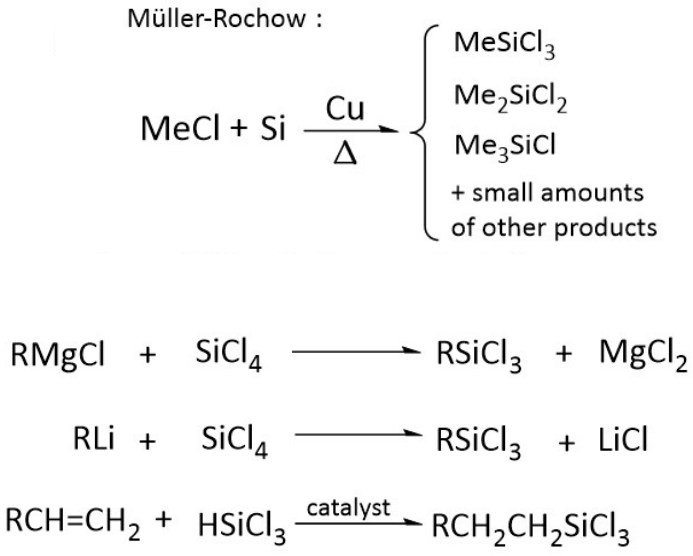

Figure 2: Müller-Rochow synthesis; reaction scheme for organic substitution of chlorosilanes

While the first Grignard reagent was prepared in 1901,[26] the first synthesis of organosilicon compounds, reacting ethyl or phenyl magnesium bromide with $SiCl_4$ was reported in 1904 by Kipping and Dilthey.[27] The reaction can be explained by an oxidative addition with insertion of magnesium into the carbon-halogen bond.[28] The Grignard reagent generates a polarization change at this bond and the so formed carbanion reacts as a nucleophile that forms a new *σ*-bond. The distribution of the mono-, di- , tri- and tetrasubstituted products depend on the stoichiometry of Grignard reagent to $SiCl_4$ and the bulkiness of the substituent. The second reaction procedure uses organolithium reagents. These compounds are frequently used for the formation of organosilanes. In 1954, Sommer *et al.* described one of the first procedures towards *t*-butyltrichlorosilane and di-*t*-butylchloro(methyl)silane using *t*-BuLi.[29] In this reaction, the nucleophilic carbanion is created by a halogen-metal exchange. The lithiated species reacts with an electrophilic compound to generate the new σ-bond and a lithium halide salt. Organolithium reagents show a high reactivity towards $SiCl_4$, which makes the reaction often difficult to control. Grignard Reagents, in comparison have a lower reactivity as well as a sensitivity to the bulkiness of the substituent but show a higher selectivity of the reaction.[30]

Organosilicon halides are one of the most important groups of functional organosilanes and through a vast variety of substitution reactions, are versatile precursors to diverse organosilicon derivatives. Due to the high affinity of silicon to oxygen, the silicon halides (except fluorides) are usually easily hydrolyzed by water or alcohols, leading to the corresponding mostly unstable (poly)silanoles and silyl alcoholates. The reaction with water is particularly important in that it provides a basis for silicone

manufacture. The chemistry of polysilanols is extensive and is of particular importance in the silicone polymer industry and sol gel processing, but there is also a growing interest in other applications, like anion-recognition by silanediol-based receptors[31-33] or silanediol protease inhibitors.[34,35] Chlorosilanes react with other protic materials like alcohol to form alkoxysilanes or with primary and secondary amines to form aminosilanes. Diorgano dichlorosilanes are the most popular precursor compounds to create functionalized oligo- and polyorganosilanes[1] *via* Wurtz couling with alkali metals (see also 2.5.1). In addition, treatment of organochlorosilanes with LAH (lithium aluminum hydride) in ethereal solvents (see Figure 3) leads to hydrogen rich silanes, which have shown to serve as important substrates for many applications, such as the single-source precursors in CVD (chemical vapour deposition) processes, as monomeric substrates for sigma-bond metathesis and hydrosilylation, as well as ligands for transition metal catalysts[36] or as colour stabilizer in polycarbonate composite material.[37] Furthermore, hydrogen rich silanes are used to generate polysilanes via dehydrogenative coupling.[36] Hydrogen bound to silicon can behave as reducing agent and triethylsilane and diphenylsilane are employed in the reduction of ketones and esters.[38]

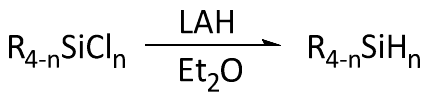

Figure 3: Preparation of hydrogen-rich silanes with LAH

2.2 Crystal structures and interactions

The importance of aromatic non-covalent interactions in the stabilization of compounds in the solid state and their significance in chemical and biological processes has been well documented.[39,40] The nature of the aromatic substituent directly affects the type of electrostatic interaction present which can vary from π-π to CH-π interactions.[41,42] Figure 4 summarizes the types of aromatic non-covalent interactions present in the organo silane species included in this work and acceptable ranges found in biological and organic systems.[39,40,43]

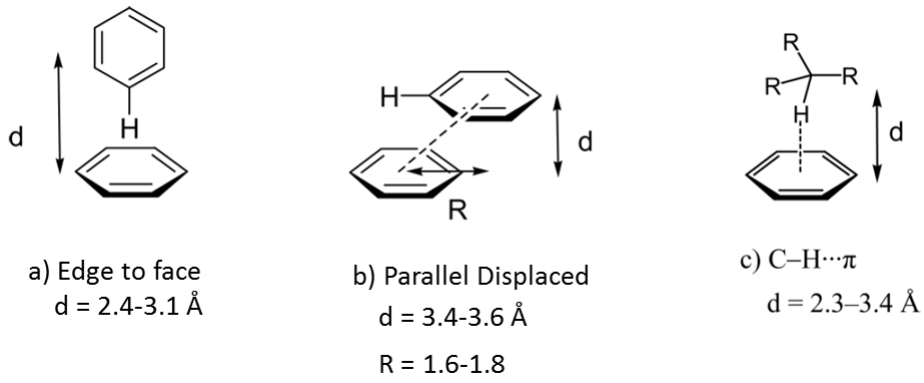

Figure 4: Orientations of aromatic non-covalent interactions and accepted ranges[39,40,43]

In the arrangement of aromatic rings one can distinguish generally between a stacked arrangement and an edge to face conformation. Stacking does not necessarily have to be a perfect face-to face alignment of the atoms but most of the organo species presented show a parallel displacement. Even though these interactions are weaker than the classical hydrogen bond, they play a notable role in the determination and stabilization of the solid state structure.[39]

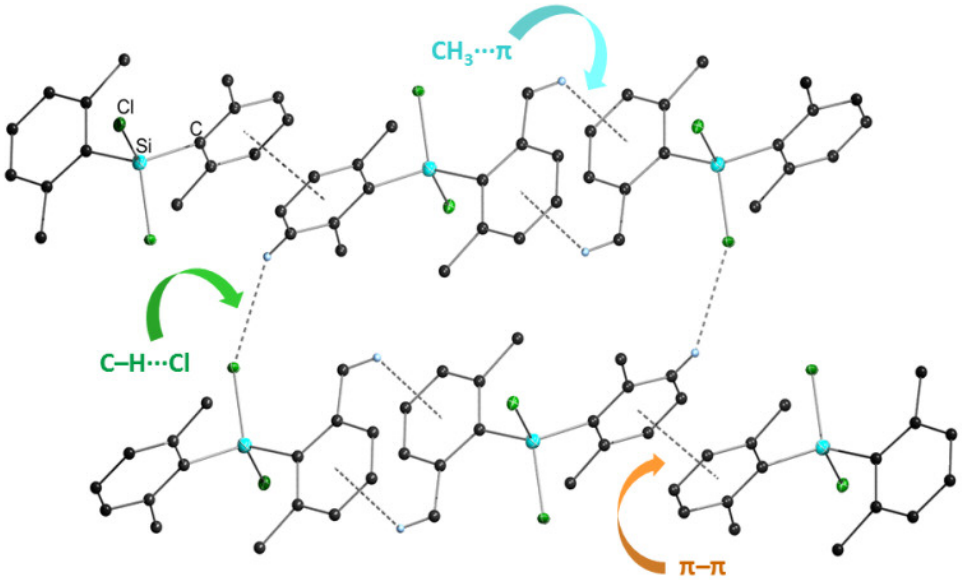

Figure 5: Crystal structure of 2,6-xylyl$_2$SiCl$_2$ (11)

In addition to the aforementioned aryl substituent based intermolecular interactions, weaker interactions including C–H···Cl (see Figure 5) can be present in the structure. For a detailed view on the intermolecular forces and discussion of the nature of these interactions see Hunter *et al.*[41]

2.3 Thermolysis

Thermolysis of (organo)silanes has been extensively studied and has led to a wide-area of applications. Polysilazanes, polysiloxanes, and polycarbosilanes can be used in order to produce small-diameter Si_3N_4 or SiC ceramic fibers for high-temperature applications, fiber-reinforced composite materials and coatings.[44,45] The polymer precursors can provide ceramics with a tailored chemical composition and a defined nanostructural organization when a certain thermal treatment under a controlled atmosphere is applied.[45]

An additional application for thermic decomposition of silanes is the field of photovoltaic and optoelectronic devices. Due to the increasing global energy demand and simultaneous shrinking of fossil reserves, renewable resources are becoming increasingly important. A special position in this case takes the sun, with its seemingly endless energy reserves. On this reason the photovoltaic industry experiences a continuous upward trend. Recent systems use polycrystalline silicon or thin film technologies like PECVD (plasma enhanced chemical vapor deposition). For PECVD methods, monosilane (SiH_4) is the most common precursor.[46] Additionally, this vapor deposition of gaseous silanes to form silicon thin films is a widely used technique in the production of advanced electronic devices.[8] Beside monosilane, higher hydrosilanes can also form silicon *via* thermal decomposition. These compounds, as well as SiH_4, have the disadvantage of a thermal decomposition temperature higher than the boiling point. Handling of the resulting gaseous and self-igniting compounds is problematic. Recently, the liquid processing of cyclohexasilane had been reported as a possible approach toward printable amorphous silicon films that can be thermally recrystallized. However, in this case, the handling of the explosive chemical, is also rather problematic, with limited perspective for large-scale industrial utilization.[47]

In 2001 Coleman *et al.* showed that aryl substituted silanes might also be promising materials for silicon formation. In a process using supercritical solvents, the preparation of silicon nanowires was successfully achieved. However, the mechanism of formation is complex and not all intermediates could be defined.[48]

In the heat treatment of organo silanes and polysilanes, oxygen is in many cases inevitably included in the resulting solids, due to its affinity to silicon. Nevertheless SiC_xO_y compounds can be used for super low-*k* materials due to their low dielectric constant and their thermal stability.[49]

In case of solid organosilanes, described in the present work, the thermolytic degradation might lead to solvent-processable silicon or silicon-carbon composite material that could be used in solar cell technology or in electronic devices like transistors.

2.4 Reactivity

2.4.1 UV-Irradiation

The photodimerization of anthracene, having been first studied by Fritzsche in 1867, is one of the oldest known photochemical reactions.[50] Anthracenes combine the advantages of easily accessible absorption spectra, exhibiting monomer (or eximer) fluorescence and high photoreactivity, with solubility in organic solvents.[51] The dimerization across the 9,10-positions of anthracene occurs by exposure of a saturated benzene solution to sunlight or by irradiation with an incandescent lamp. The dimeric nature can be identified by the bridgehead proton ^{1}H-NMR signal at 4.53 ppm in $CDCl_3$ as well as by the UV spectrum. Thermolysis at approximately 280 °C leads to a quantitative conversion to the educt. The resonance stabilization per π-electron is higher for a benzene ring than for a naphthalene ring which causes the preferred formation of the photo dimer **2**, which contains the maximum possible number of benzene rings and the most stable arrangement of aromatic systems. An excited molecule **1*** combines with an non excited molecule of **1** to form the bimolecular complex **[1·1]*** (the so called excimer). Excimer decay *via* cycloaddition gives **2** (Figure 6).[52]

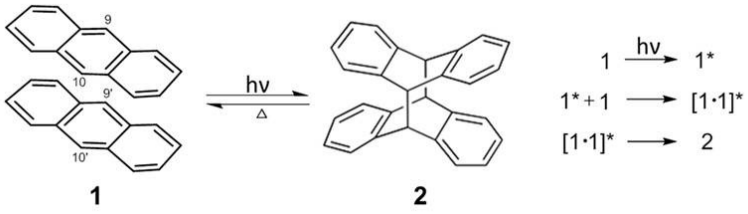

Figure 6: [4+4] photodimerization of anthracene[52]

In addition to photodimerization intramolecular reactions are also known. Di-9-anthrylmethane gives the [4+4] addition product with a cyclopropane structure. The irradiation reaction of di-9-anthryldimethylsilane was expected to give the analogous structure with a silacyclopropane structure, which may allow interesting chemistry due to its high reactivity. Unexpectedly the formation of the [2+4] cycloadduct (Type I, see

Figure 7) was observed in 90% yield. Thermolysis at 250 °C afforded quantitative amounts of the educt, showing the reversibility of the reaction.[53] A subsequent study by Takahashi *et al*.[54] investigated the cycloaddition of di-9-9'-anthracene conjugates linked by permethylsilyl chains. It was shown that the A2S*n* gives one of three cycloadducts depending on the chain length.

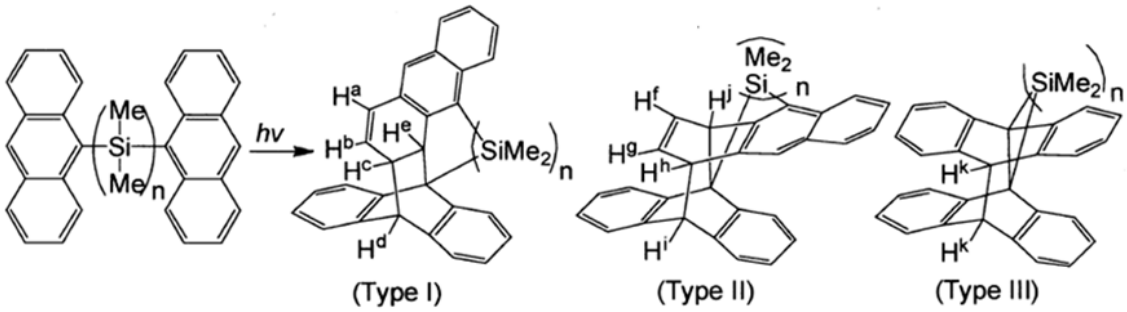

Figure 7: Photochemical reaction of A2Sn(n=1,2 and 3)[54]

Irradiation of di-9-anthryldimethylsilane afforded two intramolecular cyclisation products. The main product was a [2+4] adduct (Type I, Figure 7), which is in agreement to the earlier studies, but also the [4+4] adduct (Type III, Figure 7), was observed. The products were characterized using ^{1}H-NMR and the ratio of Type I: Type III was determined as 2:1. A2S2 gave the Type II adduct.

In comparison to anthracene, naphthalenes are much less photoreactive and less is known about their photodimerization. Neither 1-substituted naphthalene nor naphthalene itself is known to undergo photodimerization. Nevertheless, several groups reported on [4+4] cyclodimers from certain naphthalenes. It was also shown by Noh *et al.* that the 1-substituted naphthalenes, methyl-1-naphthoate and naphthalene-1-carbonitrile give the *syn*-[2+2] cyclodimer upon low temperature irradiation.[55]

2.5 Linear and cyclic oligo- and polysilanes

Oligo- as well as polysilanes, with their unbroken chains of catenated silicon atoms are the prototypical conjugated systems. Diarylpolysilanes with tightly locked Si-backbones are candidates for ideal one-dimensional (1-D) structures that would show 1-D semiconductor and/or quantum wire properties.[56] They can be regarded as one-dimensional analogs to elemental silicon, on which, of course, nearly all of modern electronics is based. Delocalization of the σ-electrons in the Si–Si bonds gives the polysilanes unique optoelectronic properties.[57] Silylarene units in the main chain generate a so called σ-π conjugation resulting from the interaction between Si-Si σ-orbitals and

C=C π-orbitals (Figure 8), leading to a decreased optical band gap (bathochromic shift of absorption maximum) when compared to alkyl substituted polysilanes.[58]

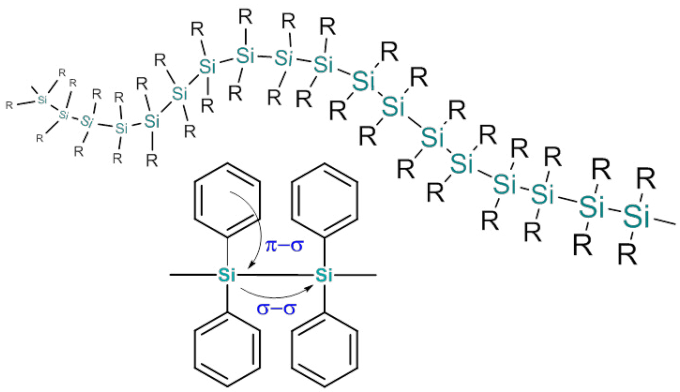

Figure 8: Polysilane chain; *σ–π* and *σ–σ* conjugation of silylarene and main chain

The first Si-homocycles Si_4Ph_8 and Si_5Ph_{10} were synthesized by Kipping and Sands in 1921 by reacting dichlorodiphenylsilane with sodium.[59] Shortly after that, the *para*-tolyl substituted ring systems could be synthesized.[60] Today, the most common method to produce Si_5Ph_{10} is the reductive coupling of Ph_2SiCl_2 with lithium in THF, with yields of about 70-80% and 20-30% Si_4Ph_8 as side product. Gilman *et al.* concluded that this product distribution is due to thermodynamic reasons because of the higher stability of the five-membered ring.[61] An attempt to synthesize the *ortho*-tolyl substituted cycles failed[62] and also no literature is known about bigger substituents like e.g. naphthyl groups. The only other example of an aryl substituted ring system is $benzyl_6Si_6H_6$, which was synthesized by Harrod.[63] Si_5Ph_{10} serves as precursor for cyclopentasilane,[64] which can be used to form silicon films after ring-opening polymerization with UV-light.[65] The so derived silicon films were also tested as high capacity graphite-silicon composite material for lithium-ion batteries.[46] Benzene solutions of Si_5Ph_{10} can be spin-coated on substrates, followed by thermolysis to obtain inorganic silicon-based thin films with tunable dielectric properties.[49] The use of Si_4Ph_8 and Si_5Ph_{10} as active material in lithium-ion batteries was as well investigated in our research group.[66]

The first polysilane derivative, polydiphenylsilane, was probably prepared along with the ring systems by Kipping in 1921. It attracted little scientific interest due to its insolubility and infusibility. Besides polydiphenylsilane, only a small number of other diarylpolysilanes are described in literature.[67] Recent findings showed the possible applicability of C_{60} with PDHOF (polydiphenylhydrosilane)[58] in bulk heterojunction solar cells.[68] Phenyl substituted branched polysilanes were also tested as anode material in rechargeable lithium ion batteries, performing well in electrochemical operations.[69] Poly[bis(*p*-*n*-butylphenyl)silane attracted some attention because of its high room

temperature luminescence.[70] Unfortunately, polymer yields and the molecular weight are very sensitive towards steric bulk of the substituents. When one of the aryl goups is exchanged by an alkyl (e.g. methyl) an important number of soluble polysilanes, including homopolymers and copolymers have been synthesized and studied. A well-known representative is polymethylphenylsilane, which can be easily obtained and is highly soluble in in common organic solvents. Attempts to polymerize sterically more demanding compounds like methyl-α-naphtyldichlorosilane or methyl-α-phenanthryldichlorosilane were unsuccessful.[67]

2.5.1 Wurtz-type coupling

The so called Wurtz-type reductive dehalogenative coupling is the most common method for the synthesis of polysilanes. A dichlorodiorganosilane is reacted with a slight stoichiometric excess of dispersed sodium in an inert, high-boiling solvent (in most cases toluene) by refluxing, to yield the desired polysilane (Figure 9).[7]

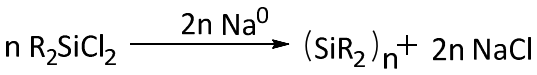

Figure 9: Wurtz-type coupling of chlorosilanes with sodium

The mechanism of the reaction seems to be a condensation reaction involving a chain mechanism, with various active species including silyl radicals, silyl anions, silyl anion radicals and disilenes. It has been discussed wether the polymodal weight distribution results from the many different chain carriers. A proposed mechanism for the coupling reaction (see Figure 10) is initiated *via* a silyl anion radical to a silyl radical.[7]

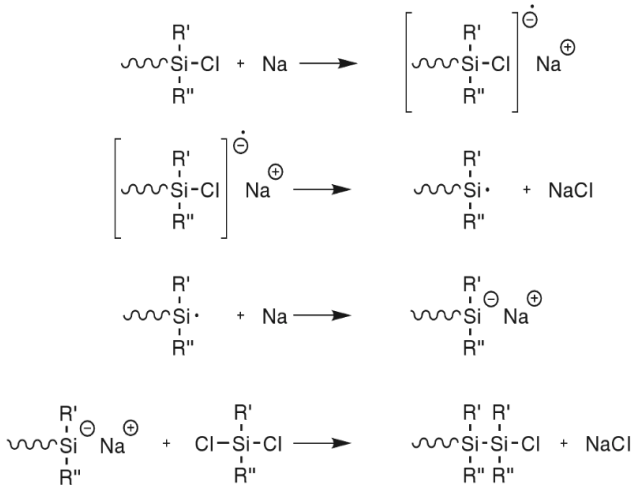

Figure 10: Proposed chain mechanism for the Wurtz-type coupling[7]

The polymeric species is then formed by four stage propagation step.The functionalities that can be introduced *via* the monomer are limited due to the harsh reaction conditions. Also the stereochemical control in the polymerization is marginal, yields are often low and a big dependency on the steric bulk of the substituents is observed. Control over the degree of polymerization is difficult and the weight distribution is in many cases trimodal with a low weight region (cyclic products), a middle and a high weight region, which can not be separated easily. Besides solvent and temperature the used alkali metal also has an influence on the reaction. An exchange of sodium by lithium leads to a higher degree of cyclooligomerization.[67]

Many modifications of the Wurtz-coupling reaction have been developed, including ultrasound assisted polymerization at room temperature,[71,72] addition of crown ether[73] or diglyme.[58,59]

2.5.2 Catalysis with titanocene derivatives

The dehydrogenative coupling of hydrosilanes is a powerful technique for the formation of Si-Si bonds. A catalyst has to be used since the rate-determining step is the kinetically unfavourable dissociation of hydrogen from silicon. Generally, the homodehydrocoupling of silanes proceeds *via* a silicon-silicon bond formation, forming the corresponding dimer and elimination of one molecule of dihydrogen. There are three basic metallocene catalyst variations that have been developed. Cp_2MMe_2 (M=Ti, Zr)[74], CpCp*M(SiR_3)X (M=Zr, Hf; R=Me, Ph, $SiMe_3$; X=Cl, alkyl)[75] and Cp_2MCl_2/*n*-BuLi (M=Ti, Zr, Hf).[76] Only the titanium catalysts and aryl substituted hydrosilanes will be discussed here.

Referring to Harrod,[77] the dehydrocoupling reaction of hydrosilanes with Cp_2TiMe_2 occurs in two stages . The induction period is followed by a rapid, autocatalytic reaction which transforms Cp_2TiMe_2 into the active catalyst. In this stage one equivalent each of Si-Me and CH_4 are produced (Eq.1, Figure 11). The second step is the formation of the deep blue coloured titanocene(III) silyl complexes **a** and **b** through the reaction of titanocene with Si-H. Complex **a** appears first and is then converted into **b**. This stage is followed by the polymerization reaction (Eq.2, Figure 11). This reaction provides relatively low molecular weight polysilane (when using $PhSiH_3$) and a relatively large quantity of cyclic polysilanes. The precise manner in which the Si-Si bonding occurs is not clear, but the most widely accepted mechanism of Group IV metallocene promoted dehydrocoupling reactions is based on the σ-bond metathesis mechanism proposed by Tilley.[78]

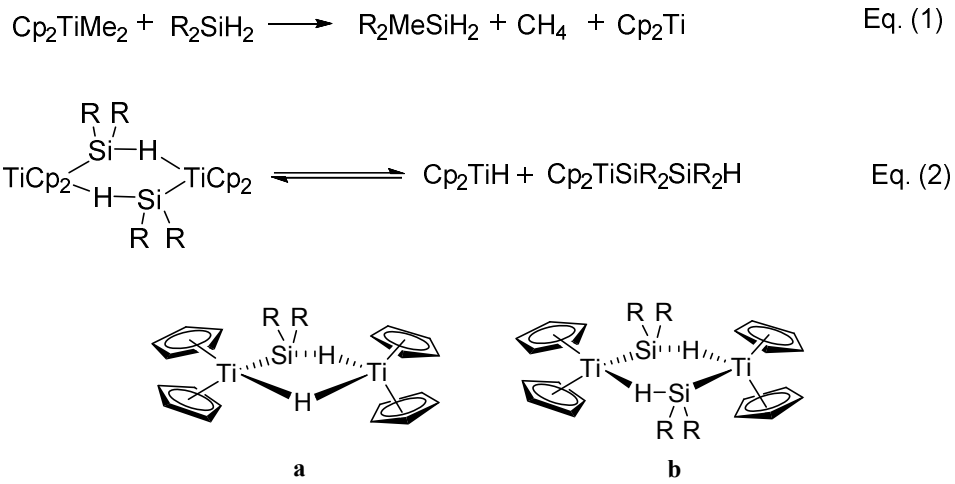

Figure 11: Reaction of Cp_2TiMe_2 with hydrosilanes; Titanocene(III) silyl complexes a and b[77]

The combined catalyst system Cp_2TiCl_2 with *n*-BuLi was introduced by Corey and co-workers.[79] No induction period is observed and secondary silanes can be coupled at reasonable rates at higher temperatures. Metallocene dichlorides do not react with hydrosilanes in the absence of an activation agent. For the reaction of Cp_2MCl_2 with *n*-BuLi no general agreement about the mechanistic details exist so far.

Primary silanes: In most cases the reaction of $PhSiH_3$ was investigated. There is no standard set of conditions used by the different studies, therefore comparison of the results is difficult, as different reaction times, silane/complex ratio, solvent, temperature and work-up procedure were used. Nevertheless, there are some conclusions that can be drawn. Most catalyst systems produce a bimodal distribution of the polysilane product. In general, for Cp_2MMe_2 (M=Ti, Zr, Hf), the M_w increases with Ti < Zr < Hf , and the % of cyclics is in the order Hf < Zr < Ti . When the phenyl ring is substituted with a methyl group in *ortho* position no homopolymer could be obtained. Substituents in *meta* or *para* position show a higher polymerization rate under similar conditions. When the aryl group is moved to a position one unit away from the silicon center (like in R=benzyl), the rate of dehydrocoupling decreases and a mixture of cyclic products is obtained. Electron donating groups as substituents of the phenyl ring show a reduction in the rate of the coupling reaction. It can be concluded that the degree of polymerization is affected by electronic and steric effects.[80]

Secondary silanes: The polymerization of secondary silanes proceeds much the same way as it does for primary silanes, but the problem of steric hindrance becomes a more serious problem, slowing down the reaction and requiring higher temperatures.[79,80]

Tertiary silanes: There are no conditions yet reported for the coupling of tertiary silanes with organic substituents with the catalyst types described above.

Beside Wurtz- and dehydroganative coupling of silanes some other routes were as well established, including masked disilenes, ring opening polymerization (ROP) or the stepwise formation of the polymer from the reaction of dichlorosilanes with dilithiated silanes.[81] Due to the complex and in many ways difficult polymerization, polysilanes still are not used commercially, even though they show interesting electro- and photochemical properties.

In our case the reaction of Cp_2TiMe_2 on primary silanes with sterically demanding substituents like 1-naphtylSiH_3 (**30**) and 2,6-xylylSiH_3 (**37**) as well as the catalyst system Cp_2TiCl_2/*n*-BuLi with the corresponding secondary silanes was examined. Beside that the reaction of 1-naphtyl$_2$SiCl_2 (**8**) with lithium and magnesium was investigated. The goal was to obtain novel oligomers or polymers but also new cyclic products, which could then be used in thermolysis processes followed by screening for their applicability in battery materials or thin film formation for optoelectronic devices.

3 Results and Discussion

3.1 Synthesis

Various organo(chloro)silanes with varying steric bulk were synthesized in which the silicon atom is bonded to either a sp^3 carbon (Figure 12, Compound 1 and 2) or bonded directly to the sp^2 carbon of an aromatic system (Figure 12, Compound 3–11). The compounds show *ortho*, *meta* or *para* substitution of the phenyl ring, as well as double substitution in 2,6- and 2,4-position towards the silicon atom. In addition, polyclyclic substituents were as well investigated.

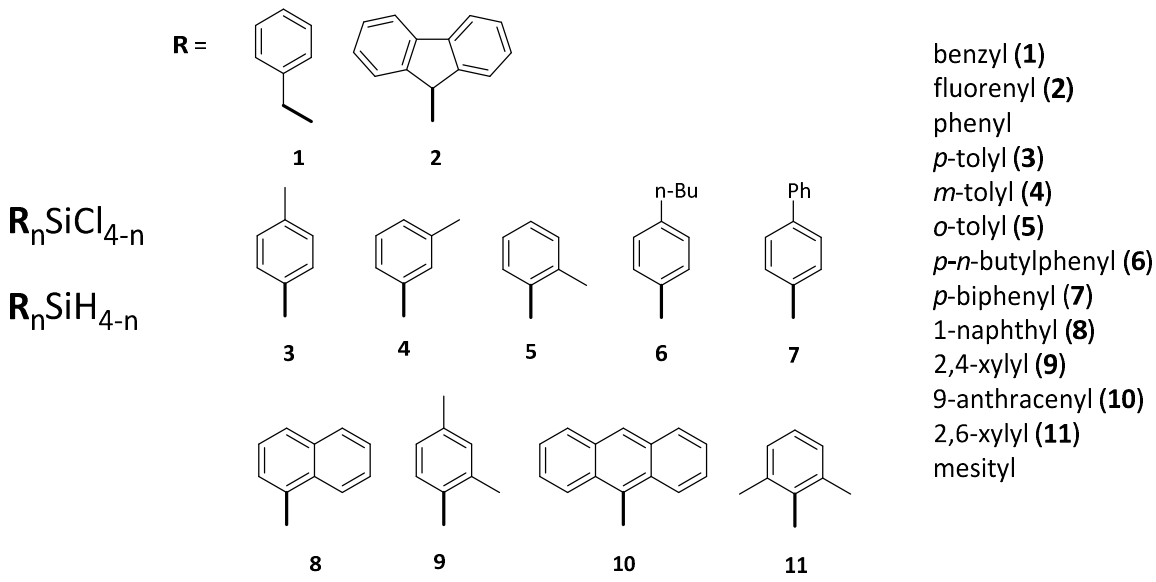

Figure 12: Organo(chloro)silane target molecules; R= substituent

Synthesis of organochlorosilanes follows two different reaction pathways with varying stoichiometry of the active reagent towards $SiCl_4$. In all cases, a Grignard or lithiation reaction leads to the desired product. In the case of dichlorosilanes, R_2SiCl_2, a ratio of 1:0.5 of the lithiation or Grignard reagent to $SiCl_4$ leads to good yields of the product with minor formation of side products (Figure 13, reaction A and B). To obtain the trichlorinated $RSiCl_3$ species a large excess of $SiCl_4$ is required to obtain high yields (Figure 13, reaction C). A ratio of 1:0.3 of the lithiation reagent to $SiCl_4$ gives the monochlorinated species R_3SiCl (Figure 13, reaction D).

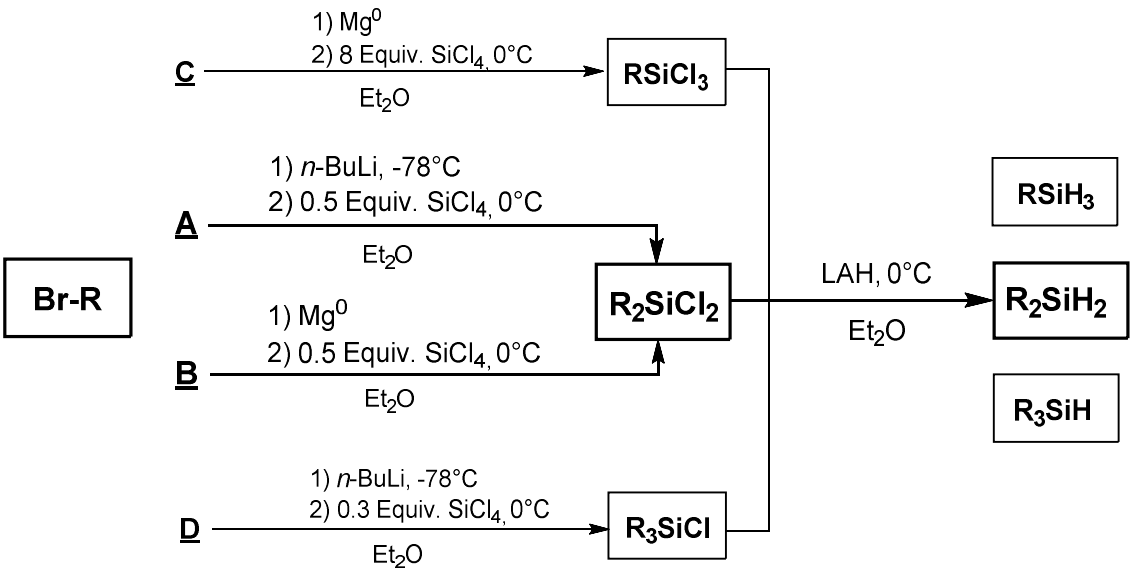

Figure 13: General synthetic procedures towards organo(chloro)silanes. R = benzyl (1), fluorenyl (2), *p*-tolyl (3), *m*-tolyl (4), *o*-tolyl (5), *p*-*n*-butylphenyl (6), *p*-biphenyl (7), 1-naphthyl (8), 2,4-xylyl (9), 9-anthracenyl (10), 2,6-xylyl (11).

Subsequently the organochlorosilanes are reacted with a slight excess of LAH in ethereal solution at 0 °C to obtain the corresponding hydrogen rich organosilanes.

3.1.1 Organochlorosilanes R_nSiCl_{4-n}

R_2SiCl_2: For both novel and previously synthesized dichlorides presented (Figure 12), a lithiation reaction (Figure 13, reaction A) was preferred over published procedures.[82-84] In a typical experiment, the aryl/alkyl bromide was reacted with *n*-BuLi at -78 °C in Et_2O. The solution was transferred *via* cannula to $SiCl_4$, in ether, cooled to 0 °C. Salt formation was observed and the reaction stirred. After filtering, the solvent was evaporated and the compound purified by distillation or recrystallization.

In the case of the fluorenyl substituent, lithiation of the aryl bromide did not result in the desired compound but rather formation of product mixtures including fluorene. However, direct lithiation of fluorene at 0 °C resulted in formation of pure fluorenyl$_2$SiCl$_2$ (**2**). 9-anthracenyl$_2$SiCl$_2$ (**10**) was prepared similar to literature,[85] however despite several attempts, the pure compound could not be isolated. Compound **10** was purified by sublimation, to remove anthracene as a major byproduct which led to a melting point of 161–162 °C which is notably higher than the one presented in literature, reported at 128 °C.[85] Due to availability of the appropriate Grignard for compounds *p*-*n*-butylphenyl$_2$SiCl$_2$ (**6**) and *p*-biphenyl$_2$SiCl$_2$ (**7**), a Grignard reaction was used for compound formation. In this route, the Grignard was added to a solution of $SiCl_4$ in Et_2O cooled to 0 °C. The reaction was stirred for 4 hours and allowed to warm to room

temperature. Et_2O was removed and the resulting residue was redissolved in hot toluene. Insoluble salts were removed *via* filtration and washed with hot toluene. To obtain benzyl$_2$SiCl$_2$ (**1**) general procedure B was used. As already stated in earlier publications, preparation of the dichlorosilane using benzyllithium leads mainly to the coupling product dibenzyl. This is caused by the reactivity of benzyllithium and the ease with which benzyl halides undergo displacement of the halide ion by organometallic compounds.[86]

For all solid compounds, recrystallization from toluene, pentane or Et_2O afforded crystals suitable for single crystal X-ray diffraction studies. In some cases, compounds were first purified *via* distillation under reduced pressure to remove mono- or trisubstituted byproducts (benzyl, *o*-tolyl, 2,4-xylyl, 2,6-xylyl).

RSiCl$_3$: Organotrichlorosilanes were prepared *via* reaction of the respective Grignard reagent with $SiCl_4$ in THF according to literature.[87] The ratio between $SiCl_4$ and the Grignard reagent was modified to reduce the formation of byproducts (Figure 13, reaction C).[30] An increase of the stoichiometric ratio ($SiCl_4$: R-MgBr) to 8:1 leads to higher yields of the organotrichlorosilane, but complicates the solvent recovery due to the similar boiling points of $SiCl_4$ (57.6 °C) and THF (65.5 °C). Therefore large amounts of the excess $SiCl_4$ need to be carefully quenched with alcohol and water. 1-naphthylSiCl$_3$ (**15**) was obtained in 85% yield, *p*-tolylSiCl$_3$ (**13**) in 66%. The formation of 2,6-xylylSiCl$_3$ failed in a previous study performed in our working group.[30] Moving one of the methyl groups from *ortho* to the *para* position allowed the successful formation of 2,4-xylylSiCl$_3$ (**12**) in fair yield (20%). BenzylSiCl$_3$ (**14)** was not synthesized directly but showed to be the major byproduct in the synthesis of the corresponding disubstituted chlorosilane. The pure compound was obtained as a low boiling fraction in the distillation of benzyl$_2$SiCl$_2$ (**1**). With the exception of 1-naphthylSiCl$_3$ (**15**), which was obtained as colourless solid by recrystallization from toluene, the reported monosubstituted chlorosilanes are colourless oils, which were purified by distillation.

R$_3$SiCl: To obtain 1-naphthyl$_3$SiCl (**16**), 1-naphthylbromide was reacted with *n*-BuLi at -78 °C in Et_2O, according to literature (Figure 13, reaction D).[88] The solution was transferred *via* cannula to $SiCl_4$, in ether, cooled to 0 °C. Salt formation was observed and the reaction stirred filtered. The pure compound was recrystallized from toluene.

3.1.2 Organosilanes R_nSiH_{4-n}

R$_2$SiH$_2$: Diorgano silicon dihydrides were prepared by the addition of an Et_2O or THF (in case of compound **21**, **24**, **25** and **27** the addition of THF was necessary because of bet-

ter solubility of the chlorosilane) solution of the corresponding chlorosilane (see 3.1.1) to a suspension of LAH in Et_2O at 0 °C (Figure 13). After complete addition, the solution was stirred for 1 hour at room temperature. Excess LAH was quenched carefully with aqueous H_2SO_4 (10%). The organic layer was separated *via* cannula. The extraction of the aqueous phase with Et_2O was repeated twice. The organic solution was dried over $CaCl_2$ for 1 hour without further stirring followed by filtration. $CaCl_2$ was washed 3-4 times with Et_2O to increase the overall yield of the reaction. The solvent was removed and the product purified. Pure benzyl$_2$SiH$_2$ (**20**), *p*-tolyl$_2$SiH$_2$ (**34**) and *m*-tolyl$_2$SiH$_2$ (**22**) were obtained *via* distillation. 2,6-Xylyl$_2$SiH$_2$ (**28**) was as well distilled to remove the more volatile 2,6-xylylSiH$_3$ (**37**), leading to the pure 2,6-xylyl$_2$SiH$_2$, which solidified in the flask after several hours at room temperature. Fluorenyl$_2$SiH$_2$ (**21**), 1-naphthyl$_2$SiH$_2$ (**25**), *p*-biphenyl$_2$SiH$_2$ (**24**) and 2,4-xylyl$_2$SiH$_2$ (**26**) were recrystallized from toluene. Pure *p*-*n*-butylphenyl$_2$SiH$_2$ (**23**) was obtained *via* bulb-to-bulb distillation under reduced pressure, with a heating gun (Temp. > 500 °C) due to the extreme high boiling point. 9-Anthracenyl$_2$SiH$_2$ (**27**) was purified by vacuum sublimation at 60 °C, to remove anthracene as a major byproduct. Completeness of anthracene removal was monitored by ^{1}H-NMR. The pure silane was recrystallized from ethyl acetate yielding bright yellow needles. The side reaction, formation of anthracene, was already observed in synthesis of the corresponding chlorosilane. *p*-Tolyl$_2$SiH$_2$ (**34**)[89] and *o*-tolyl$_2$SiH$_2$ (**3**)[90] were prepared similar to literature. All literature reported ^{1}H-, ^{13}C- and ^{29}Si-NMR shifts were obtained in $CDCl_3$. For better comparability ^{1}H and ^{29}Si-NMR data was measured in C_6D_6 as well.

All of the obtained secondary silanes show no distinctive reactivity towards decomposition when in contact with air. Compounds **26**-**28** were stored under air for several weeks without any changes in properties. This finding is in contrast to alkyl or phenyl substituted silanes which are classified as air and moisture sensitive. The sterically more demanding substituents like 1-naphthyl or 9-anthracenyl seem to lead to a lower reactivity and higher stability towards those conditions.

RSiH$_3$: The primary silanes benzylSiH$_3$ (**32**), 2,4-xylylSiH$_3$ (**29**), 1-naphthylSiH$_3$ (**30**) and *p*-tolylSiH$_3$ (**31**) were obtained by reaction of the corresponding chlorosilanes with LAH in Et_2O at 0 °C (see Figure 13). All compounds were purified by distillation and were obtained as colourless oils.

R$_3$SiH: 1-naphthyl$_3$SiH (**30**), was obtained by reaction of the corresponding chlorosilane with LAH in Et_2O at 0 °C (see Figure 13). The pure compound was recrystallized from toluene.

3.2 X-Ray Crystallography

Only a few crystal structures of chlorosilanes[10-13] and hydrogen-rich organosilanes[14-20] have been published thus far, therefore, there is little information on how the substituent affects the solid state structures of these compounds. In particular, the presence of stabilizing factors in the form of non-covalent secondary interactions including π–π stacking, edge to face or $CH_3\cdots\pi$ interactions attributed to the nature of the aromatic substituents in the solid state has not been reported. However, understanding and utilization of all non-covalent interactions, including π-π stacking, is of fundamental importance for the further development of supramolecular chemistry and prediction of crystal structures.

3.2.1 Organochlorsilanes R_nSiCl_{4-n}

R_2SiCl_2: This section summarizes the crystallographic data of solid compounds **1**, **2**, **5**, **8**, **9**, and **11** and compares it to already published compounds.[10-13] In each case, the silicon atom is found in a near distorted tetrahedral environment bound to two chlorine atoms and two substituents (Figure 14). For crystallographic data and details of measurements and refinement for presented compounds see Appendix. Table 1 summarizes average bond lengths and angles for presented compounds and comparable silicon dichlorides.

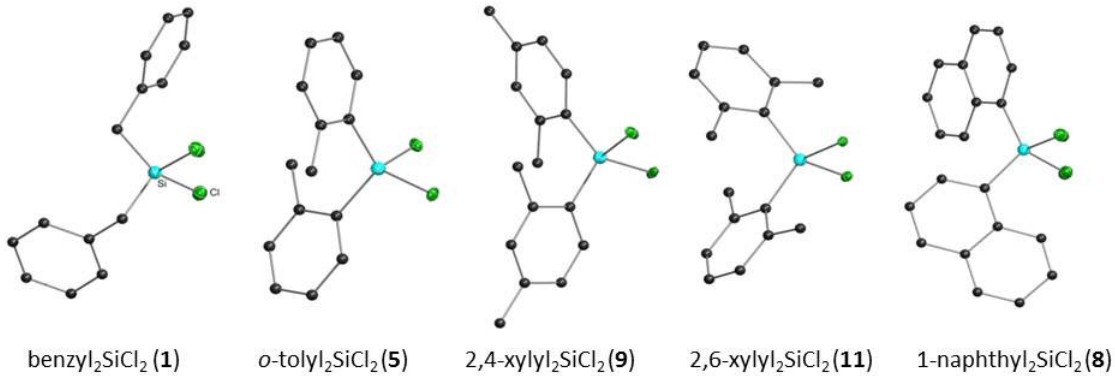

Figure 14: Crystal structures of presented compounds. All non-carbon atoms shown as 30% shaded ellipsoids. Hydrogen atoms interactions removed for clarity.

Both *o*-tolyl$_2$SiCl$_2$ (**5**) and 2,4-xylyl$_2$SiCl$_2$ (**10**) display averaged Si–C bond lengths of 1.858(3) Å, with a similar value for 1-naphthyl$_2$SiCl$_2$ (**8**) (1.859(3) Å) (Table 1). As expected, the addition of a methyl group at the 6-position of the aryl substituent in 2,6-xylyl$_2$SiCl$_2$ (**11**) results in a longer averaged Si-C bond length (1.877(2) Å) comparable to

mesityl$_2$SiCl$_2$ (1.875(2) Å).[12] The longest averaged Si–C bond length (1.881(3) Å) is attributed to the highly substituted aryl moiety in 2,3,5,6-tetramethylphenyl$_2$SiCl.[11] Not surprisingly, this substituent also results in the longest averaged Si–Cl bond length (2.073(1) Å), however a clear trend is not observed in the compounds with the less bulky substituents, with averaged Si–Cl bond lengths ranging from 2.059(2)–2.069(2) Å.

Table 1: Selected bond lengths (Å) and angles (°) for presented silicon dichlorides.

	Space Group	Si–C (Å)(avg.)	Si–Cl (Å)(avg.)	C–Si–C (°)	Cl–Si–Cl (°)
benzyl$_2$SiCl$_2$ (**1**)	P2$_1$/n	1.857(3)	2.081(2)	113.53(1)	107.04(4)
tetramethylcyclopentadienyl$_2$SiCl$_2$[10]	P2$_1$/n	1.875(3)	2.062(3)	120.27(1)	101.71(1)
pentamethylcyclopentadienyl$_2$SiCl$_2$[13]	C2/c	1.885(5)	2.073(3)	122.51(3)	101.08(3)
fluorenyl$_2$SiCl$_2$ (**2**)	P-1	1.878(4)	2.059(4)	117.65(5)	105.01(2)
o-tolyl$_2$SiCl$_2$ (**5**)	P2$_1$/c	1.858(3)	2.065(3)	116.94(2)	104.79(5)
2,4-xylyl$_2$SiCl$_2$ (**9**)	P-1	1.858(3)	2.059(2)	118.15(9)	104.95(4)
2,6-xylyl$_2$SiCl$_2$ (**11**)	P-1	1.877(2)	2.069(2)	113.72(7)	102.66(3)
mesityl$_2$SiCl$_2$[12]	P-1	1.875(2)	2.064(2)	113.42(8)	102.96(4)
2,3,5,6-tetramethylphenyl$_2$SiCl$_2$[11]	P2$_1$/c	1.881(3)	2.073(1)	119.61(1)	101.14(5)
1-naphthyl$_2$SiCl$_2$ (**8**)	P2$_1$/n	1.859(3)	2.063(2)	116.84(10)	106.18(4)

The position of methyl substitution on the aryl ring also has a marked effect on the C–Si–C and Cl–Si–Cl angles. As mentioned above, each silicon atom is found in a near tetrahedral environment, and depending on the position of methyl substitution on the aryl ring, the angles around the silicon atom are varying considerably. Both *o*-tolyl$_2$SiCl$_2$ (**5**) and 2,4-xylyl$_2$SiCl$_2$ (**9**) display Cl–Si–Cl angles of 104.79(5)° and 104.95(4)° respectively, while the additional methyl group in the aryl moiety of 2,6-xylyl$_2$SiCl$_2$ (**11**) and mesityl$_2$SiCl$_2$ (102.96(4)°) results in more narrow angles. This is a direct result of increased steric demand on the chlorine atoms. In addition, the C–Si–C angles in 2,6-xylyl$_2$SiCl$_2$ (**11**) (113.72(7)°) and mesityl$_2$SiCl$_2$ (113.42(8)°) are much narrower than seen for the other presented dichlorides coinciding with the added steric demand of the methyl groups on the 2 and 6-position on the chlorine atoms. This added stress is not seen in 1-naphthyl$_2$SiCl$_2$ (**8**) which displays a wider Cl–Si–Cl (106.18(4)°) and a C–Si–C angle (116.84(10)°) similar to that of *o*-tolyl$_2$SiCl$_2$ (**5**). The bulkier 2,3,5,6-tetramethylphenyl$_2$SiCl$_2$ displays a Cl–Si–Cl angle of 101.14(5)° and the largest C–Si–C angle (119.61(1)°) accommodated by a large torsion angle of nearly 76° between the aryl substituents.[11]

The molecular structure of fluorenyl$_2$SiCl$_2$ (**2**) (Figure 15) varies significantly for the abovementioned aryl species. In this case, the fluorenyl substituents adopt a parallel orientation as seen for HR$_2$SiEt$_2$[91] and (MeR)(Me$_3$SiR)SiMe$_2$[92] (R = fluorenyl). Parallel substituents are also seen for both tetramethylcyclopentadienyl$_2$SiCl$_2$[10] and pentamethylcyclopentadienyl$_2$SiCl$_2$.[13] Despite this substituent arrangement, Si–C (1.878(4) Å) and Si–Cl (2.059(4) Å) bond lengths fall in expect ranges (Table 3) The planar nature of the fluorenyl substituent results in similar C–Si–C (117.65(5)°) and Cl–Si–Cl (105.01(2)°) angles as in 1-naphthyl$_2$SiCl$_2$ (**8**). Finally, benzyl$_2$SiCl$_2$ (**1**) displays the longest Si–Cl (2.801(2) Å) bond length and widest Cl–Si–Cl (107.04(4)°) angle among presented silicon dichloride species. This wider angle is attributed to the decreased steric demand of the benzyl substituent on the chlorine atoms.

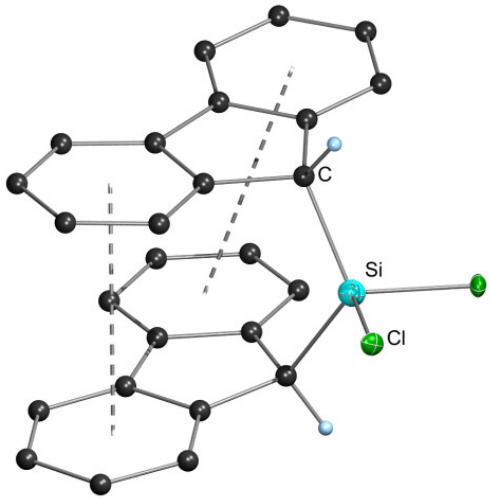

Figure 15: Crystal structure of fluorenyl$_2$SiCl$_2$ (2). All non-carbon atoms shown as 30% shaded ellipsoids. All hydrogen atoms except the hydrogen on the methanide carbon on the fluorenyl substituent removed for clarity.

Because of the lack of representative examples, the presence of aromatic secondary interactions and their importance as stabilizing factors for silicon dichloride species in the solid state has been rarely discussed. Specifically, interactions attributed to the nature of the aromatic substituents including π–π stacking, edge to face or CH$_3$···π interactions are present and should be studied (see also 2.2). These stabilizing interactions are described and compared to those present in previously reported species (see Table 2). Not surprisingly, 1-naphthyl$_2$SiCl$_2$ (**8**) shows a π–π stacking conformation in the solid state, where the molecules are arranged in a way to maximize these interactions creating infinite columns of parallel stacked naphthalene derivatives with a specific distance (d = 3.58 and 3.60 Å) between the ring centers (Figure 16). They are also found to be parallel-displaced to each other with a certain off-set (R = 1.54 and 1.23).

These values are in accordance to reported ranges of 3.4-3.6 Å for benzene[39] or 3.35 Å in graphite[93] and has been described for related aryl tin species.[94,95]

Table 2: List of non-covalent interactions for presented silicon dichlorides.

	π–π Stacking (Å)		**Edge to Face** (Å)	**CH_3–π** (Å)	**C–H···Cl** (Å)
	d	R			
benzyl$_2$SiCl$_2$ (**1**)	–	–	3.13	3.14	–
fluorenyl$_2$SiCl$_2$ (**2**)	3.35	0.96	–	–	2.84
o-tolyl$_2$SiCl$_2$ (**5**)	–	–	2.69–3.07	–	–
2,4-xylyl$_2$SiCl$_2$ (**9**)	–	–	3.26	2.99	–
2,6-xylyl$_2$SiCl$_2$ (**11**)	3.45	1.46	–	3.24	2.99
1-naphthyl$_2$SiCl$_2$ (**8**)	3.58	1.54	2.95	–	2.91

The chlorine atoms also aid in propagating these columns through C–H···Cl interactions (2.91 Å) with the hydrogens of the naphthyl substituents of the molecules above. In addition, the molecules are connected to the adjacent π–π stacking columns through edge to face interactions (2.95 Å) between naphthyl substituents (see Table 2).

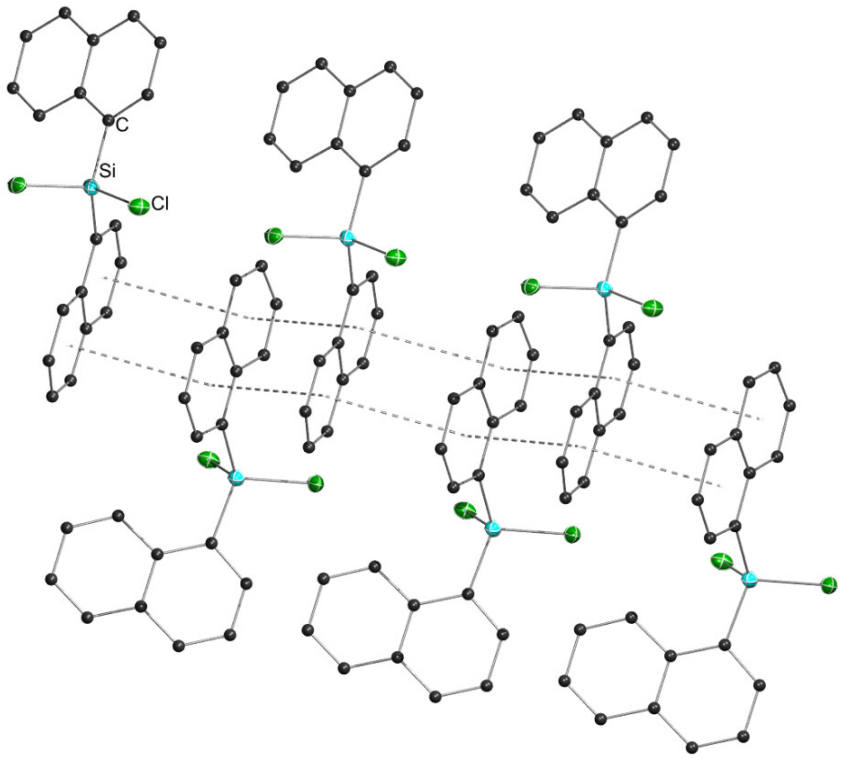

Figure 16: Crystal packing diagram for 1-naphthyl$_2$SiCl$_2$ (8). π–π stacking interactions are highlighted by dashed bonds. All non-carbon atoms shown as 30% shaded ellipsoids. All hydrogen atoms, edge to face and C–H···Cl interactions removed for clarity.

Edge to face interactions are exclusively present in the extended solid state of structure *o*-tolyl$_2$SiCl$_2$ (**5**) (2.69–3.07 Å) (Figure 17) consistent with the availability of phenyl hydrogens. The addition of a methyl group onto the aryl substituent of 2,4-xylyl$_2$SiCl$_2$ (**9**) results in CH$_3$···π interactions (2.99 Å) through the methyl in the 4-position and elongated edge to face interactions with neighboring molecules (3.26 Å) (Figure 18). However, methyl addition at the 6-position in 2,6-xylyl$_2$SiCl$_2$ (**11**) results in infinite chains propagated through both π–π stacking (d = 3.45 Å, R = 1.46) and CH$_3$···π interactions (3.24 Å) (Figure 19) These chains are then bridged by C–H···Cl interactions (2.99 Å).

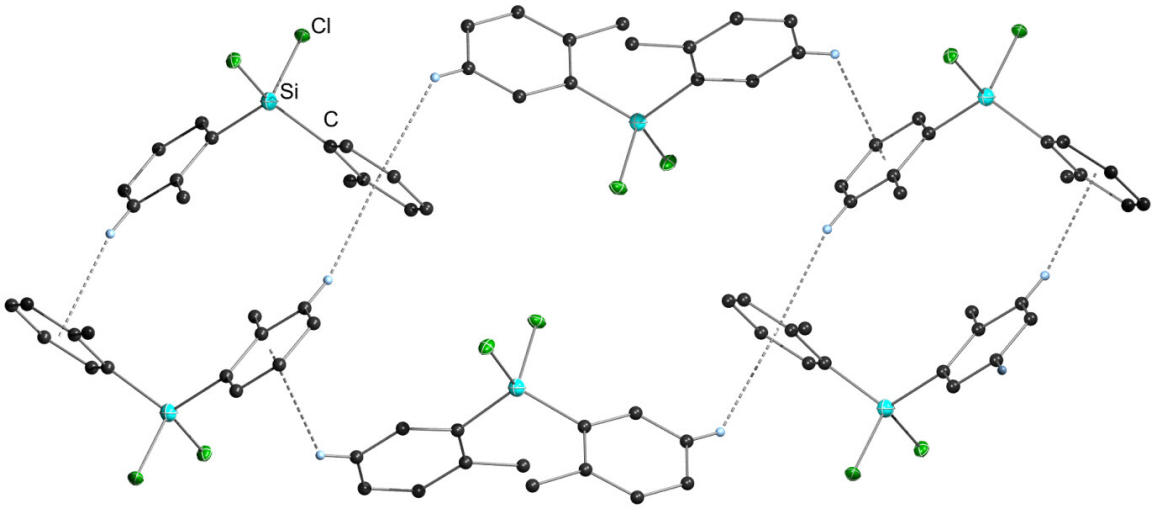

Figure 17: Crystal packing diagram for *o*-tolyl$_2$SiCl$_2$ (5). Edge to face interactions are highlighted by dashed bonds. All non-carbon atoms shown as 30% shaded ellipsoids. Hydrogen atoms not involved in intermolecular interactions removed for clarity.

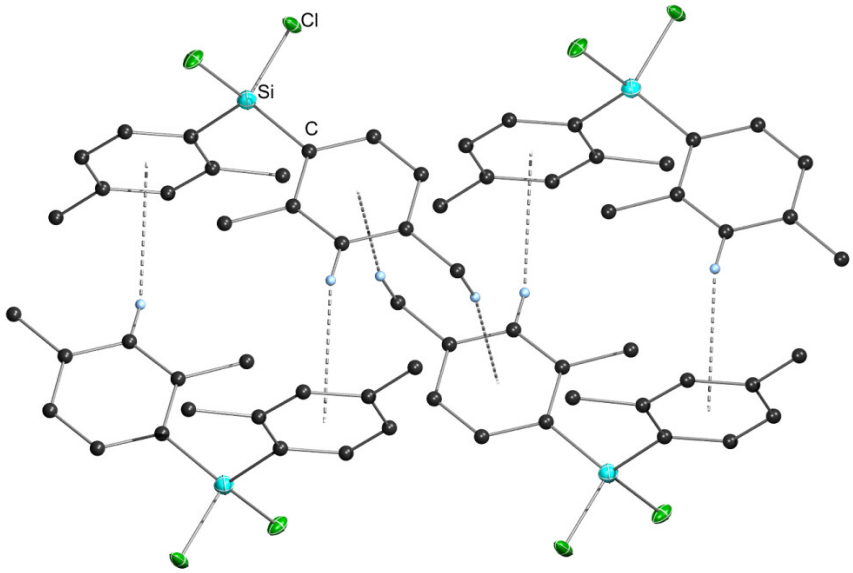

Figure 18: Crystal packing diagram for 2,4-xylyl$_2$SiCl$_2$ (9). Edge to face interactions and CH$_3$···π interactions are highlighted by dashed bonds. All non-carbon atoms shown as 30% shaded ellipsoids. Hydrogen atoms not involved in intermolecular interactions removed for clarity.

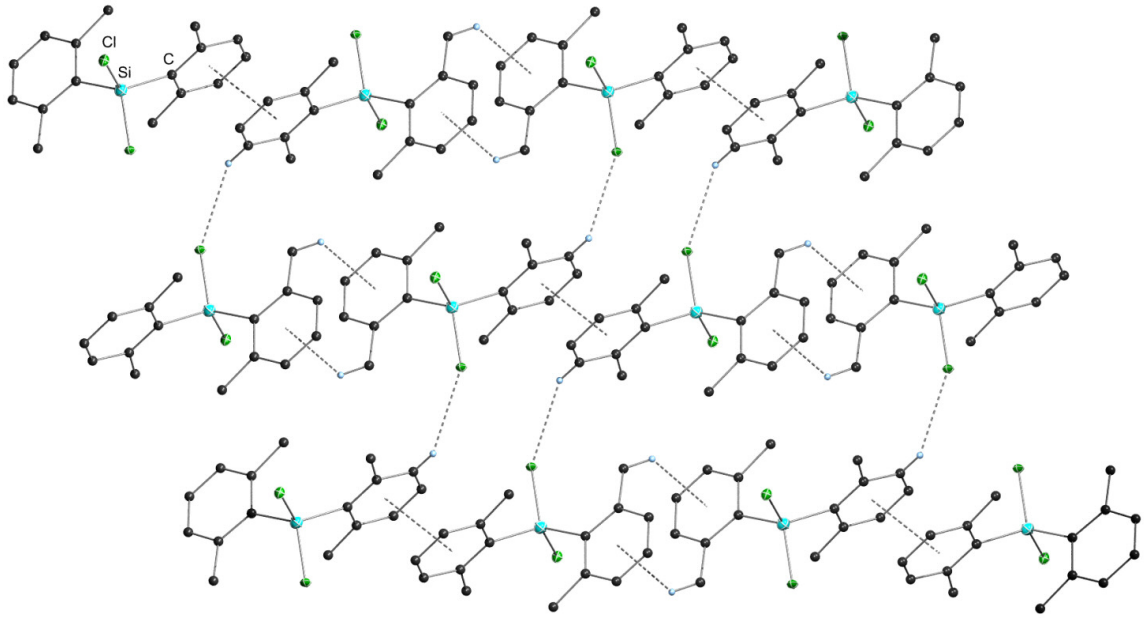

Figure 19: Crystal packing diagram for 2,6-xylyl$_2$SiCl$_2$ (11). CH$_3$···π and C–H···Cl interactions are highlighted by dashed bonds. All non-carbon atoms shown as 30% shaded ellipsoids. Hydrogen atoms not involved in intermolecular interactions removed for clarity.

As mentioned above, the fluorenyl substituents in the molecular structure of fluorenyl$_2$SiCl$_2$ (**2**) adopt a parallel orientation with a π–π stacking distance of 3.35 Å (R = 0.96). This substituent conformation and similar π–π stacking distances are also observed in the molecular structures of HR$_2$SiEt$_2$[91] (d = 3.47 Å) and

(MeR)($SiMe_3$R)$SiMe_2$[92](d = 3.45 Å) (R = fluorenyl). The stacked fluorenyls then interact with a neighboring molecule through more π–π stacking (d = 3.53 Å, R = 1.23) resulting in π-stacked oligomeric chains (Figure 20). Similar solid state interactions have been described for compounds resulting from the anionic initialized polymerization of dibenzofulvene.[96] As seen in 2,6-xylyl$_2$$SiCl_2$ (**11**), these π-stacked oligomeric chains are also bridged by C–H···Cl interactions through the phenyl hydrogens of the fluorenyl substituent (2.84 Å).

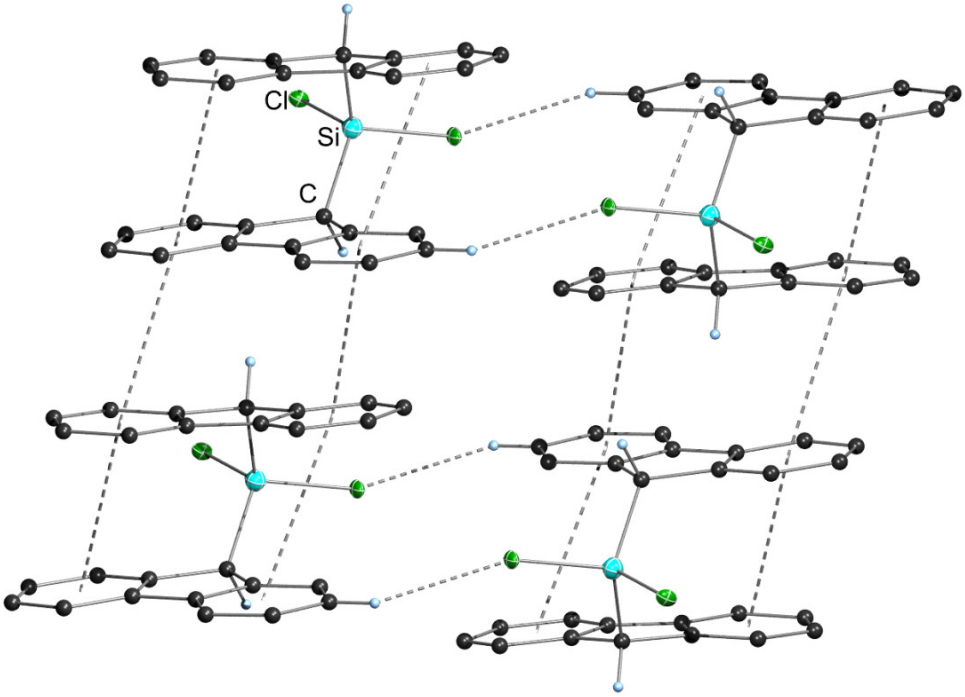

Figure 20: Crystal packing diagram for fluorenyl$_2$$SiCl_2$ (2). π–π stacking and C–H···Cl interactions are highlighted by dashed bonds. All non-carbon atoms shown as 30% shaded ellipsoids. Hydrogen atoms not involved in intermolecular interactions removed for clarity.

The benzyl$_2$$SiCl_2$ (**1**) species also shows intermolecular interaction in the solid state. In this case, the lack of methyl substitution on the phenyl ring does not circumvent CH_3-pi interactions. In the extended structure (Figure 21), we see neighboring molecules oriented so as to maximize CH_3-π interactions from one of the methanide (C*H*$_2$-Ph) hydrogens with the phenyl substituent of the other compound (3.14 Å). However, in contrast to 2,6-xylyl$_2$$SiCl_2$ (**11**), oligomeric chains are not formed. Rather edge to face interactions (3.13 Å) are preferred.

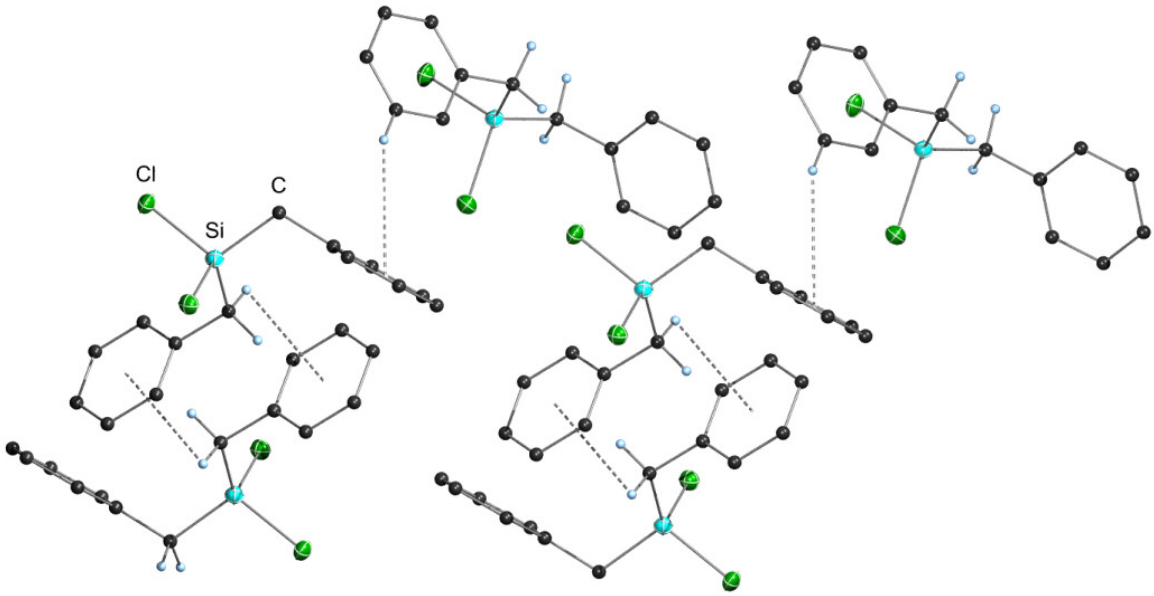

Figure 21: Crystal packing diagram for benzyl$_2$SiCl$_2$ (1). Edge to face interactions and CH$_3$···π interactions are highlighted by dashed bonds. All non-carbon atoms shown as 30% shaded ellipsoids. Hydrogen atoms not involved in intermolecular interactions removed for clarity.

RSiCl$_3$/R$_3$SiCl: 1-naphthyl$_3$SiCl (**16**) crystallizes in a triclinic space group P-1. Selected bond lengths and angles are given in Table 3. For crystallographic data and details of measurements and refinement for presented compounds see Appendix**.**

Table 3: Selected bond lengths (Å) and angles (°) for presented 1-naphthyl substituted chlorosilanes.

	Space Group	Si–C (Å)(avg.)	Si–Cl (Å)(avg.)	C–Si–C (°)	Cl–Si–Cl (°)	C–Si–Cl (°)
1-naphthylSiCl$_3$ (**15**)	P2$_1$/c	1.841(2)	2.034(8)	–	106.9(4)	111.9(7)
2-naphthylSiCl$_3$ [30]	P2$_1$/n	1.841(3)	2.034(10)	–	107.2(4)	111.7(9)
1-naphthyl$_2$SiCl$_2$ (**8**)	P2$_1$/n	1.859(3)	2.063(2)	116.84(10)	106.18(4)	108.33(3)
1-naphthyl$_3$SiCl (**16**)	P-1	1.873(4)	2.089(9)	111.23(8)	–	107.65(9)

Comparison of 1-naphthylSiCl$_3$ (**15**), 1-naphthyl$_2$SiCl$_2$ (**8**) and 1-naphthyl$_3$SiCl (**16**) shows that by stepwise exchange of chlorine with a naphthyl group the bond lengths change notably. The Si-C bond length elongates with increasing number of naphthyl substituents from 1.841(2) Å for 1-naphthylSiCl$_3$ (**15**) to 1.873(4) Å for 1-naphthyl$_3$SiCl (**16**). The same trend can be seen for the Si-Cl bond length showing the largest value for 1-naphthyl$_3$SiCl (**16**). The C-Si-Cl and the C-Si-Cl angle decrease with an increase in number of naphthyl substituents, due to the higher steric demand of the naphthyl group compared to chlorine. The obtained bond lengths and angles of 2-naphthylSiCl$_3$ are in a similar range than the one for the corresponding 1-naphthyl substituted compound.

Aromatic secondary interactions present in 1-naphthyl and 2-naphtyl substituted chlorosilanes are listed in Table 4.

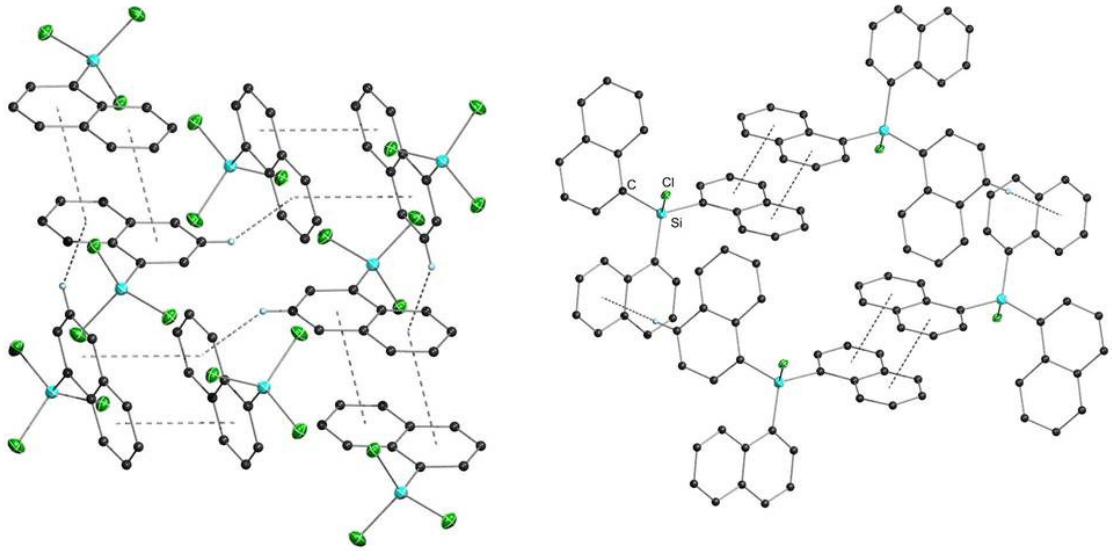

1-naphthylSiCl$_3$ (**X**) 1-naphthyl$_3$SiCl (**X**)

Figure 22: Crystal packing diagram for 1-naphthyl substituted chlorosilanes. π–π stacking interactions are highlighted by dashed bonds. All non-carbon atoms shown as 30% shaded ellipsoids. Hydrogen atoms not involved in intermolecular interactions removed for clarity.

In 1-naphthylSiCl$_3$ (**15**) two adjacent naphthyl groups are parallel stacked with a specific distance of 3.41 Å between the ring centers and a certain off-set of 1.72 Å. The same naphthyl group forms an edge to face interaction (2.94 Å) to the naphthyl group of the neighboring molecule. No columns are formed as observed in 1-naphthyl$_2$SiCl$_2$ (**8**). Unexpectedly no C–H···Cl interactions can be detected.

Table 4: List of non-covalent interactions for 1-naphthyl substituted chlorosilanes

	π–π Stacking (Å)		**Edge to Face** (Å)	**C-H···Cl** (Å)
	d	R		
1-naphthylSiCl$_3$ (**15**)	3.41	1.72	2.94	–
1-naphthyl$_2$SiCl$_2$ (**8**)	3.58	1.54	2.95	2.91
1-naphthyl$_3$SiCl (**16**)	3.45	1.60	2.78-3.15	–
2-naphthyl$_2$SiCl$_2$	–	–	2.78-2.87	2.91

In 1-naphthyl$_3$SiCl (**16**) two naphthyl groups are connected to the adjacent molecule *via* edge to face interactions (2.78-3.15 Å). The third group is parallel stacked to the naphthyl group of the neighboring molecule with a specific distance of 3.45 Å between the ring centers and a certain off-set of 1.60 Å. No C–H···Cl interactions can be detect-

ed (Figure 22). 2-Naphthyl$SiCl_3$ cocrystallizes with naphthalene. No π–π interaction is observed since the 2-naphthyl group forms an edge to face interaction (2.78-2.87 Å) with an adjacent naphthalene molecule (Figure 23).

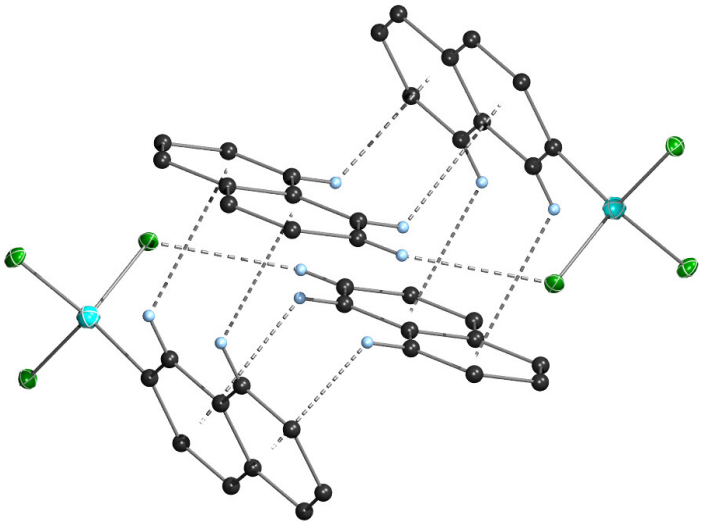

Figure 23: Crystal packing diagram for 2-naphthyl$SiCl_3$ substituted chlorosilanes. Edge to face interactions are highlighted by dashed bonds. All non-carbon atoms shown as 30% shaded ellipsoids. C–H···Cl interactions and hydrogen atoms not involved in intermolecular interactions removed for clarity.

3.2.2 Organosilanes R_nSiH_{4-n}

R_2SiH_2: This section summarizes the crystallographic data of solid compounds **21, 25-28** and **34** and compares it to already published compounds. In each case, the silicon atom is found in a near distorted tetrahedral environment bound to two hydrogen atoms and two substituents (Figure 24).

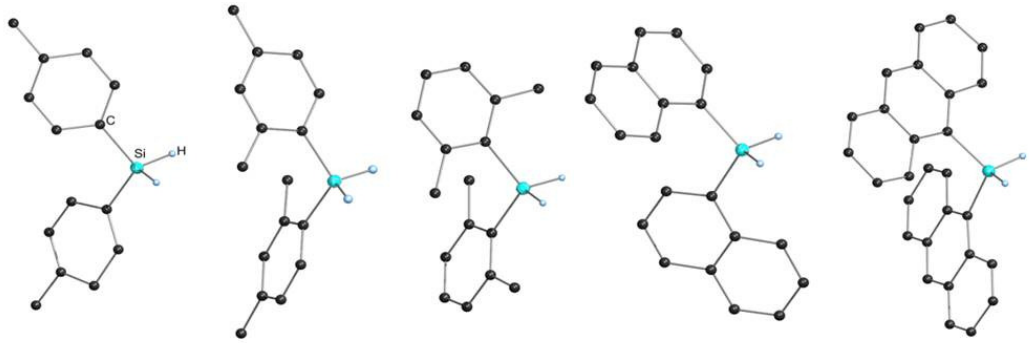

Figure 24: Structure of presented aryl silicon dihydrides. All non-carbon atoms shown as 30% shaded ellipsoids. All hydrogen atoms except Si–H atoms removed for clarity.

All hydrogen atoms bound to silicon were located in the difference map. While compounds **21**, **25**, **26**, **27** and **28** were isolated as discrete crystals by recrystallization from

solution, crystals of liquid *p*-tolyl$_2$SiH$_2$ (**34**) were formed *via in situ* crystallization inside a capillary. This method was quite successful in the isolation of X-ray quality crystals for this compound, and is a technique that has allowed for characterization for a variety of compounds (see 3.2.3).[97,98] Table 5 summarizes average bond lengths and angles for presented compounds and comparable silicon dihydrides. For crystallographic data and details of measurements and refinement for presented organosilanes see Appendix**.**

Table 5: Selected bond lengths and angles for all presented compounds and similar aryl silicon dihydrides known in literature.

Compounds	**Space Group**	**Si–C (Å) (avg.)**	**Si–H (Å)**	**C–Si–C (°)**	**H–Si–H (°)**
fluorenyl$_2$SiH$_2$ (**21**)	P2$_1$/n	1.897(3)	1.372(2) 1.401(2)	110.10(5)	111.8(9)
p-tolyl$_2$SiH$_2$ (**34**)	P2$_1$2$_1$2$_1$	1.870(2)	1.395(3) 1.407(3)	110.54(1)	109.9(17)
2,4-xylyl$_2$SiH$_2$ (**26**)	P2$_1$/c	1.869(2)	1.389(2)	117.18(6)	109.7(11)
2,6-xylyl$_2$SiH$_2$ (**28**)	P2$_1$/c	1.885(2)	1.354(2) 1.398(2)	114.05(7)	102.2(11)
mesityl$_2$SiH$_2$[17,18]	C2/c	1.883(2)	1.42(2)	114.16(11)	108(2)
1-naphthyl$_2$SiH$_2$ (**25**)	Pbca	1.869(3)	1.385(2) 1.403(2)	109.90(6)	110.5(9)
9-anthracenyl$_2$SiH$_2$ (**27**)	P2$_1$/c	1.898(2)	1.359(2) 1.407(2)	113.73(8)	106.9(11)
2,3,4-triphenylnaphthyl$_2$SiH$_2$[20]	P-1	1.896(1)	1.38(2) 1.40(2)	112.78(7)	104(1)

As reported for the series of R$_2$SiCl$_2$ (R = benzyl, fluorenyl, *o*-tolyl, 2,4-xylyl, 2,6-xylyl, 1-naphthyl), an increase in steric demand around the silicon central atom results in slightly elongated average Si–C bond lengths when bulkier aryl substituents are present (see 3.2.1). *p*-Tolyl$_2$SiH$_2$ (**34**) and 2,4-xylyl$_2$SiH$_2$ (**26**) display averaged Si–C bond lengths of 1.870(2) and 1.869(2) Å respectively, with a similar value for 1-naphthyl$_2$SiH$_2$ (**25**) (1.869(3) Å)**.** The addition of a methyl group at the 6-position of the aryl substituent in 2,6-xylyl$_2$SiH$_2$ (**28**) results in a longer averaged Si–C bond length (1.885(2) Å) comparable to mesityl$_2$SiH$_2$ (1.875(2) Å).[17,18] Not surprisingly, the longest averaged Si–C bond lengths of 1.898(2) and 1.896(1) Å are attributed to the highly substituted aryl moiety in 9-anthracenyl$_2$SiH$_2$ (**27**) and 2,3,4-triphenylnaphthyl$_2$SiH$_2$.[20] Curiously, this

bulky substituent does not result in the longest Si–H bond length which is attributed to mesityl$_2$SiH$_2$ (1.42(2) Å). All other Si–H bond lengths range from 1.354(2)–1.407(3) Å.

Methyl substitution on the aryl ring also has an effect on the C–Si–C and H–Si–H angles as also observed in the aforementioned R_2SiCl_2 species. As mentioned above, each silicon atom is found in a near tetrahedral environment, and depending on the position of methyl substitution on the aryl ring, the angles around the silicon atom are varying considerably. Both *p*-tolyl$_2$SiH$_2$ (**34**) and 2,4-xylyl$_2$SiH$_2$ (**26**) display similar H–Si–H angles of 109.9(17) and 109.7(11)° respectively (Table 5). *p*-tolyl$_2$SiH$_2$ (**34**) also displays the closest to ideal tetrahedral geometry around the silicon atom with a C–Si–C angle of 110.54(1)°. However, the additional methyl group in the aryl moiety of 2,6-xylyl$_2$SiH$_2$ (**28**) results in the most narrow H–Si–H angle of 102.2(11)° among presented aryl substituents. Despite having a wider H–Si–H angle, mesityl$_2$SiH$_2$ and 2,6-xylyl$_2$SiH$_2$ (**28**) display quite similar C–Si–C angles of 114.05(7) and 114.16(11)° respectively. This added stress is not seen in 1-naphthyl$_2$SiH$_2$ (**25**) which displays the widest H–Si–H angle (110.5(9)°) and most narrow C–Si–C angle (109.90(6)°). Surprisingly, the widest C–Si–C angle (117.18(6)°) is observed for 2,4-xylyl$_2$SiH$_2$ (**26**) and not in 9-anthracenyl$_2$SiH$_2$ (**27**) (113.73(8)°) and 2,3,4-triphenylnaphthyl$_2$SiH$_2$ (112.78(7)°) as expected. These compounds display average H–Si–H angles of 106.9(11)° and 104(1)° respectively.

In fluorenyl$_2$SiH$_2$ (**21**), the planar fluorenyl substituents are perpendicular to each other or in an H-in-H-out conformation (Figure 25), which has been shown to be the lowest energy conformer (gas phase) found by AM1 molecular orbital calculations in bisfluorenyl silicon species.[99] This conformation is also observed in fluorenyl$_2$SiMe$_2$,[91,99] difluorenylsilacyclobutane,[91] 9-methylfluoren-9-yl$_2$SiMe$_2$[100] and (9-methylfluoren-9-yl)(fluoren-9-yl)SiMe$_2$.[100] While Si–H (1.372(2) and 1.401(2) Å) bond lengths fall in expect ranges (Table 5), the averaged Si–C (1.897(3) Å) of fluorenyl$_2$SiH$_2$ (**21**) resembles that of the bulkier substituted 9-anthracenyl$_2$SiH$_2$ (**27**) (1.898(2) Å) and 2,3,4-triphenylnaphthyl$_2$SiH$_2$ (1.896(1) Å).[20]

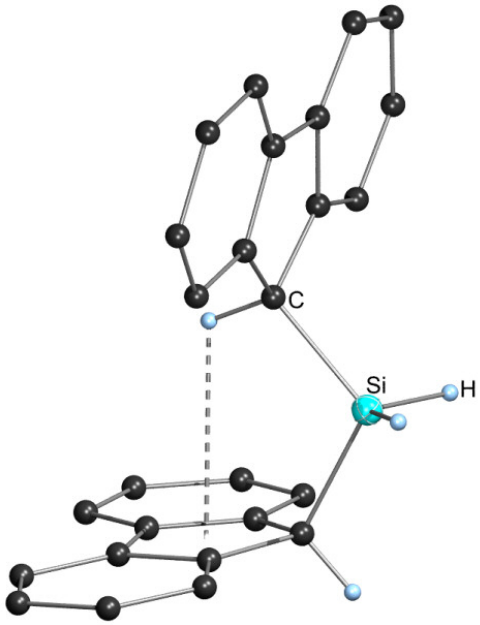

Figure 25: Crystal structure of fluorenyl$_2$SiH$_2$ (21). All non-carbon atoms shown as 30% shaded ellipsoids. All hydrogen atoms except Si–H removed for clarity.

Despite this substituent arrangement, the C–Si–C (110.15(5)°) and H–Si–H angle (111.8(9)°) of fluorenyl$_2$SiH$_2$ (**21**) resemble those found for *p*-tolyl$_2$SiH$_2$ (**34**). In addition, the H-in-H-out substituent conformation in fluorenyl$_2$SiH$_2$ (**21**) allows for an intramolecular Si–H···π interactions (2.84 Å) between one of the silyl hydrogens and the centroid of the opposite fluorenyl substituent. These intramolecular interactions are also reported for 9-methylfluoren-9-yl$_2$SiMe$_2$ (2.65 Å) and (9-methylfluoren-9-yl)(fluoren-9-yl)SiMe$_2$ (2.88 Å).[100]

In fluorenyl$_2$SiH$_2$ (**21**), the planar fluorenyl substituents are perpendicular to each other. However, the corresponding chloride compound, fluorenyl$_2$SiCl$_2$ (**2**), shows a parallel arrangement of the fluorenyl groups. DFT calculations (DFT: MPW1PW91/6-31+G*) showed that in the case of fluorenyl$_2$SiCl$_2$ (**2**) the parallel and the perpendicular structure (Figure 26) have no major difference in energy between the two arrangements. A change from one form to the other does not lead to a notably energy gain. None of the two arrangements is thermodynamically favored, so both could possibly be obtained in the solid state structure. For fluorenyl$_2$SiH$_2$ (**21**) the perpendicular form shows a lower energy than the parallel one. A change to the parallel form is as well unfavorable due to the higher energy barrier between the two forms. The obtained solid state structure corresponds to the thermodynamically favored arrangement.

Due to the lack of representative examples, the presence of aromatic secondary interactions and their importance as stabilizing factors for silicon dihydride species in the solid state has been rarely discussed. Specifically, interactions attributed to the nature

of the aromatic substituents including π–π stacking, edge to face or C–H···π interactions should be studied.

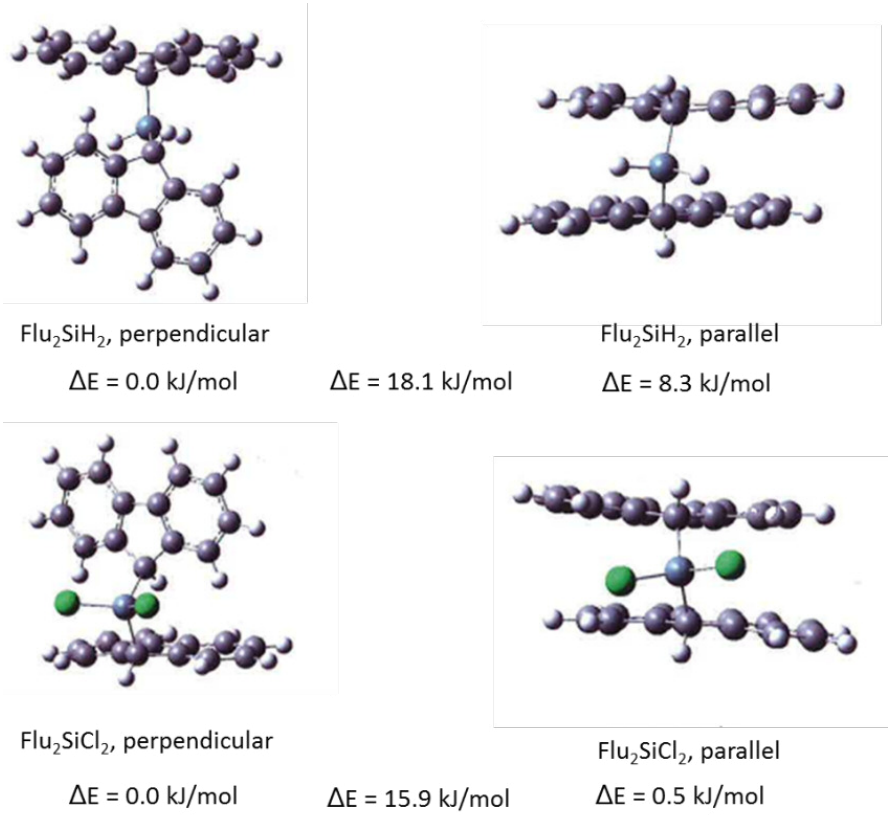

Figure 26: Calculated energy for perpendicular and parallel arrangement of the fluorenyl groups in fluorenyl$_2$SiCl$_2$ (2) and fluorenyl$_2$SiH$_2$ (21); (DFT: MPW1PW91/6-31+G*)

These stabilizing interactions are described and compared to those present in previously reported species (Table 6). In both 1-naphthyl$_2$SiH$_2$ (**25**) (Figure 27) and 9-anthracenyl$_2$SiH$_2$ (**27**) (Figure 28), the fused aromatic ring substituents show a large propensity towards π–π stacking. In each case, the molecules arrange in solid state to maximize these interactions, with a specific distance between the ring centers (d). They are also found to be parallel-displaced to each other with a certain offset (R). This is in stark contrast to the herringbone structure present for naphthalene and anthracene, which are dominated by edge to face interactions and corresponds more to larger polycyclic aromatic molecules, such as coronene, kekulene, or graphite.[93,101,102]

1-naphthyl$_2$SiH$_2$ (**25**) has an interplanar distance of 3.50 Å with a displacement of 1.45 (Table 6). These findings are in accordance with a reported range of 3.4–3.6 Å for benzene[101] or 3.35 Å in graphite,[93] and also observed for a series of aryl tin[94,95] and aryl silicon halides.[103]

Table 6: Secondary non-covalent interactions for all presented compounds and similar aryl silicon dihydrides known in literature. Intramol.=intramolecular; Intermol.=intermolecular;

Compounds	π–π Stack- (Å)		Edge to (Å)	CH_3–π (Å)	Si–H···π (Å)
	d	R			
fluorenyl$_2$SiH$_2$ (**21**)	3.45	1.51	2.89-3.22	–	2.84, intramolecular
p-tolyl$_2$SiH$_2$ (**34**)	–	–	2.96-3.18	–	–
2,4-xylyl$_2$SiH$_2$ (**26**)	–	–	3.18	2.83	–
2,6-xylyl$_2$SiH$_2$ (**28**)	–	–	2.95	2.76-	–
mesityl$_2$SiH$_2$[17,18]	–	–	–	–	–
1-naphthyl$_2$SiH$_2$ (**25**)	3.50	1.45	2.79-2.83	–	–
9-anthracenyl$_2$SiH$_2$ (**27**)	3.42	1.84	–	–	2.49, intermolecular
2,3,4-triphenylnapththyl$_2$SiH$_2$[20]	–	–	2.81	–	3.08, intermolecular

While not creating infinite chains as seen for the precursor to the hydride, 1-naphthyl$_2$SiCl$_2$ (**8**),[103] molecules of 1-naphthyl$_2$SiH$_2$ (**25**) displaying π–π stacking exhibit edge to face interactions (2.79, 2.83 Å) with neighboring pairs of molecules (Figure 27).

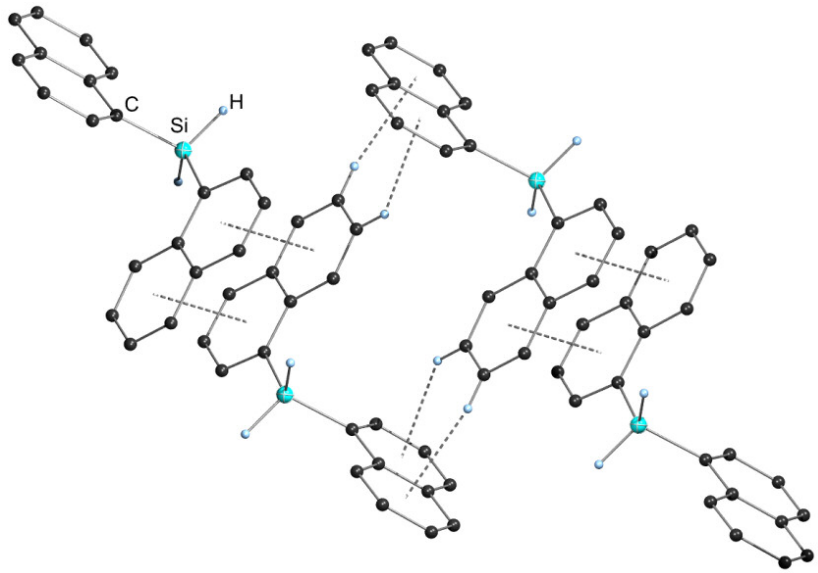

Figure 27: Crystal packing diagram for 1-naphthyl$_2$SiH$_2$ (25). π–π stacking and edge to face interactions are highlighted by dashed bonds. All non-carbon atoms shown as 30% shaded ellipsoids. All hydrogen atoms not involved in intermolecular interactions except Si–H atoms removed for clarity.

9-anthracenyl$_2$SiH$_2$ (**27**) shows a slightly shorter interplanar distance of 3.42 Å, but larger displacement of 1.84 (Table 6). Offset distances for other aromatic systems are found in the range 1.6–1.8 Å.[101] In this case, not only are linear chains propagated by π–π stacking through the anthracenyl substituents, but very close Si–H···π interactions

(2.49 Å) occur between one of the silyl hydrogens and the inner aromatic ring of the neighboring molecule. This interaction is also observed in 2,3,4-phenylmethyl$_2$SiH$_2$ (3.08 Å) despite the sterically crowded substituent.[20]

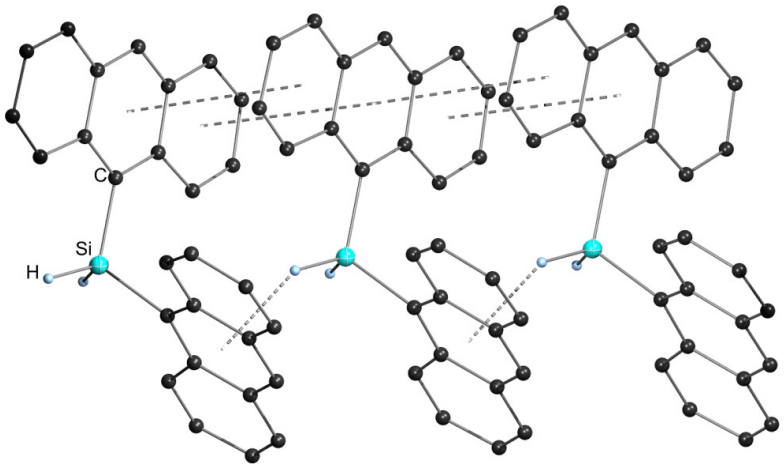

Figure 28: Crystal packing diagram for 9-anthracenyl$_2$SiH$_2$ (27). π–π stacking and Si–H···π interactions are highlighted by dashed bonds. All non-carbon atoms shown as 30% shaded ellipsoids. All hydrogen atoms not involved in intermolecular interactions except Si–H removed for clarity.

Despite presence of a methyl group in the *para* position of the aryl substituent in *p*-tolyl$_2$SiH$_2$ (**34**) (Figure 29), only edge to face interactions are observed (2.96, 3.18 Å). However in 2,4-xylyl$_2$SiH$_2$ (**26**) and 2,6-xylyl$_2$SiH$_2$ (**28**), the addition of a second methyl group on the aryl substituent leads to CH$_3$···π interactions being preferred in packing motifs.

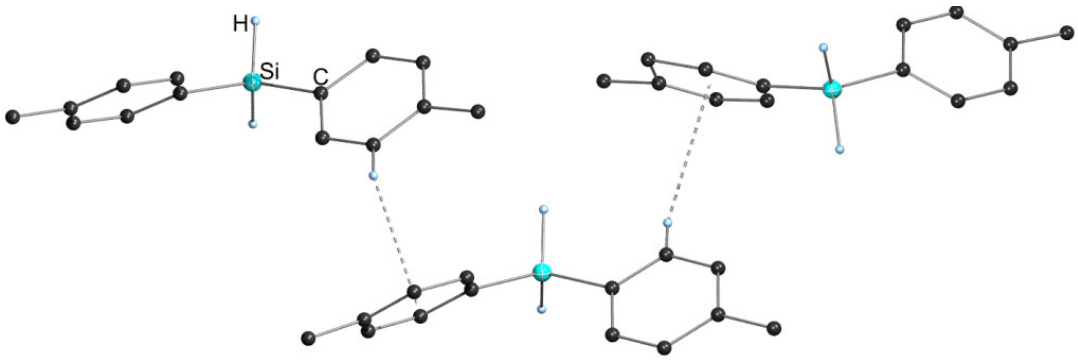

Figure 29: Crystal packing diagram for *p*-tolyl$_2$SiH$_2$ (34). Edge to face interactions are highlighted by dashed bonds. All non-carbon atoms shown as 30% shaded ellipsoids. All hydrogen atoms not involved in intermolecular interactions except Si–H atoms removed for clarity.

The solid state packing motif 2,4-xylyl$_2$SiH$_2$ (**26**) (Figure 30) closely resembles that of 2,4-xylyl$_2$SiCl$_2$ (**9**) with the exception of slightly longer CH3···π (3.26 Å) and edge to face (2.99 Å) interactions in this compounds as compared to 2,4-xylyl$_2$SiH$_2$ (**26**) (3.18, 2.83 Å). These interactions are well within range for reported CH$_3$···π interactions (2.3–3.4

Å).[94,101,103] These latter are also visible in the solid state packing motif for toluene,[104] which in addition to edge to face interactions (2.78 Å), exhibits closer $CH_3\cdots\pi$ interactions from the methyl group (2.61 Å). Even closer $CH_3\cdots\pi$ (2.95 Å) and edge to face (2.76 Å) interactions are observed in 2,6-xylyl$_2$SiH$_2$ (**28**) resulting in a tighter packed structure (Figure 31).

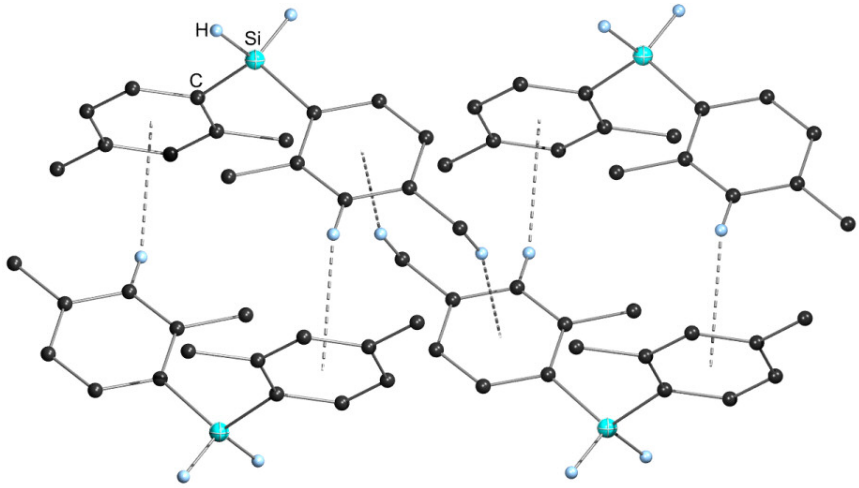

Figure 30: Crystal packing diagram for 2,4-xylyl$_2$SiH$_2$ (26). Edge to face interactions and $CH_3\cdots\pi$ interactions are highlighted by dashed bonds. All non-carbon atoms shown as 30% shaded ellipsoids. All hydrogen atoms not involved in intermolecular interactions except Si–H removed for clarity.

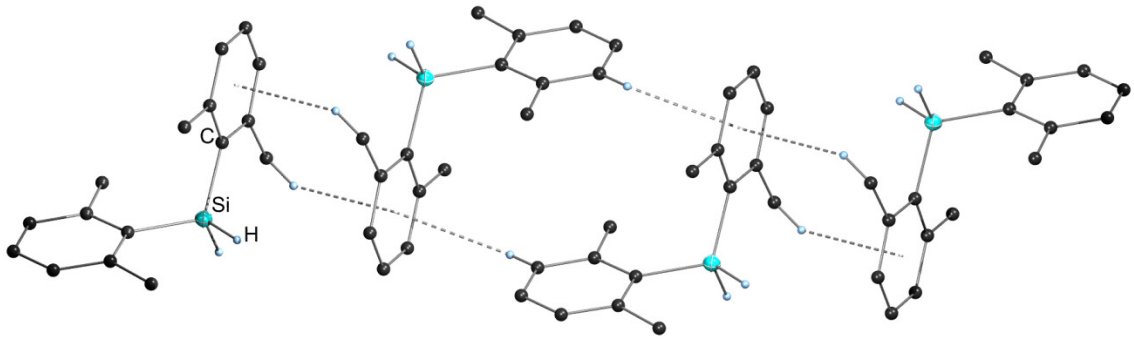

Figure 31: Crystal packing diagram for 2,6-xylyl$_2$SiH$_2$ (28). $CH_3\cdots\pi$ and edge to face interactions are highlighted by dashed bonds. All non-carbon atoms shown as 30% shaded ellipsoids. All hydrogen atoms not involved in intermolecular interactions except Si–H removed for clarity.

Also exhibiting close intermolecular π–π stacking interactions between neighboring molecules (d = 3.45, R = 1.51 Å) in the solid state is H-in-H-out fluorenyl$_2$SiH$_2$ (**21**) (Figure 32), which creates sheets further propagated by edge to face interactions (2.89–3.22 Å) (Table 4). No interactions are observed between these sheets. This is in stark contrast to fluorenyl$_2$SiCl$_2$ (**2**) which crystallizes in an H-out-H-out substituent arrangement as π–π stacked oligomeric chains bridged by C–H···Cl interactions through the phenyl hydrogens of the fluorenyl substituent (2.84 Å).[103]

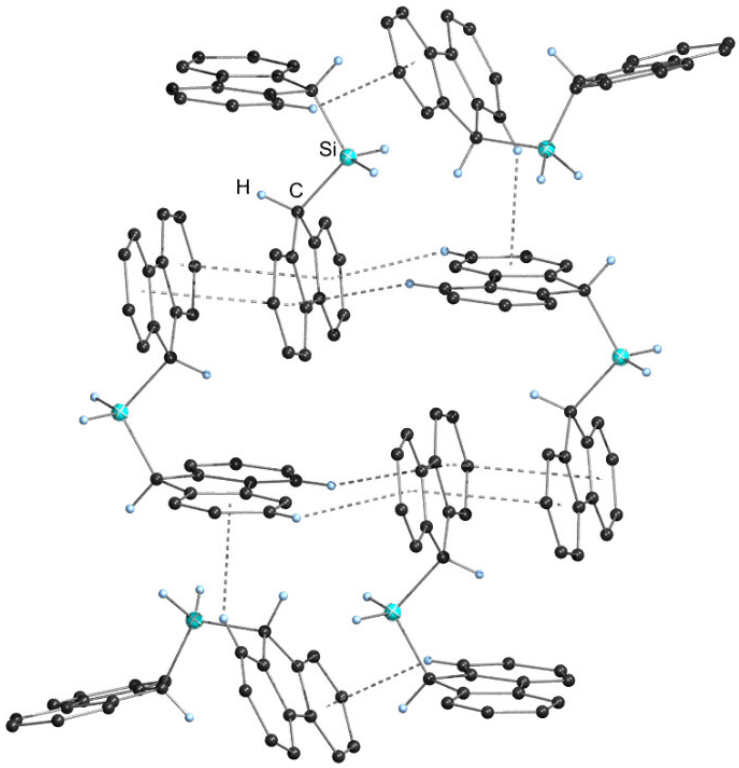

Figure 32: Crystal packing diagram for fluorenyl$_2$SiH$_2$ (21). π–π stacking and edge to face interactions are highlighted by dashed bonds. All non-carbon atoms shown as 30% shaded ellipsoids. All hydrogen atoms not involved in intermolecular interactions except Si–H removed for clarity.

3.2.3 Capillary Crystallization

Crystal structure determination of low melting *p*-tolyl$_2$SiH$_2$ (**34**) was made possible by growing crystals inside of sealed glass capillaries mounted on the singel crystal diffractometer.[1]

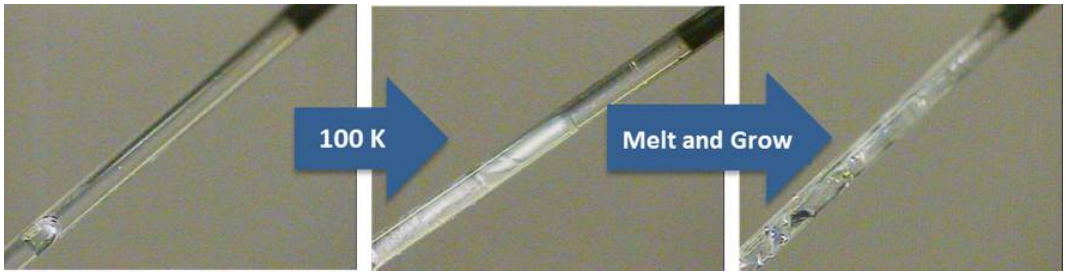

Figure 33: Procedure of *in situ* crystallization

Samples were cooled to 100 K and subsequently warmed up and cooled down very slowly until seed crystals were formed (Figure 33). This was done either by exposing the capillary to a focused IR laser beam (OHCD Laser)[105] or by manually warming up

[1] measurements were performed at the University of Bielefeld with the help of Dr. H. G. Stammler

the sides of the capillary. Diffraction studies were subsequently carried out at the temperature of initial crystal formation and 100 K (Figure 34). Twin refinement was required for *p*-tolyl$_2$SiH$_2$ (**34**). Hydrogen atoms next to heavy atoms were found in the difference map.[106,107]

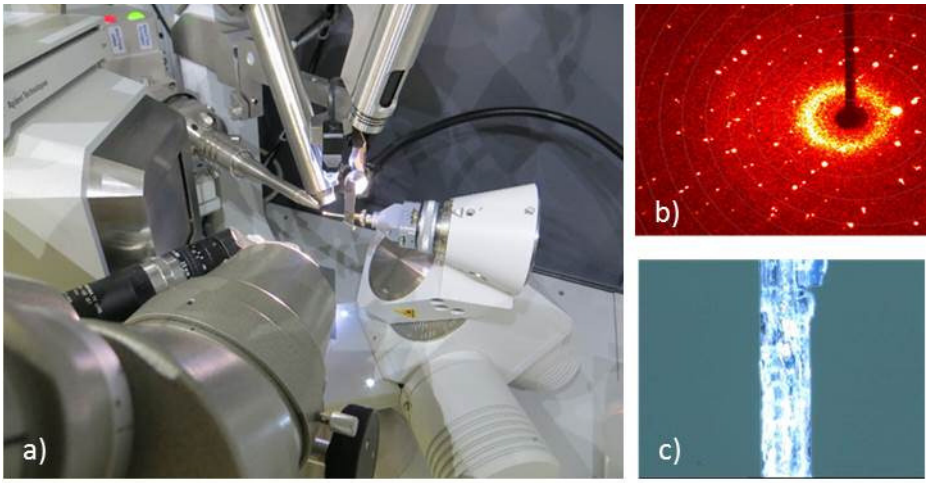

Figure 34: a) Measurement setup with SuperNova diffractometer; b) diffraction pattern; c) crystal inside glass capillary

3.3 ^{29}Si-NMR – experimental and calculated data

^{29}Si-NMR measurements were performed with relaxation delay times ranging from 25-60 seconds, with the sterically hindered compound 9-anthracenyl$_2$SiCl$_2$ (**10**) and the corresponding hydride 9-anthracenyl$_2$SiH$_2$ (**27**) requiring the longest delay. For compounds bearing a proton in position *ortho* to the silicon, population transfer pulse programs such as DEPT were used for measurement. ^{29}Si-NMR studies are supplemented by density functional calculations. Table 7 shows the obtained experimental and calculated ^{29}Si-NMR shifts for organo dichlorosilanes R$_2$SiCl$_2$

Table 7: Experimental and M06L/Iglo-II calculated ^{29}Si-NMR shifts of diorgano dichlorosilanes in C_6D_6. C.No.: Compound number (see 4); calc = calculated; exp = experimental.

R$_2$SiCl$_2$ R=	C. No.	δ ^{29}Si$_{exp}$ [ppm]	δ ^{29}Si$_{calc}$ [ppm]
benzyl	(**1**)	22.7	26.7
fluorenyl	(**2**)	17.3	22.3
phenyl [108]	-	6.20	8.7
p-tolyl	(**3**)	6.65	8.7
m-tolyl	(**4**)	6.37	9.6
3,5-xylyl [90]	-	not reported	9.2
o-tolyl	(**5**)	6.57	10.0
p-*n*-butylphenyl	(**6**)	6.49	7.8
p-biphenyl	(**7**)	6.24	7.8
1-naphthyl	(**8**)	7.58	11.6
2,4-xylyl	(**9**)	7.23	11.0
9-anthracenyl	(**10**)	3.02	8.4
2,6-xylyl	(**11**)	2.08	7.6
mesityl [109]	-	4.30	7.5

Benzyl$_2$SiCl$_2$ (**1**) exhibits the largest low field shift in the row of presented compounds followed by the cyclopentadienyl-like fluorenyl$_2$SiCl$_2$ (**2**). As expected, when silicon is bonded to an *sp*^{2} hybridized carbon these are shifted to higher fields compared to usual silicon organic variety with an *sp*^{3} hybridized carbon. 1-naphthyl$_2$SiCl$_2$ (**8**) with only one proton in *β*-position of the rather flat naphthyl group shows a slightly downfield shift compared to the phenyl derivatives with a substituent in the *para* position. The substitution on the phenyl ring with a methyl group in *ortho*-, *meta*- or *para*-position does not show a clear trend, but all exhibit a similar shift in the range of 6.5 ppm. Un-

expectedly, 2,4-xylyl$_2$SiCl$_2$ (**9**) shows a slight downfield shift compared to the *meta*-substituted phenyl. Introduction of a second group in the *ortho* position as in 2,6-xylyl$_2$SiCl$_2$ (**11**) and mesityl$_2$SiCl$_2$ or 9-anthracenyl$_2$SiCl$_2$ (**10**) leads to increased shielding towards silicon, expressed by a notably high field shift.

Table 8 shows the obtained experimental and calculated ^{29}Si-NMR shifts for organo trichlorosilanes (RSiCl$_3$) and triorgano chlorosilanes (R$_3$SiCl). Again, benzylSiCl$_3$ (**14**) shows the largest low field shift. All other compounds exhibit a shift in the range of -0.4 to -1.1 ppm. The influence of the substituent on the ^{29}Si-NMR shift for organo trichlorosilanes is not as distinctive as for diorgano dichlorosilanes, due to a higher availability of space around the silicon atom, which allows an unhindered arrangement of the substituent. Triaryl chlorosilanes (R$_3$SiCl) exhibit a shift in the range of 1.2 to 4.58 ppm.

Table 8: Experimental and M06L/Iglo-II calculated ^{29}Si-NMR shifts of organo trichlorosilanes and tri organo chlorosilanes in C_6D_6. C.No.: Compound number (see 4); calc = calculated; exp = experimental.

RSiCl$_3$ R=	C. No.	δ ^{29}Si$_{exp}$ [ppm]	δ ^{29}Si$_{calc}$ [ppm]
phenyl	-	-0.8	9.3
benzyl	(**14**)	7.66	17.8
p-tolyl	(**13**)	-0.52	9.4
o-tolyl[30]	-	-0.72	9.2
1-naphthyl	(**15**)	-1.1	10.1
2,4-xylyl	(**12**)	-0.432	9.4
2-naphthyl[30]	-	-0.93	8.4
R$_3$SiCl			
phenyl	-	1.2	2.5
p-tolyl	(**17**)	2.9	2.5
p-biphenyl	(**19**)	2.33	2.0
2,4-xylyl	(**18**)	4.58	-0.3
1-naphthyl	(**16**)	4.0	3.4

A typical feature of silicon chemical shifts is the so called “sagging behavior” upon successive exchange of substituents on the silicon, which results in a bell shape curve if the R group is substituted by chlorine in a stepwise fashion. ^{29}Si-NMR Shifts are located on the bell shaped curve if plotted against the sum of electronegativities of the substituents of the silicon. In case of aryl substituted silanes, only the phenyl substituted compounds have been studied so far.[110] Figure 35 shows the obtained chemical ^{29}Si-

NMR shifts for 1-naphthyl, *p*-tolyl and 2,4-xylyl substituted chlorosilanes plotted against the sum of electronegativities of the ligand. For simplification, the values for phenyl were used due to a lack of data, concerning electronegativities of aryl substituents. This approach is appropriate, since it was stated that group electronegativity is mainly due to the contribution of the first atom which links the group to the remainder of the molecule and only to a small extend from the contribution of the residual atoms of the group. The used values were calculated using the method of Huheey.[111,112] Since no literature about the successful formation of a sterically hindered tetraarylsilane with a group bearing a substituent in *ortho* position is available, the ^{29}Si-NMR shift of 1-naphthyl$_3$phenylSi was used as value for the tetrasubstituted compound. This compound was prepared by the addition of phenylithium to 1-naphthyl$_3$SiCl. In addition, the shift of Ph$_4$Si was used due to the lack of data concerning *p*-tolyl$_4$Si.

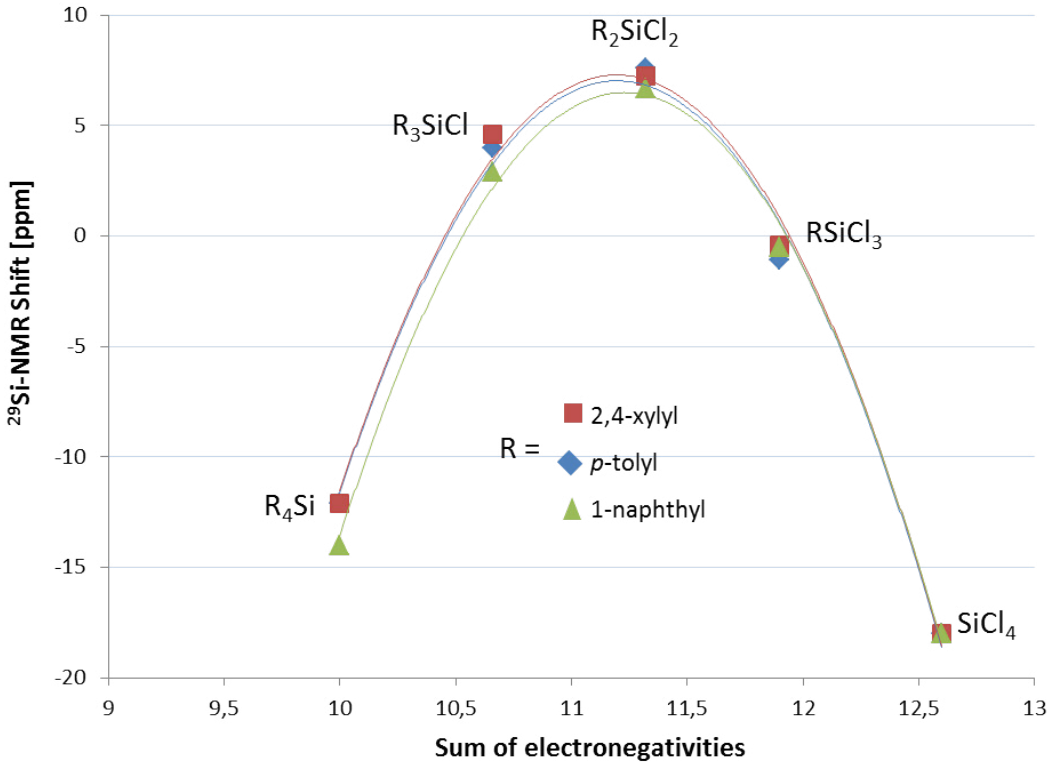

Figure 35: ^{29}Si-NMR chemical shifts of 1-naphthyl, *p*-tolyl and 2,4-xylyl substituted chlorosilanes plotted against the sum of electronegativity

All presented compounds can be located on a bell shaped curve, which is in agreement with literature. The appearance of the curve is connected to the shielding of the silicon atom. For a more detailed discussion see Ernst *et al.* [113]

The DFT calculated ^{29}Si-NMR chemical shifts of diorgano dichlorosilanes are all only +2 ppm to +5.4 ppm higher than the observed peaks (see Table 7). This agreement be-

tween measured and DFT calculated ^{29}Si-NMR chemical shifts is remarkably good with the maximum deviation of +5.4 ppm in the case of the 9-anthracenyl substituted compound **10**. The calculated ^{29}Si-NMR chemical shifts of organo trichlorosilanes show a deviation of 9.3 ppm to 10.0 ppm, which is somewhat higher than the one observed for the corresponding dichloro-species. In case of the monochlorinated compounds, the calculated values are as well in exceptional good agreement to the experimental obtained data.

The DFT calculations demonstrate that by a stepwise substitution of chlorine by an organic substituent the deviation decreases. This finding can be explained by the specifications of the used basic set, in which halogen atoms can not be described accurately due to relativistic effects. This characteristic increases with the atomic number and would lead to an even larger deviation for heavier halogens such as bromine. Additionally, the possibility of interactions of the chlorine atoms with solvent molecules has to be considered. DFT-calculations display single molecules in gas phase, without interactions. The more chlorine atoms present in the structure, the more interactions with the solvent are possible, which leads to a larger deviation between experimental and calculated values.

Table 9 shows the obtained experimental ^{29}Si-NMR shifts for arylsilanes R_2SiH_2. Benzyl$_2$SiH$_2$ (**20**) exhibits the highest low field shift in the row of presented compounds followed by the cyclopentadienyl-like fluorenyl$_2$SiH$_2$ (**21**)**.** As expected, when silicon is bonded to a sp^2 hybridized carbon these are shifted to higher fields compared to usual silicon organic variety with sp^3 hybridized carbon. Phenyl$_2$SiH$_2$ as well as its *para*-substituted analogs show a silicon shift around -33 ppm. Comparing *para* and *meta* substitution on the aromatic ring no trend on the shift or the coupling constant can be observed. The *ortho* substituted ring *s*hows a slight downfield shift which could be caused by an increase of shielding towards the silicon atom. 1-Naphthyl$_2$SiH$_2$ (**25**) with only one proton in β-position of the rather flat naphthyl group shows a slightly downfield shift compared to the phenyl derivatives with substituent in *para* position. Unexpectedly, *p*-*n*-butylphenyl$_2$SiH$_2$ (**23**) shows a slight downfield shift compared to the substituted phenyl compounds. Introduction of a second group in the *ortho* position like in 2,6-xylyl$_2$SiH$_2$ (**28**) and mesityl$_2$SiH$_2$ leads to a notably shielding effect and therefore to a high field shift.

Table 9: Experimental and B3LYP/Iglo-II calculated ^{29}Si-NMR shifts of diorgano silanes in C_6D_6. C.No.: Compound number (see 4); calc = calculated; exp = experimental.

R_2SiH_2 R=	C. No.	δ $^{29}Si_{exp}$ [ppm]	δ [ppm]	$^1J(^1H\text{-}^{29}Si)_{exp}$ [Hz]	$^1J(^1H\text{-}^{29}Si)_{calc}$ [Hz]
benzyl	(**20**)	-24.3	-25.4	196.5	-187.4
fluorenyl	(**21**)	-17.3	-20.8	208	-199.2
phenyl	-	-34.1[114]	-36.9	198.3	-187.6
p-tolyl	(**34**)	-33.6	-37.5	197.9	-186.4
m-tolyl	(**22**)	-33.5	-36.5	197.3	-186.4
3,5-xylyl [1]	-	-33.2[115]	-36.3	not reported	-185.9
o-tolyl	(**35**)	-34.2	-35.4	197.6	-186.4
p-*n*-butylphenyl	(**23**)	-38.8	-38.0	196.6	-186.3
p-biphenyl	(**24**)	-33.9	-37.2	198.8	-187.8
1-naphthyl	(**25**)	-39.3	-30.0	199.5	-190.2
2,4-xylyl	(**26**)	-40.4	-36.1	195.4	-185.4
9-anthracenyl	(**27**)	-61.4	-70.9	202.1	-190.3
2,6-xylyl	(**28**)	-62.2	-70.6	196.5	-186.1
mesityl	-	-62.1[3]	-70.9	not reported	-185.2

The same trend is as well observed for 9-anthracenyl$_2$SiH$_2$ (**27**), which may be attributed to the sterical demand of the substituent despite its rather flat molecular geometry. Due to only small differences in the value of the coupling constants ranging from 195.4 Hz for 2,4-xylyl$_2$SiH$_2$ (**26**) to 208 Hz for fluorenyl$_2$SiH$_2$ (**21**), no clear trend can be observed for the different substituents.

For R_2SiH_2, the obtained data shows that the increasing steric demand of the substituent in *ortho* position leads to a ^{29}Si-NMR high-field shift caused by shielding effects towards the silicon atom (see Figure 36). The same trend is observed for R_2SiCl_2.

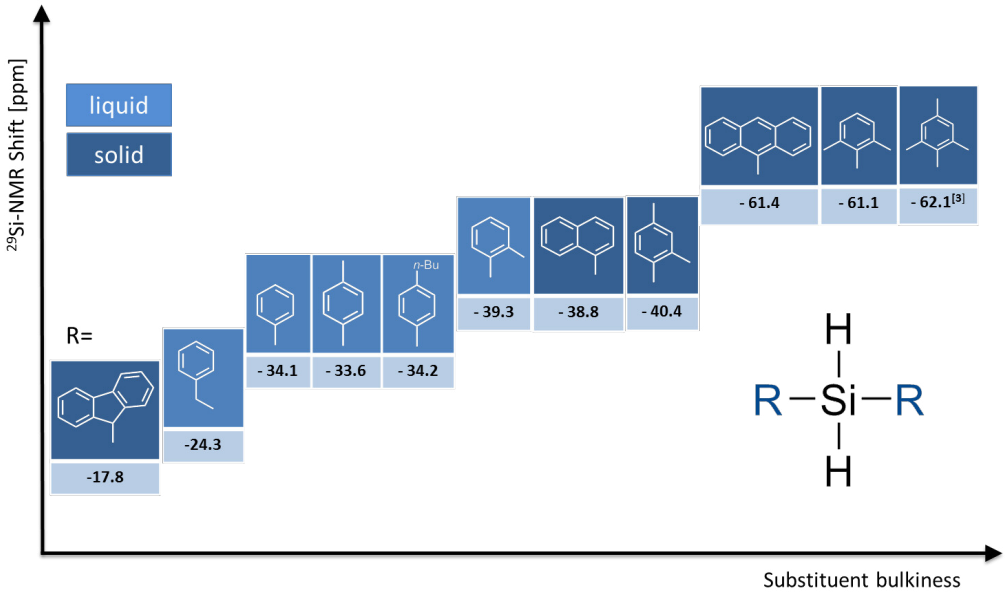

Figure 36: ^{29}Si-NMR shifts in dependency of the substituent bulkiness

The DFT calculated ^{29}Si-NMR chemical shifts for dihydrides differ from the experimentally obtained ones with a deviation of 0.8 to 9.5 ppm (Figure 37). This agreement between measured and DFT calculated ^{29}Si-NMR chemical shifts is exceptionally good with the maximum deviation of +9.5 ppm in the case of the 9-anthracenyl substituted compound **27**. The calculated coupling constant fits very well to the experimental data with a mean deviation of 10.4 Hz (Figure 38).

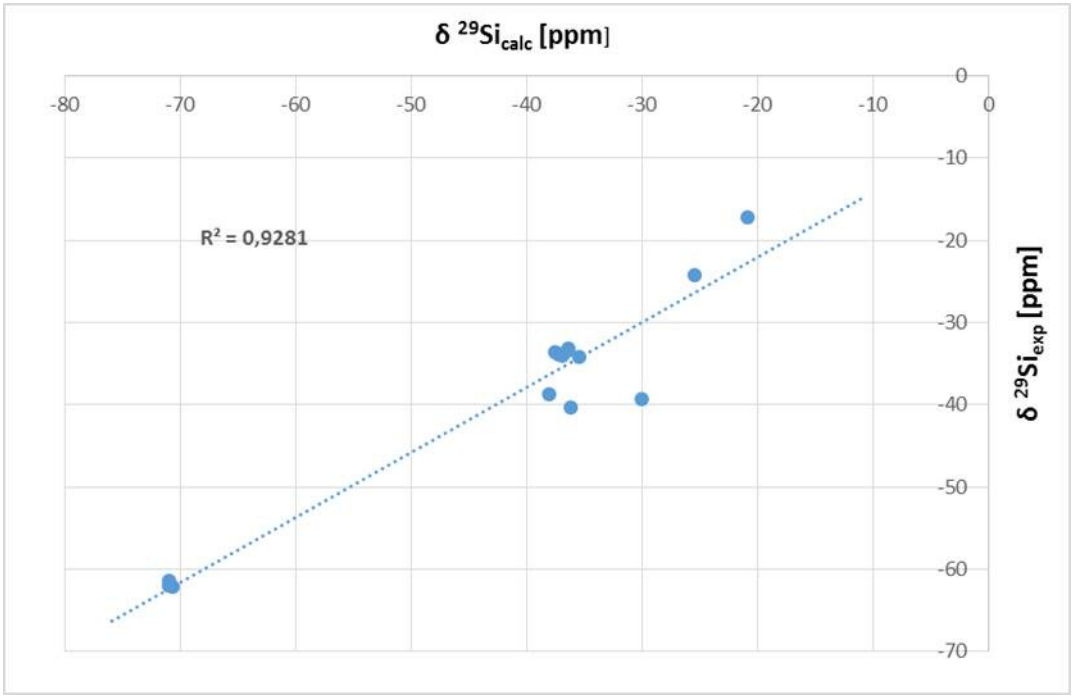

Figure 37: Comparison of the $^{29}Si_{exp}$ and $^{29}Si_{calc}$ shifts for R_2SiH_2

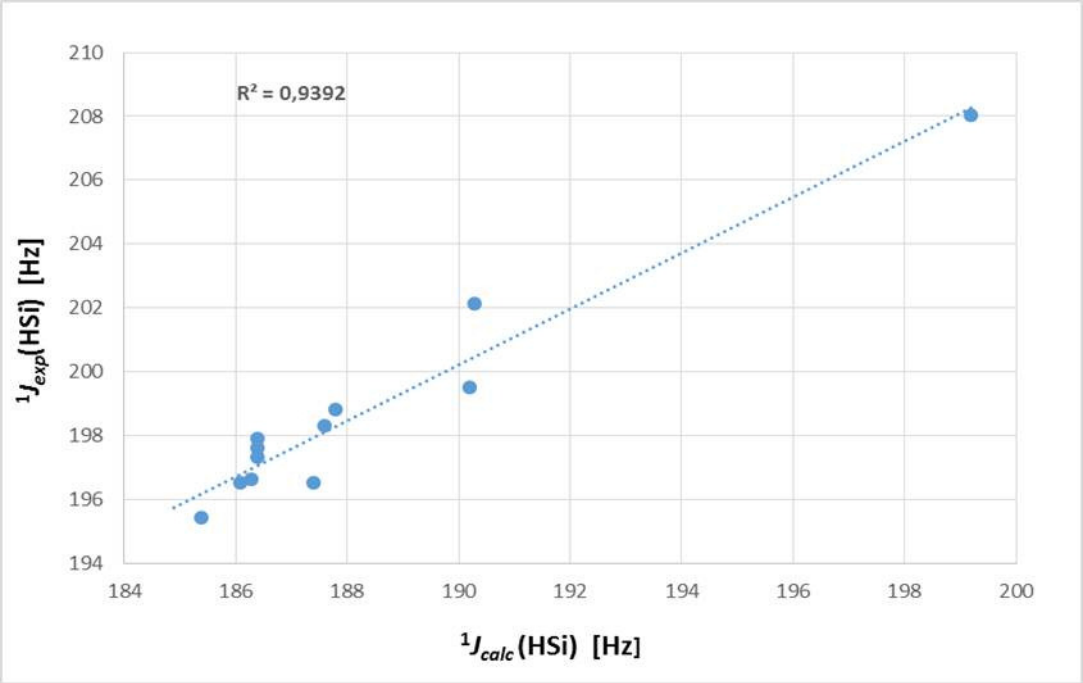

Figure 38: Comparison of $^1J_{exp}$(HSi) and $^1J_{calc}$(HSi) shifts for R_2SiH_2

Table 10 shows the obtained experimental and calculated ^{29}Si-NMR shifts for organo silanes $RSiH_3$ and R_3SiH. The increasing steric demand of the substituent in *ortho* position leads to a ^{29}Si-NMR high-field shift caused by shielding effects towards the silicon atom. DFT-calculations show a deviation of 6.5-10.46 ppm in case of $RSiH_3$, and 0.6 ppm in case of R_3SiH. These values are in exceptional good agreement to the experimental obtained data.

Table 10: Experimental and B3LYP/Iglo-II calculated ^{29}Si-NMR shifts of organo silanes $RSiH_3$ and R_3SiH in C_6D_6. C.No.: Compound number (see 4); calc = calculated; exp = experimental.

$RSiH_3$ R=	C. No.	$\delta\,^{29}Si_{exp}$ [ppm]	$\delta\,^{29}Si_{calc}$ [ppm]	$^1J(^1H\text{-}^{29}Si)_{exp}$ [Hz]	$^1J(^1H\text{-}^{29}Si)_{calc}$ [Hz]
benzyl	(**32**)	-55.4	-61.9	199.3	192.0
phenyl	-	-60.5	-68.8	201.0	189.3
p-tolyl	(**31**)	-60.9	-69.4	197.9	188.6
1-naphthyl	(**30**)	-62.8	-69.1	200.7	189.2
2,4-xylyl	(**29**)	-63.9	-72.0	197.8	191.8
R_3SiH					
phenyl[116]	-	-17.7	-23.3	200	189
1-naphthyl	(**33**)	-29.0	-	195.4	-

3.4 Thermolysis

The formation of silicon, Si(SiO_2) and $Si_xC_yO_z$ from organosilanes *via* thermolysis under inert gas conditions was investigated. In the tube furnaces, a continuous argon flow was applied during the experiments. In case of the Anton Paar DHS 1100 the reaction chamber was held under slight over pressure of the inert gas. The goal was to efficiently remove carbon from the obtained particles or layers. Therefore silanes with aromatic substituents, which could act as leaving groups *via* breaking of the Si-C bond, were chosen.

SEM and EDX measurements were performed on the obtained thermolyzed samples. Si_5Ph_{10} (**36**), 1-naphthyl$_2SiH_2$ (**25**) and 9-anthracenyl$_2SiH_2$ (**27**) were regarded as the most promising candidates, due to their high melting point and were additionally analyzed *via* thermogravimetric analysis (TGA) in combination with differential scanning calorimetry (DSC) and coupled mass spectroscopy (MS).

The given values for EDX measurements have to be considered in a qualitative rather than quantitative way. The carbon content can only be reported with a high uncertainty of measurement. This results from the low atomic number of carbon (accuracy increases with Z) and the possibility of the existence of residual hydrocarbon species in the measurement chamber, which influences the resulting data. Nevertheless trends in the carbon value as well its absence can be reported with a certain accuracy.

Substrates

Samples were prepared on stainless steel, platinum and in most cases molybdenum foil. Steel and platinum were rinsed with isopropanol and dried in a nitrogen stream prior to use. The molybdenum foil was polished to reduce the oxygen content and thereby the probability of a reaction of the surface oxygen with silicon formed during thermolysis. Figure 39 shows a cross section of the molybdenum foil. In “Spektrum 1” and “Spektrum 2“ no oxygen was observed. About 25-30% oxygen content were detected in “Spektrum 3” and “Spektrum 5”.

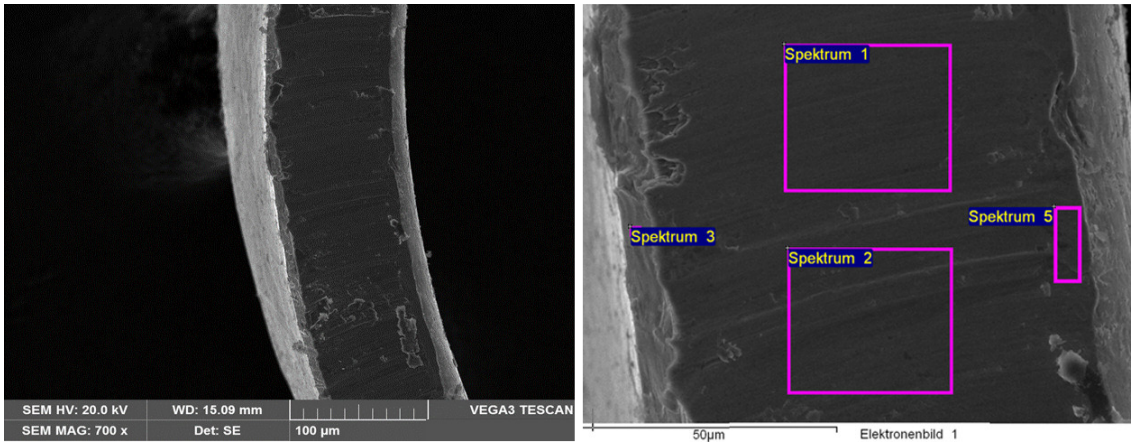

Figure 39: Cross section of molybdenum foil (left); spectra analyzed *via* EDX (right)

Figure 40 shows the unpolished surface with an oxygen content of about 24%. Polishing with glass wool reduces this content to about 21%. Polishing with sandpaper (1200) led to about 17%. A further reduction of the oxygen content was not possible with the given methods. Due to the easy preparation, it was decided to use glass wool polished molybdenum foils for all experiments.

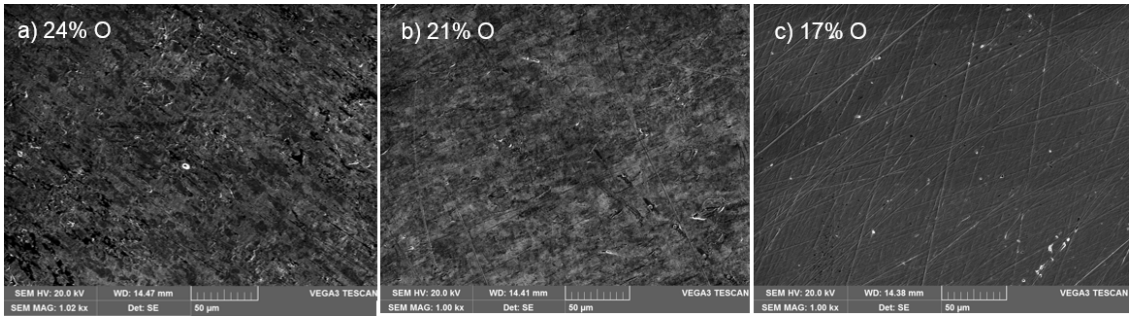

Figure 40: Molybdenum foil; a) unpolished; b) polished with glass wool; c) polished with sandpaper

3.4.1 TGA/DSC/MS

The most promising silanes Si_5Ph_{10} (**36**), 1-naphthyl$_2$SiH$_2$ (**25**) and 9-anthracenyl$_2$SiH$_2$ (**27**) (Figure 41) were analyzed *via* thermogravimetric analysis (TGA) in combination with differential scanning calorimetry (DSC) and coupled mass spectroscopy (MS).

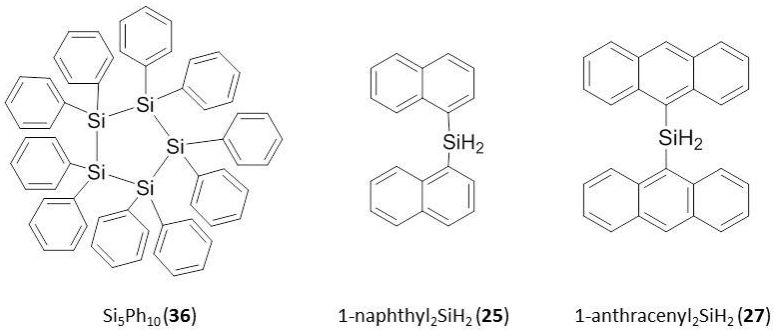

Figure 41: Organo silanes analyzed *via* TGA/DSC/MS

Approximately 10 mg of the silane were heated to 1000 °C in helium atmosphere with a rate of 10 K/min. The observed melting and decomposition, in combination with mass analysis allow conclusions about the reaction behavior during thermolysis. Table 11 shows the elemental composition of compound **25**, **27** and **36**.

Table 11: Elemental composition of Si_5Ph_{10} (36), 1-naphthyl$_2SiH_2$ (25) and 9-anthracenyl$_2SiH_2$ (27)

	Si_5Ph_{10} (36) M_W=911.5 g/mol	**1-naphthyl$_2SiH_2$ (25)** M_W=284.1 g/mol	**9-anthracenyl$_2SiH_2$ (27)** M_W= 384.6 g/mol
Element	**%**	**%**	**%**
Si	15.4	9.9	7.3
C	79.1	84.5	87.5
H	5.5	5.7	5.2

Si_5Ph_{10} (36): The thermolytic decomposition of Si_5Ph_{10} was already described detailed in an earlier study of our working group.[117] The TGA/DSC measurement shows an initial mass increase that results from the condensation of residual moisture in the measuring instrument (Figure 42). The actual mass loss step is located between 283 °C and 541 °C with a decrease in mass of 87.1%. It is derived from the decomposition (possibly at the beginning with superimposed melting peak) of the sample. Assuming that all 10 phenyl (C_6H_5) substituents are released during thermolysis, this would correspond to a weight loss of 84.6%, which is in the range of the observed value.

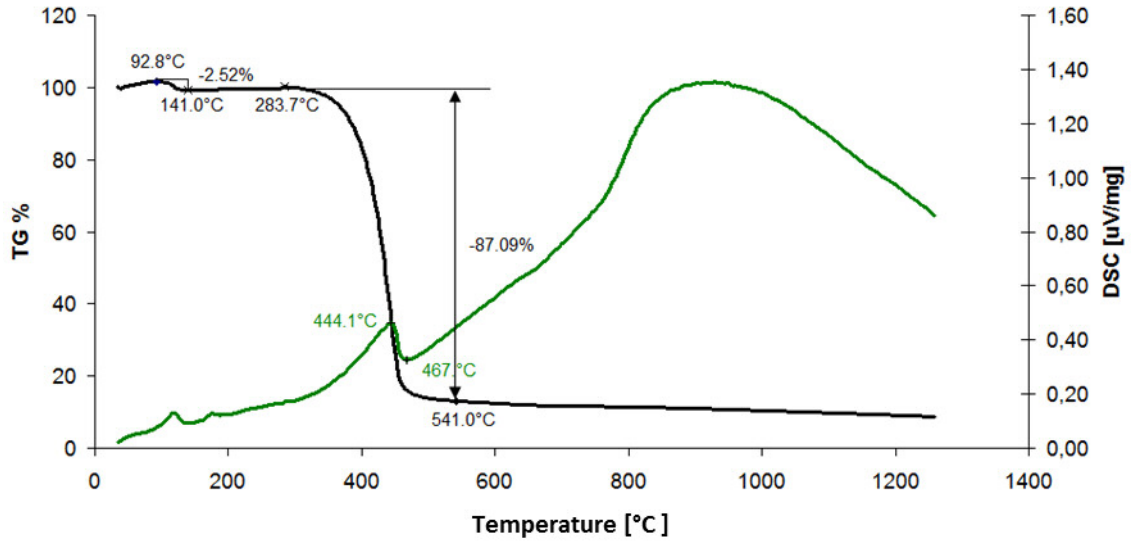

Figure 42: TGA/DSC of Si_5Ph_{10} (36); helium atmosphere; heating to 1000 °C

Subsequent to the mass loss step, with a short delay time, due to the measurement setup of the coupled mass spectrometer, an increase of carbon containing fragments

can be observed (Figure 43). Values for carbon [12] and CO_2 [44] (formed with residual oxygen) show a parallel run and serve as control for one another.

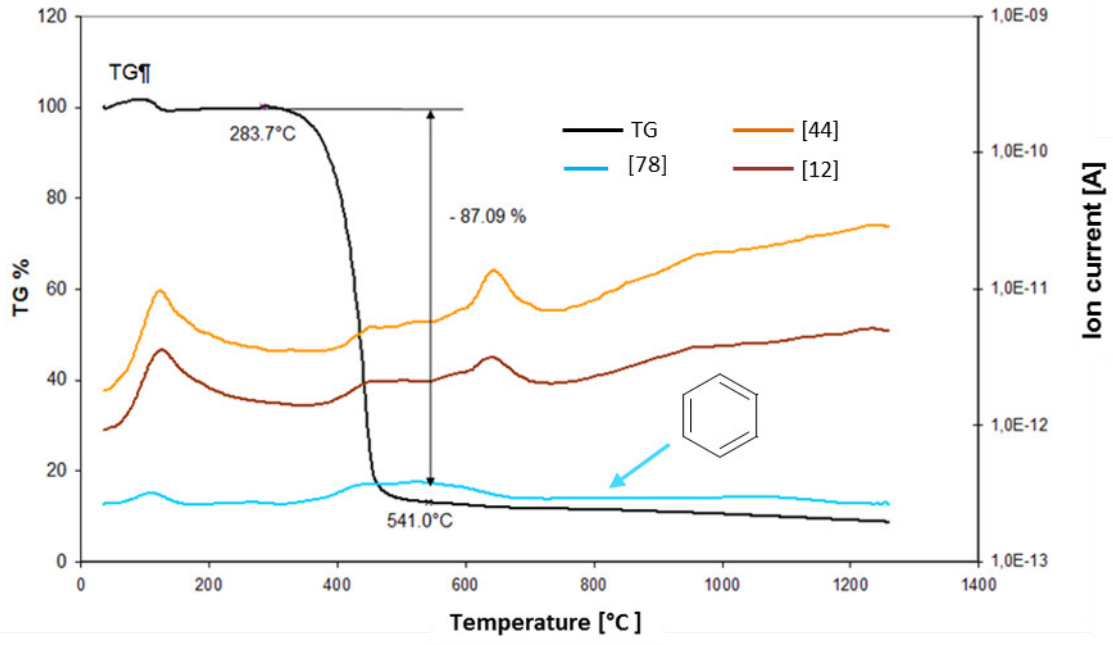

Figure 43: TGA/MS of Si_5Ph_{10} (36); helium atmosphere; heating to 1000 °C

Phenyl and its fragments with m/z values of 78, 63, 51, 39 and 26,[118] as well as products from the phenyl radicals such as biphenyl can be detected in low quantities *via* coupled MS-analysis. This finding suggests that a cleavage of phenyl groups takes place but only to a small amount. The TGA/DSC data file containing all detected mass fragments can be found in the Appendix.

1-naphthyl$_2$SiH$_2$ (25): The TGA/DSC measurement shows an endothermic peak at about 117 °C, which is related to the melting of the sample (Figure 44). The narrow and sharp appearance of this peak is a sign for the high purity of the silane. The melting point observed in the TGA/DSC measurement is notably higher than the value reported under air (98-99 °C). This increase results from the change to a helium atmosphere and is a commonly observed trend in TGA/DSC analysis. The decomposition reaction is located between 265 °C and 341 °C with a decrease in mass of 77.1%. At 297 °C the highest reaction speed (in combination with mass loss) is observed (see Appendix). After the main decomposition step additional weight loss of the sample takes place, until a temperature of about 650 °C. An overall decrease in mass of 93.2% observed. Assuming the cleavage of the two naphthyl substituents ($C_{10}H_7$) during thermolysis,

this would correspond to a weight loss of about 90.1%, which is in the range of the observed value.

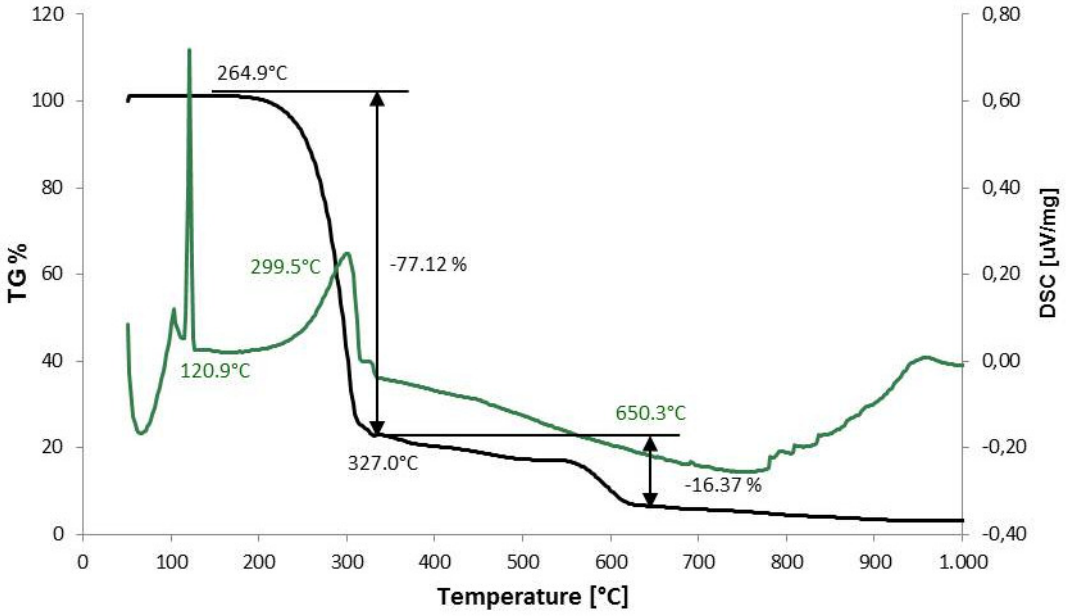

Figure 44: TGA/DSC of 1-naphthyl$_2$SiH$_2$ (25); helium atmosphere; heating to 1000 °C

Subsequent to the mass loss step an increase of carbon containing fragments can be observed (Figure 45). The naphthyl group with an m/z of 128 as well as its fragments at 102, 77, 75, 64, 51 and 39 m/z can be observed in the mass analysis.[118]

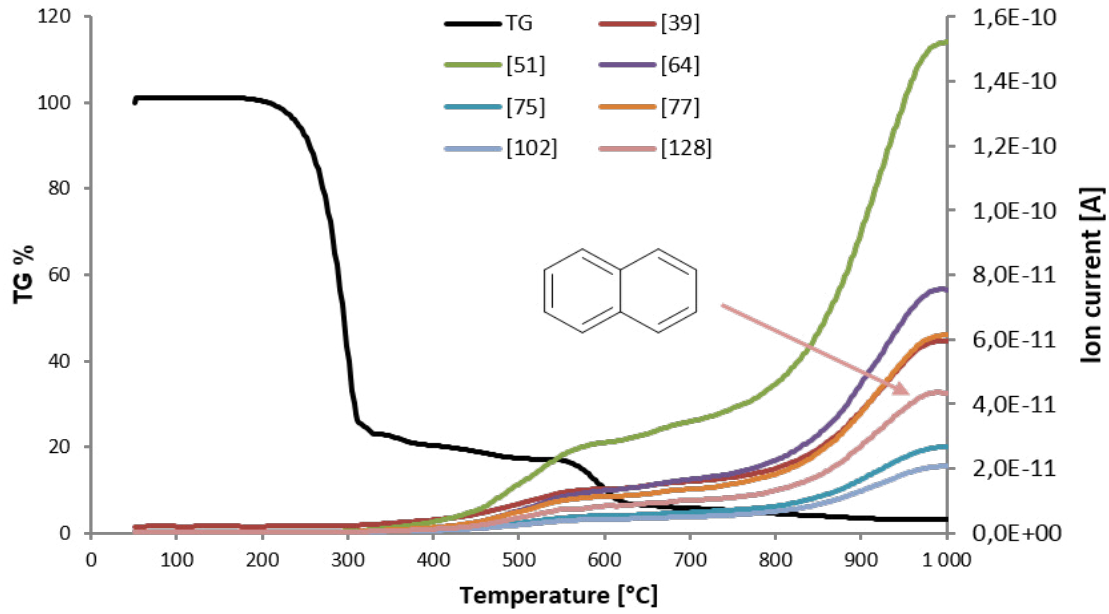

Figure 45: TGA/MS of 1-naphthyl$_2$SiH$_2$ (25); helium atmosphere; heating to 1000 °C

The observed naphthalene is most likely derived from the decomposition, but might as well be formed from reaction products.

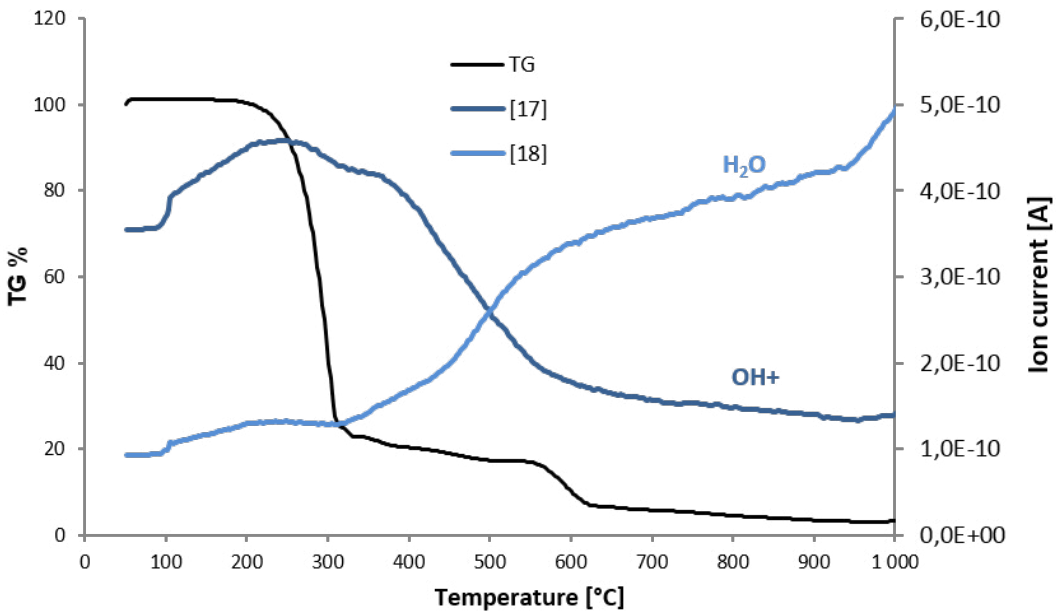

Figure 46: TGA/MS of 1-naphthyl$_2$SiH$_2$ (25); H_2O, OH+; helium atmosphere; heating to 1000 °C

Traces of water can be detected in the MS due to condensation of residual moisture in the measuring instrument. Typically, the [OH+] and [H_2O] line show a parallel run and serve as control for one another (since OH+ is a fragment of H_2O). In the MS analysis of 1-naphthyl$_2$SiH$_2$, an increase of H_2O and a decrease of OH+, simultaneously to the decomposition step, is observed (Figure 46). This behavior is in most cases a sign that hydrogen (H+) is evolved from the sample which reacts with OH+ to form H_2O. The TGA/DSC data file containing all detected mass fragments can be found in the Appendix.

In summary, the TGA/DSC/MS analysis of 1-naphthyl$_2$SiH$_2$ shows with high possibility the cleavage of naphthyl groups as well as the formation of hydrogen.

9-anthracenyl$_2$SiH$_2$ (27): The TGA/DSC measurement shows an endothermic peak at about 220 °C, which is related to the melting of the sample (mp_{Air}=200-202 °C). The decomposition reaction is located between 237 °C and 609 °C with a decrease in mass of 79.5% (Figure 47). At 368 °C the highest reaction speed (in combination with mass loss) is observed (see Appendix). An additional weight loss of the sample takes place, until a temperature of about 1000 °C. An overall decrease in mass of 88% observed. Assuming the cleavage of the two anthracenyl substituents ($C_{14}H_9$) during thermolysis, this would correspond to a weight loss of about 92%, which is in the range of the observed value.

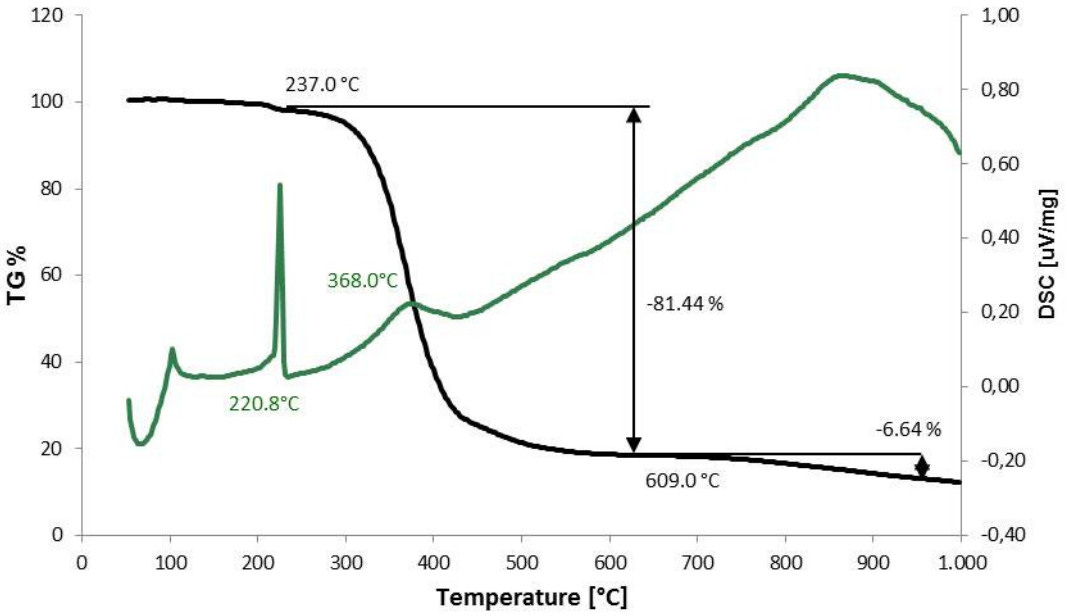

Figure 47: TGA/DSC of 9-anthracenyl$_2$SiH$_2$ (27); helium atmosphere; heating to 1000 °C

Subsequent to the mass loss step an increase of carbon containing fragments can be observed (Figure 48). The anthracenyl group with an m/z of 178 can not be detected directly due to limitations of the coupled MS concerning m/z values >130.

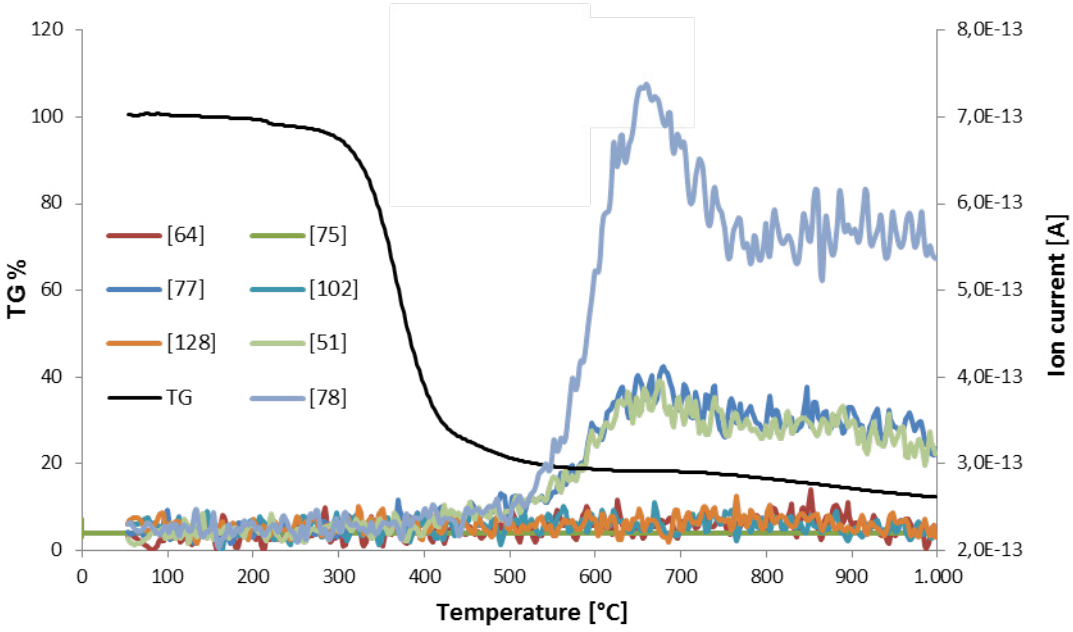

Figure 48: TGA/MS of 9-anthracenyl$_2$SiH$_2$ (27); helium atmosphere; heating to 1000 °C

Fragments of the anthracenyl group at 128, 102, 77, 75, 64 and 51 m/z can be observed in the mass analysis.[118] All mass fragments can be detected in low amounts with a high background noise level. This might be caused by clogging of the capillary which is located in front of the MS. In the case of 9-anthracenyl$_2$SiH$_2$ (**27**) a decrease in the OH+ value was not observed in the same amount as in 1-naphthyl$_2$SiH$_2$ (**25**). The

TGA/DSC data file containing all detected mass fragments can be found in the Appendix**.**

In summary, the TGA/DSC/MS analysis of 9-anthracenyl$_2$SiH$_2$ (**27**) shows the formation of mass fragments of the anthracenyl group, but an uncertainty of measurement remains due to the high noise level caused by difficulties in the detection of fragments of higher m/z values.

The temperature of thermolysis of the organo silanes was chosen in accordance to the TGA data, to ensure that the end temperature is higher than the one observed for-decomposition.

3.4.2 Characterization of thermolysis products

Organo silanes Si$_5$Ph$_{10}$ (**36**), 1-naphthyl$_2$SiH$_2$ (**25**), 9-anthracenyl$_2$SiH$_2$ (**27**), benzyl$_2$SiH$_2$ (**20**), *p*-tolyl$_2$SiH$_2$ (**34**), *p*-butylphenyl$_2$SiH$_2$ (**23**) and 1-naphthylSiH$_3$ (**30**) were thermolyzed with varying reaction parameters, using a Carbolite single zone horizontal tube furnace GHA 12/600, a Carbolite horizontal tube furnace HZS 12/200/1200 and an Anton Paar Domed Hot Stage DHS 1100. The samples were prepared as loose powders and as layers on different substrates. For experimental details see section 4.7.

3.4.2.1 Powder samples

This section gives a short overview about thermolyzed powder samples of Si$_5$Ph$_{10}$ (**36**). A detailed description was done in an earlier study of our working group.[117] Si$_5$Ph$_{10}$ was thermolyzed in a ceramic sample holder (using a Carbolite single zone horizontal tube furnace GHA 12/600) and the resulting glass like solid analyzed *via* SEM/EDX and elemental analysis.

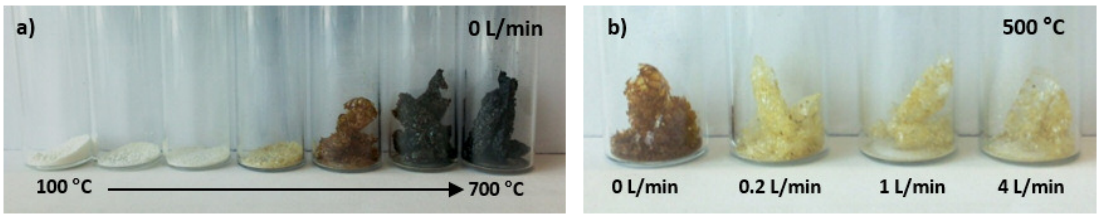

Figure 49: Resulting powders from thermolysis of Si$_5$Ph$_{10}$ (36); a) 0 L/min Ar; 100 °C -700 °C; (right) 500 °C 0-4 L/min gas flow

During the experiments reaction parameters were varied (Figure 49). Especially the gas flow rate showed an influence on the obtained products. The sample with 0 L/min gas flow showed a different appearance in all experiments (Figure 49). This might be

caused by less removal of reaction gases and a higher temperature (gas flow slightly cools the sample). In the elemental analysis the sample with 0 L/min gas flow and a thermolysis temperature of 500 °C shows the best elemental distribution, with a carbon content of about 60% and 33% silicon, which is the highest obtained value for this test setting.

a)

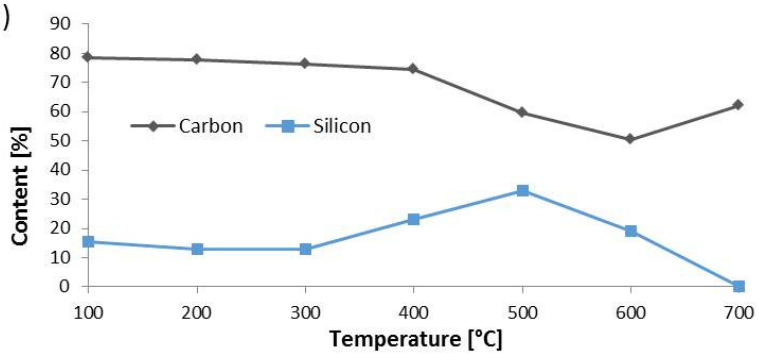

b)

V_{Gas} [L/min]	Carbon [%]	Silicon [%]
4	69.4	24
1	68.9	24
0.2	68.7	24
0	59.6	33

Figure 50: Si- and C-content of Si_5Ph_{10} (36) thermolysis at a) 100-700 °C with 0 L/min gas flow (=V_{Gas}) and b) 0-4 L/min gas flow at 500 °C

A special behavior was observed for the sample at 700 °C with 0 L/min gas flow. No silicon could be detected in the resulting powder sample, but in the gas stream spherical, orange-brown particles were obtained (Figure 51), which differ notably from the appearance of the thermolyzed, residual glass like powder samples (Figure 52).

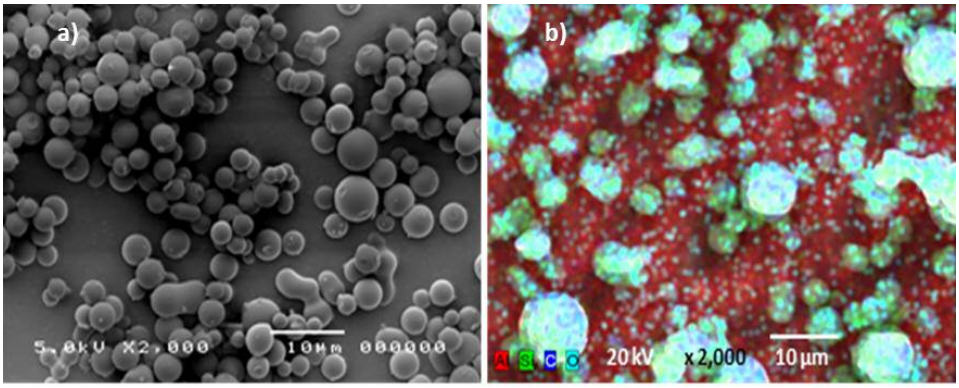

Figure 51: Spherical particles obtained from thermolysis of Si_5Ph_{10} (36) at 700 °C / 0 L/min; a) SEM image; b) elemental mapping on aluminum foil

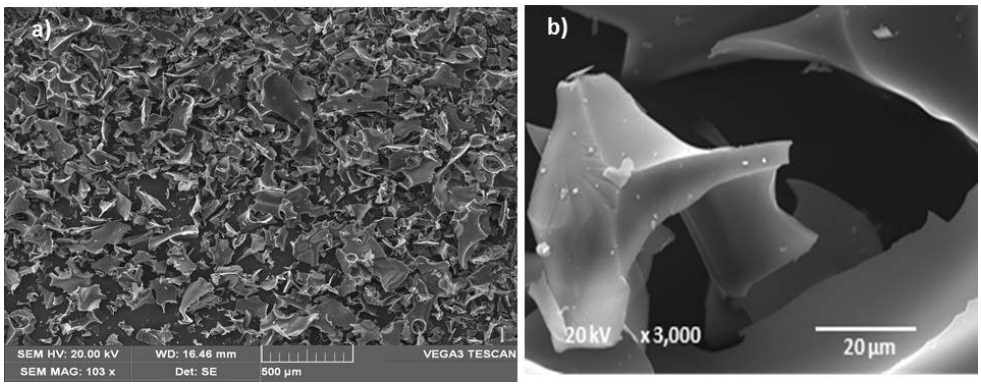

Figure 52: Thermolyzed powder samples of Si_5Ph_{10} (36); a) magnification 100x; b) magnification 3000x

Only a small amount of the spherical particles could be obtained. EDX analysis show that the particles mainly consist of silicon and oxygen. It seems that due to very fast heating, a release of small silicon particles takes place. This finding is supported by the absence of silicon in the residual powder. A similar formation of Si nanoparticles was already observed for the reaction of phenylsilane under certain reaction conditions.[48]

In conclusion the formation of silicon from Si_5Ph_{10} seems to be possible at high temperatures with very fast heating. But only very small amounts of the silicon particles can be obtained. This results from the low silicon content of the precursor (15.4%). In a typical experiment, using 0.2 g Si_5Ph_{10}, a maximum of 30 mg silicon can be formed. Lower temperatures led to a silicon content of up to 33%. Nevertheless powders with a higher carbon content may also show interesting properties for applications as in low *k* materials.[49]

3.4.2.2 Samples on substrates

Organo silanes Si_5Ph_{10} (**36**), 1-naphthyl$_2SiH_2$ (**25**), 9-anthracenyl$_2SiH_2$ (**27**), benzyl$_2SiH_2$ (**20**), *p*-tolyl$_2SiH_2$ (**34**), *p*-butylphenyl$_2SiH_2$ (**23**) and 1-naphthylSiH_3 (**30**) were thermolyzed with varying reaction parameters, using a Carbolite single zone horizontal tube furnace GHA 12/600, a Carbolite horizontal tube furnace HZS 12/200/1200 and an Anton Paar Domed Hot Stage DHS 1100. Samples were prepared on stainless steel, platinum and molybdenum foil.

GHA 12/600

Si_5Ph_{10} (**36**) and 1-naphthyl$_2SiH_2$ (**25**) were thermolyzed using a Carbolite single zone horizontal tube furnace GHA 12/600. For experimental details see Table 12.

Table 12: Experimental details for thermolysis of Si_5Ph_{10} (36) and 1-naphthyl$_2SiH_2$ (25) with GHA 12/600; Fe=stainless steel, Mo= molybdenum; heating rate = 5 °C/min

Sample No.	Silane	Method	Surface	T [°C]
OE 1	Si_5Ph_{10} (**36**)	THF solution	Fe	750
OE 2	1-naphthyl$_2SiH_2$ (**25**)	Toluene solution	Mo	450
OE 3	1-naphthyl$_2SiH_2$ (**25**)	Toluene solution	Mo	450
OE 4	1-naphthyl$_2SiH_2$ (**25**)	powder	Mo	450
OE 5	1-naphthyl$_2$SiH2 (**25**)	powder	Mo	450/700
OE 6	1-naphthyl$_2SiH_2$ (**25**)	melting	Mo	450/700

For experiment OE 1, thin films were prepared directly by applying the powdered silane on a stainless steel substrate. Figure 53 shows the obtained sample after thermolysis at 750 °C and 0.5 L/min gas flow, using a Carbolite single zone horizontal tube furnace GHA 12/600. The obtained layers are mainly homogeneous with fragmented sections (possibly due to the difference in heat expansion of sample and surface). A high silicon content is accompanied by an even higher carbon content. Similar to powder samples a release of the phenyl groups does not take place, preventing complete removal of carbon from the sample.

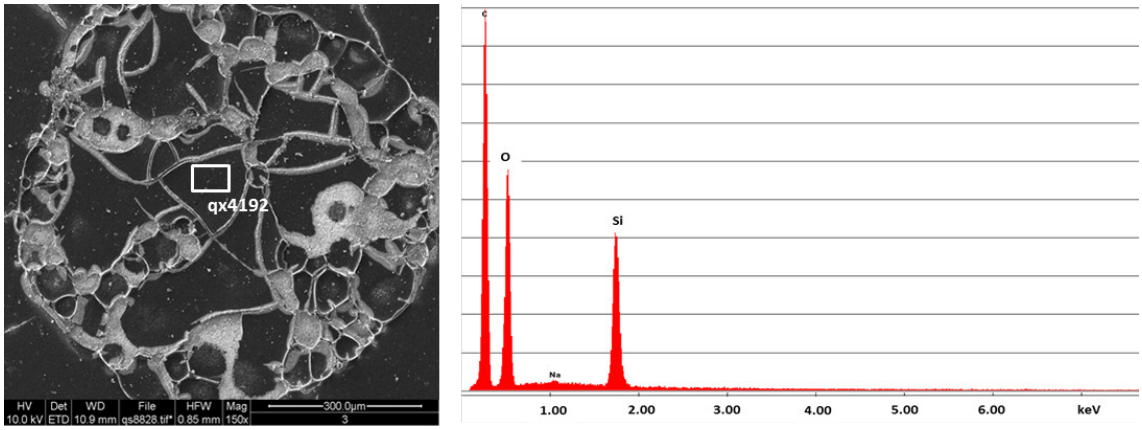

Figure 53: SEM/EDX measurement of OE 1[2]

For a more detailed description of the thermolysis of Si_5Ph_{10}, including additional substrates and reaction parameters see master thesis Binder.[117]

In experiment OF 2 and OF 3 a toluene solution of 1-naphthyl$_2SiH_2$ (**25**) was prepared and applied onto the surface until complete covering. In the case of OF 2 a more concentrated silane solution was used. The solvent was removed *in vacuo* and the samples

[2] measurement was performed at FELMI Graz

thermolyzed at 450 °C. The resulting surfaces are shown in Figure 54. For OE 2 structures are arranged from droplets of the solution. For the more diluted sample OE 3 only isolated particles can be observed.

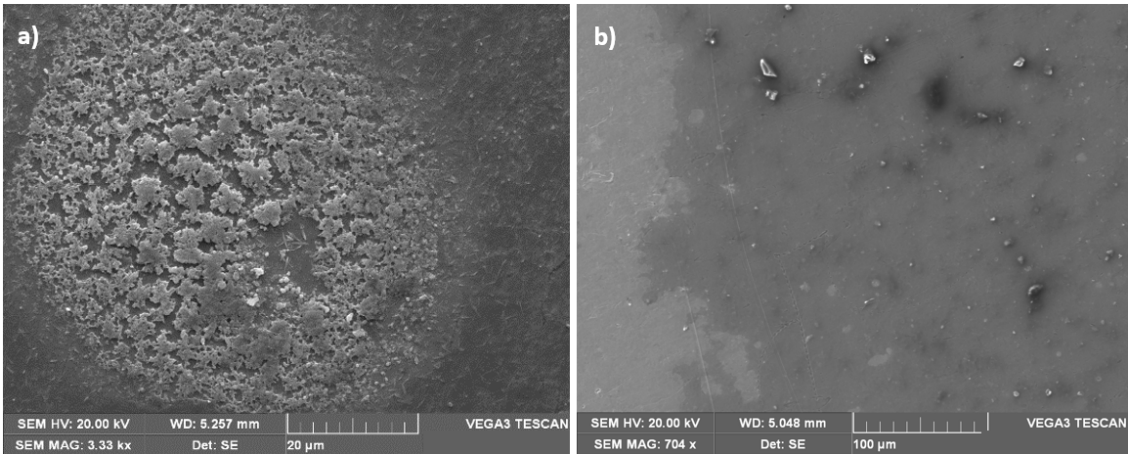

Figure 54: SEM image of a) OE 2; b) OE 3; after thermolysis at 450 °C

An EDX analysis, performed as elemental mapping, shows the composition of isolated particles of OE 2 (Figure 55). A silicon content of about 20% as well as a carbon content of 18% is observed. This distribution may result from an increased release of carbon containing fragments, compared to the thermolysis of Si_5Ph_{10} (**36**). This possible reaction behavior is supported by the TGA analysis, showing naphthalene fragments.

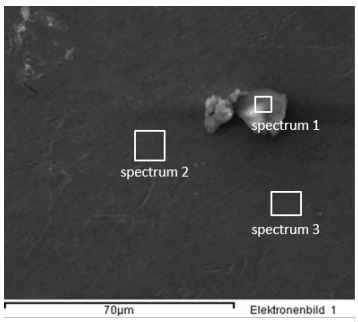

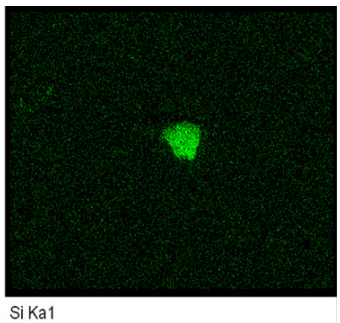

Element	spectrum 1 Atom%	spectrum 2 Atom%	spectrum 3 Atom%
O K	57.2	17.8	42.8
Si K	20.6	-	-
Mo L	4.0	82.2	57.2
C K	18.2	-	-

Figure 55: OE 2; SEM image and elemental mapping (EDX) of silicon

The elemental mapping of OF 3 shows similar values to OF 2 (Figure 56). Again a silicon content of about 20% and a carbon content of 16% is observed. For both experiments, a high oxygen content is present. This may result from residual oxygen in the gas stream. Furthermore, the samples are exposed to air before measurement, due to instrument set up. In addition, the oxygen value of the molybdenum surface varies notably. This might be caused by inhomogeneity of the polishing and therefore different oxidation behavior.

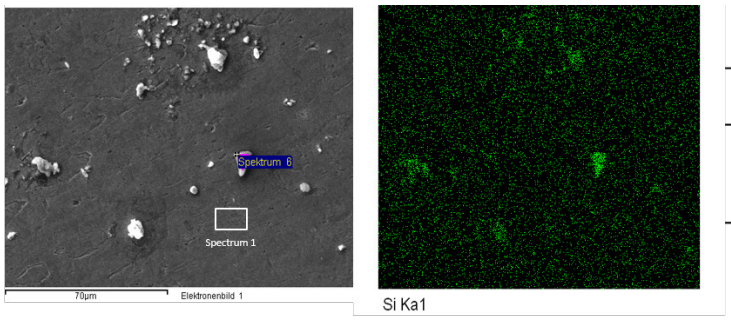

Element	spectrum 1 Atom%	"Spektrum 6" Atom%
O K	29.4	50.1
Si K	-	21.7
Mo L	70.6	12.7
C K	-	15.5

Figure 56: OE 3; SEM image and elemental mapping (EDX) of silicon

In experiment OF 4 and OF 5, powdered 1-naphthyl$_2$SiH$_2$ (**25**) was applied onto the molybdenum surface, resulting in a thick layer that was compressed slightly with a spatula. The resulting surfaces after thermolysis are shown in Figure 57. OE 4 shows a thin glass like layer with fragmented sections. A rather high carbon content (50%) is observed. This may be caused by hindered removal of reaction gases from more thick layers. For OF 5 a second heating step to 700 °C was introduced. The resulting surface shows dark, unordered particles with a high carbon content, similar to OF 4.

The usage of powder samples seemed to lead to an increase of the carbon content, therefore a sample preparation for more thin layers was tested.

In OE 6, single crystals of 1-naphthyl$_2$SiH$_2$ (**25**) were applied onto a molybdenum surface and heated until melting (100 °C). The liquid silanes was dispersed on the foil by tilting until a thin layer was obtained.

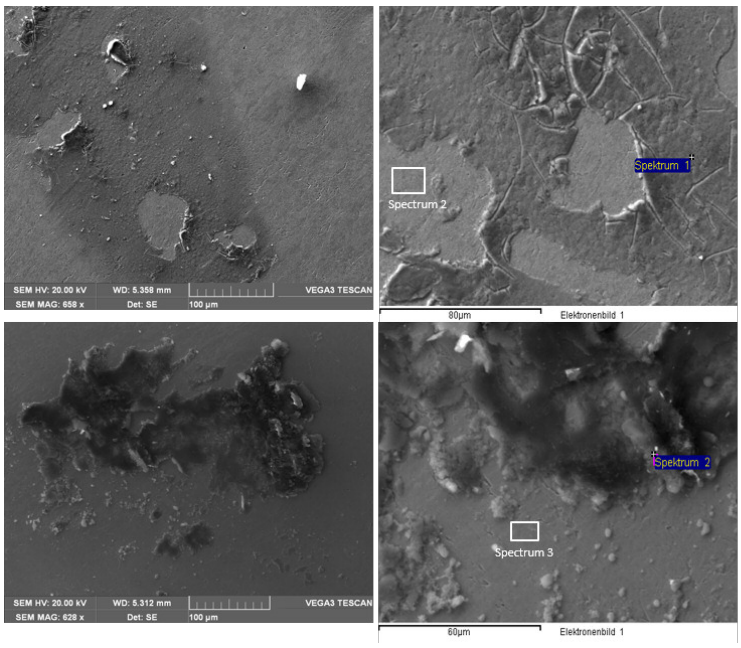

Element	"Spektrum 1" Atom%	spectrum 2 Atom%
O K	15.3	14.6
Si K	11.9	-
Mo L	21.6	85.4
C K	51.2	-

Element	"Spektrum 2" Atom%	Spectrum 3 Atom%
O K	29.6	22.7
Si K	6.8	-
Mo L	4.0	75.0
C K	59.6	2.3

Figure 57: SEM/EDX of OE 4 (top) and OE 5 (bottom)

OE 6 was thermolyzed in a two-step process (450/700 C °). SEM analysis shows rod like structures on the surface (Figure 58). The EDX analysis reveals a lower carbon content (10%) than for the powdered samples. Also in the mapping, the composition from mainly silicon (and oxygen) is apparent.

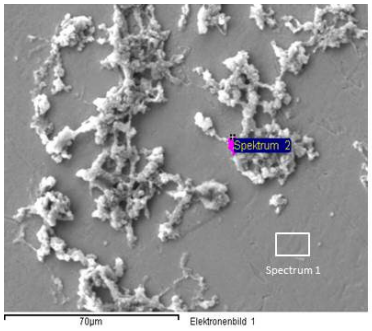

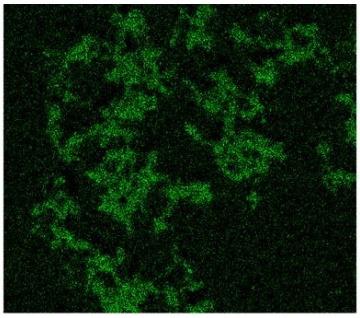

Element	Spectrum 1 Atom%	"Spektrum 2" Atom%
O K	23.1	65.2
Si K	-	12.4
Mo L	76.9	2.4
C K	-	10.1

Figure 58: OE 6; SEM image and elemental mapping (EDX) of silicon

A preferable thin layer of precursor in combination with a thermolysis at 700 °C gave the best results for the GHA 12/600. 1-naphthyl$_2$SiH$_2$ (**25**) allows for the formation of particles/layers with a notably lower carbon content than Si$_5$Ph$_{10}$ (**36**).

HZS 12/200/1200

1-naphthyl$_2$SiH$_2$ (**25**), 9-anthracenyl$_2$SiH$_2$ (**27**), benzyl$_2$SiH$_2$ (**20**), *p*-tolyl$_2$SiH$_2$ (**34**), *p*-*n*-butylphenyl$_2$SiH$_2$ (**23**) and 1-naphthylSiH$_3$ (**30**) were thermolyzed with a Carbolite horizontal tube furnace HZS 12/200/1200. For experimental details see Table 13**.**

Table 13: Experimental details for thermolysis of various silanes with GHA 12/600; Mo= molybdenum; heating rate = 10 °C/min

Sample No.	Silane	Method	Surface	T [°C]
OE 7	blank	-	Mo	450/700
OE 8	benzyl$_2$SiH$_2$ (**20**)	pure	Mo	450/700
OE 9	*p*-tolyl$_2$SiH$_2$ (**34**)	pure	Mo	450/700
OE 10	1-naphthylSiH$_3$ (**30**)	pure	Mo	450/700
OE 11	1-naphthyl$_2$SiH$_2$ (**25**)	melting	Mo	450/700
OE 12	9-anthracenyl$_2$SiH$_2$ (**27**)	toluene solution	Mo	450/700
OE 13	*p*-*n*-butylphenyl$_2$SiH$_2$ (**23**)	pure	Mo	450/700

Figure 59 shows the surface of the molybdenum blank after thermolysis up to 700 °C. EDX analysis suggests the oxidation of molybdenum, by forming small platelets, which grow from the surface. These structures were not observed in the experiments for the

GHA 12/600, which might be caused by the shorter reaction time or a lower oxygen content. The GHA 12/600 was evacuated prior to thermolysis, followed by flushing with argon. This procedure could not be applied for the HZS 12/200/1200. In this case, a purging of the working tube with nitrogen for 1 hour was performed prior to thermolysis.

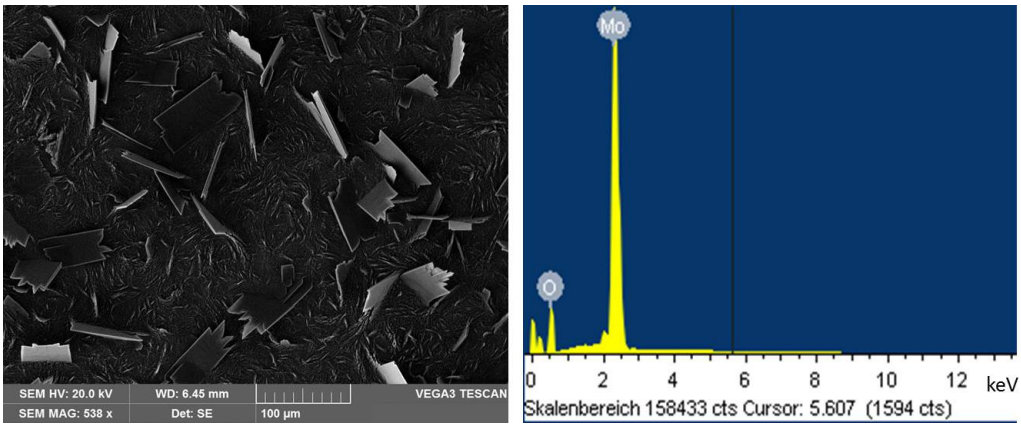

Figure 59: SEM/EDX of Mo blank, 450 °C/700 °C

Figure 60 shows the SEM images of OE 8 and OE 9, which are similar to the one obtained from the blank molybdenum foil. In the EDX analysis, only oxygen and molybdenum are detected. It seems reasonable that the volatile substances *p*-tolyl$_2$SiH$_2$ (**34**) and benzyl$_2$SiH$_2$ (**20**) boil off the surface and are removed within the gas flow.

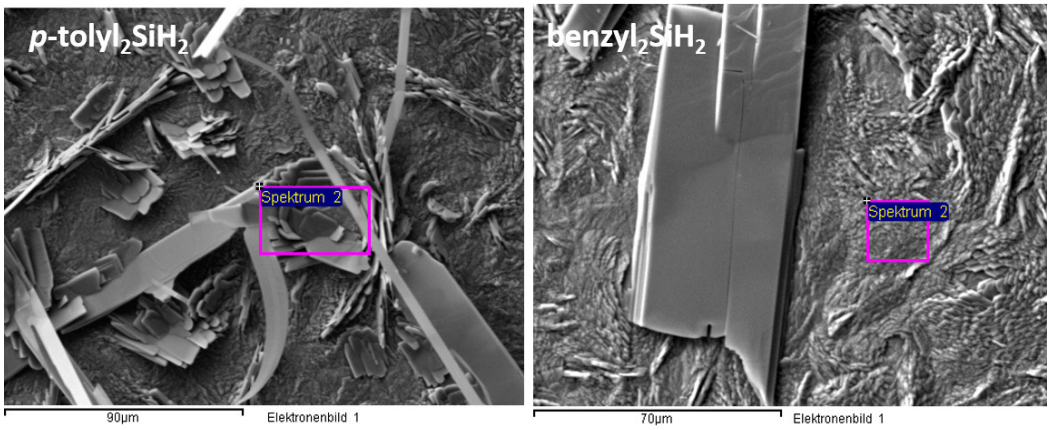

Figure 60: SEM images of OE 8 and OE 9 after thermolysis at 450/700 °C

Figure 61 shows the obtained SEM image and EDX data of OF 10. The surface differs from the previous described. No platelet structures are observed, but only traces of silicon are detected on the surface. Due to this finding a reaction of 1-naphthylSiH$_3$ (**30**) with the surface, forming a porous structure might be possible. Nevertheless, a film formation with the volatile silane is not possible.

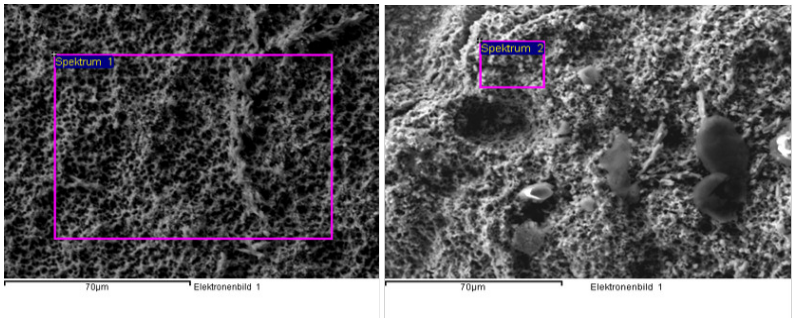

Element	"Spektrum 1" Atom%	"Spektrum 2" Atom%
O K	75.4	76.4
Si K	-	1.1
Mo L	24.6	22.3
C K	-	-

Figure 61: SEM/EDX of OE 10 after thermolysis at 450/700 °C

Figure 62 shows the obtained SEM image and EDX data of OF 11. In this case the silane was molten on the surface prior to thermolysis. The obtained layers are quite homogeneous and show a carbon content of 2-6%. On the molybdenum substrate a formation of platelets due to oxidation can as well be observed. The oxygen content of the layers is again very high, which can be explained by the high affinity of silicon to oxygen and the impossibility of its exclusion in the experimental setup.

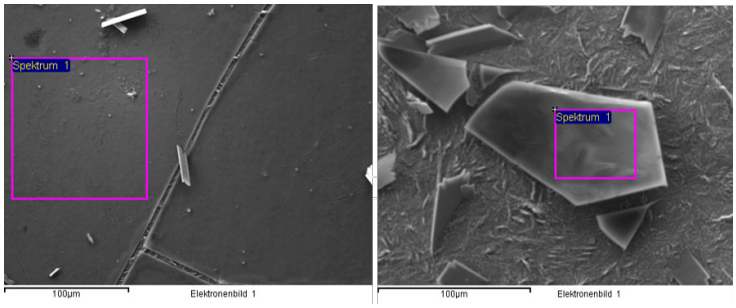

Element	"Spektrum 1" Atom%	"Spektrum 1a" Atom%
O K	70.1	68.4
Si K	10.6	25.6
Mo L	13.32	3.45
C K	6.1	2.5

Figure 62: SEM/EDX of OE 11 after thermolysis at 450/700 °C

Figure 63 shows the obtained SEM image and EDX data of OF 12. A toluene solution of the silane was dispensed onto the surface until complete coating. On the surface thin fragmented platelets with a glass like appearance can be detected.

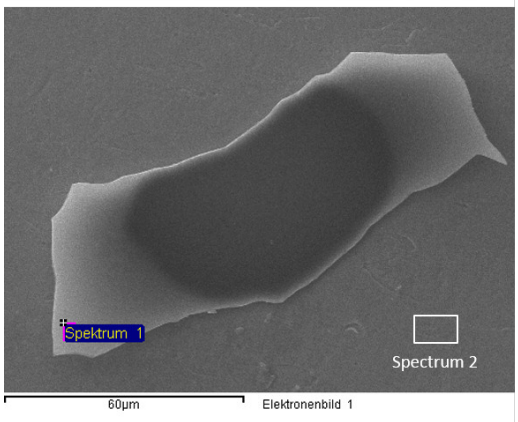

Element	"Spektrum 1" Atom%	Spectrum 2 Atom%
O K	69.8	21.3
Si K	24.2	-
Mo L	6.1	78.7
C K	-	-

Figure 63: SEM/EDX of OE 12 after thermolysis at 450/700 °C

For the thermolyzed 9-anthracenyl$_2$SiH$_2$ (**27**), no carbon at all could be detected in the resulting films. This value was accompanied with a quite high silicon content of about 25%.Figure 64 shows the obtained SEM image and EDX data of OF 13. The pure silane was applied to the surface. In the SEM image only isolated particles can be detected after thermolysis. The EDX analysis reveals a high carbon content (67%).

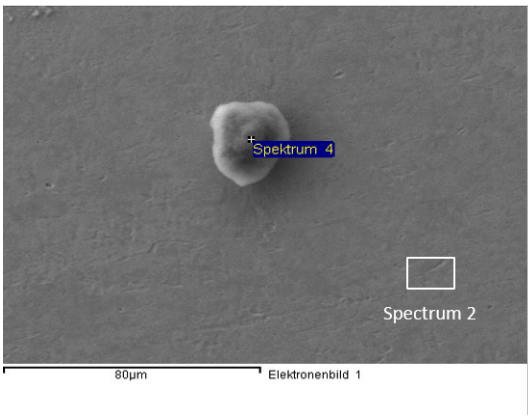

Element	"Spektrum 1" Atom%	Spectrum 4 Atom%
O K	11.1	17.6
Si K	21.1	-
Mo L	-	82.4
C K	67.9	-

Figure 64: SEM/EDX of OE 13 after thermolysis at 450/700°C

Thin layers of the precursor in combination with a two-step thermolysis up to 700 °C gave the best results for the HZS 12/200/1200. Benzyl$_2$SiH$_2$ (**20**), *p*-tolyl$_2$SiH$_2$ (**34**), and 1-naphthylSiH$_3$ (**30**) turned out to be too volatile for an efficient thermolysis. *p*-*n*-butyl$_2$phenylSiH$_2$ (**23**) gave particles with a rather high carbon content. 1-Naphthyl$_2$SiH$_2$ (**25**) and 9-anthracenyl$_2$SiH$_2$ (**27**) resulted to be the most promising candidates for further experiments.

DHS 1100

Thermolysis of 1-naphthyl$_2$SiH$_2$ (**25**) was investigated in detail with an Anton Paar DHS 1100, which allows a very fast heating rate (up to 100 °C/min) and easy handling, due to the comparatively small instrument (Figure 65).

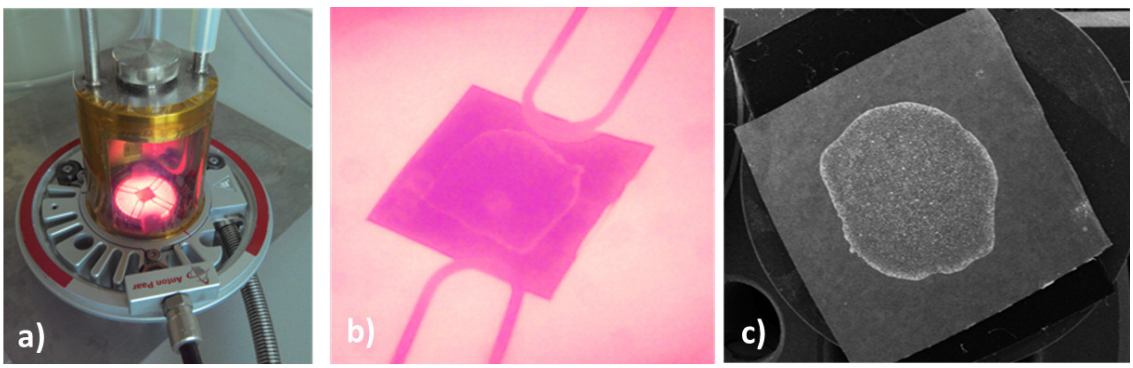

Figure 65: Experimental setup with modified dome. a) sample during thermolysis b) obtained surface coating

For experimental details of thermolysis experiments with the DHS 1100 see Table 14.

Table 14: Experimental details for thermolysis of 1-naphthyl$_2$SiH$_2$ (25) on molybdenum (Mo) or platinum (Pt) foil with DHS 1100

Sample No.	Method	Surface	T [°C]	T_{Rate} [°C/min]
OE 14	powder	Mo	700	50
OE 15	powder	Mo	700	100
OE 16	melting	Mo	700	100
OE 17	melting	Mo	700	100
OE 18	melting	Mo	700	100
OE 19	melting	Pt	700	100
OE 20	melting	Pt	700	100
OE 21	melting	Pt	700	100
OE 22	melting	Pt	700	100

Figure 66 shows the obtained SEM image and EDX data of OF 14 and OF 15. In both cases, a powdered silane sample was directly applied to the molybdenum surface.

OF 14 shows a carbon content of about 30%, which is notably lower than the one observed for powder samples from the GHA 12/600. In the case of OF 14 only a thin powder layer was applied and a higher heating rate (100 °C/min) used. In the observed particles no carbon could be detected.

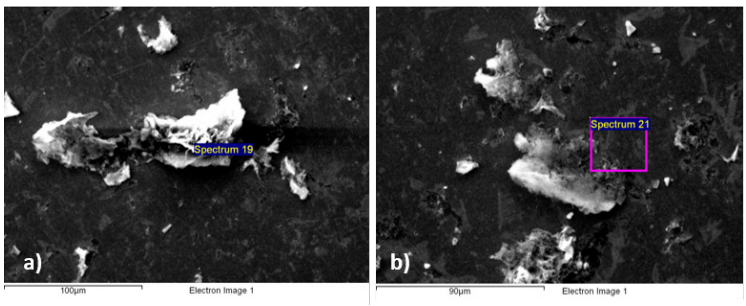

Element	"Spektrum 19" Atom%	"Spektrum 21" Atom%
O K	49.8	46.0
Si K	19.5	12.4
Mo L	1.6	41.51
C K	29.1	-

Figure 66: SEM/EDX of OE 14 and OE 15 after thermolysis at 700 °C

Figure 67 shows an elemental mapping of an additional part of OE 15, indicating the composition from mainly silicon (and oxygen).

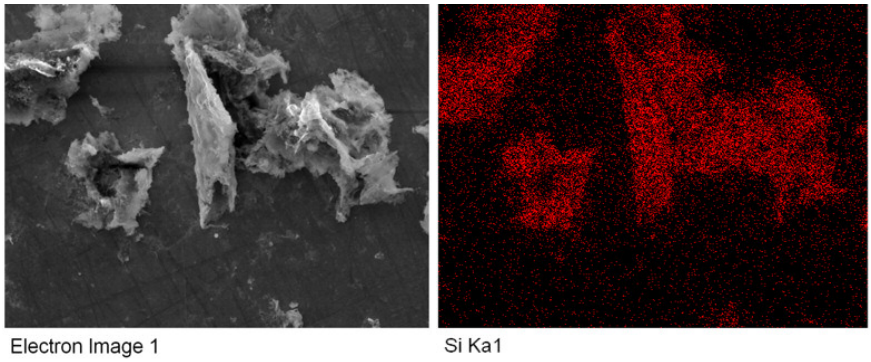

Figure 67: OE 15; SEM image and elemental mapping (EDX) of silicon

Figure 68 shows an overview of the surface of sample OE 16. In this experiment (and the following) the silane was molten on the surface *prior* to thermolysis. Instead of unordered solids or layers, small particles are formed.

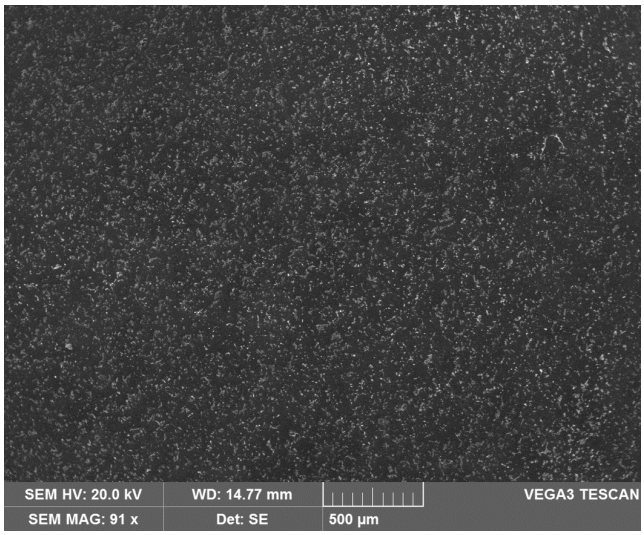

Figure 68: SEM image of OE 16

Figure 69 shows the SEM and EDX data for OF 16 and OF 17. In both cases carbon was not detectable in the resulting sample. The silicon content ranges from 10-25%, depending also on the thickness of the particle (also related to the observed molybdenum content)

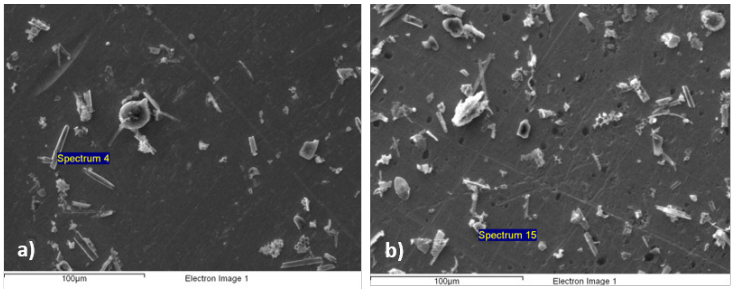

Element	"Spektrum 4" Atom%	"Spektrum 15" Atom%
O K	79.5	73.5
Si K	10.6	25.3
Mo L	9.9	1.2
C K	-	-

Figure 69: SEM/EDX of OE 16 and OE 17 after thermolysis at 700 °C

Figure 70 shows an elemental mapping of OE 18, indicating the composition of the resulting particles from mainly silicon and oxygen.

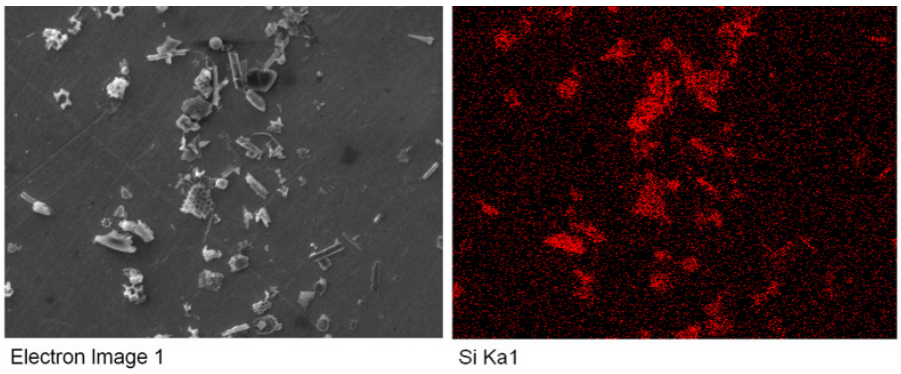

Figure 70: OE 18; SEM image and elemental mapping (EDX) of silicon

To eliminate oxygen derived from the molybdenum surface, which could react with silicon, a second test row (OE 19-22) was performed on platinum substrates. Figure 71 shows an overview of the surface of sample OE 19. Similar to molybdenum, small particles are formed.

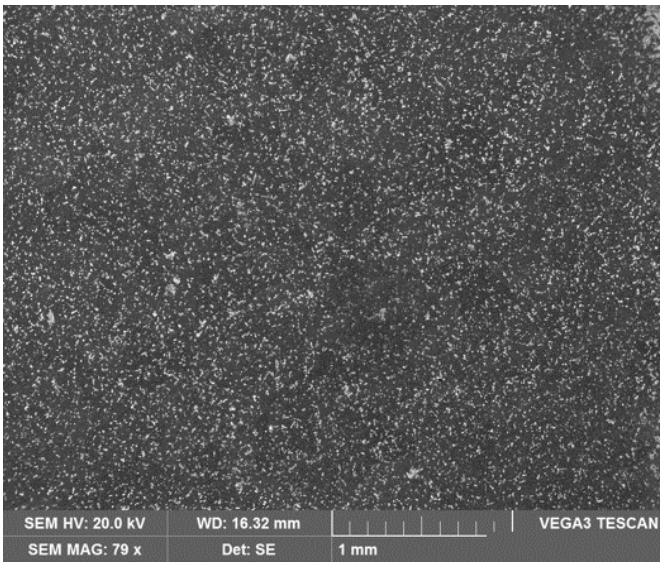

Figure 71. SEM image of OE 17

To ensure the reproducibility of the previous measurements regarding the absence of carbon in the obtained samples, a test row of 4 equal samples was prepared (OF 19-OF22). Figure 72 shows the SEM and EDX analysis of the resulting particles. All samples show a good conformity regarding the elemental composition. A silicon content of 16-23%, accompanied by an high oxygen content was observed. No carbon could be detected.

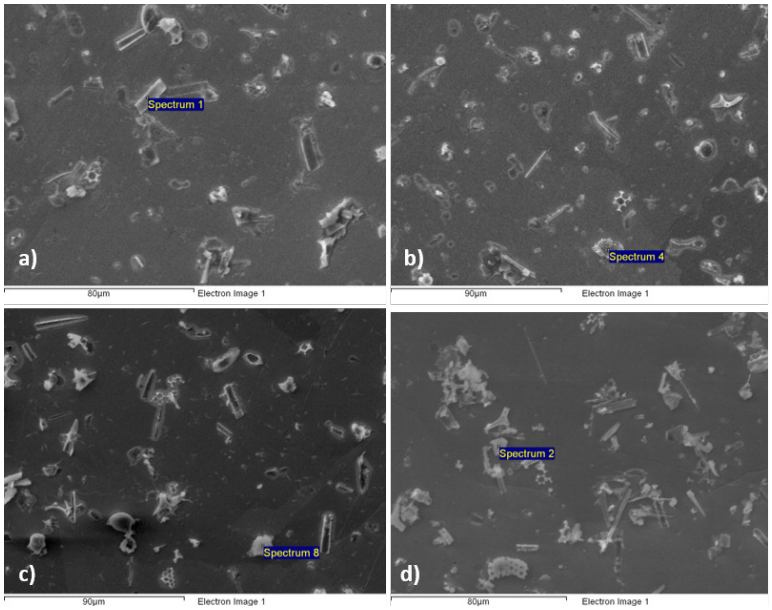

Element	"Spektrum 1" Atom%	"Spektrum 4" Atom%
O K	78	78.3
Si K	16.5	18.8
Pt M	55	2.9
C K	-	-

Element	"Spektrum 8" Atom%	"Spektrum 2" Atom%
O K	76.0	76.3
Si K	23.0	22.5
Pt M	1.0	1.2
C K	-	-

Figure 72: SEM/EDX of a) OE 19, b) OE 20, c) OE 21 and d) OE 22 after thermolysis at 700 °C

An interesting feature of all experiment performed with the highest heating rate (100°C/min) is the formation of comb-like structures on the surface (Figure 73), which are possibly derived from the fast release of reaction products during thermolysis.

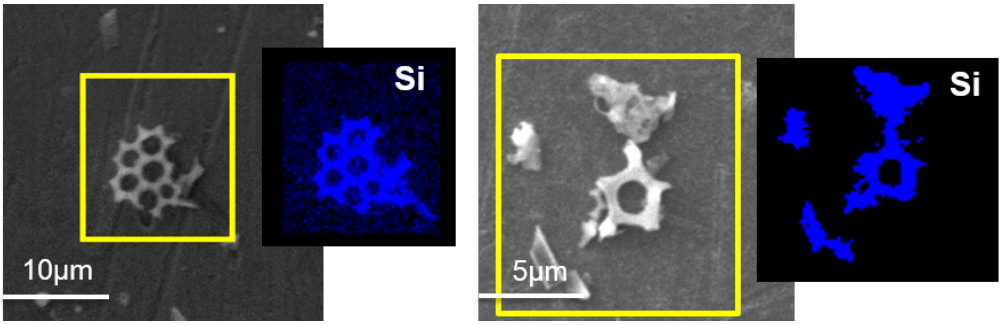

Figure 73: SEM images of observed comb structures formed at high heating rates (100 °C/min); elemental mapping (EDX) of silicon

Summing up, the formation of silicon (or SiO) from organosilanes was successfully performed. Variation of the reaction parameters show that the temperature, preparation of the sample (especially regarding the thickness of the silane layer) as well as the heating rate have a major influence on the reaction products. 1-naphthyl$_2$SiH$_2$ (**25**) and 9-anthracenyl$_2$SiH$_2$ (**27**) proved to generate carbon free particles under certain conditions. Due to the easier synthetic accessibility of the former, 1-naphthyl$_2$SiH$_2$ (**25**) might be the more interesting candidate for further applications. Even though silanes with other substituents than naphthyl or anthracenyl (which might be the better leaving groups in thermolysis) produce layers or particles with a higher carbon content, this might as well lead to the interesting possibility to "tune" the carbon content by intentionally choosing the organic substituent of the organo silane (Figure 74).

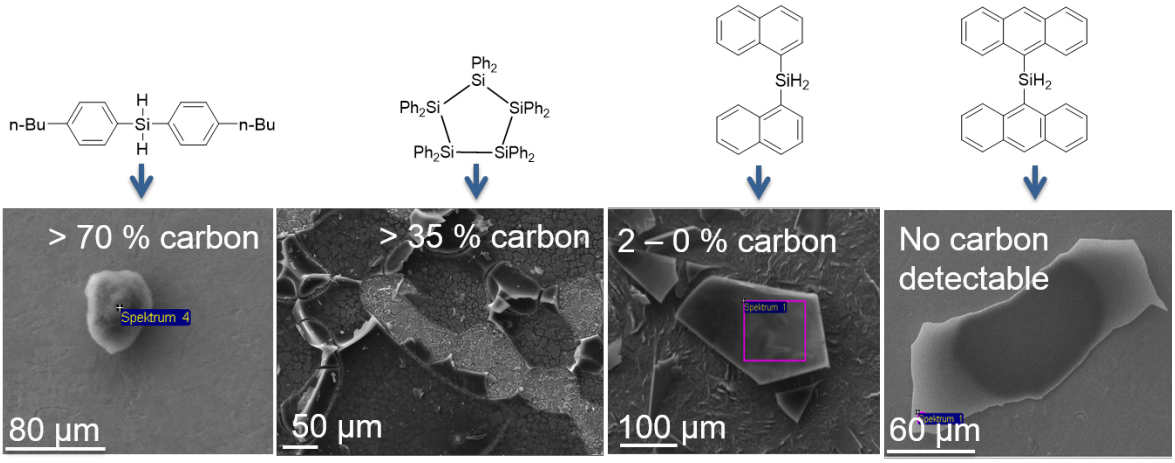

Figure 74: Dependency of carbon content on substituent of the organo silane.

In the heat treatment of organo silanes and polysilanes, oxygen is in many cases inevitably included in the resulting solids due to its affinity to silicon. Nevertheless, SiC_xO_y compounds can be used for super low-*k* materials due to the low dielectric constant and their thermal stability.[49]

3.4.3 Battery Material

In this study, which was performed in our working group,[119] the influence of octaphenyl-cyclotetrasilane (Ph_8Si_4) and decaphenylcyclopentasilane ($Ph_{10}Si_5$) on the capacity of graphite in lithium-ion half-cells has been tested (Figure 75). For this purpose, the silanes were pretreated differently depending on the preparation procedure of the electrodes used. Pretreatments included pyrolysis of the silanes, mixing and/or ball-milling of the same with graphite, polymeric binder, carbon and solvent.

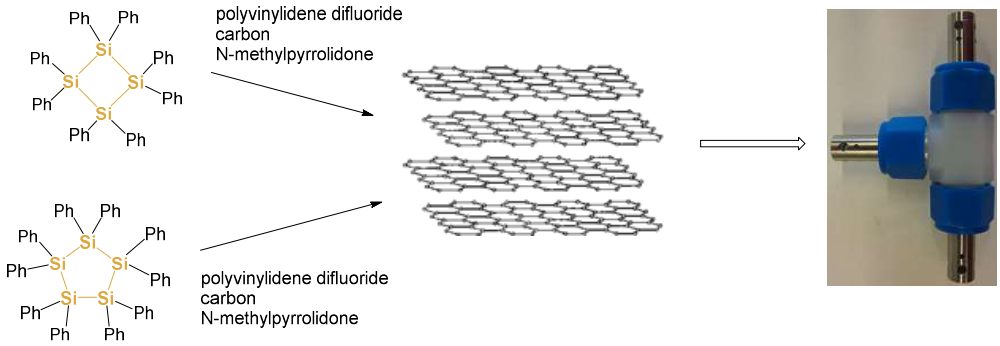

Figure 75: Scheme for the usage of phenylated cyclosilanes in lithium-ion half-cells

Testing of these electrodes was carried out using Galvanostatic Cycling and Cyclic Voltammetry protocols. The silane containing electrodes showed lower capacities than the comparably prepared graphite electrodes. The capacities found for Si_4Ph_8 were slightly

higher than for its five-membered analogue in all of the experiments performed. The Galvanostatic Cycling of the perphenylated cyclopolysilanes was carried out with electrodes from different preparation methods. The used electrodes differed in composition, particle size and treatment during the preparation. The resulting determined practical capacities were 250 mAh g^{-1} for graphite, 227 mAh g^{-1} for Si_4Ph_8 and 202 mAh g^{-1} for Si_5Ph_{10} (Figure 76).

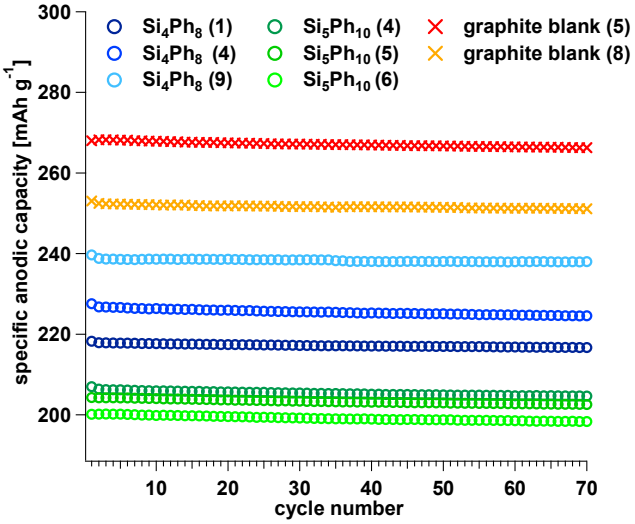

Figure 76: Ball-milled graphite blank vs. ball-milled Si_4Ph_8 and Si_5Ph_{10}

Exceptional results were found for electrodes containing pyrolysed silanes, which elevated the average capacity significantly from 216 mAh g^{-1} (graphite blank) to 347 mAh g^{-1} (Si_4Ph_8, 60% vs. blank) and 297 mAh g^{-1} (Si_5Ph_{10}, 37% vs. blank) (Figure 77).

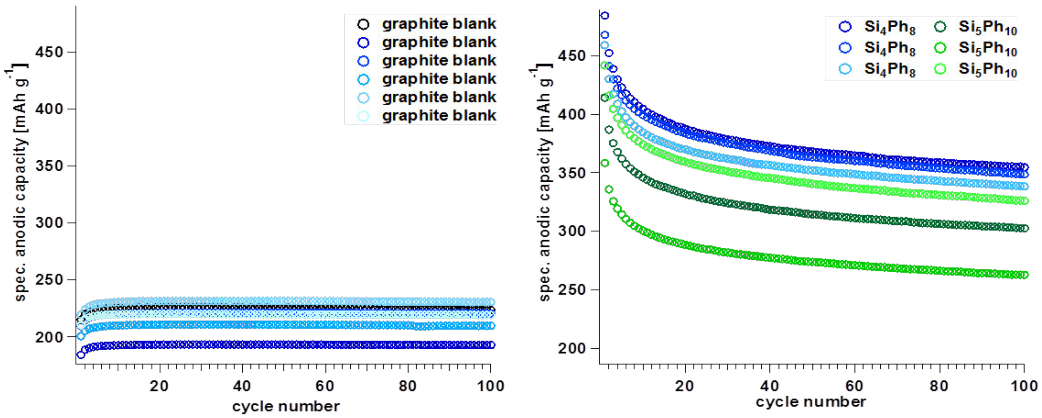

Figure 77: Ball-milled graphite blank (left) vs. pyrolysed & ball-milled Si_4Ph_8 and Si_5Ph_{10} (right)

This may be explained by a ring opening during the pyrolysis at 700 °C, which resulted in shorter polymeric silicon structures. The pyrolysis might lead to higher capacity m terials with experimentally found specific capacities of 131 mAh g^{-1} for pyrolysed Si_4Ph_8 and 82 mAh g^{-1} for pyrolysed Si_5Ph_{10}.

3.5 Reactivity

3.5.1 Oligo-/Polymerization

Oligomerization of aryl(chloro)silanes was investigated using two different reaction pathways. Dehydrogenative coupling of arylsilanes with the metallocene catalysts Cp_2TiMe_2 and *n*-BuLi/Cp_2TiCl_2 as well as a Wurtz-type coupling reaction of arylchlorosilanes with the alkali metals lithium and magnesium.

Reaction with metallocene catalyst

In literature the dehydrogenative coupling has been described only for a few other aromatic systems besides phenyl. When the phenyl ring is substituted with a methyl group in the *ortho* position, no homopolymer could be obtained. Substituents in the *meta* or *para* position show a higher polymerization rate under similar conditions. In the present work, the reaction of the arylsilanes with Cp_2TiMe_2 was performed like described by Harrod *et al.*[120] with the goal to obtain an oligomer or a Si-ring system with a arylSiH-group. Reaction of the secondary silanes with the combined *n*-BuLi/Cp_2TiCl_2 was performed similar to Corey et al.[79] to obtain the corresponding homooligomers or polymers (Figure 78).

The reaction was performed with two different substituent systems. In comparison to phenyl, the naphthyl group shows an increase in the steric bulk in the *ortho* position, but has a rather flat geometry. 2,6-Xylyl has an even higher bulk, due to the two methyl groups in the *ortho* positions towards the silicon atom.

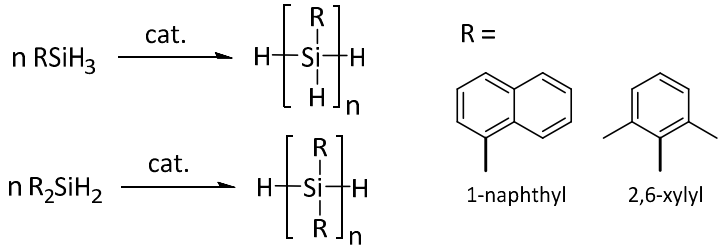

Figure 78: Reaction scheme for homogeneous dehydrogenative coupling

All reactions were carried out in toluene. The addition of *n*-BuLi in the combined catalyst system was done at 0 °C because of the instability of the organolithium reagent at higher temperatures. After complete addition, the reaction was heated to 90 °C. For trihydrides, a toluene solution of Cp_2TiMe_2 was added at room temperature (see Table

15). A colour change indicating the formation of the deep blue coloured titanocene(III) silyl complexes was observed (see Figure 79).

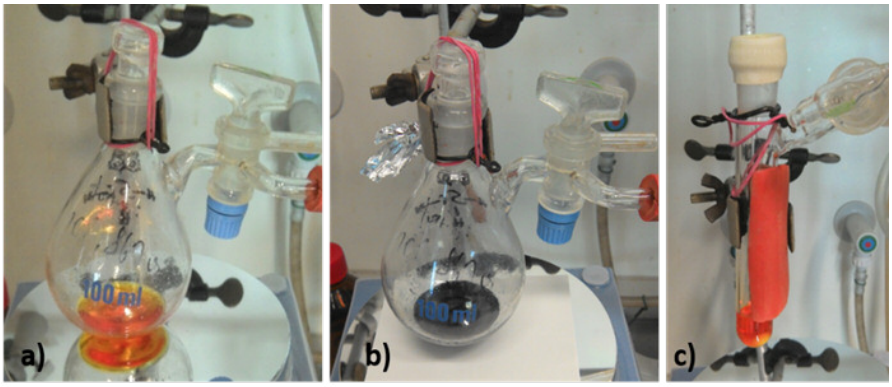

Figure 79: a) reaction solution of 1-naphthylSiH$_3$ (30) with Cp$_2$TiMe$_2$, b) reaction after 30 minutes; c) reaction solution of 2,6-xylyl$_2$SiH$_2$ (28) with *n*-BuLi/Cp$_2$TiCl$_2$ after 10 hours reflux

The reaction of 2,6-xylyl$_2$SiH$_2$ (**28**) with *n*-BuLi/Cp$_2$TiCl$_2$ gives a large ^{29}Si-NMR signal at -62.1 ppm (D$_2$O). In the ^{1}H-NMR spectra, the hydride signal can be seen at 5.08 ppm (D$_2$O) with an integral ratio to the methyl protons of 2:12, which correspond to the unreacted educt. No colour change could be observed in this reaction.

Table 15: Reaction of arylsilanes R$_2$SiH$_2$ and RSiH$_3$ with metallocene catalysts

Monomer	Catalyst	Conditions	Colour change	^{29}Si–NMR [ppm]
1-naphthyl$_2$SiH$_2$ (**25**)	*n*-BuLi/Cp$_2$TiCl$_2$	0 °C/ 90 °C	black; 30 min	-39.4
1-naphthylSiH$_3$ (**30**)	Cp$_2$TiMe$_2$	RT	dark blue; 30 min	-62.8, -39.8
2,6-xylyl$_2$SiH$_2$ (**28**)	*n*-BuLi/Cp$_2$TiCl$_2$	0 °C/ 90 °C	orange (no change)	-62.1
2,6-xylylSiH$_3$ (**37**)	Cp$_2$TiMe$_2$	RT	dark blue; 20 min	-45.5, 62.2

Reaction of 1-naphthyl$_2$SiH$_2$ (**25**) with *n*-BuLi/Cp$_2$TiCl$_2$ gives one ^{29}Si-NMR signal at -39.4 ppm (D$_2$O). In the ^{1}H-NMR spectra, the hydride signal can be seen at 5.4 ppm (D$_2$O) with an integral ratio of 2:2 to the dublet of the aryl-protons in α-position to the silicon. Also in this case the shifts can be assigned to unreacted educt. The colour change in the reaction of 1-naphthyl$_2$SiH$_2$ (**25**) may occur from a reaction of the catalyst with residual moisture. In the reaction of 2,6-xylylSiH$_3$ (**37**) with Cp$_2$TiMe$_2$ a colour change to dark blue is observed after 20 minutes. The ^{29}Si-NMR shows a large peak at -62.2 ppm, which can be attributed to the unreacted educt and a smaller peak at -45 ppm (see Figure 80). GC-MS analysis of the solution was inconclusive. Unfortunately it was not possible to characterize the reaction product, but from comparison of the reaction with 1-naphSiH$_3$ (**25**) it is obvious that the reaction of 2,6-xylylSiH$_3$ (**30**) seems to be slower due to the larger sterical hindrance.

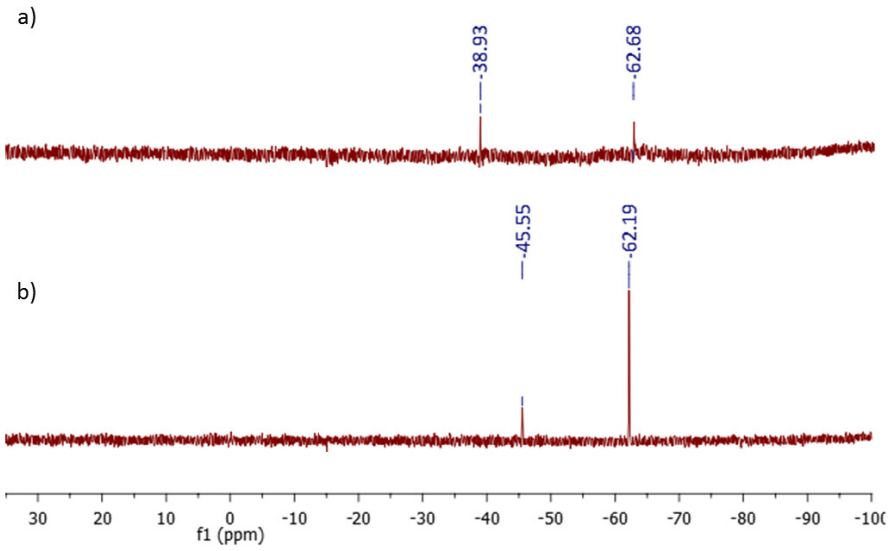

Figure 80: ^{29}Si-NMR of the reaction of Cp_2TiMe_2 with a) 1-naphthylSiH$_3$ (30), b)2,6-xylylSiH$_3$ (30) after one week

After 3 days, the reaction of 1-naphthylSiH$_3$ (**30**) turns to a dark brown colour and a yellowish-white precipitate is formed. The precipitate was filtered off and dried. In the residual solution, two ^{29}Si-NMR shifts were measured overnight. A small one at -62.8 ppm, which can be assigned to unconverted educt and a larger one at -39.8 ppm. A GC-MS analysis did not yield any results, which may be caused by a too large molecular weight or problems in the injector system. The shift might correspond to a low weight oligomer. The white precipitate was washed *via* soxhlet extractor with toluene for 10 hours. The resulting white powder is insoluble in common organic solvents. The bad solubility would be an indication for a compound bearing more than one naphthyl moiety. If compared to the monomers the solubility decreases from 1-naphthyl$_2$SiH$_2$ (**25**) to 1-naphthyl$_3$SiH (**33**). The same effect can be seen for the corresponding chlorosilanes. The ATR-IR Analysis (see Figure 81) of the precipitate shows a strong band at 2100 cm^{-1}, which can be attributed to the Si-H group. In the region between 3100-3000 cm^{-1} the symmetric and asymmetric stretching vibration of the aryl C-H can be seen. The bands between 2000 and 1600 cm^{-1} can be assigned to combination vibrations. A strong C=C valence vibration shows at 1500 cm^{-1}. The "fingerprint" region from 1300-1000 cm^{-1} is very similar to the ATR-IR spectra of naphthalene (see Appendix), but showing less bands in the region 600-1000cm^{-1} compared to 1-naphthyl$_2$SiH$_2$ (**25**) (see Appendix), which could be caused by the absence of the second aryl substituent. The two naphthyl groups show a wider variety of rocking, wagging and twisting modes compared to the mononaphthyl substituted silane. The same effect can be observed for phenylsilanes.[121] The ATR-IR spectra allows the conclusion, that the ob-

tained solid has both a naphthyl moiety and a Si-H group, which would fit to the desired product of the dehydrogenation.

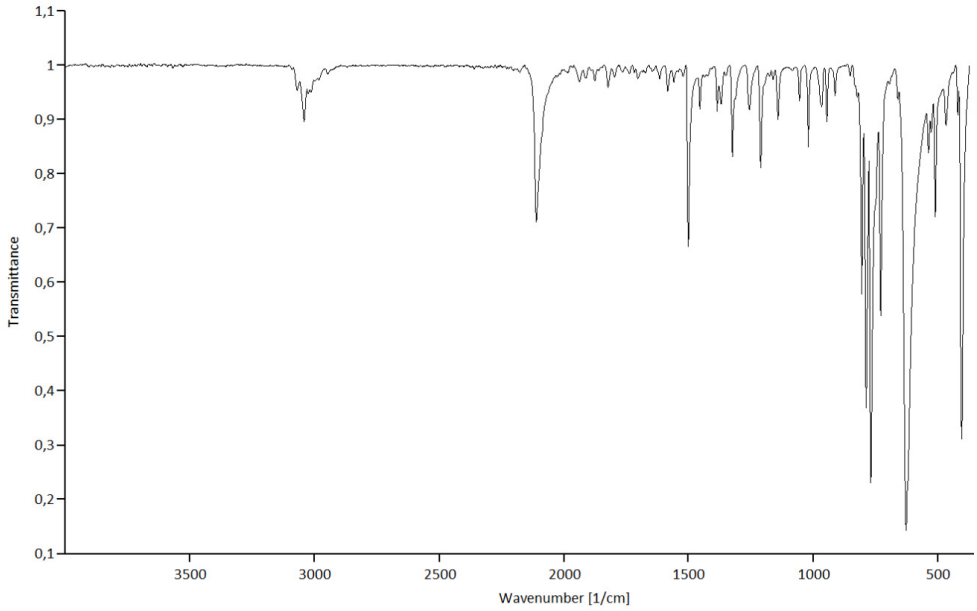

Figure 81: ATR-IR spectra of the precipitate of NaphthylSiH$_3$ (30) with Cp$_2$TiMe$_2$

The electron impact mass spectrum with direct ionization is shown in Figure 82. Spectra were continuously acquired while the sample was heated from room temperature to 550 °C.

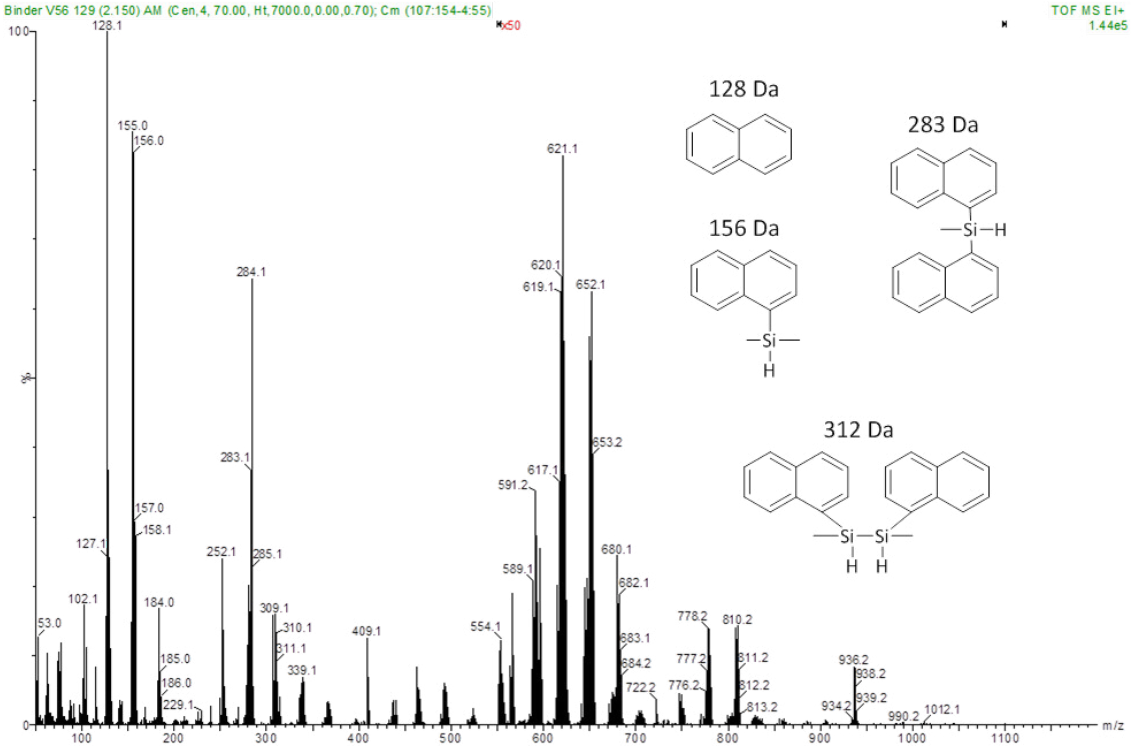

Figure 82: Enlarged (50x) DI-EI spectra of the precipitate [Naphthyl$_x$SiH$_y$] with some of the detected MS fragments

Up to 150 °C, toluene was detected which was possibly enclosed in the sample. At approximately 400 °C, the above-mentioned spectra was obtained. Due to the high temperature, the visible peaks might not only be the precipitate, but also its thermal degradation products. Fragments with the weight distance of the naphthylSiH group (156 Da) as well as the naphthyl group (128 Da) can be detected. The mass of 283 Da (bzw. 284 Da) would fit to a fragment with two naphthyl groups attached to the silicon atom. The rearrangement of aromatic substituents when exposed to heat was already observed in the thermolysis of $Ph_{10}Si_5$.[122] The fragment at 621 Da would fit to a tetramer of naphthylSiH-units, which is evidence for the succesful oligomerization, beyond the disilane state. Noticeable is the fragement at 936 Da which would fit peculiar good to the cyclohexamer of naphthylSiH. It might have been formed thermally during the heating, but also the direct formation during the reaction is possible. The theoretical isotope pattern M^+ of $(1\text{-naphthylSiH})_6$ and the observed pattern can be seen in Figure 83. Both patterns fit very well.

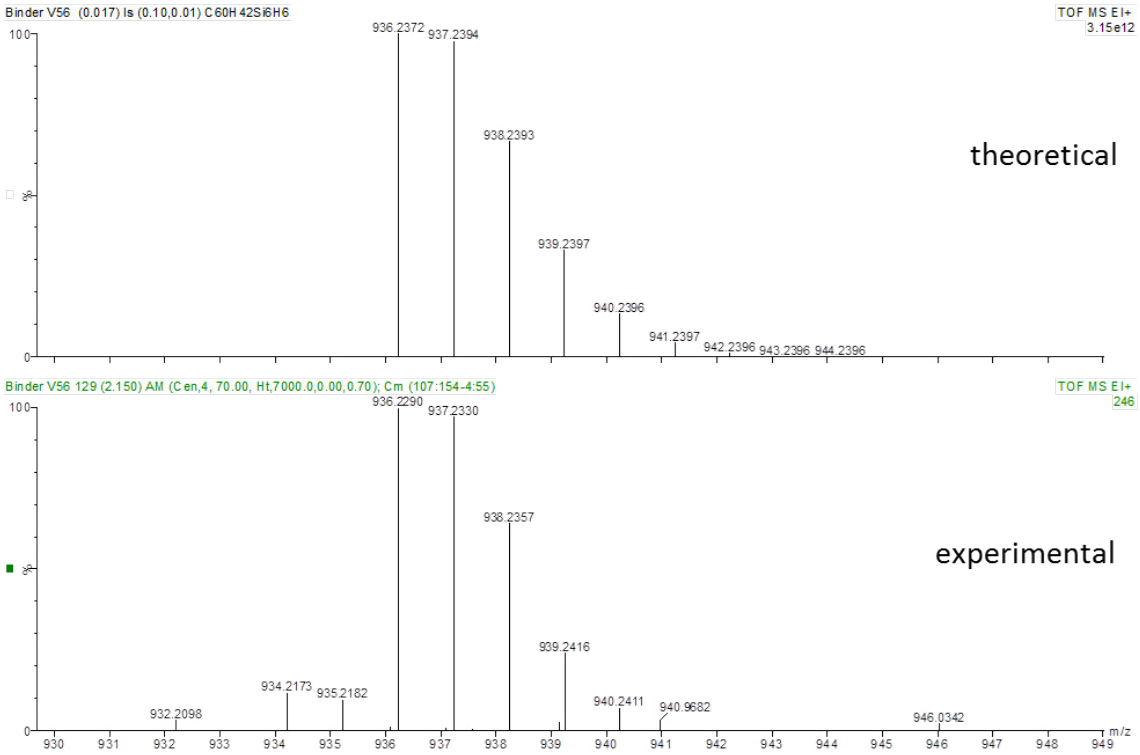

Figure 83: Theoretical and experimental isotope pattern of $(1\text{-naphthylSiH})_6$

The MALDI-TOF spectra also shows the formation of an oligomeric 1-naphthylSiH compound (Figure 84). The largest fragment at 1187 Da could be attributed to a cyclic compound or a linear hexamer. In both cases again, a rearrangement of the naphthyl groups seems to take place.

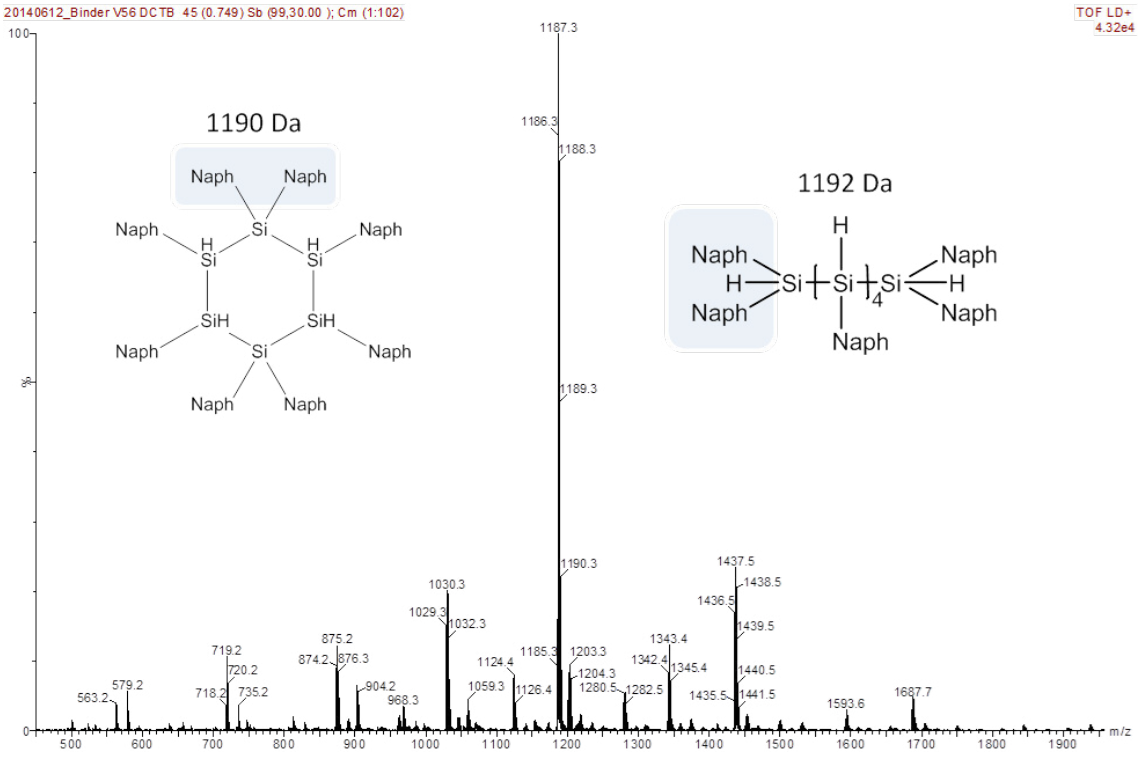

Figure 84: MALDI-TOF of the precipitate [1-naphthyl$_x$SiH$_y$]

The pattern of the mass spectra clearly shows the oligomerization of the monomer. The difference in mass between the major peaks is in nearly all cases 156 Da, which can be assigned to the 1-naphthylSiH-group. For the detailed MALDI-TOF spectra of the specific m/z regions see Appendix. Because of the bad solubility of the oligomer, no crystal structure could be obtained, but the conclusion can be drawn that the dehydrogenative coupling of 1-naphthylSiH$_3$ (**30**) with Cp_2TiMe_2 is successful beyond the disilane stage. The flat geometry of the naphthyl group does not hinder the coupling. A similar reaction as described by Harrod[120] seems to take place. For some fragments the theoretical mass differs from the experimental by the weight of one or two protons. Perhaps also in this case a reaction between the naphthyl moietys takes place as is sugested for the Wurtz-reaction of 1-naphthyl$_2$SiCl$_2$ (**8**) with lithium (see subsequent section). To obtain compounds with higher mass than the oligomer, it would be interesting to use also other catalyst systems with hafnium or zirconium, as well as other aryl substituents including anthracenyl. The oligomers of (1-naphthylSiH) could be interesting materials for different applications, combining the Si-Si chain with a large conjugated π-system. The poor solubility might be improved by proper substitution of the naphthyl ring.

It could be shown that the reaction of 1-naphthylSiH$_3$ (**30**) with Cp_2TiMe_2 leads to the desired oligmerization. Polymerization could not be observed, possibly due to the higher steric demand of the naphthyl group compared to phenyl. For 2,6-xylylSiH$_3$, a

reaction takes place but no characterization was possible so far. After one week reaction time, only a small amount of a reaction product is observed *via* ^{29}Si-NMR. Dehydrogenative coupling of secondary silanes R_2SiH_2 with *n*-BuLi/Cp_2TiCl_2 was not sucessful under the used conditions.

Wurtz coupling with alkali metal

The Wurtz coupling of 1-naphthyl$_2$SiCl$_2$ (**8**) was performed with lithium and magnesium analogous to the reaction with phenyl$_2$SiCl$_2$ (see 4.8.1) to obtain novel ring systems, oligomers or polymers.

The reaction was carried out with 3 different types of lithium: flakes (finely cut lithium band), granules and powder. In the reaction with lithium flakes, a green-black solution was obtained after one hour. This colour would be typical for a lithium naphthalenide (Figure 85). This anion is strongly basic and might lead to many side reactions. It was as well shown that lithium naphthalenide reacts with protic solvents and THF at elevated temperatures.[123] The discolouration of the solution when in contact with air can also be an indication for this reaction.

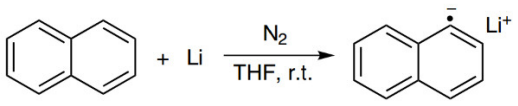

Figure 85: Preperation of lithium naphthalenide in THF

The ^{1}H-NMR showed peaks similar to naphthalene, but no educt was detected. The obtained yellow white solid seemed to be amorphous. ATR-IR spectra did not give a clear answer about the composition. No ^{29}Si-NMR shift could be detected. The precipitate might be an oligomeric product, due to its bad solubility and the many possible side reactions occurring does not allow for characterization. When using lithium powder neither a warming of the solution nor a strong colour change was observed. Several ^{29}Si-NMR shifts were detected, but the largest one at 7.67 ppm can be assigned to unreacted educt. A small amount of a yellow-white precipitate was formed but it could as well not be characterized due to its inhomogeneity, giving unclear results in all further analysis. Due to the large surface, the lithium powder might have already been to unreactive, which would go along with the observations during the reaction concerning warming and colour. In the reaction with lithium granules, a colour change was observed leading to a slightly greenish solution, which would again fit to the formation of lithium naphthalenide. Several ^{29}Si-NMR silicon shifts were detected as well in this

case, but no educt. Again the yellow-white precipitate did not give any clear results. Table 16 shows a summary of the obtained ^{29}Si-NMR shifts for the reactions.

Table 16: ^{29}Si-NMR Shifts of various Wurtz type coupling reactions of 1-naphthyl$_2$SiCl$_2$ (8) with alkali metal (=M). Li=lithium, Mg=magnesiumThe highest intensity peaks are indicated in bold fond.

M	Exp.No.	Preparation	δ ^{29}Si-NMR [ppm]
Li	W1	band	no signal
	W2	powder	8.9, **7.7**, -10.5, **-16.2**, -30.6, -35.5, -40.9
	W3	granules	**-17.7**, -24.4, -39.4, **-45.3**, -41.5
	W4	freshly cut band[124]	-24.9, **-29.0**, -37.2, -38.9, -**39.7**, -41.8
	W5	band[124]	7.0, 39.3, 57.5
Mg[124]	W6	activated with iodine	**-6.6**, -21.9, -43.9
	W7	activated with ethereal HCl	**-17.1,** -18.2**,** -35.5, **-38.3, -39.8,** -45.8
	W8	rasped	4.0, **-6.6,** -21.9

A second study performed in our working group[124] using magnesium showed similar results. With lithium band (W4 and W5) completely different results were obtained in the two reaction runs. Magnesium as well led to unreproducible results, showing various ^{29}Si shifts. MS analysis of W5 showed 1-naphthyl$_2$Si chains with different lengths, which would indicate a successful oligomerization. Besides that, fragments with the loss of two hydrogens could also be detected, which led to a proposed reaction scheme depicted in Figure 86.

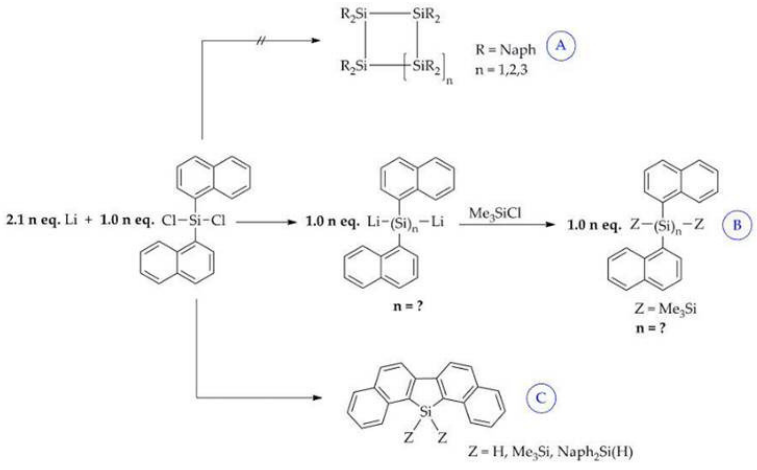

Figure 86: Depicted reaction scheme for W5[124]

Investigation of the ^{29}Si-NMR shifts shows a repeating signal in the range of -22 to -25 ppm which would fit to a cyclotetrasilane when compared to the shifts of similar perarylated compounds. Also, signals in the range of -36 to -39 ppm could belong to

the cyclopentasilane derivative. For a comparison to already known and predicted shifts of aryl substituted disilanes and ring systems see Appendix**.** Unfortunately no product could be isolated.

Despite our attempts to work under well defined reaction conditions, Wurtz coupling reactions seem to be hard to control and results were hardly reproducible. In all experiments, reaction mixtures were obtained that were difficult or even impossible to separate. This problem was increased by the insolubilty of all oligomeric reaction products bearing naphthyl groups. The same applies to polymers with phenyl substituents, which are today only used in applications were the diphenyl- substituted monomer is connected with a better soluble monomer such as the dimethyl group in a copolymer or in case of polymers containing PhSiMe groups. This approach could as well be successful in the usage of naphthyl substituted oligomers. Still the problem of many unwanted side reactions is always existing. Unfortunately, naththyl groups seem to show a wider variety of side reactions (including naphthalenide formation or forming of intermolecular bonds) than phenyl groups. All obtained solids were inhomogeneous in colour and texture and could not be purified further. Also direct ionization in mass analysis failed in many cases.

When compared to the dehydrogenative coupling of 1-naphthylSiH_3 (**30**) with a titanocene catalyst, the latter led to a much more homogeneous product, that was easier to analyze. It seems that this reaction is better controlled with fewer side reactions than the Wurtz type coupling which goes along with the results in many literature studies.

3.5.2 UV-Irradiation

Due to the sucessful photodimerization of di-9-anthracenyldimethylsilane and several 1-substituted naphthalenes (see 2.4.1), the reactivity of 9-anthraceny_2SiH_2 (**27**), 1-naphthylsilane (**30**) and dibenzylsilane (**20**) under irradiation was examined. The reactions were investigated regarding the possible formation of cycic adducts as well as photoinduced polymerization of the hydrogen rich silanes, which was reported in literature for cyclic silanes.[65] The reactions were carried out in deuterated benzene in a standard NMR tube. The UV-Vis spectra of various silanes were measured and compared to the absorption of glass to identify the usable range of wavelengths (Figure 87).

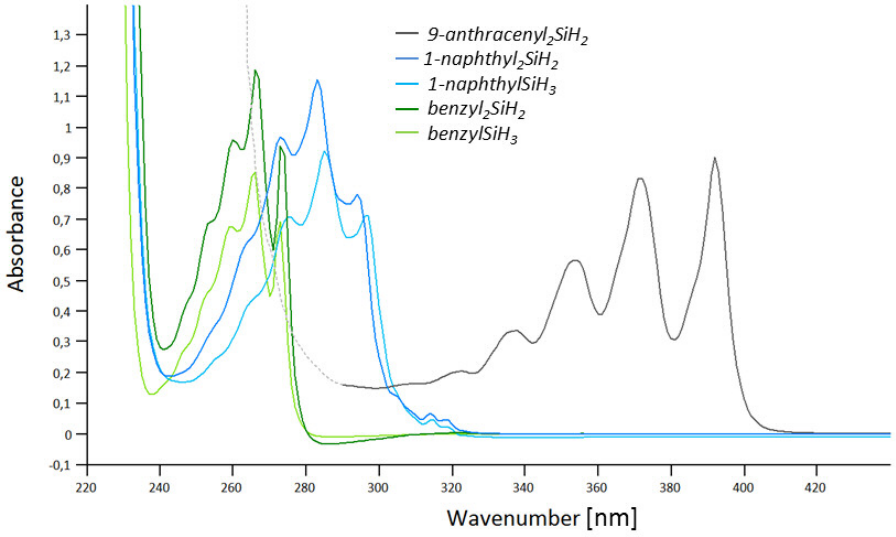

Figure 87: UV-Vis spectra the *p*-band region of 9-anthracenyl$_2$SiH$_2$ (27), 1-naphthyl$_2$SiH$_2$ (25), 1-naphthylSiH$_3$ (30), benzyl$_2$SiH$_2$ (20) and benzylSiH$_3$ (32)

The absorption maxima of 9-anthracenyl$_2$SiH$_2$ (**27**) at 392 nm, 372 nm, 353 nm and 336 nm are located near to the visible region, due to the larger π-system. 1-naphthylSiH$_3$ (**30**) shows absorbance maxima at 296 nm, 285 nm, 275 nm and 265 nm. The values for 1-naphthyl$_2$SiH$_2$ (**25**) are about 2 nm lower. The maxima of benzyl$_2$SiH$_2$ (**20**) and benzylSiH$_3$ (**32**) can be found at 273 nm, 266 nm, 260 nm and 253 nm.

9-anthracenyl$_2$SiH$_2$ (**27**) seemed to be the most promising candidate for the irradiation experiments. It shows absorption bands in the visible region of the spectrum and is the only coloured substance in the experiment. Anthracene, as a polycyclic aromatic molecule with sp^2-hybridisation of the binding orbitals of its carbon atoms, has a π-π* transition as lowest electronic transition (S0-S1). The visible *p*-band with the vibronic structure appears in solution as a broad band with four major absorption peaks between

300 and 400 nm. Figure 88 shows the comparison of the *p*-bands of anthracene and 9-anthracenyl$_2$SiH$_2$ (**27**) in benzene. 9-anthracenyl$_2$SiH$_2$ shows a bathochromic shift of the absorption maximum to 398 nm, which is in agreement with the observed colour change from the colourless anthracene to the bright greenish yellow of 9-anthracenyl$_2$SiH$_2$.

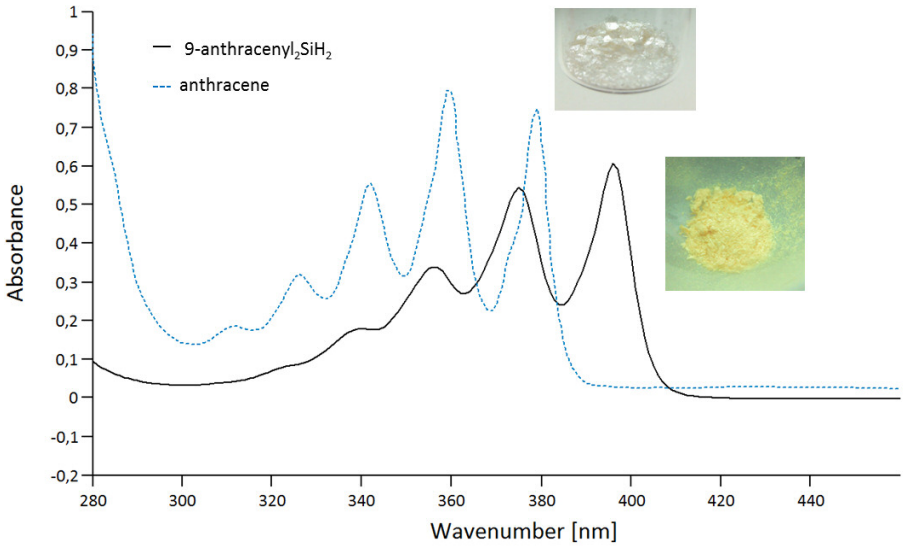

Figure 88: UV-Vis spectra of the *p*-band of a) 9-anthracenyl$_2$SiH$_2$ (27) and b)anthracene in benzene

A 0.1 mol/l solution of (**27**) was prepared in deuterated benzene, which was stored over potassium to minimize the water content. The sample was filled into a NMR-tube under inert gas and was mounted beside the brightest spot of the UV-lamp (for details see 4.8.2). ^{1}H-NMR spectra of the sample were measured prior to irradiation, after 5, 10, 20 and 30 minutes. A last measurement was taken after 6 hours of irradiation.

Figure 89 shows the ^{1}H-NMR spectrum of 9-anthracenyl$_2$SiH$_2$ (**27**) in C_6D_6 (spectrum referenced to the solvent peak at 7.16 ppm). The removal of anthracene was achieved by 24 hours vacuum sublimation at 60 °C followed by recrystallization from ethyl acetate at -4 °C. Residual anthracene can be identified *via* ^{1}H-NMR, by the absence of three peaks. A singlet at 8.16 ppm and a multiplet at 7.8 ppm and 7.24 ppm (see Appendix).

9-Anthracenyl$_2$SiH$_2$ (**27**) shows a dublet at 8.78 ppm and 7.74 ppm which can be assigned to the protons in position 4 and 5, as well as the protons in position 1 and 8. The singlet at 8.22 ppm belongs to the proton in position 10. The shifts of the protons in position 2,3,6 and 7 combine to a multiplet in the range of 7.04 – 7.14 ppm. The protons of the Si-H group show a singlet at 6.50 ppm, with a Si-H coupling constant of 202 Hz.

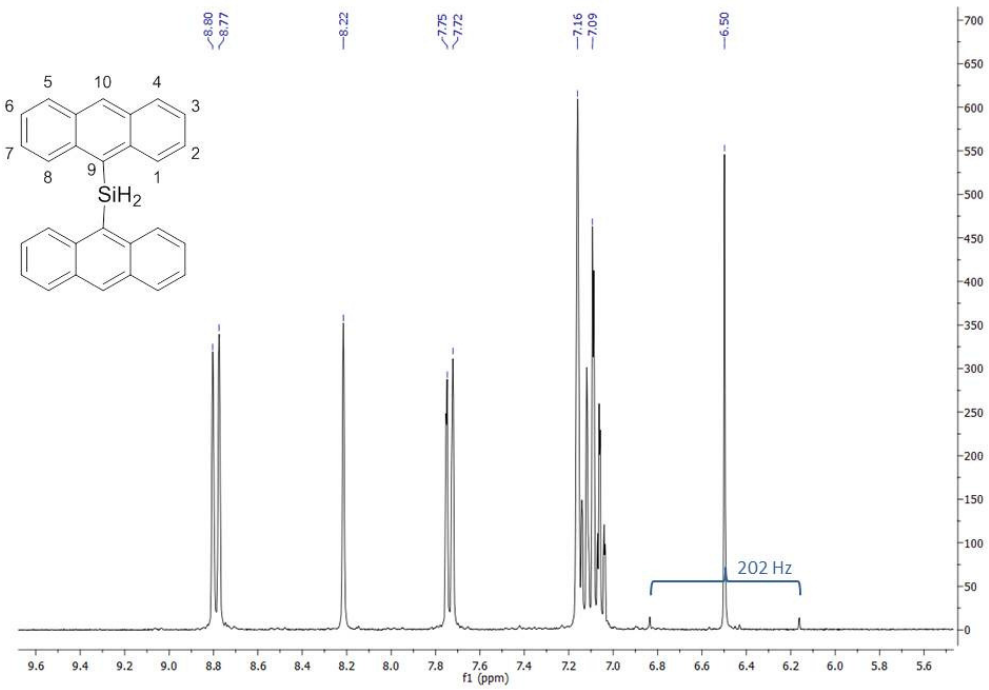

Figure 89: ^{1}H-NMR spectrum of 9-anthracenyl$_2$SiH$_2$ (27) in C_6D_6

After 5 minutes irradiation of 9-anthracenyl$_2$SiH$_2$ with UV light (see Figure 90) already a significant difference in the spectrum can be observed.

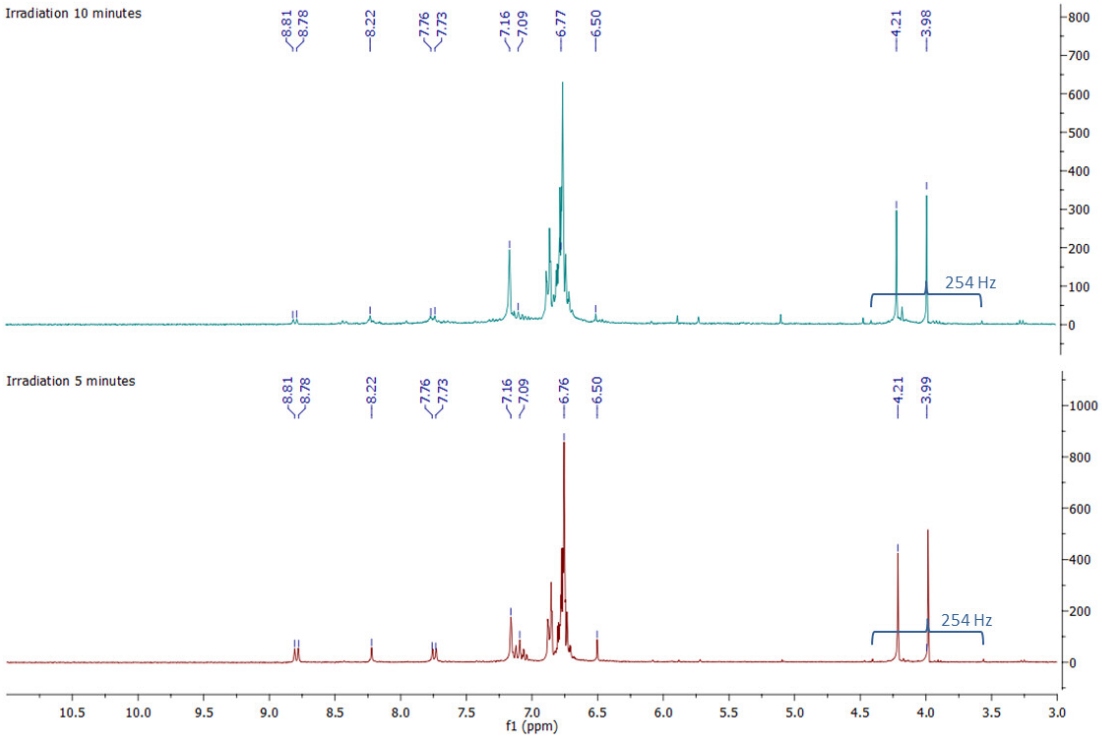

Figure 90: UV-Irradiation of 9-anthracenyl$_2$SiH$_2$ (27) in C_6D_6 at 60-900 nm after 5 min (red) and 10 min (blue)

The educt related peaks can still be detected, but the intensity has strongly decreased. Instead, new multiplet shitfts are appearing in the range of 6.7 – 6.8 ppm. Two singlet shifts, one at 4.21 ppm and one at 3.99 ppm are formed. When compared to results from literature, the similarities to the reported Type III side-product of the irradiation of di-methyl-dianthracenyl silane are noticeable.[54] Regarding the proposed structure of this reaction, an assignment of the obtained shifts is possible. The strong singlet at 3.98 ppm corresponds to the Si-H proton, which could be proved by the allocation of the satellite signals due to the Si-H coupling. The coupling constant increases from 202 Hz of the educt to 254 Hz, which would also mean a difference in the structure of the molecule.

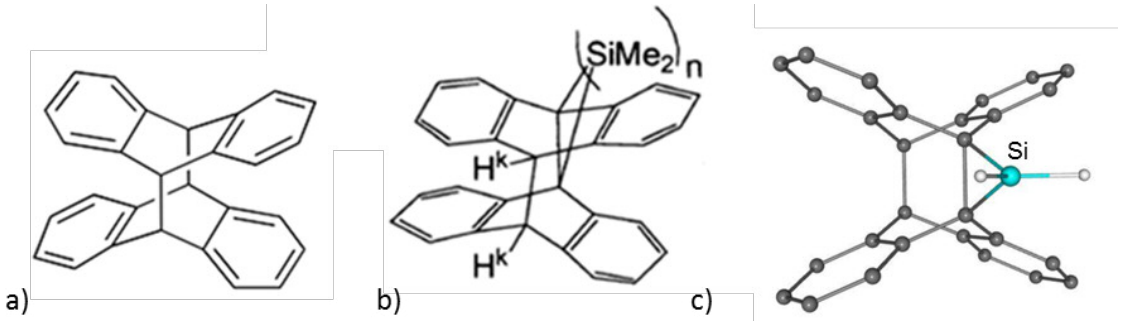

Figure 91: a) photodimer of anthracene; b) side product of irradiation of di-9-anthryldimethylsilane;[54] b) predicted structure of irradiation product of 9-anthracenyl$_2$SiH$_2$ (27)

The shift at 4.21 ppm is characteristic of the bridged backbone proton in position 10 of the anthracene substituent.[54] A similar shift can also be observed in the irradiation of anthracene. The proposed structure for the irradiation product, bearing a silacyclopropane structure is shown in Figure 91.

Progressive irradiation leads to a decrease of the Si-H proton shift. After 6 hours only the backbone proton shift at 4.20 ppm and a broad multiplet at 6.79 ppm can be observed (Figure 92). These shifts fit very well to the reported data of the photodimer of anthracene (see Figure 91). For this compound, one multiplet at 6.80 ppm and 6.87 ppm respectively, as well as a singlet at 4.53 ppm were detected when measured in $CDCl_3$. Solutions that were only irradiated for a short time, showed the same spectrum as the ones with the longest irradiation times, when stored at room temperature (or in the freezer) for some time. This allows the conclusion that the formed photodimer seems to be quite unstable. The absence of the Si-H shift in the resulting spectrum is also a strong indication for compound decomposition. It seems that upon irradiation in a first step the [4+4] cyclodimer is formed, which can be identified in the ^{1}H spectrum.

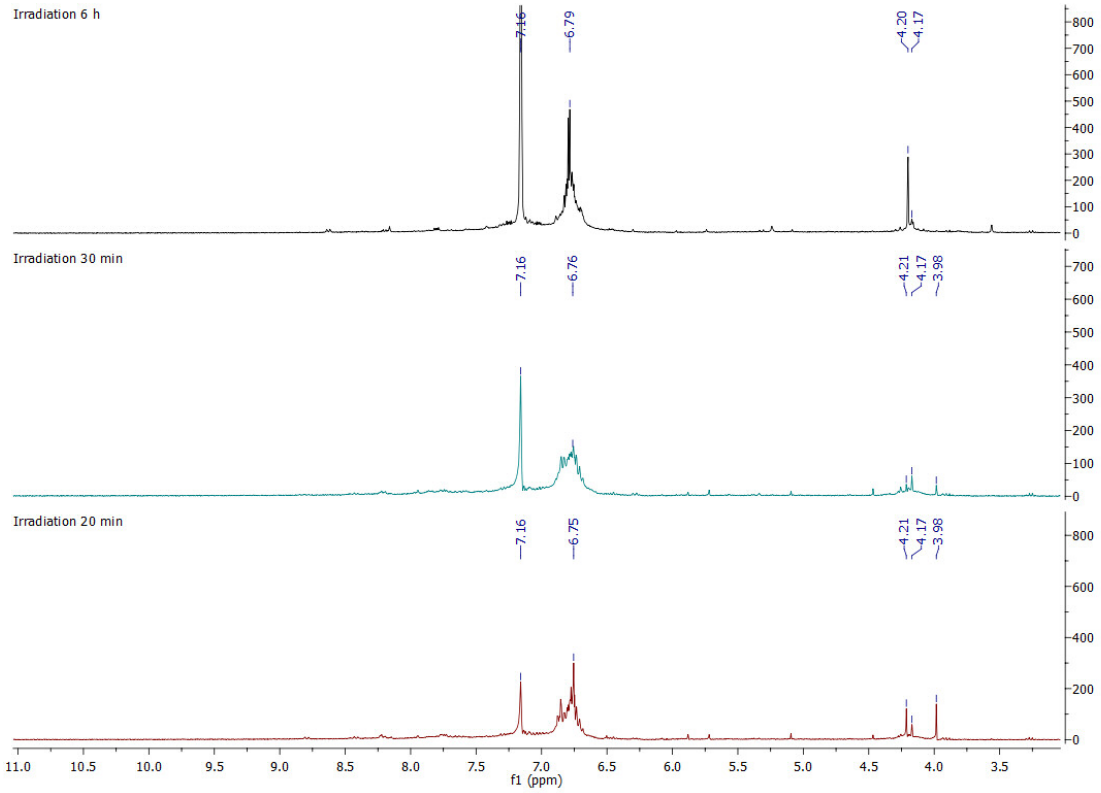

Figure 92: UV-Irradiation of 9-anthracenyl$_2$SiH$_2$ (27) in C_6D_6 at 60-900 nm after 20 min (red) and 30 min (blue) and 6 hours (black)

Already after 20 min irradiation the ratio of the backbone-H shift to the Si-H shift changes, and the latter decreases until it disappears. This may be due to a Si-C bond cleavage, affording the anthracene dimer and an unknown silicon species. During irradiation, the colour of the solution turned from slightly yellow to bright yellow and after 6 hours to a darker orange with a cloudy precipitate on the bottom (see Figure 93). This process was accompanied by a deterioration of the solubility, which made it difficult to get a sufficient "Lock Level" on the NMR machine. Therefore, due the low concentration it was not possible to obtain a reproducible ^{29}Si-NMR shift. A measurement over two days, with a relaxation time of 60 sec showed one shift at -21 ppm. After evaporation of the solvent, small orange crystals were formed, but due to their poor quality it was not possible to get a crystal structure.

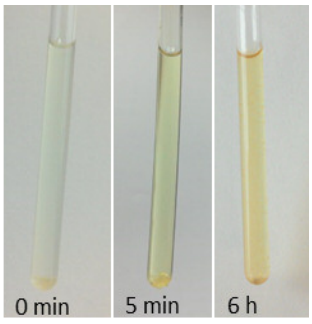

Figure 93: Colour change of the solution during irradiation

Beside the shifts attributed to the [4+4] photodimer, after 5 min irradiation also shifts in the range 5–6.5 ppm appear, that may be attributed to a structure similar to the reported type I (see Figure 6). The intensity does not change notably with continuing irradiation time. The observed shifts fit to the literature data, but the distribution of the formed products differs. The ratio

of Type I: Type III was determined as 2:1 for the irradiation of di-9-anthracenyldimethylsilane,[54] whereas in our case the Type III adduct is the main reaction product. An explanation for this different reaction behavior may be the different steric demand of the hydride protons compared to the methyl groups. Unfortunately, the authors do not give any information about stability of the photodimers or possible isolation. Only ^{1}H-NMR data is provided.

Irradiation of 1-naphthylSiH_3 (**30**) was performed similar to literature at room temperature and at -78 °C with EtOH/N_2.[55] After 60 minutes a slight change in colour was observed, but only the educt shifts can be detected in the ^{1}H-NMR. Also, the irradiation of benzylSiH_3 (**32**) only afforded the educt.

In summary the irradiation of 9-anthracenyl$_2SiH_2$ (**27**) leads to an intramolecular [4+4] adduct, which was characterized *via* ^{1}H-NMR. Due to the instability of the compound no further isolation and characterization was possible. Compounds with a smaller π-system (benzyl, naphthyl) did not undergo a reaction under the given conditions.

3.5.2.1 Grazing Incidence Small Angle Scattering (SAXS) and Deep X-ray Lithography (DXRL) of 9-anthracenyl$_2SiH_2$ (27) in PMMA

To study the effect of high radiation doses on 9-anthracenyl$_2SiH_2$ (**27**), it was embedded into a PMMA (polymethylmethacrylate) matrix and irradiated with hard X-ray radiation between 2 and 20 keV at the Deep X-ray Lithography Beamline of the electron storage ring ELETTRA, Trieste, Italy.[125] The sample was prepared, first, by mixing the silane and the polymer and second, the mixtures were spin coating on a Si-wafer. For details of the sample preparation see 4.8.3.1. Irradiation was performed with increasing radiation doses up to 250 kJ and analyzed with Grazing incidence Small Angle Scattering at the Austrian SAXS beamline at ELETTRA.[126] The incidence angle was set to 0.5°.

Figure 94 shows the vertical cuts of the GISAXS images of PMMA and in comparison with the silane containing PMMA sample. In the latter, a growth of nanostructures can be observed instantly with beginning of the irradiation. In case of the sole polymer, a formation of larger structures (>10 nm) can as well be detected but with a much slower rate.

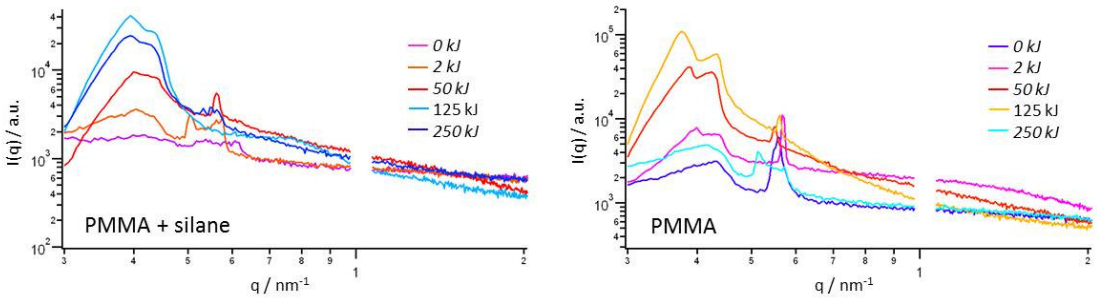

Figure 94: Vertical cuts of the GISAXS images of silane containing PMMA (left) and PMMA (right) at different radiation doses

A curve fit of the GISAXS data of the silane containing polymer (Figure 95) allows a more detailed description of the irradiation induced nanostructure formation. For the analysis a model consisting spherical particles with a Schultz distribution for the particle sizes and a sticky hard sphere model for the structure factor was used.

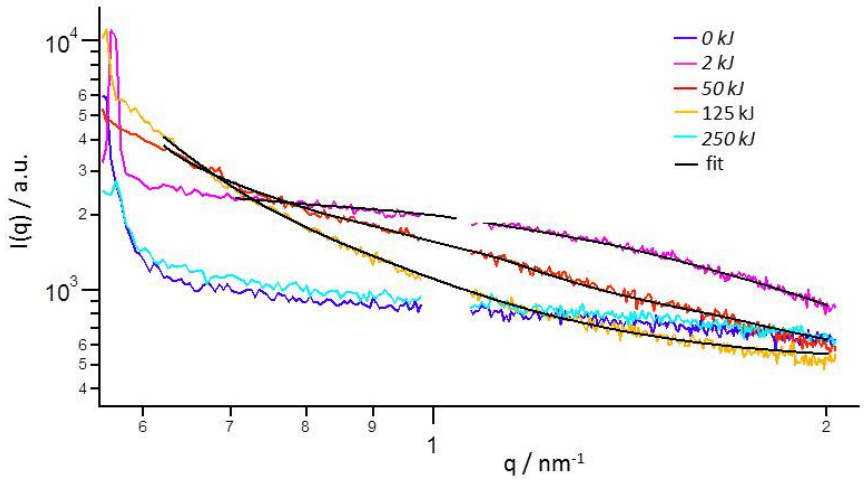

Figure 95: Vertical cuts of the GISAXS data of silane containing PMMA with the resulting fits of the model (described in the text)

Additionally a general Porod term was added for the large structures.[127,128] At a dose of about 2 kJ, particles with a diameter of approximately 3 nm with a spacing of 7 nm can be detected (Figure 96). Upon continued irradiation an increase of size (5 nm) alongside with a wider spacing (11 nm) is observed, which might be attributed to the growth of larger nanostructures by aggregation of the initial smaller ones. The nanostructures continuously grow, until they reach a diameter larger than 10 nm at the highest irradiation dose, which was limited by the resolution of the technique.

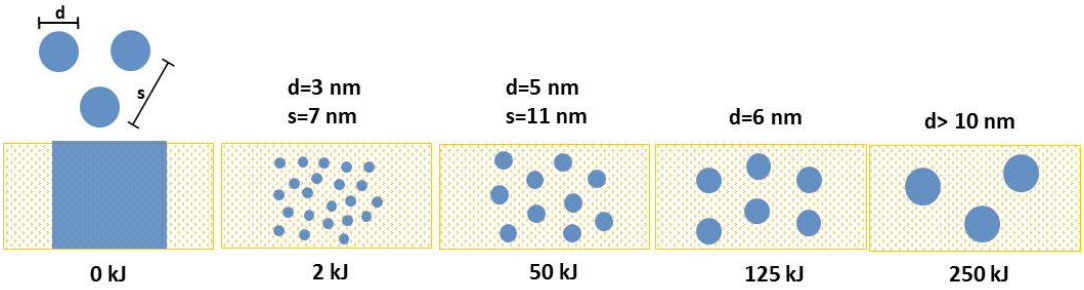

Figure 96: Formation of nanostructures in irradiated silane containing PMMA; d= diameter of particle, s= spacing between particles

The obtained GISAXS data supplements the UV irradiation experiments of 9-anthracenyl$_2$SiH$_2$ (**27**) that led to an intramolecular [4+4] adduct, which rapidly decomposes due to the unstable silacyclopropane structure. In the PMMA films, it seems that the anthracene structure stays unaltered since its typical blue fluorescence can still be observed after the highest irradiation dose (Figure 97). A formation of silicon nanostructures and the anthracene dimer *via* Si-C bond cleavage seems to be probable and is supported by the ^{1}H-NMR data and GISAXS measurements.

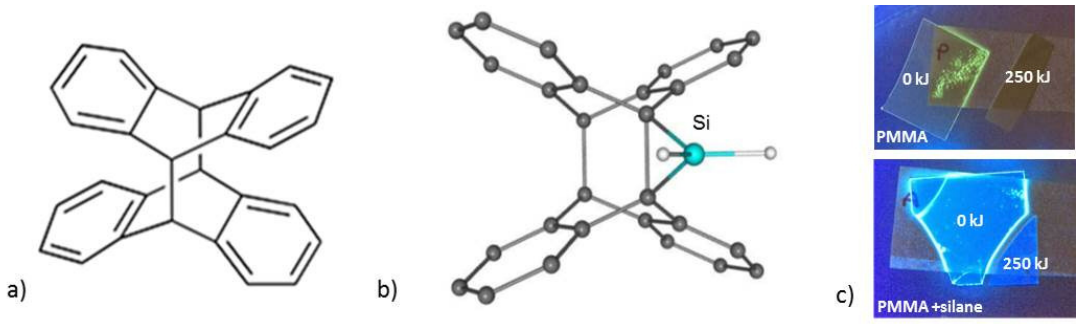

Figure 97: a) photodimer of anthracene; b) proposed structure of irradiation product of 9-anthracenyl$_2$SiH$_2$ (27); c) fluorescence of PMMA (top) and silane containing PMMA (bottom) at different energy doses

3.5.2.2 Time resolved *in situ* GISAXS of 9-anthracenyl$_2$SiH$_2$ (27) in PMMA

For investigating the thermolysis of unaltered and irradiated 9-anthracenyl$_2$SiH$_2$ (**27**) an in situ structural study was performed under gracing incidence conditions. Therefore 9-anthracenyl$_2$SiH$_2$ (**27**) was embedded into a PMMA (polymethylmethacrylate) matrix and spin coated on a Si-wafer (for the exact methods see 4.8.3.1). The final film (unaltered and with 250 kJ dose) was heated to 440 °C with an Anton Paar DHS 1100 under argon atmosphere. The reaction was monitored by *in situ* GISAXS measurement.

Figure 98 shows the vertical cuts of the GISAXS pattern of PMMA and silane containing PMMA. A different reaction behavior can be observed. In case of the silane containing

sample a sudden formation of particles is detected, which is independent from the irradiation dose.

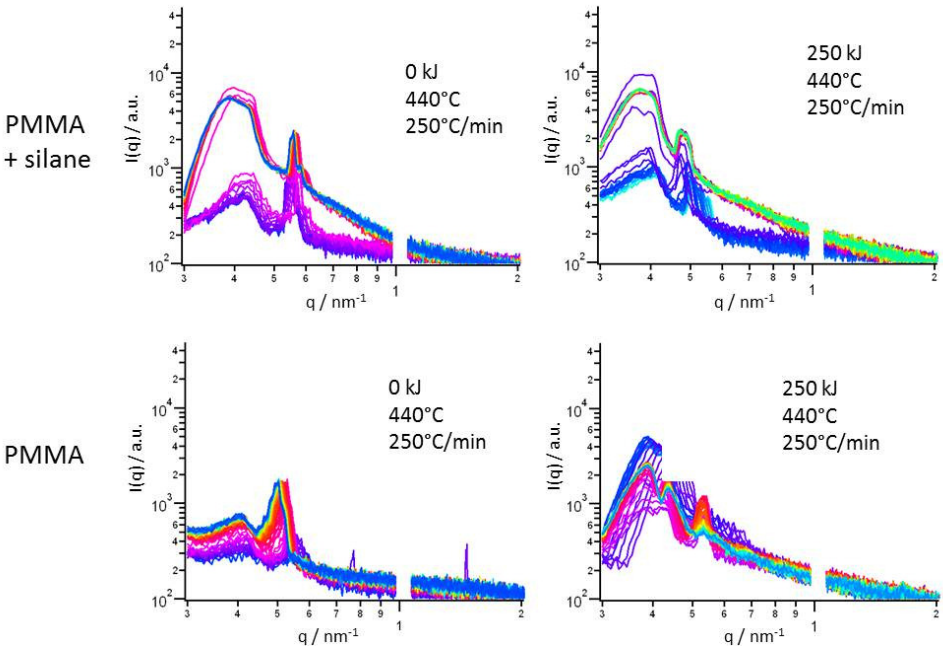

Figure 98: GISAXS of silane containing PMMA (top) and PMMA (bottom) and at different energy doses and heating to 440 °C

An easy accessible quantity is the correlation length of the particles derived by dividing the moments of the scattering pattern.[129] As a sensitive indicator the differential correlation length given by the difference of the correlation length to its initial value was used.

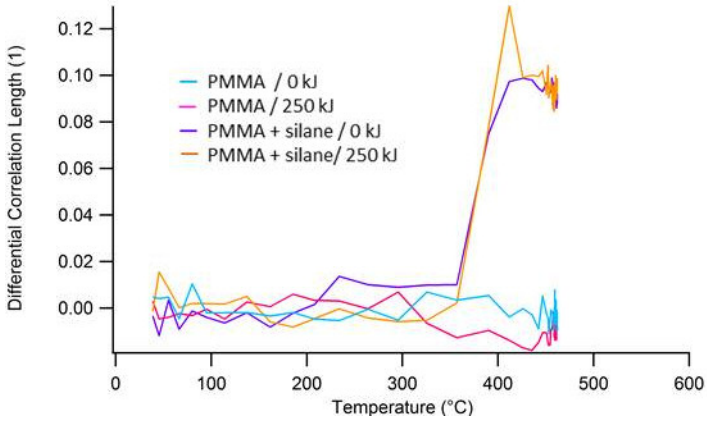

Figure 99: Correlation lengths of observed particles

Plotting of the differential correlation lengths against the temperature (Figure 99) shows the rapid formation of particles in the range of 380-400 °C, which fits very well to the observed decomposing temperature of 9-anthracenyl$_2$SiH$_2$ (**27**), detected by TGA/DSC analysis. These findings match the detected particle formation observed in thermolysis experiments.

3.5.3 Deep X-Ray Lithography (DXRL) of organo silane films

The influence of irradiation on thin films of various silanes was investigated. The samples were irradiated with increasing energy doses on double sided polished Si-wafers (IR transparent) and analyzed *via* IR measurement. To prevent interference of the subjacent silicon during EDX measurements, the substrate was changed to molybdenum. Only the highest dose (7044 J/cm^2) was applied to these samples. Figure 100 shows the exemplified IR-spectrum of 1-naphthyl$_2$SiH$_2$ (**25**), which was spin coated on a Si-Wafer.

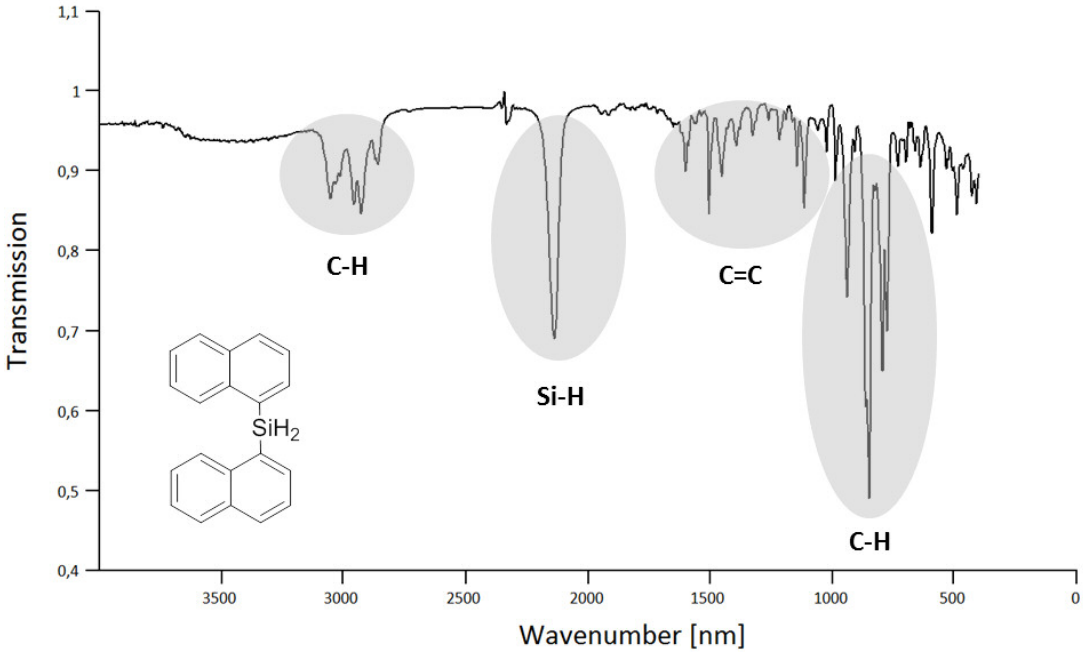

Figure 100: IR-spectrum of 1-naphthyl$_2$SiH$_2$ (25) thin film on a Si-wafer

The silane shows a strong band at 2100 cm^{-1}, which can be attributed to the Si-H group. In the region between 3100-3000 cm^{-1}, the symmetric and asymmetric stretching vibration of the aryl C-H can be seen. The bands between 2000 and 1600 cm^{-1} can be assigned to C=C vibrations of the aromatic system. Around 900 nm the vibrations of the aromatic C-H can be found. The samples were mounted on a carrier and irradiated at five different energy doses. Figure 101, Figure 103, Figure 105, Figure 107 and Figure 109 show the IR-spectra of the different silanes before irradiation, after a dose of 1760 J/cm^{-1} and after the maximum dose of 7044 J/cm^{-1}. All other doses are omitted for clarity.

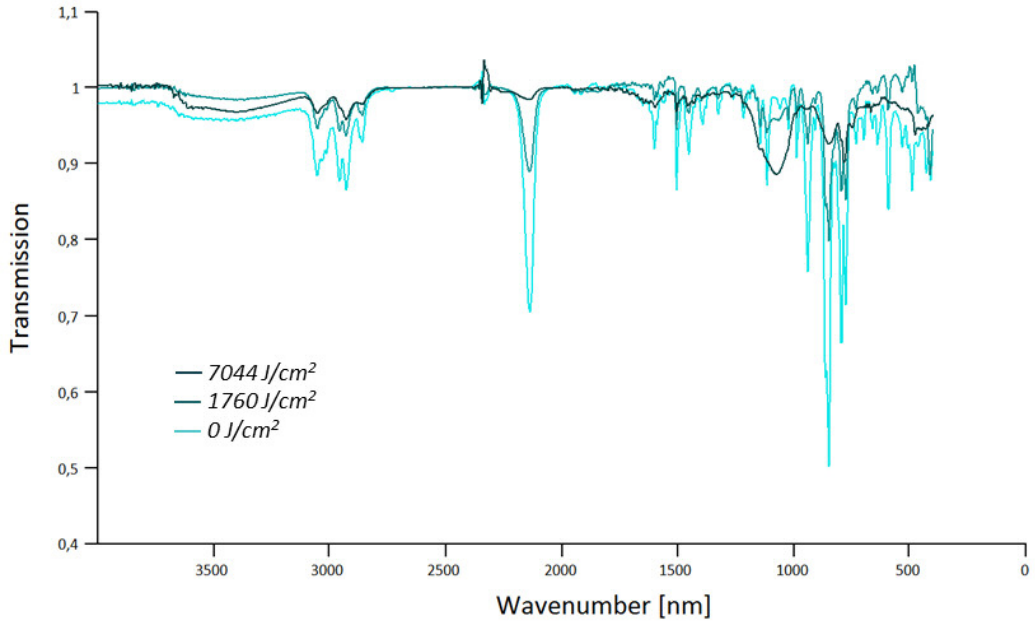

Figure 101: IR of 1-naph$_2$SiH$_2$ (25) at different doses.

1-Naphthyl$_2$SiH$_2$ (**25**) (see Figure 101) shows a decrease in the 2100 cm^{-1} band with increasing doses, accompanied by the formation of a strong broad band at 1100 cm^{-1} and a weaker band in the range of 3200 – 3600 cm^{-1}. At the highest dose, the band at 2100 cm^{-1} has almost disappeared. Figure 102 shows the exposed and unexposed 1-naphthyl$_2$SiH$_2$. The unexposed side shows an arrangement of the crystallites that is lost on the exposed side. EDX analysis showed a slight decrease in the carbon content and an increase in the oxygen value (for details see Appendix).

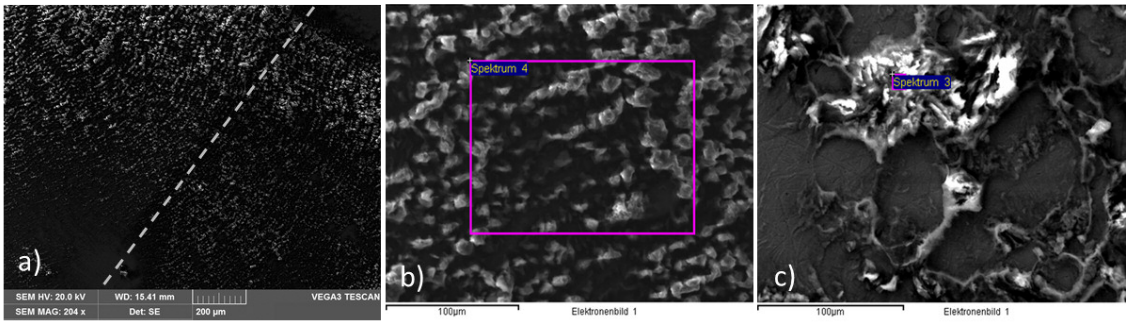

Figure 102: SEM/EDX of 1-naph$_2$SiH$_2$ (25), 7044 J/cm^2

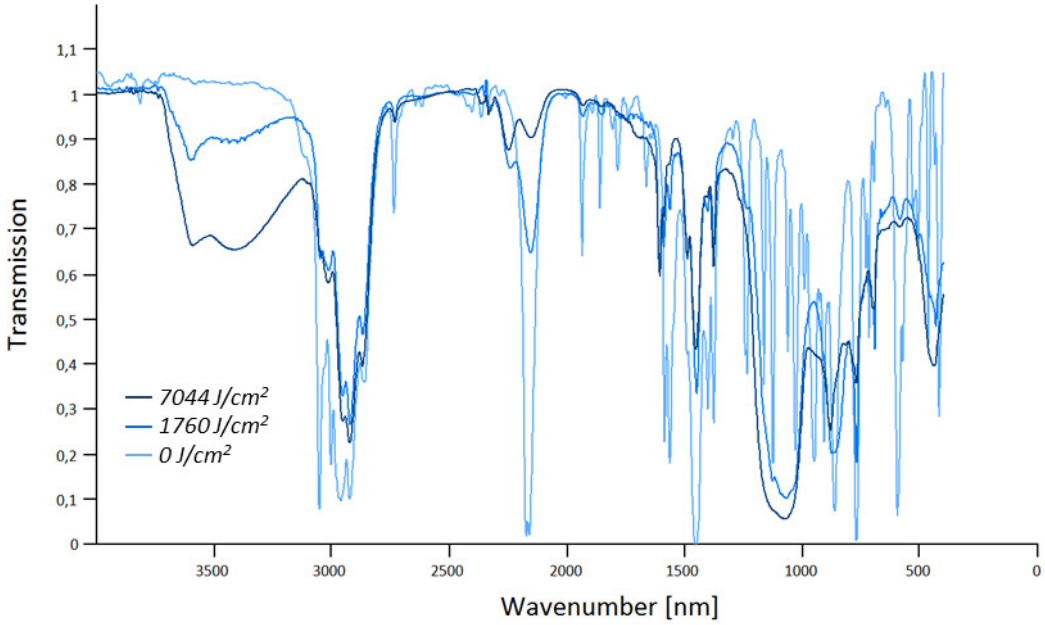

Figure 103: IR of 2,6-xyly$_2$SiH$_2$ (28) at different doses.

2,6-Xylyl$_2$SiH$_2$ (**28**) (see Figure 103) shows a decrease in the 2100 cm^{-1} band with increasing doses. At the highest dose the Si-H peak can still be detected, but a second band at 2260 cm^{-1} starts forming at 1760 cm^{-1}. The increase of the dose leads to the formation of a strong broad band at 1100 cm^{-1} and second band in the range of 3200 – 3700 cm^{-1} that overlaps with a strong peak at 3600 cm^{-1}. Figure 104 shows the exposed and unexposed 2,6-xylyl$_2$SiH$_2$. Irradiation leads to a glass-like homogenous layer that differs clearly from the unexposed sample. EDX analysis showed a slight decrease in the carbon content and an increase in the oxygen value (for details see Appendix).

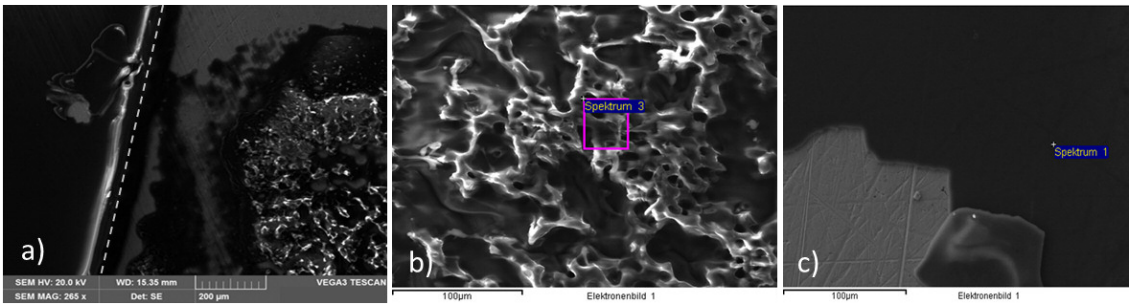

Figure 104: SEM/EDX of 26-xylyl$_2$SiH$_2$ (28), 7044 J/cm^2

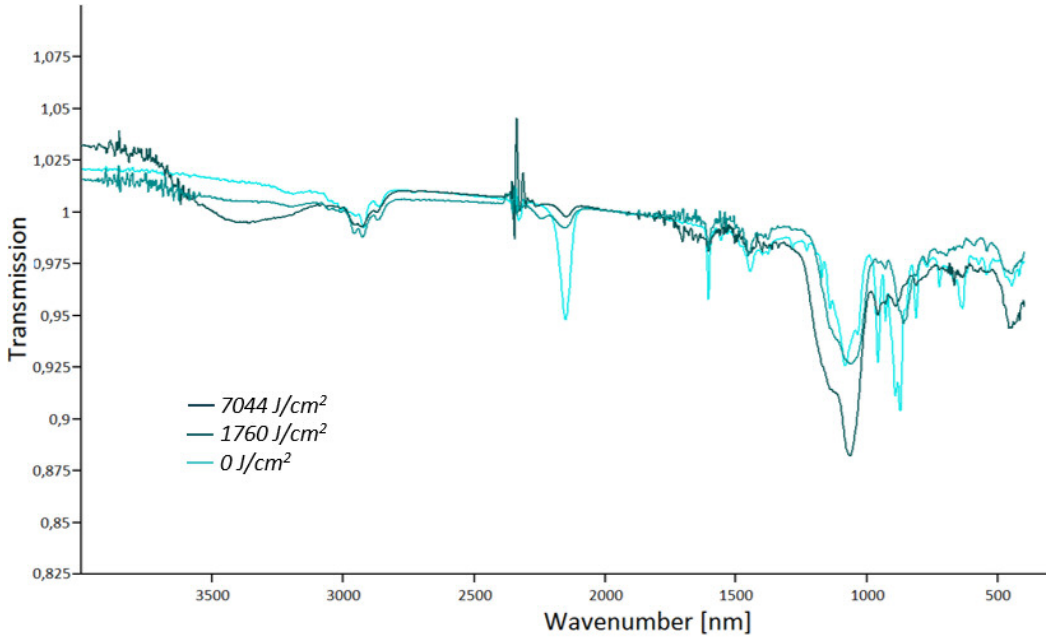

Figure 105 : IR of 2,4-xylylSiH$_3$ (29) at different doses

2,4-xylylSiH$_3$ (**29**) (see Figure 105) shows a decrease in the 2100 cm^{-1} band with increasing doses. At the highest dose the Si-H peak can still be detected, but a second band at 2260 cm^{-1} starts forming at 1760 J/cm^2. The increase of the dose leads to the formation of two strong broad overlapping bands at 1140 and 1070 cm^{-1}, accompanied by a second band in the range of 3100 – 3700 cm^{-1}. Figure 106 shows the exposed and unexposed 2,4-xylylSiH$_3$. The coating of the unexposed side is rather inhomogeneous, showing also uncoated areas. Exposure leads to a very thin glass-like homogeneous layer. EDX analysis shows no significant difference in the carbon and oxygen content (see Appendix) for the exposed and unexposed sample.

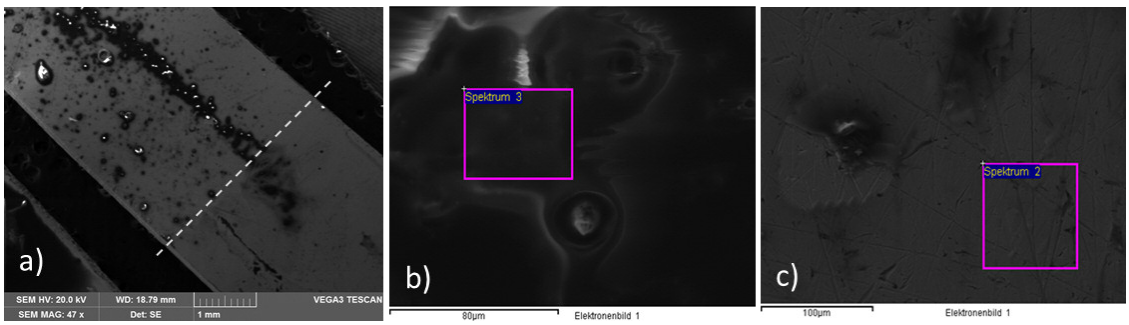

Figure 106: SEM/EDX of 2,4-xylylSiH$_3$ (29), 7044 J/cm^2

p-*n*-Butylphenyl$_2$SiH$_2$ (**23**) (see Figure 107) shows a decrease in the 2100 cm^{-1} band with increasing doses, accompanied by the formation of a broad band at 1100 cm^{-1} and a weaker band in the range of 3200 – 3600 cm^{-1}. At the dose of 7044 J/cm^{-1} the band at 2100 cm^{-1} has disappeared. Figure 108 shows the exposed and unexposed *p*-*n*-

butylphenyl$_2$SiH$_2$. Irradiation leads to a glass-like homogeneous layer that differs clearly from the unexposed sample. EDX analysis shows no significant difference in the carbon and oxygen content (for details see Appendix for the exposed and unexposed sample.

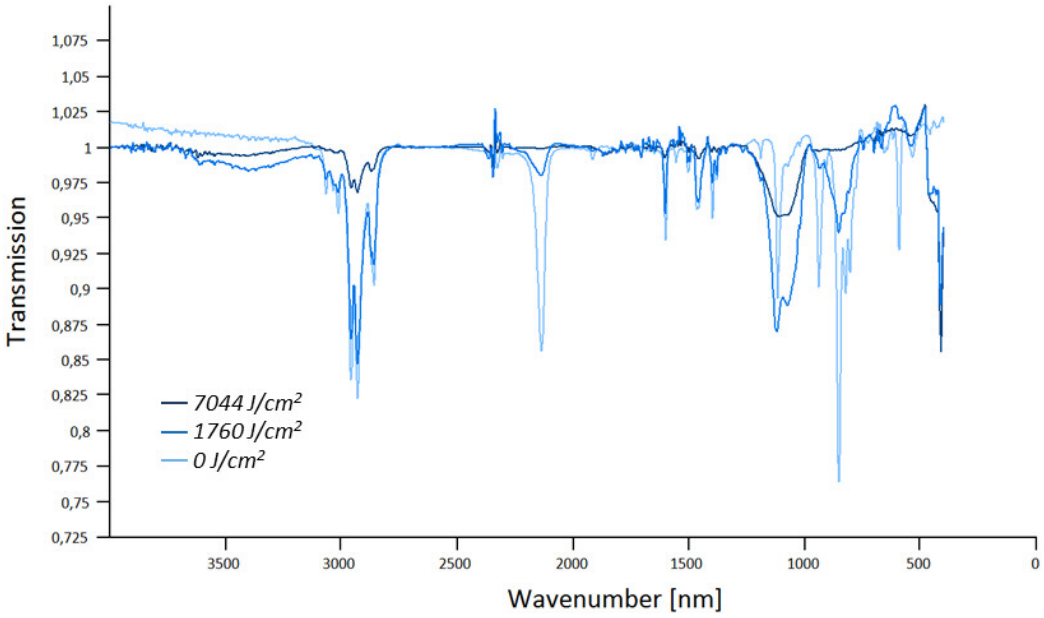

Figure 107: IR of p-n-butylphenyl$_2$SiH$_2$ (23) at different doses.

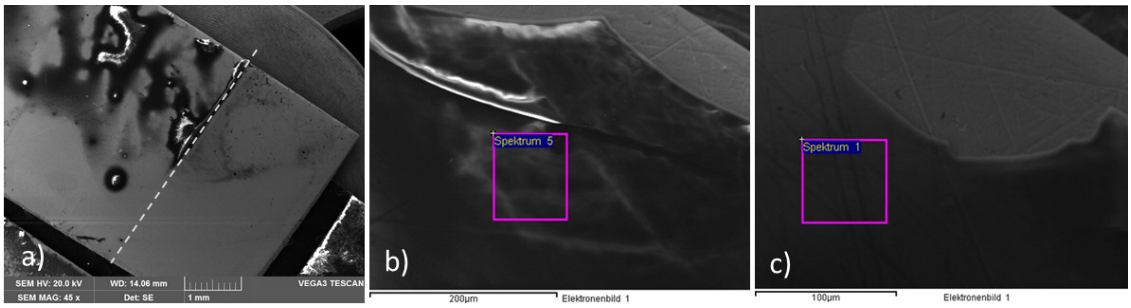

Figure 108: SEM/EDX of *p-n*-butylphenyl$_2$SiH$_2$ (23), 7044 J/cm^2

Spin coating of 9-anthracen$_2$SiH$_2$ (**27**) did not give a layer on the surface, but needles formed on the edges of the molybdenum substrate. The sample was irradiated as a whole. Despite of the coating problems an effect of the irradiation on the IR spectra of the compound can be detected. Again a decrease in the 2100 cm^{-1} band with increasing doses can be seen, accompanied by the formation of a strong broad band at 1100 cm^{-1} and very weak band in the range of 3200 – 3600 cm^{-1} (see Figure 109) . At the highest dose the band at 2100 cm^{-1} has disappeared. Figure 110 shows the exposed 9-anthracen$_2$SiH$_2$. EDX analysis showed a high oxygen content of the sample (for details see Appendix).

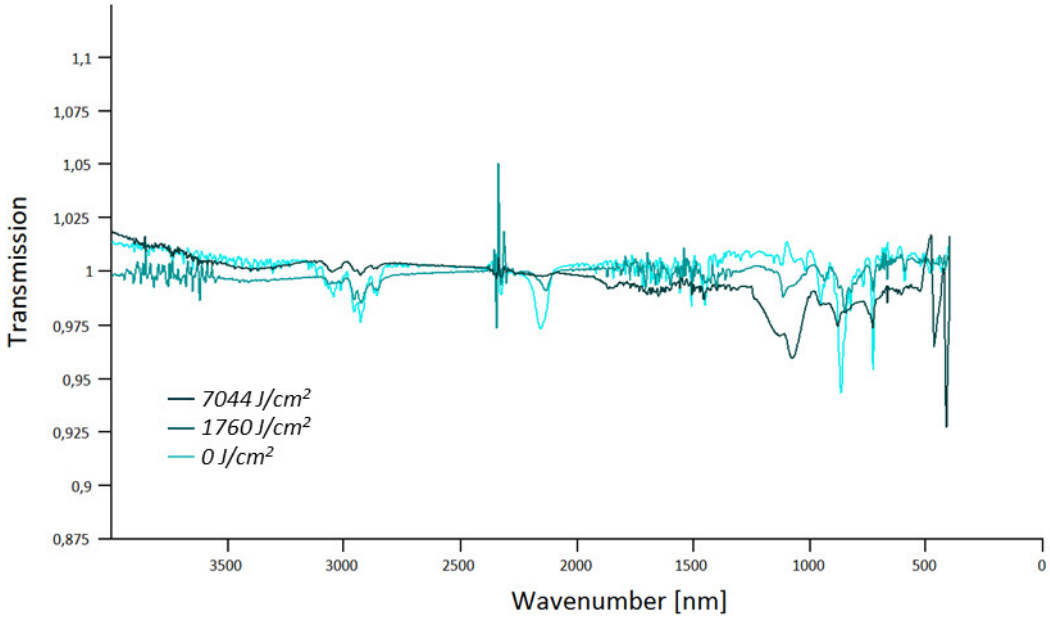

Figure 109: IR of anthracenyl$_2$SiH$_2$ (27) at different doses.

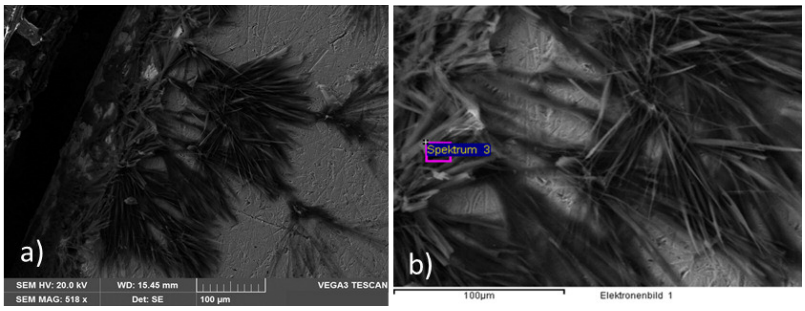

Figure 110: SEM/EDX of 9-anthracenyl$_2$SiH$_2$ (27), 7044 J/cm^2

The spin coating of phenyl$_8$Si$_4$ and [phenyl$_2$Si]$_n$ did not give any visible films on the surface. No analysis was possible.

The irradiation of the arylsilanes leads in all cases to an intensity decrease or disappearance of the Si-H peak at 2100 cm^{-1}. To confirm that this finding is caused by the irradiation and not by the reactivity of the silane itself towards air or moisture, further experiments were performed. 2,6-xylyl$_2$SiH$_2$ (**28**) and 9-anthracenyl$_2$SiH$_2$ (**27**) were stored under air for 24 h and the IR-spectra compared to silane samples which were stored under inert conditions (see Appendix). No change in the spectra was observed, which leads to the conclusion that no reaction with air takes place.

A possible explanation of the decrease of the 2100 cm^{-1} peak would be the breaking of the Si-H bond. A similar behavior was investigated for the irradiation of CPS (cyclohexasilane) with UV-irradiation. The observed Si-H bond breaking led to a polymerization of the compound. This reaction would also be possible for the arylsilanes and would fit to the finding that the composition of the formed layer does not differ very much from

the starting material. C-H vibrations can be observed even after the highest doses, which suggests that the organic groups are generally not influenced by the irradiation. The broad peaks at ~ 3700 cm^{-1}, 3200 – 3600 cm^{-1} as well as the peak at 1080 – 1100 cm^{-1} would suggest various Si-O and Si-OH moieties, which would fit to the finding that the oxygen value of the exposed sample is slightly higher than the unexposed ones.

In summary a breaking of the Si-H bond followed by a oxidation is presumed to be occuring. A breaking of the Si-C bond is not supposed. In addition a breaking of the C-C bond of the aryl moiety is unlikely, due to the existence of the C-H vibrations even after the highest irradiation doses. The EDX spectra as well shows a high carbon content in the resulting films. The irradiation seems to lead to glass like layers which show a much higher homogeneity than the unexposed films. Further analysis and characterization might lead to interesting properties.

3.5.4 Selective Chlorination with TCCA

Up to date various methods are used to synthesize chlorosilanes *via* the corresponding silicon hydrides. Transformation of the Si-H bond to Si-Cl can be achieved by acyl chloride,[130,131] thionyl chloride,[132,133] phosphorus trichloride,[131,134] phosphorus pentachloride,[135] and oxalyl chloride with aluminum trichloride[136] based methodologies. Only few methods for a selective monochlorination of silanes have been described thus far, including reaction with tintetrachloride in dibutylether,[137] an iron-catalyzed method with acetyl chloride as the chlorine donor[138] as well as the use of stoichiometric copper chloride in combination with catalytic amounts of copper iodide.[139] A brief review on the halogenation of silanes and the applications of halosilanes has also been given by Kunai and Ohshita.[140]

Many of the above mentioned methods suffer from difficulties in handling the often toxic reagents, low yields, or tedious workup procedures.[141] In 2007 Stutts *et al.* reported on the efficient chlorination of silicon hydrides with the inexpensive and easy to handle trichloroisocyanuric acid (TCCA). In this chloroimide, all three chlorine atoms are available for the reaction due to the lower energy state resulting from the aromatization following the substitution of the 3 chlorine atoms by hydrogen (see Figure 111).[141]

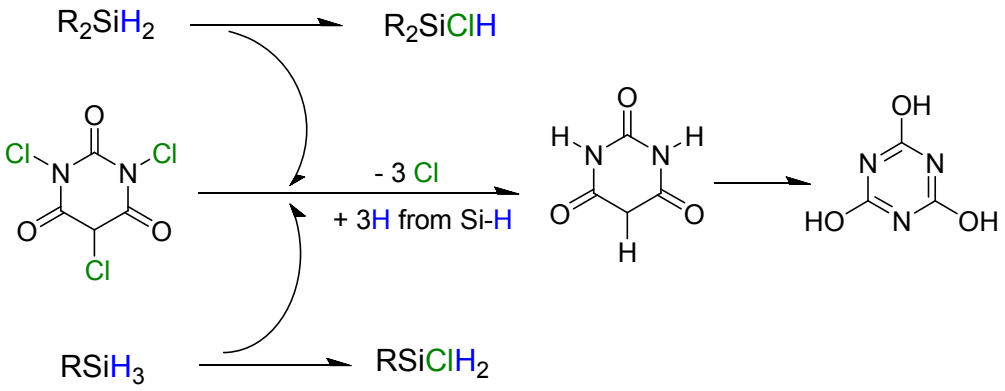

Figure 111: Reaction scheme for the chlorination of R_2SiH_2 and $RSiH_3$ with TCCA

Several silanes including phenyl$_3$SiH, *t*-butyl$_3$SiH, phenylmethylSiH$_2$ as well as siloxanes such as (methylHSiO)$_4$ were reacted with a slight excess of TCCA to obtain the corresponding chlorosilanes in yields of 90% or greater. The reaction time showed to be dependent on the number of hydrogen atoms and the sterical demand of the starting silane. THF proved to be suitable for most reactions with the necessity to perform the

TCCA addition at -20 °C to control the exothermic reaction and prevent chlorination of THF. [141]

In our working group the utility of TCCA in the selective chlorination of α-ω-dihydrosiloxanes was already investigated. Tetramethyldisiloxane gave the monochlorinated chlorotetramethyldisiloxane in a yield of 70%. 15% remained as unreacted educt alongside with 15% of the dichlorinated 1,2-dichlorodisiloxane.[142] In the present study the substitution of a single hydride by a chlorine atom in secondary and primary aryl and alkyl silanes with a stoichiometric amount of TCCA was investigated. 1-naphthyl$_2$SiH$_2$ (**25**), 1-naphthylSiH$_3$ (**30**), phenyl$_2$SiH$_2$, phenylSiH$_3$, 9-anthracenyl$_2$SiH$_2$ (**27**), ethyl$_2$SiH$_2$ and *t*-butyl$_2$SiH$_2$ were used as starting silanes.

In a typical reaction, 1 mmol of the silane was dissolved in 3–5 mL dry THF, cooled to -20 °C. 0.33 mmol TCCA was added portionwise while vigorously stirring the solution. After complete addition, the cooling bath was removed and the solution warmed to room temperature. The reactivity was investigated without refluxing of the solution. After a certain reaction time (depending on concentration and used silane) a clouding of the solution was observed. The solution was filtered and analyzed *via* GC-MS and NMR to monitor the reaction.

The chlorination of phenyl$_2$SiH$_2$ with 0.33 mmol TCCA did not result in the formation of the desired monochlorinated product. To investigate the optimum reaction conditions, stoichiometry, solvent amount and reaction/addition times were varied (see Table 17 and Table 18).

Table 17: Reaction of phenyl$_2$SiH$_2$ (= educt) with TCCA; variation of stoichiometry. E:TCCA describes the ratio of Si-H to chlorine atoms of TCCA

Exp.	Educt [mmol]	TCCA [mmol]	E:TCCA	Ph$_2$SiHCl [%]	Ph$_2$SiH$_2$ [%]	Ph$_2$SiCl$_2$ [%]
A	0.99	0.33	1:1	53.2	46.8	0
B	0.99	0.36	1:1.1	51.5	48.5	0
C	0.99	0.49	1:1.5	66.0	34.0	0
D	0.99	0.59	1:1.78	76.2	1.60	22.5
E	0.99	0.60	1:1.82	76.4	0	23.6
F	0.99	0.66	1:2	86.3	0	13.7
G	0.99	0.70	1:2.12	73.0	0	27.0
H	0.99	0.74	1:2.24	73.5	0	26.5

Reaction of phenyl$_2$SiH$_2$ with TCCA in the ratio 1:1 (Si-H to available chlorine atoms) leads to a formation of 50% product, alongside with 50% unreacted educt (see Figure 112).

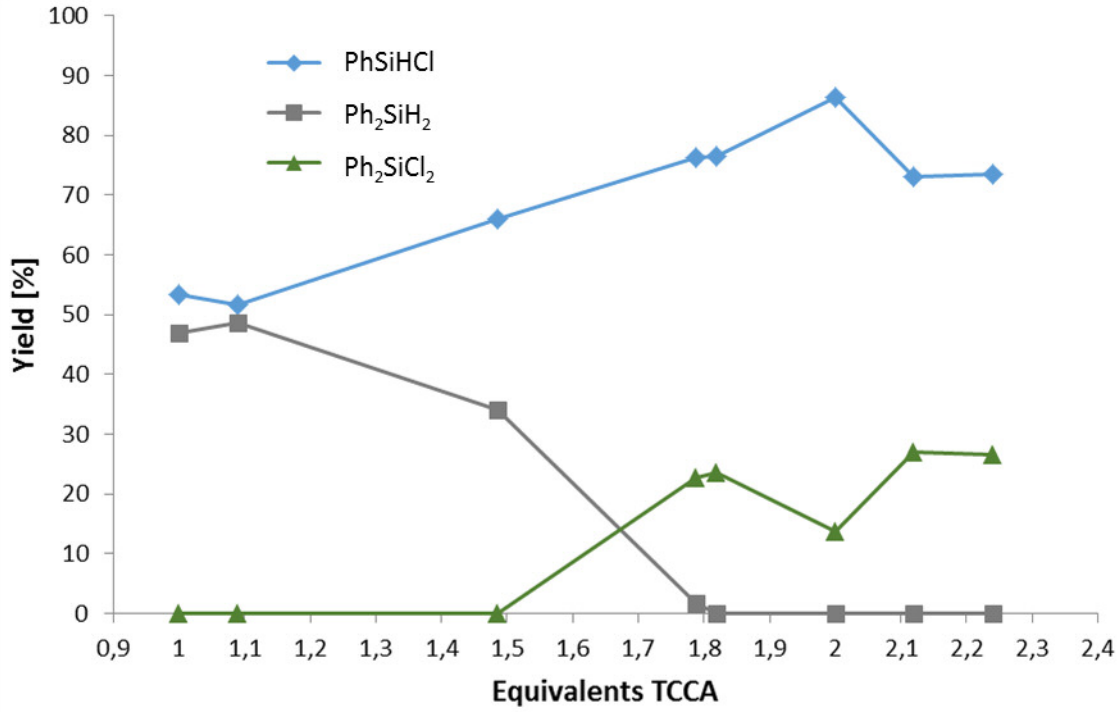

Figure 112: Reaction of phenyl$_2$SiH$_2$ (= educt) with TCCA; variation of stoichiometry

When the ratio is increased, a higher product formation can be investigated. At 1:1.5 still 34% educt are present but the formation of the dichlorinated species can as well be observed. The best distribution between educt, product and dichlorinated species can be found at a ratio of 1:2. About 86% phenyl$_2$SiHCl is formed, beside a small amount of phenyl$_2$SiCl$_2$. To eliminate the possibility of unsuitable reaction conditions as cause for the product distribution at a 1:1 ratio, the influence of a variation of the reaction parameters was investigated (Table 18). A change in the reaction time (Exp. A1, A2 and A3) did not lead to an increase in product formation. This finding would suggest a side reaction that leads to a decrease of the reactivity of the TCCA. The GC-MS of those samples shows some compounds (~360 m/z) at larger retention times (~ 18 min) that would fit to condensation products of the partly with the fully reacted TCCA. This assumption would fit to the increase of educt in the reaction when the TCCA is added more rapidly (Exp. A4). Changing the solvent volume to 2 mL did not give a certain change in the yields (Exp. A5), but an even more concentrated reaction (Exp. A6) gave rise to the formation of the dichlorinated species.

Table 18: Reaction of phenyl$_2$SiH$_2$ (= educt) with TCCA (E:TCCA=1:1); variation of reaction parameters RT=reaction time, AT= addition time, C= concentration

Exp.	Solvent [mL]	Addition time [min]	Reaction time [min]	Ph_2SiHCl [%]	Ph_2SiH_2 [%]	Ph_2SiCl_2 [%]	Var.
A1	5	10	60	52.28	47.72	0	RT
A2	5	10	120	46.17	53.83	0	RT
A3	5	10	1020	47.06	52.94	0	RT
A4	5	5	45	24.51	75.49	0	AT
A5	2	10	45	53.49	46.51	0	C
A6	1	10	45	47.76	50.98	2.57	C
A7	10	10	120	61.23	38.25	0.82	C

A more diluted sample with 120 min reaction time (Exp. A7) did give somewhat higher product yields but still a large amount of unreacted silane is present. The product educt ratio of all experiments with a 1:1 stoichiometry is in the same range (see Figure 113). This reproducibility shows that for the selective chlorination of phenyl$_2$SiH$_2$ a different TCCA to educt ratio might be favorable.

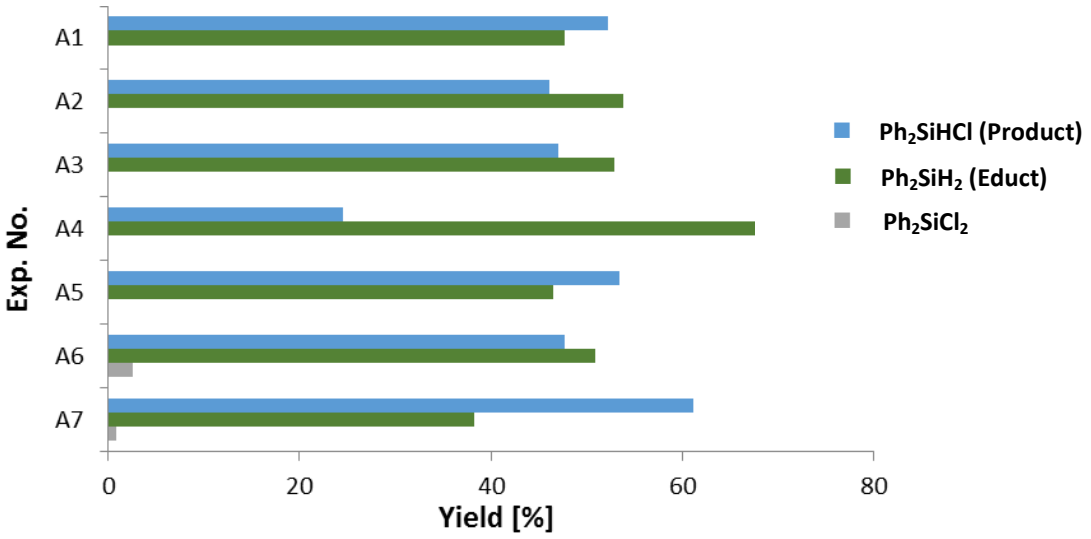

Figure 113: Variation of parameters for educt:TCCA=1:1; yield of Ph_2SiHCl, Ph_2SiH_2 and Ph_2SiCl_2

The 1:2 ratio of educt to TCCA gave the best product distribution in the preliminary test, hence the influence of a variation of the reaction parameters was investigated for this reaction as well (see Table 19). If the reaction solution is concentrated to 2 mL (Exp. F1) an increased amount of the dichlorinated species is observed. Diluting to 10 ml (Exp. F2) leads to very good product distribution. 86% of the desired monochlorinated product are formed aside with a small amount of phenyl$_2$SiCl$_2$. A five times scale up (Exp. F3), followed by bulp to bulp distillation gave 80% of phenyl$_2$SiHCl (Exp. F4).

Table 19: Reaction of Ph_2SiH_2 (= educt) with TCCA (E:TCCA=1:2); variation of reaction parameters RT=reaction time, AT= addition time, C= concentration; $TCCA^1$= TCCA powder, $TCCA^{2=}$ THF solution of TCCA

Exp.	Solvent [mL]	Addition time [min]	Reaction time [min]	Ph_2SiHCl [%]	Ph_2SiH_2 [%]	Ph_2SiCl_2 [%]	Var.
F1	2	10	45	72.96	0	27.04	C
F2	10	10	60	83.66	0	16.34	C
F3	50	30	60	79.02	0	20.98	scale up
F4	50	30	60	80.93	0.62	18.56	work-up
F5	5	30	45	86.78	0	13.22	AT
F6	50	60	45	66.90	0	33.10	scale up
F7	50	60	45	70.37	0	29.62	work-up
F8	10	10	1080	79.67	3.62	17.34	RT
F9	5	10	45	50.51	48.39	2.14	$TCCA^1$
F10	20+10	30	60	40.74	59.26	0	$TCCA^2$

When the addition time is increased to 30 minutes (Exp. F5) the highest product yield is observed. A 10 times scale up (Exp. F6), followed by work up (Exp. F7) led to 70% yield of the product. A more diluted sample with long reaction time (Exp. F8) gave good yields but also a slightly increased $phenyl_2SiCl_2$ formation is detected. Using a powdered TCCA (Exp. F9) did give lower product yield aside with unreacted educt. This might be caused by the difficult addition of the very fine powder in the counter gas flow. A THF solution of TCCA, which was added drop wise to the dissolved silane (Exp. F10) led to a rather low product yield. The solution was cooled to -20 °C before addition. Due to the long addition time the solution warmed to approximately 0 °C. This temperature might be insufficient to prevent side reactions of the TCCA with the THF. Figure 114 shows the product distribution for the 2:1 ratio of educt to TCCA.

In summary slow addition of TCCA to an approx. 0.2 molar silane solution and a reaction time of 45-60 minutes with the appropriate stoichiometry led to the best product distribution.

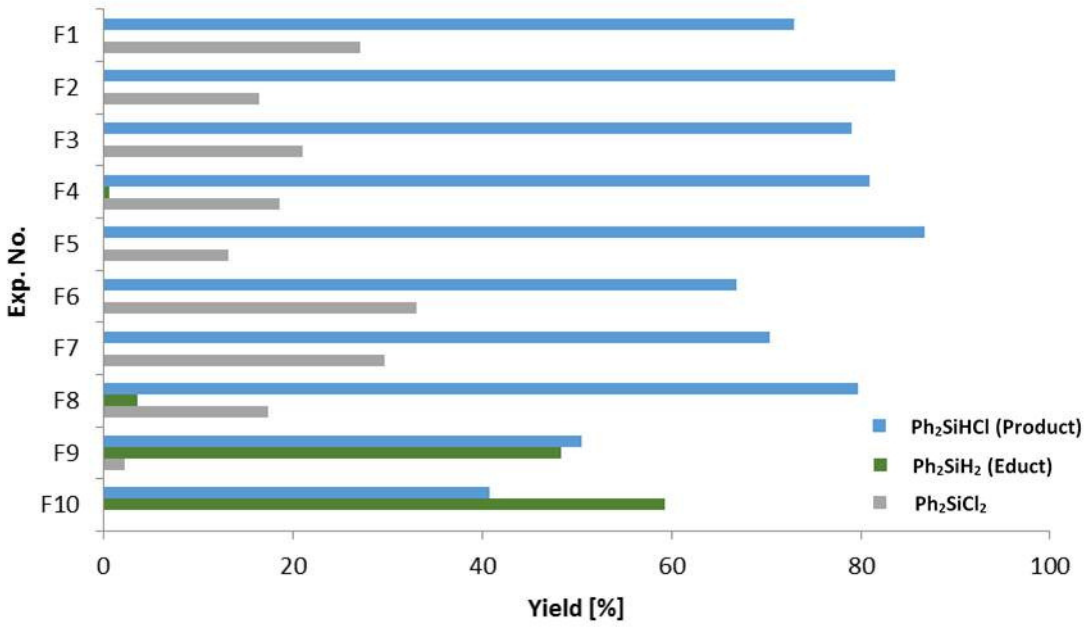

Figure 114: Variation of parameters for educt:TCCA=1:2; yield of Ph_2SiHCl, Ph_2SiH_2 and Ph_2SiCl_2

The reaction with the best product distribution (F5) was filtered and purified *via* bulb to bulb distillation, followed by NMR analysis. The ^{1}H- and ^{29}Si-NMR spectra are shown in Figure 115.

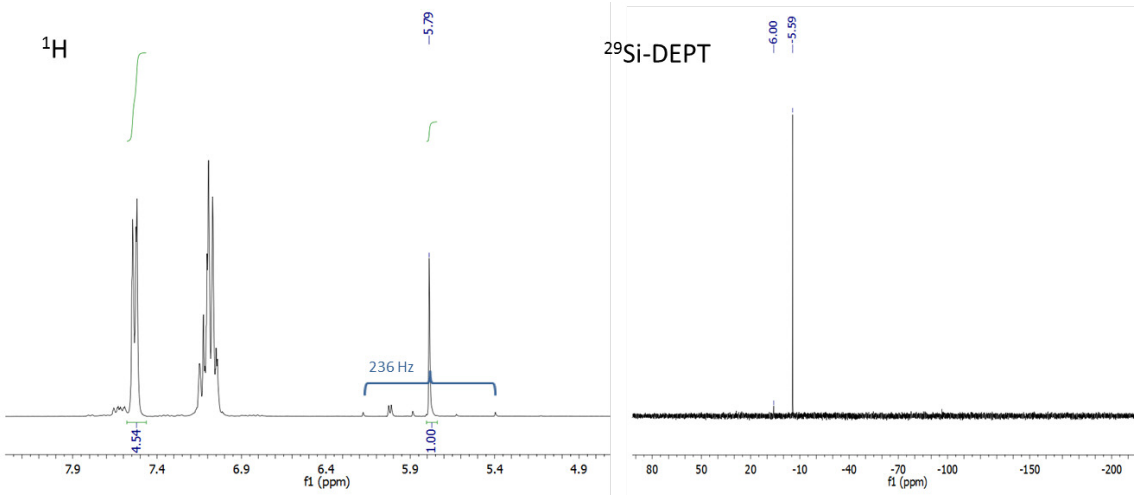

Figure 115: ^{1}H-NMR and ^{29}SiDEPT spectrum of F5 in C_6D_6

The ^{1}H-NMR spectrum shows the newly formed Si-H hydrogen shift at 5.79 ppm. A coupling constant of 236 Hz is observed, which differs from the value for the educt. $Phenyl_2SiH_2$ shows a Si-H hydrogen shift at 5.11 ppm and a coupling constant of 198 Hz. The observed integral intensities of the Si-H proton to the proton in position *ortho* to the silicon are 1:4.5, which fits to the product distribution. The Si-DEPT spectrum shows a peak at -5.59 ppm, which is attributed to product diphenylchlorosilane. A sec-

ond shift at 6.00 ppm shows the dichlorinated species. According to the GC-MS data, about 10% of diphenyldichlorsilane are formed.

The selective chlorination of the secondary silane 1-naphthyl$_2$SiH$_2$ (**25**) (Table 20) was investigated at a 1:1 ratio of educt to TCCA, with different concentrations (Exp. K; L and M). The best product distribution was obtained with a 0.3 molar silane solution and an addition time of 30 minutes.

Table 20: Reaction of secondary silanes (= educt) with TCCA; n.d = not detectable

Exp.	Silane	E:TCCA	Solvent [mL]	Reaction time [min]	R_2SiH Cl [%]	R_2SiH_2 [%]
K	1-naphthyl$_2$SiH$_2$ (**25**)	1:1	5	40	82.93	17.07
L	1-naphthyl$_2$SiH$_2$ (**25**)	1:1	10	60	62.23	37.77
M	1-naphthyl$_2$SiH$_2$ (**25**)	1:1	3	60	96.12	3.88
N	ethyl$_2$SiH$_2$	1:1	5	60	29.19	26.83
O	*t*-butyl$_2$SiH$_2$	1:1	5	60	56.52	43.47
P	9-anthracenyl$_2$SiH$_2$ **(27)**	1: 2	5	60	n.d	n.d

The ^{1}H-NMR spectrum (see Figure 116) shows the newly formed Si-H hydrogen shift at 6.42 ppm. A coupling constant of 236 Hz is observed, which differs from the value for the educt. A small amount of educt can still be detected in this reaction, which can be identified via the Si-H hydrogen shift. 1-naphthyl$_2$SiH$_2$ shows a Si-H hydrogen shift at 5.47 ppm and a coupling constant of 199 Hz.

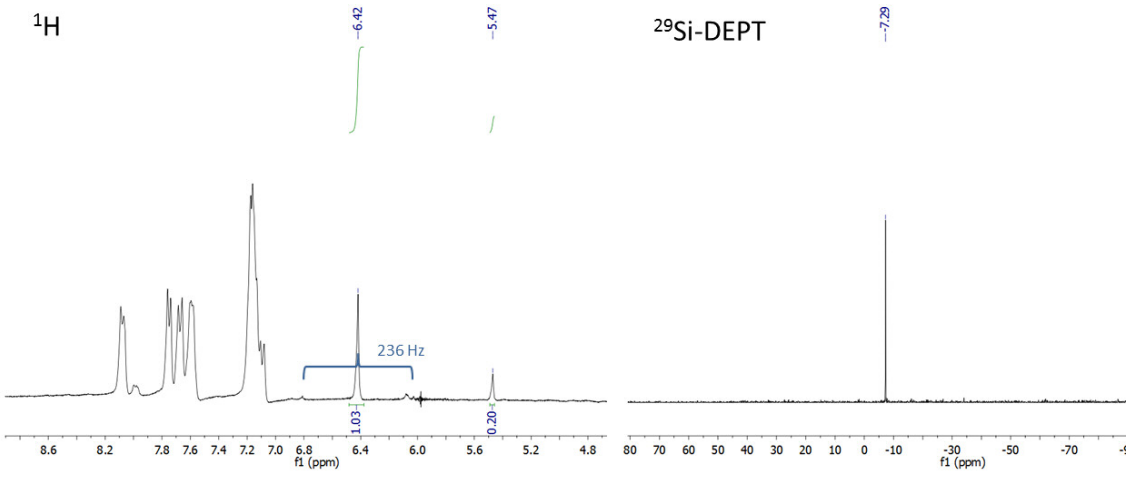

Figure 116: ^{1}H-NMR and ^{29}SiDEPT spectrum of TCCA reaction of 1-naphthyl$_2$SiH$_2$ (25) in C_6D_6 (Exp.M)

The Si-DEPT spectrum shows a peak at -7.28 ppm, which is attributed to product di-1-naphthylchlorosilane (Figure 116). The shift of the educt at -39 ppm can not be detected, which might be due to the low signal to noise ratio despite using an overnight measurement with long relaxation delay (d1=60 sec).

The selective chlorination of diethylsilane (Exp. N) with TCCA gave the product in 30% yield, aside with 26% unreacted educt. The product distribution shows about 44% siloxanes. The MS-data allows the characterization of various siloxanes like tetraethyldisiloxane, 1-chlorotetraethyldisiloxane, 1,2-dichloro-tetraethylsiloxane, hexaehtyltrisiloxane and 1,3-dichloro-hexaethyltrisiloxane which are formed through reaction of the monochlorinated and the dichlorinated product with OH-functionalities *via* HCl elimination. It is not sure if those hydrolysis products are derived from a reaction of the chlorinated silane with moisture or from the fully reacted TCCA (see Figure 117).

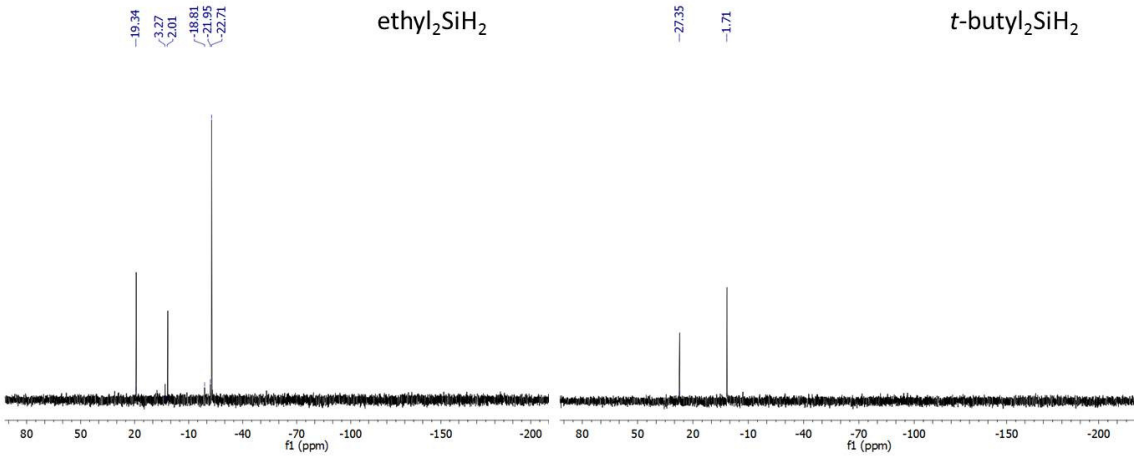

Figure 117: ^{29}SiDEPT spectrum of TCCA reaction of ethyl$_2$SiH$_2$ (Exp. N) and *t*-butyl$_2$SiH$_2$ in C$_6$D$_6$ (Exp. O)

Due to overlapping of the residual THF solvent peaks (reaction was performed in THF) with the Si-H hydrogen of the silanes, the ^{1}H-NMR spectrum of this reaction did not allow significant conclusions. The Si-DEPT spectrum (see Figure 117) shows several peaks in the region from 19 to –22 ppm. The peak at -22.71 ppm is attributed to the educt. The peak at 2 ppm might show the product. The small peaks around -20 ppm lie within the usual range for siloxanes. Unfortunately no ^{29}Si-NMR data of the product or related siloxanes is available to allow a better shift assignment.

The selective chlorination of di-*t*-butylsilane (Exp.O) with TCCA gave the product in 56% yield, aside with 43% unreacted educt. No siloxane formation was observed. Due to overlapping of the residual THF solvent peaks with the Si-H hydrogen of the silanes, the ^{1}H spectrum of this reaction did not allow significant conclusions (reaction was performed in THF). The Si-DEPT spectrum (see Figure 117) shows two peaks. The shift at 27 ppm can be assigned to the product, the educt shows a signal at 1.71 ppm. The obtained shifts fit to the GC-MS data.

A GC-MS analysis, even with elongated measurement times, of the product distribution of the selective chlorination of the secondary silane 9-anthracenyl$_2$SiH$_2$ (**27**) (Exp. P) failed because of the high molecular mass of the chlorinated product.

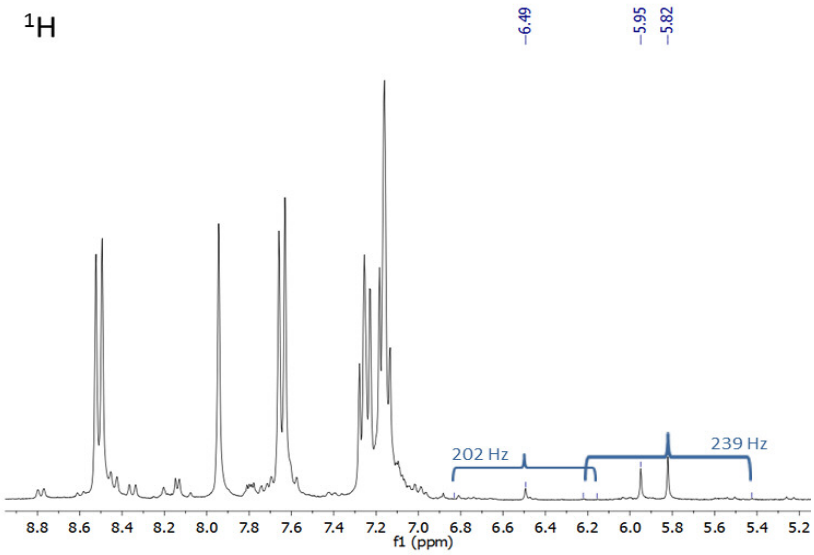

Figure 118: ^{1}H-NMR spectrum of 9-anthracenyl$_2$SiH$_2$ (27) in C$_6$D$_6$ (Exp.O)

Figure 118 shows the ^{1}H spectrum of the filtered reaction solution. The educt can be identified *via* the Si-H hydrogen shift at 6.49 ppm and the coupling constant of 202 Hz. The Si-H hydrogen shift of the product is formed at 5.82 ppm with a coupling constant of 239 Hz that fits very well to the coupling constant for the rather similar di-1-naphthylchlorosilane. Despite using a ^{29}Si-NMR overnight measurement for 14 hours with a long relaxation delay (d1=90 sec), no signal of the reaction products could be observed. This difficulty in the measurement of anthracenyl substituted silanes was already experienced for similar compounds (see 3.3)

The selective chlorination of the primary silanes 1-naphthylSiH$_3$ (**30**) and phenylSiH$_3$ was investigated at a 1:1 ratio of educt to TCCA (Table 21).

Table 21: Reaction of primary silane (= educt) with TCCA

Exp.	Silane	E:TCCA	Solvent [mL]	Reaction time [min]	RSiH$_2$Cl [%]	RSiH$_3$ [%]
I	1-naphthylSiH$_3$ (**30**)	1:1	10	30	0.98	99.02
I1	1-naphthylSiH$_3$ (**30**)	1:1	10	120	68.00	32.00
I2	1-naphthylSiH$_3$ (**30**)	1:1	10	120	73.23	26.77
J	phenylSiH$_3$	1:1	5	120	53.85	46.15

The selective chlorination of 1-naphthylSiH$_3$ (**30**) with 10 minutes reaction time shows mainly educt in the solution (Exp. I). After 120 minutes (Exp. I1) followed by work up

(Exp. I2) 73% product aside with 27% educt can be observed. The ^{1}H-NMR spectrum (see Figure 119) shows the newly formed Si-H hydrogen shift at 5.39 ppm. A coupling constant of 240 Hz is observed, which differs from the value for the educt. 1-naphthylSiH$_3$ (**30**) shows a Si-H hydrogen shift at 4.36 ppm and a coupling constant of 200 Hz.

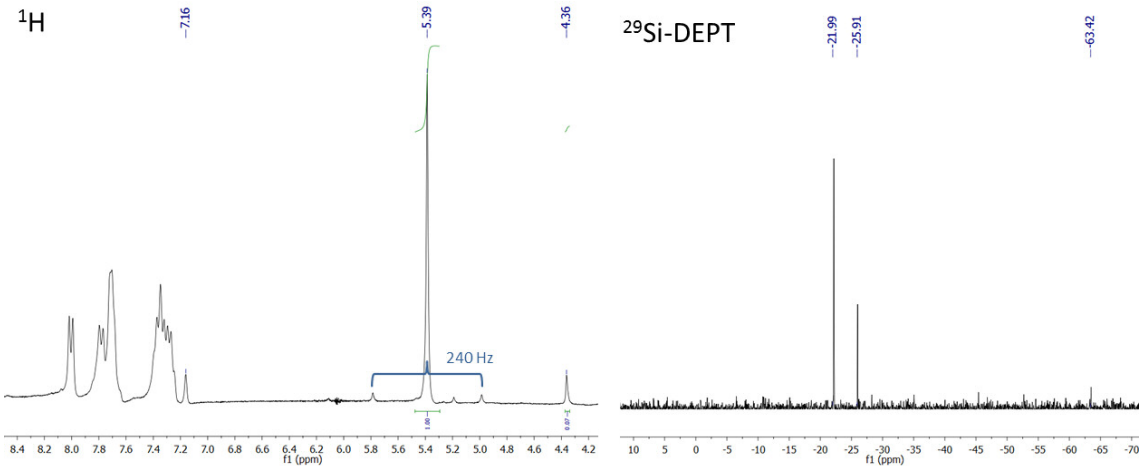

Figure 119: ^{1}H-NMR and ^{29}SiDEPT spectrum of TCCA reaction of 1-naphthylSiH$_3$ (30) in C$_6$D$_6$ (Exp.I2)

The Si-DEPT spectrum (see Figure 119) shows three peaks. The shift at -22 ppm can be assigned to the product 1-naphthylchlorosilane. The rather similar 1-naphthylbromosilane was reported by Hassler in 1990[143] showing a ^{29}Si-NMR shift at -27.9 ppm and a Si-H coupling constant of 239.8 Hz. The observed shift at -25.9 would fit to the formation of 1,2-dinaphthyldisiloxane. The corresponding phenyl substituted compound shows a shift at -25.1 ppm.[144] This siloxane was not detected in the GC-MS analysis which would suggest its formation during the overnight ^{29}Si-NMR measurement (14 hours). In this case, the measurement was not performed in the dry solvent but in C$_6$D$_6$ that was stored under air, due to the supposed low reactivity of naphthylchlorosilanes, which was observed in the handling of similar compounds. The shift at -63.4 ppm can be assigned to the unreacted educt.

The selective chlorination of phenylSiH$_3$ (Exp. J) after 120 minutes reaction time shows 54% product yield, aside with 46% unreacted educt. Figure 120 shows the ^{1}H-NMR and ^{29}Si-NMR spectrum of the reaction solution after filtering. The educt can be identified *via* the Si-H hydrogen shift at 4.15 ppm and the coupling constant of 201 Hz. The Si-H hydrogen shift of the product phenylchlorosilane is formed at 5.13 ppm with a coupling constant of 241 Hz. The large signal at ~ 3.5 ppm is attributed to the THF solvent signal. The ^{29}Si-NMR spectrum shows two peaks. The signal at -60.45 ppm can be assigned to the unreacted educt and the shift at -18 ppm to the product.

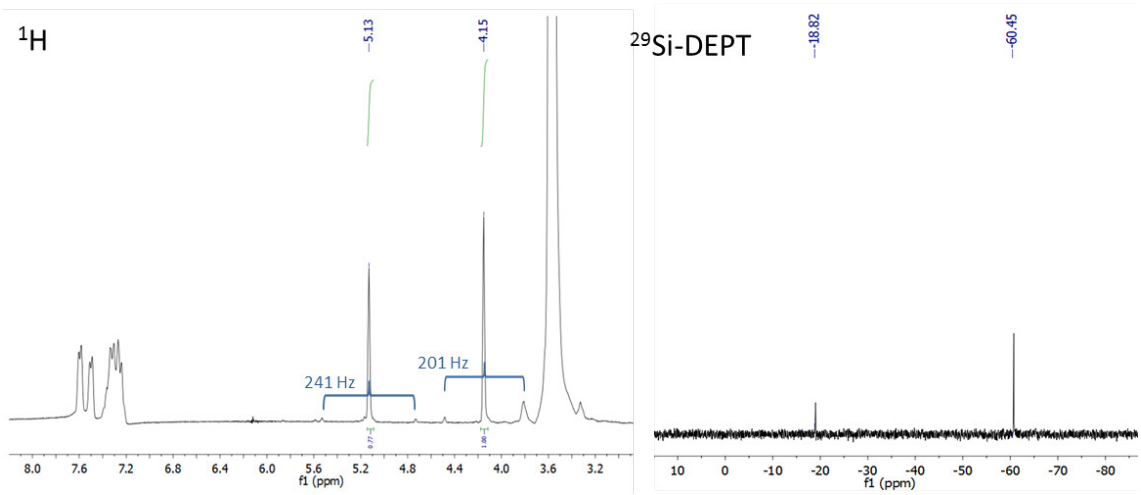

Figure 120: ^{1}H-NMR and ^{29}SiDEPT spectrum of TCCA reaction of phenylSiH$_3$ in C$_6$D$_6$ (Exp.J)

Table 22 and Table 23 show the comparison of the ^{29}Si-NMR data of educt and product of the selective chlorination of the silanes. With the exception of 9-anthracenyl$_2$SiH$_2$ (**27**), the selective chlorination leads to a downfield NMR-shift of the Si-H hydrogen in the ^{1}H and the silicon shift in the ^{29}Si-NMR spectrum, due to the higher electronegativity of the chlorine atoms compared to the hydrogen atom. The coupling constants of the obtained monochlorinated compounds show a notably conformance and fit to the literature known data.

Table 22: Comparison of the ^{29}Si-NMR data of R$_2$SiH$_2$ (educt) and R$_2$SiClH (product); n.d = not detectable

R=	δ R$_2$SiH$_2$ [ppm]	δ Si-**H** [ppm]	^{1}J(^{1}H-^{29}Si) [Hz]	R$_2$SiClH [ppm]	δ Si-**H** [ppm]	^{1}J(^{1}H-^{29}Si) [Hz]
phenyl	-34.1*	5.11	198.3	-5.59	5.79	236
1-naphthyl	-39.4*	5.47	199.5	-7.28	6.42	236
ethyl	-22.6*	3.64	184.8	2/19	n.d	n.d
t-butyl	1.56*	3.67*	181.5*	27.4	4.27*	211.5*
anthracenyl	-61.22*	6.5	202*	n.d.	5.82	236

*pure sample measured in C$_6$D$_6$

Table 23: Comparison of the ^{29}Si-NMR data of RSiH$_3$ (educt) and RSiClH$_2$ (product)

R=	RSiH$_3$ [ppm]	δ Si-**H** [ppm]	^{1}J(^{1}H-^{29}Si) [Hz]	RSiClH$_2$ [ppm]	δ Si-**H** [ppm]	^{1}J(^{1}H-^{29}Si) [Hz]
phenyl	-60.45	4.15	201	-18.82	5.13	241
1-naphthyl	-63.42	4.36	200	-21.99	5.39	240

In summary, the selective chlorination of secondary and primary aryl and alkyl silanes with TCCA could be successfully performed. For phenyl$_2$SiH$_2$ a yield of 86% product could be obtained. Siloxane formation was detected for the chlorination of diethylsilane but not for *tert*-butylsilane or the aryl substituted compounds. The formation of 1,2-dinaphthyldisiloxane might be caused by the usage of wet C_6D_6.These findings suggests the higher reactivity towards moisture for alkyl- substituted or less sterically crowded silanes

All reactions showed the importance of suitable reaction conditions, especially the stoichiometry turned out to be a crucial point and should be performed for all silanes in a future study. Also the influence of a higher temperature on the reaction time should be investigated.

4 Experimental

4.1 Materials and methods

All reactions, unless otherwise stated, were carried out using standard Schlenk line techniques under nitrogen atmosphere, using oven-dried glassware. All dried and deoxygenated solvents were obtained from a solvent drying system (Innovative Technology Inc.). C_6D_6 was distilled over sodium and stored under nitrogen. $SiCl_4$ was purchased from ABCR and distilled before use. All other chemicals from commercial sources were utilized without further purification. Melting point measurements were carried out by threefold determination with a Stuart Scientific SMP 10 (up to 300 °C). Degassed H_2SO_4 (10%) was diluted with deionized water. GC-MS measurements were performed on an Agilent Technologies GC system (column: HP-5MS) with mass selective detector Type Agilent 5975C using EI at 70 eV. An Agilent Technologies Cary 60 spectrometer was used for UV-VIS measurements. IR spectra were performed on a Bruker APHA FT-IR spectrometer with platinum ATR diamond top. TGA/DSC/MS measurements were performed on a NETSCH STA 409. DXRL experiments were performed at the DXRL beamline at ELETTRA using a DEX02 scanner (Jenoptik GmbH).

4.2 NMR Spectroscopy

^{1}H (300.22 MHz), ^{13}C (75.5 MHz), and ^{29}Si (59.64 MHz) NMR spectra were recorded on a Mercury 300 MHz spectrometer from Varian at 25 °C. Chemical shifts for ^{1}H, ^{13}C and ^{29}Si were recorded in part per million with either TMS (0.00 ppm), $CDCl_3$ (7.26 ppm for ^{1}H or 77.0 ppm for ^{13}C) or C_6D_6 (7.16 ppm for ^{1}H or 128.0 ppm for ^{13}C) as a reference. Coupling constants (*J*) are reported in Hertz (Hz).

4.3 Crystal structure determination

All crystals suitable for single crystal X-ray diffractometry were removed from a Schlenk flask and immediately covered with a layer of silicone oil. A single crystal was selected, mounted on a glass rod on a copper pin, and placed in the cold N_2 stream provided by an Oxford Cryosystems cryometer. XRD data collection was performed on a Bruker APEX II diffractometer with use of Mo Kα radiation (λ = 0.71073 Å) and a CCD

area detector. Empirical absorption corrections were applied using SADABS.[145] The determination of compound *p*-tolyl$_2$SiH$_2$ (**34**) was obtained by crystallization of the sample in a capillary tube while mounted on an Agilent SuperNova diffractometer with use of Mo Kα radiation (λ= 0.71073 Å). Data collection, cell refinement and data reduction was performed with CrysAlisPro. The structures were solved with use of either direct methods or the Patterson option in SHELXS and refined by the full-matrix least-squares procedures in SHELXL.[146,147] The space group assignments and structural solutions were evaluated using PLATON.[148,149] Non-hydrogen atoms were refined anisotropically. Hydrogen atoms bonded to silicon atoms were located in a difference map. All other hydrogen atoms were located in calculated positions corresponding to standard bond lengths and angles. Intermolecular interactions for presented and published compounds were determined by the calculation of centroids and planes feature of the programs Mercury[150] and Diamond.[151]

4.4 SEM/EDX

Scanning electron microscopy (SEM) analysis was performed on a Vega 3 SBU SEM with a tungsten hair-pin cathode. Samples were sputtered with gold for topographic characterization. Qualitative and quantitative analysis of the layers and particles was performed *via* energy dispersive X-ray microanalysis (Oxford Instruments, model INCA x-act). Selected samples were characterized at FELMI Graz.

4.5 Computational Details

All calculations have been carried out using the Gaussian09 program package[152] on a computing cluster with blade architecture. The mPW1PW91 hybrid functional[153] has been used together with the 6-31+G* basis sets for geometry optimizations and vibrational frequency calculations. Magnetic shieldings have been obtained using IGLO-II basis sets[154] in combination with the B3LYP functional for the silanes and the M06L functional[155] for the chlorosilanes. The magnetic shielding of tetramethylsilane (($\sigma(Si)_{B3LYP}$ = 337.8 ppm, $\sigma(Si)_{M06L}$ = 372.7 ppm) was used as reference for calculating ^{29}Si-NMR chemical shifts.

4.6 Synthesis

4.6.1 Organochlorosilanes R_nSiCl_{4-n}

General procedure A for R_2SiCl_2 – compounds 2–5 and 8–11

A flask furnished with a dropping funnel was charged with the aryl/alkylbromide in Et_2O. *n*-BuLi (1.6 M in hexane), diluted with Et_2O was added dropwise at -78 °C. After addition the reaction was kept at -78 °C for 10 min and was then allowed to warm to room temperature and stirred for 30 min. The solution was transferred *via* cannula to $SiCl_4$ dissolved in Et_2O at 0 °C. The reaction was stirred for 2 hours and was allowed to warm to room temperature. The solvent was removed under reduced pressure and the residue dissolved in boiling toluene. Insoluble salts were removed *via* filtration through cellite and washed with hot toluene. The solvent from the resulting clear solution was removed under reduced pressure, followed by purification *via* distillation or recrystallization.

*fluorenyl$_2$SiCl$_2$ (**2**)*

0.94 g fluorene (5.5 mmol) was dissolved in 20 mL Et_2O. The solution was cooled to 0 °C and 3.6 mL *n*-BuLi (1.6 M in hexane, 5.7 mmol, 1.1 equiv.) was added dropwise via syringe. The resulting orange solution was stirred for 1h at room temperature. Completeness of lithiation was monitored by ^{1}H-NMR. 20 mL Et_2O were added to the solution followed by slow addition of 0.314 mL of $SiCl_4$ (2.76 mmol, 0.5 equiv.) at 0 °C. The resulting cloudy yellow solution was stirred for 4 h. Et_2O was removed under reduced pressure and the residue dissolved in boiling toluene. Insoluble salts were removed via filtration through cellite and washed with hot toluene. The resulting clear solution was concentrated under reduced pressure. Crystals suitable for X-ray diffraction analysis were grown at room temperature. Yield 60% (0.71 g, 1.6 mmol), mp = 173 °C. ^{1}H NMR (300 MHz, $CDCl_3$) δ 7.58 (d, *J* = 7.6 Hz, 1H), 7.45 (d, *J* = 7.7 Hz, 1H), 7.25 (t, *J* = 7.5 Hz, 2H), 7.07 (t, *J* = 7.5 Hz, 1H), 4.16 (s, 1H). ^{13}C NMR (75.5 MHz, $CDCl_3$) δ 141.4, 139.9, 126.9, 126.4, 125.2, 120.2, 43.0 ppm. ^{29}Si NMR (59.64 MHz, C_6D_6): δ 17.33 ppm. MS (70 eV, m/z) = 428 (M^+).

*p-tolyl$_2$SiCl$_2$ (**3**)*

17.5 mL 4-bromotoluene (142 mmol, 1 equiv.) in 150 mL Et_2O. Addition of 97.76 mL *n*-BuLi (1.6 M in hexane, 156 mmol, 1.1 equiv.). 8.16 mL $SiCl_4$ (71 mmol, 0.5 equiv.) in 100 mL Et_2O. Purification by distillation. Yield 62% (12.4 g, 44 mmol) of colourless liquid. bp(obs.) = 110-112 °C (0.4 mbar)[82]. ^{1}H NMR (300 MHz, C_6D_6): δ 7.67 (d, *J* = 7.6 Hz, 4H), 6.93 (d, *J* = 7.5 Hz, 4H), 2.00 (s, 6H) ppm. ^{13}C NMR (75.5 MHz, C_6D_6): δ 142.2, 134.6, 129.4, 129.2, 21.5 (CH_3) ppm. ^{29}Si NMR (59.64 MHz, C_6D_6): δ 6.65 ppm. MS (70 eV, m/z) = 280.1 (M^+).

*m-tolyl$_2$SiCl$_2$ (**4**)*

14.27 mL 3-bromotoluene (99%) (83 mmol, 1 equiv.) in 100 mL Et_2O. Addition of 56.8 mL *n*-BuLi (1.6 M in hexane, 91 mmol, 1.1 equiv.) in 20 mL Et_2O. 4.73 mL $SiCl_4$ (41 mmol, 0.5 equiv.) in 80 mL Et_2O. Purification by distillation. Yield 36% (4.17 g, 15 mmol) of colourless liquid. bp= 140-143 °C (3 mbar)[156]. ^{1}H NMR (300 MHz, C_6D_6): *δ* 7.65 (s, 2H), 7.58 (d, *J* = 7.0 Hz, 2H), 7.10 (t, *J* = 7.4 Hz, 2H), 7.03 (d, *J* = 7.2 Hz, 2H), 2.04 (s, 6H) ppm. ^{13}C NMR (75.5 MHz, C_6D_6): *δ* 138.8, 134.9, 132.9, 132.3, 131.6, 128.7, 21.5 (CH_3) ppm. ^{29}Si NMR (59.64 MHz, C_6D_6): *δ* 6.4 ppm. MS (70 eV, *m/z*) = 280.0 (M^+).

*o-tolyl$_2$SiCl$_2$ (**5**)*

12.8 mL 2-bromotoluene (106 mmol, 1 equiv.) in 150 mL Et_2O. Addition of 73.2 mL *t*-BuLi (1.6 M in hexane, 117 mmol, 1.1 equiv.) in 20 mL Et_2O. 6.1 mL $SiCl_4$ (53 mmol, 0.5 equiv.) in 100 mL Et_2O. Purification by distillation. Crystals suitable for X-ray diffraction analysis were grown from toluene at 4 °C. Yield 67% (10.0 g, 36 mmol). mp = 74–75 °C. bp(obs.) = 114-116 °C (0.4 mbar). ^{1}H NMR (300 MHz, C_6D_6): δ 7.95 (dd, *J* = 7.5, 1.5, 2H), 7.08 (td, *J* = 7.5, 1.5, 2H), 6.98 (td, *J* = 7.5, 0.5, 2H), 6.85 (dd, *J* = 7.6, 0.5, 2H), 2.24 (s, 6H) ppm. ^{13}C NMR (75.5 MHz, C_6D_6): δ 144.0, 135.6, 132.2, 131.3, 131.1, 126.0, 22.8 (CH_3) ppm. ^{29}Si NMR (59.64 MHz, C_6D_6): δ 6.57 ppm. MS (70 eV, m/z) = 280.0 (M^+).

*1-naphthyl$_2$SiCl$_2$ (**8**)*

36.56 g 1-bromonaphthalene (176.5 mmol, 1 equiv.) in 250 mL Et_2O. Addition of 121.34 mL *n*-BuLi (1.6 M in hexane, 194.2 mmol, 1.1 equiv.) in 70 mL Et_2O. 10.14 mL $SiCl_4$ (88.2 mmol, 0.5 equiv.) in 200 mL Et_2O. Crystals suitable for X-ray diffraction analysis could be grown from toluene at room temperature . Yield: 76% (23.7 g, 67 mmol). mp = 138–139 °C. ^{1}H NMR (300 MHz, C_6D_6): δ 8.59 – 8.50 (m, 2H), 8.14 (d, *J* = 6.9, 2H), 7.60 (d, *J* = 8.1, 2H), 7.55 – 7.47 (m, 2H), 7.14 – 7.01 (m, 6H) ppm. ^{13}C NMR (75.5 MHz, C_6D_6): δ 136.1, 135.6, 133.7, 133.0, 129.7, 129.1, 127.9, 126.9, 126.1, 124.9 ppm. ^{29}Si NMR (59.64 MHz, C_6D_6): δ 7.58 ppm. MS (70 eV, m/z) = 352.1 (M^+).

*2,4-xylyl$_2$SiCl$_2$ (**9**)*

18.1 g 2,4-xylylbromide (97.7 mmol, 1 equiv.) in 50 mL Et_2O. Addition of 67.17 mL *n*-BuLi (1.6M in hexane, 107 mmol, 1.1 equiv.) in 40 mL Et_2O. 5.61 mL $SiCl_4$ (48.8 mmol, 0.5 equiv.) in 70 mL Et_2O. 2,4-xylyl$SiCl_3$ could be identified as side product and was removed under vacuum (distillation). Yield 46% (6.94 g, 22.5 mmol) of slightly yellow oil. Colourless crystals suitable for X-ray diffraction analysis were grown from the neat solution at 4 °C. mp = 60–62 °C. ^{1}H NMR (300 MHz, C_6D_6): δ 7.67 (d, *J* = 7.7, 2H), 6.75 (d, *J* = 7.7, 2H), 6.68 (s, 2H), 2.42 (s, 6H), 1.99 (s, 6H) ppm. ^{13}C NMR (75.5 MHz, C_6D_6): δ 143.5, 141.9, 135.4, 131.66, 126.3, 22.4 (CH_3), 20.9 (CH_3) ppm. ^{29}Si NMR (59.64 MHz, C_6D_6): δ 7.23 ppm. MS (70 eV, m/z) = 308.1 (M^+).

*9-anthracenyl$_2$SiCl$_2$ (**10**)*

6 g 9-bromoanthracene (23 mmol, 1 equiv.) in 50 mL Et_2O and 50 mL THF. Addition of 16 mL *n*-BuLi (1.6 M in hexane, 26 mmol, 1.1 equiv.). 1.33 mL $SiCl_4$ (12 mmol, 0.5 equiv.) in 50 mL Et_2O. Purification by vacuum sublimation at 60°C (0.04 mbar) to remove anthracene as major byproduct. Yield 35% (1.84g, 4.1 mmol) of yellow solid. mp = 161–162 °C. ^{1}H NMR (300 MHz, C_6D_6): δ 8.98 (d, *J* = 8.9, 4H), 8.21 (s, 2H), 7.67 (d, *J* = 9.0, 4H), 7.07 – 6.97 (m, 4H), 6.97 – 6.84 (m, 4H) ppm.^{13}C NMR (75.5 MHz, C_6D_6): δ 136.5, 134.0, 131.8, 129.7, 128.1, 126.7, 125.3, 119.7 ppm. ^{29}Si NMR (59.64 MHz, C_6D_6): δ 3.02 ppm. MS (70 eV, m/z) = 452.03 (M^+).[30]

*2,6-xylyl$_2$SiCl$_2$ (**11**)*

24.0 g 2,6-xylylbromide (129 mmol, 1 equiv.) in 100 mL Et_2O. Addition of 97.31 mL *n*-BuLi (1.6 M in hexane, 155 mmol, 1.2 equiv.) in 50 mL Et_2O. 7.45 mL $SiCl_4$ (64.9 mmol, 0.5 equiv.) in 100 mL Et_2O. Small amount of 2,6-xylyl$SiCl_3$ could be identified as side product and was removed under vacuum (distillation). Crystals suitable for X-ray Diffraction Analysis could be grown from pentane at room temperature. Yield: 73% (14.65 g, 47.3 mmol). mp = 85 °C. ^{1}H NMR (300 MHz, C_6D_6): δ 6.97 (t, *J* = 7.6, 2H), 6.75 (d, *J* = 7.5, 4H), 2.42 (s, 12H) ppm. ^{13}C NMR (75.5 MHz, C_6D_6): δ 143.4, 133.9, 131.1, 129.7, 24.5 (CH_3) ppm. ^{29}Si NMR (59.64 MHz, C_6D_6): δ 2.08 ppm. MS (70 eV, m/z) = 308.1 (M^+).

General procedure B for R_2SiCl_2 – compounds 1, 6 and 7

A flask equipped with a dropping funnel and a reflux condenser was charged with Mg in THF (or Et_2O). The dropping funnel was charged with the arylbromide in THF. After addition of approximately 10% of the aryl bromide to the Mg, the solution was carefully heated to start the reaction. The aryl bromide was subsequently added slowly. After complete addition, the reaction was refluxed for 2–12h, until complete consumption of magnesium. The content of Grignard reagent was determined by diluting small volume of the solution with deionized water and titration with 1M HCl using phenolphthalein as indicator. The Grignard solution was slowly added to $SiCl_4$ in THF (or Et_2O) at 0 °C. The reaction was stirred for 4 hours and was allowed to warm up to room temperature. The solvent was removed under reduced pressure and the residue dissolved in boiling toluene. Insoluble salts were removed *via* filtration through cellite and washed with hot toluene. The solvent of the resulting clear solution was removed under reduced pressure, followed by purification *via* distillation or recrystallization.

*benzyl$_2$SiCl$_2$ (**1**)*

2.63 g Mg (108 mmol, 1 equiv.) in 100 mL Et_2O. Addition of 13 mL benzylbromide (108 mmol, 1 equiv.) in 40 mL Et_2O. 2 h Reflux. 6 mL $SiCl_4$ (52 mmol, 0.5 equiv.) in 80 mL Et_2O. Purification by distillation. Crystals suitable for X-ray diffraction analysis were grown from toluene at 4 °C. Yield 38% (5.9 g, 21 mmol). mp = 50–51 °C. bp (obs.) = 103-107 °C (0.4 mbar)[157]. ^{1}H NMR (300 MHz, $CDCl_3$): δ 7.3–7.1 (m, 10H, Ar-H), 2.60 (s, 4H, Si-CH_2-Ar) ppm. ^{13}C NMR (75.5 MHz, C_6D_6): δ 134.1, 129.4, 128.8, 126.1, 28.8 (CH_2) ppm. ^{29}Si (59.6 MHz, C_6D_6): δ 22.72 ppm. MS (70 eV, m/z) = 280.1 (M^+).

*p-n-butylphenyl$_2$SiCl$_2$ (**6**)*

2.03 g Mg (83.6 mmol, 1.1 equiv.) in 100 mL Et_2O. Addition of 13.46 mL 1-bromo-4-*n*-butylbenzene (76.3 mmol, 1 equiv.) in 50 mL Et_2O. 4.38 mL $SiCl_4$ (38 mmol, 0.5 equiv.) in 80 mL Et_2O. Purification by distillation. Yield 38% (10.5 g, 29 mmol). bp = 193-195 °C (0.7 mbar)[158]. ^{1}H NMR (300 MHz, C_6D_6): δ 7.83 – 7.64 (m, 4H), 7.17 – 6.97 (m, 4H), 2.56 – 2.33 (m, 4H), 1.57 – 1.37 (m, 4H), 1.31 – 1.13 (m, 4H), 0.85 (t, *J*=7.3, 6H) ppm. ^{13}C NMR (75.5 MHz, $CDCl_3$): 13.9, 22.4, 33.3, 35.8, 128.5, 129.0, 134.1, 147.0 ppm.[159] ^{29}Si NMR (59.64 MHz, C_6D_6): δ 6.49 ppm. MS (70 eV, m/z) = 364.1 (M^+).

*p-biphenyl$_2$SiCl$_2$ (**7**)*

2.5 g Mg (103 mmol, 1.1 equiv.) in 80 mL Et_2O. Addition of 16.0 mL 1-bromo-4-phenylbenzene (94 mmol, 1 equiv.) in 50 mL Et_2O. 5.37 mL $SiCl_4$ (47 mmol, 0.5 equiv.) in 80 mL Et_2O. Small amount of *p*-biphenyl$SiCl_3$ could be identified as side product and was removed under vacuum (distillation). Yield 53% (10.2 g, 25.2 mmol), mp = 96–98 °C. ^{1}H NMR (300 MHz, C_6D_6): δ 7.03–7.15 (m, 5H), 7.35–7.5 (m, 4H) ppm. ^{13}C NMR (75.5 MHz, C_6D_6): δ 145.0, 140.7, 135.1, 130.9, 129.2, 128.3, 127.6, 127.5 ppm. ^{29}Si NMR (C_6D_6, 59.64 MHz): δ 6.24 ppm. MS (70 eV, m/z) = 404.1 (M^+).

General procedure C for $RSiCl_3$ – compounds 12-15

The organo trichlorosilanes were synthesized similar to the diorgano dichlorosilanes (see general procedure B) *via* reaction of the respective Grignard reagent with 8 equivalents $SiCl_4$ in THF at 0 °C. The reaction was stirred for 4 hours and was allowed to warm to room temperature. The solvent was removed under reduced pressure and the residue dissolved in boiling toluene. Due to the similarity of boiling points of THF and $SiCl_4$ further separation of the removed solvent and the excess $SiCl_4$ is not possible. The THF/$SiCl_4$ solution has to be carefully quenched with alcohol and water. Insoluble salts formed in the reaction solution were removed *via* filtration through cellite and washed with hot toluene. The solvent of the resulting clear solution was removed under reduced pressure, followed by purification *via* distillation or recrystallization.

*2,4-xylylSiCl$_3$ (**12**)*

3.22g Mg (132.5 mmol, 1.1 equiv.) in 100 mL THF. Addition of 14.93 mL 4-bromo-*m*-xylene (111.6 mmol, 1 equiv.) in 30 mL THF. 90.5 mL $SiCl_4$ (788 mmol, 8 equiv.) in 30 mL THF. Purification by distillation. Yield 4,77g, (20%, 20 mmol) of colourless oil .^{1}H NMR (C_6D_6, 300 MHz) δ 7.52 (d, 1H), 7.49 (s, 1H), 6.59 (d, 1H), 5.18 (s, 1H), 2.26 (s, 3H), 1.83 (s, 3H) ppm. ^{13}C NMR (C_6D_6, 75.5 MHz,): δ 143.75, 135.09, 132.4, 126.53, 126.27, 22.51 (CH_3), 21.31 (CH_3) ppm. ^{29}Si NMR (C_6D_6, 59.64 MHz): δ -0,432 ppm. GC-MS: t_R=12,49 ; m/z=238.

*p-tolylSiCl$_3$ (**13**)*

2.51g Mg (103 mmol, 1.1 equiv.) in 70 mL THF. Addition of 10.47 mL 4-bromotoluene (86 mmol, 1 equiv.) in 30 mL THF. 60 mL $SiCl_4$ (750 mmol, 8.8 equiv.) in 40 mL THF. Purification by distillation. Yield 12.72g, (66%, 56.4 mmol) of colourless oil.^{1}H NMR (C_6D_6, 300 MHz,) δ 7.34 (d, 2H), 6.72 (d, 2H), 1.87(s, 3H) ppm. ^{13}C NMR ($CDCl_3$, 75.5 MHz): δ 141.9, 131.9, 127.8, 21.0 ppm. ^{29}Si NMR (C_6D_6, 59.64 MHz,): δ -0.52 ppm. GC-MS: t_R=10.99; m/z=225.9.

*benzylSiCl$_3$ (**14**)*

Obtained *via* distillation during the synthesis of benzyl$_2$SiCl$_2$ as major byproduct. Yield 6.83g (21.3%, 30.3 mmol) of colourless oil. ^{1}H NMR (C_6D_6, 300 MHz): δ 2,97 (s, 2H, CH_2), 7,41-7,29 (m, 5H). ^{13}C NMR (C_6D_6, 75.5 MHz): δ 132.1, 129.34, 128.83, 126.61, 32.95 (CH_2) ppm. ^{29}Si NMR (C_6D_6, 59.64 MHz): δ 7.66 ppm. GC-MS: t_R=10.849 ; m/z = 225.1.

*1-naphthylSiCl$_3$ (**15**)*

2.32 g Mg (95 mmol, 1.1 equiv.) in 70 mL THF. Addition of 12.19 mL 1-bromonaphthalene (87 mmol, 1 equiv.) in 30 mL THF. 80 mL $SiCl_4$ (697 mmol, 8 equiv.) in 40 mL THF. Purification by distillation. Yield 14.01g, (85%, 53.7 mmol) of colourless crystals. ^{1}H NMR ($CDCl_3$, 300 MHz,): δ 8.39(d, 1H), 8.17 (d, 1H), 8.09 (d, 1H), 7.94 (d, 1H), 7.69- 7.63 (dd, 2H), 7.59- 7.53 (dd, 2H) ppm. ^{13}C NMR ($CDCl_3$, 75.5 MHz): δ 134.9, 133.7, 133.5, 133, 128.8, 126.9, 126.8, 126.3, 125.9, 123.9 ppm. ^{29}Si NMR ($CDCl_3$, 59.64 MHz,): δ -1,1ppm. GC-MS: t_R=15.69; m/z=260.

General procedure D for R_3SiCl – compounds 16-19

Triorgano chlorosilanes were synthesized similar to the diorgano dichlorosilanes (see general procedure A) *via* lithiation of the arylbromide in Et_2O at -78 °C. The lithiated compound was added dropwise to 0.3 equivalents of $SiCl_4$ in Et_2O at 0 °C. The reaction was stirred for 2 hours and was allowed to warm to room temperature. The solvent was removed under reduced pressure and the residue dissolved in boiling toluene. Insoluble salts were removed *via* filtration through cellite and washed with hot toluene. The solvent from the resulting clear solution was removed under reduced pressure, followed by purification *via* recrystallization.

Compounds **17**-**19** were obtained as byproducts in the synthesis of the corresponding diorgano dichlorosilanes as high boiling fraction during distillation. Characterization was performed *via* GC-MS analysis and ^{29}Si-NMR.

*1-naphthyl$_3$SiCl (**16**)*

9.5 mL 1-bromonaphthalene (67.4 mmol, 3 equiv.) in 100 mL Et_2O. Addition of 4.4 mL *n*-BuLi (1.6M in hexane, 69.7 mmol, 3.1 equiv.) at -0 °C. 2.6 mL $SiCl_4$ (22.5 mmol, 1 equiv.) in 200 mL Et_2O. Colourless crystals could be grown from toluene. Yield 7.6 g (76 %, 17 mmol). mp: 205-209 °C. ^{1}H NMR (C_6D_6, 300 MHz): δ 8.548.50 (dd, 3H), 8.148.11 (d, 3H), 7.617.58 (d, 3H), 7.52–7.07 (m, 9H) ppm. ^{13}C NMR (C_6D_6, 75.5 MHz): δ 136.10, 135.57, 133.66, 132.96, 129.65, 129.07, 126.89, 126.10, 124.87, 119.31 ppm. ^{29}Si NMR (C_6D_6, 59.64 MHz): δ 4.0 ppm. GC-MS: t_R = 37.03 ; m/z = 444.1.

*p-tolyl$_3$SiCl (**17**):* GC-MS: t_R = 21.6; m/z = 336.1;
^{29}Si NMR (59.64 MHz, C_6D_6): δ 2.9 ppm;

*2,4-xylyl$_3$SiCl (**18**):* GC-MS: t_R = 23.6 ; m/z = 378.1;
^{29}Si NMR (59.64 MHz, C_6D_6): δ *4*.6 ppm.

*p-biphenyl$_3$SiCl (**19**):* GC-MS: not detectable
^{29}Si NMR (59.64 MHz, C_6D_6): δ 2.3 ppm.

4.6.2 Organosilanes R_nSiH_{4-n}

General procedure for R_nSiH_{4-n}

A flask furnished with a dropping funnel was charged with LAH (lithium aluminum hydride) pellets and Et_2O. A solution of the corresponding chlorosilane in Et_2O was added slowly *via* the dropping funnel while cooling to 0 °C. The reaction mixture was stirred for 1 hour and allowed to warm up to room temperature. The solution was cooled to 0 °C. Subsequently, diluted H_2SO_4 (10%) was added to quench the excess of LAH. The phases were separated *via* a cannula, and the aqueous layer washed twice with Et_2O. The combined organic phases were dried over $CaCl_2$. Filtration and evaporation of the solvent under reduced pressure gives the product. Purification was performed *via* recrystallization, sublimation or distillation.

Diorgano silanes R_2SiH_2

*benzyl$_2$SiH$_2$ (**20**)*

9.53 g benzyl$_2$SiCl$_2$ (**1**) (33.9 mmol, 1 equiv.) in 80 mL Et_2O, 1.54 g LAH pellets (41 mmol, 1.2 equiv.) in 80 mL Et_2O. 100 mL degassed H_2SO_4 (10%). Purification by distillation. Yield 42% (3.03g, 14.3 mmol) of colourless oil. ^{1}H NMR ($CDCl_3$, 300 MHz): δ 7.4 - 7.2 (m, 10H), 4.12 (quint, ^3J = 3.6 Hz, $^1J(^1H\text{-}^{29}Si)$ = 196.5 Hz, 2H), 2.38 (d, 4H, CH_2) ppm. ^{13}C NMR (C_6D_6, 75.5 MHz): δ 139.5, 128.9, 128.6, 125.1, 18.9 (CH_2) ppm. ^{29}Si NMR (C_6D_6, 59.64 MHz): δ -39.4 ppm. GC-MS: t_R =15.43 m/z = 212.1.

*fluorenyl$_2$SiH$_2$ (**21**)*

1.67 g fluorenyl$_2$SiCl$_2$ (**2**) (3.88 mmol, 1 equiv.) in 20 mL Et_2O and 20 mL THF, 0.18 g LAH pellets (4.7 mmol, 1.2 equiv.) in 40 mL Et_2O. 50 mL degassed H_2SO_4 (10%). The resulting solid was recrystallized from toluene to obtain colourless crystals. mp: 237-238 °C. Yield 58% (0.81g, 2.25mmol), ^{1}H NMR (C_6D_6, 300 MHz) δ 7.67 (d, 2H), 7.24-7.09 (m, 12H), 3.92 (t, ^3J = 2.6 Hz, $^1J(^1H\text{-}^{29}Si)$= 208.0 Hz, 2H), 3.68 (t, 2H, CH_2) ppm. ^{13}C NMR ($CDCl_3$, 75.5 MHz) δ 144.3, 140.6, 126.8, 126.2, 124.4, 120.4, 35.8 (CH_2) ppm. ^{29}Si NMR (C_6D_6, 59.64 MHz): δ 17.33 ppm. GC-MS: t_R= 26.2 m/z = 360.1.

*m-tolyl$_2$SiH$_2$ (**22**)*

1.30 g *m*-tolyl$_2$SiCl$_2$ (**4**) (4.6 mmol, 1 equiv.) in 20 mL Et$_2$O, 0.21 g LAH pellets (5.5 mmol, 1.2 equiv.) in 40 mL Et$_2$O. 50 mL degassed H$_2$SO$_4$ (10%). Yield 76% (0.75 g, 3.5 mmol) of colourless oil. ^{1}H NMR (C$_6$D$_6$, 300 MHz): δ 7.44-7.42 (m, 4H), 7.11 (t, 2H), 7.00 (d, 2H), 5.16 (s, $^{1}J(^{1}$H-^{29}Si) = 197.3 Hz, 2H), 2.04 (s, 3H, CH$_3$) ppm. ^{13}C NMR (C$_6$D$_6$, 75.5 MHz): δ 137.7, 136.7, 133.2, 131.8, 131.0, 128.5, 21.4 (CH$_3$) ppm. ^{29}Si NMR (C$_6$D$_6$, 59.64 MHz): δ -33.5 ppm. GC-MS: t$_R$= 11.20 m/z= 212.37.

*p-n-butylphenyl$_2$SiH$_2$ (**23**)*

8 g *p-n*-butylphenyl$_2$SiCl$_2$ (**5**) (22 mmol, 1 equiv.) in 30 mL Et$_2$O, 0.99 g LAH pellets (26 mmol, 1.2 equiv.) in 100 mL Et$_2$O. 100 mL degassed H$_2$SO$_4$ (10%). Purification *via* bulb to bulb distillation. Yield 11% (0.72 g, 2.4 mmol) of colourless oil. ^{1}H NMR (C$_6$D$_6$, 300 MHz): δ 7.53 (d, 4H), 7.06 (d, 4H), 5.13 (s, $^{1}J(^{1}$H-^{29}Si) = 196.6 Hz, 2H), 2.47 (t, 4H, CH$_2$-Ar), 1.55-1.45 (m, 4H, CH$_2$), 1.32-1.20 (m, 4H, CH$_2$), 0.87 (t, 6H, CH$_3$) ppm. ^{13}C NMR (C$_6$D$_6$, 75.5 MHz): δ 144.8, 136.4, 128.8, 128.7, 36.2 (CH$_2$), 33.9 (CH$_2$), 22.8 (CH$_2$), 14.31 (CH$_3$) ppm. ^{29}Si NMR (C$_6$D$_6$, 59.64 MHz): δ -34.14 ppm; GC-MS: t$_R$=20.11 m/z= 296.1.

*p-biphenyl$_2$SiH$_2$ (**24**)*

3 g *p*-biphenyl$_2$SiCl$_2$ (**7**) (7.4 mmol, 1 equiv.) in 40 mL Et$_2$O and 10 ml THF, 0.34 g LAH pellets (8.8 mmol, 1.2 equiv.) in 50 mL Et$_2$O. 50 mL degassed H$_2$SO$_4$ (10%). The resulting solid was recrystallized from toluene to obtain colourless crystals. Yield 61% (1.52 g, 4.5 mmol), mp.: 136 °C ^{1}H NMR (C$_6$D$_6$, 300 MHz): δ 7.63 (d, 4H), 7.49-7.45 (m, 8H), 7.22 (t, 4H), 7.14 (t, 2H), 5.21(s, $^{1}J(^{1}$H-^{29}Si) = 198.8 Hz, 2H) ppm. ^{13}C NMR (C$_6$D$_6$, 75.5 MHz): δ 143.3, 141.3, 136.7, 130.4, 129.1, 127.8, 127.5, 127.4 ppm. ^{29}Si NMR (C$_6$D$_6$, 59.64 MHz): δ -33.9 ppm. GC-MS: t$_R$= 20.708 m/z= 336.1.

*1-naphthyl$_2$SiH$_2$ (**25**)*

6 g 1-naphthyl$_2$SiCl$_2$ (**8**) (16.9 mmol, 1equiv.) in 100 mL Et$_2$O and 20 mL THF. 0.7 g LAH pellets (18.4 mmol, 1.2 equiv.) in 100 mL Et$_2$O. 150 mL degassed H_2SO_4 (10%). Crystals suitable for X-ray diffraction analysis were grown from toluene at 4 °C. Yield 59% (2.85 g, 10.3mmol), mp = 98-99 °C. ^{1}H NMR (C_6D_6, 300 MHz): δ 8.20 (m, 2H), 7.70 (d, 2H), 7.64 (d, 2H), 7.61 (m, 2H), 7.23-7.20 (m, 4H), 7.11 (dd, 2H), 5.72 (s, $^1J(^1H\text{-}^{29}Si)$ = 199.5 Hz, 2H) ppm. ^{13}C NMR (C_6D_6, 75.5 MHz): δ 137.7, 136.9, 133.4, 130.9, 129.6, 128.8, 127.9, 126.4, 125.8, 125.3 ppm. ^{29}Si NMR (C_6D_6, 59.64 MHz): δ -39.43. GC-MS: t_R = 22.483; m/z = 284.1 .

*2,4-xylyl$_2$SiH$_2$ (**26**)*

4 g 2,4-xylyl$_2$SiCl$_2$ (**9**) 1 (12.9 mmol, 1 equiv.) in 40 mL Et$_2$O, 0.59 g LAH pellets (15.5 mmol, 1.2 equiv.) in 100 mL Et$_2$O. 50 mL degassed H_2SO_4 (10%). The resulting solid was recrystallized from toluene to obtain colourless crystals. Yield 61% (1.89g, 7.87 mmol), mp: 46 - 47 °C. ^{1}H NMR (C_6D_6, 300 MHz): δ 7.51 (d, 1H), 6.87 (d, 1H), 6.83 (s, 1H), 2.33 (s, 3H, CH_3), 2.10 (s, 3H, CH_3), 5.21 (s, $^1J(^1H\text{-}^{29}Si)$ = 195.4 Hz, 2H) ppm. ^{13}C NMR (C_6D_6, 75.5 MHz): δ 144.3, 139.9, 137.0, 130.5, 126.2, 22.2 (CH_3), 21.0 (CH_3) ppm. ^{29}Si NMR (C_6D_6, 59.64 MHz): δ -40.38 ppm. GC-MS: t_R= 17.092, m/z = 240.1.

*9-anthracenyl$_2$SiH$_2$ (**27**)*

12.9 g 9-anthracenyl$_2$SiCl$_2$ (**10**) (28.4 mmol, 1 equiv.) in 200 mL Et$_2$O and 50 mL THF 1.18 g LAH pellets (31.3 mmol, 1.2 equiv.) in 150 mL Et$_2$O. 100 mL degassed H_2SO_4 (10%). Yields 83% (9.1 g, 23.7 mmol) of a brown-yellowish solid. Cold toluene was added to the solid. Insoluble byproducts were removed by filtration, followed by evaporation of the solvent and sublimation of the obtained yellow powder, to remove anthracene. Recrystallization in ethyl acetate yields 38.7% (4.23 g, 10.9 mmol) of pure product in bright yellow needles. mp: 200-202 °C. ^{1}H NMR (C_6D_6, 300 MHz): δ 8.79 (d, 4H), 8.22 (s, 2H), 7.73 (d, 4H), 7.04-7.14 (m, 8H), 6.50 (s, $^1J(^1H\text{-}^{29}Si)$ = 202.1 Hz, 2H) ppm. ^{13}C NMR (C_6D_6, 75.5 MHz): δ 125.1, 126.7, 129.9, 131.5, 131.8, 138.1 ppm. ^{29}Si NMR (C_6D_6, 59.64 MHz): δ -61.22 ppm. GC-MS: t_R= 25.813, m/z = 384.2.

*2,6-xylyl$_2$SiH$_2$ (**28**)*

22.5 g 2,6-xylyl$_2$SiCl$_2$ (**11**) 2 (72.9 mmol, 1 equiv.) in 100 mL Et$_2$O, 3.32 g LAH pellets (87.9 mmol, 1.2 equiv.) in 150 mL Et$_2$O. 70 mL degassed H$_2$SO$_4$ (10%). Purification by distillation. No recrystallization was needed. Yield 67% (11.7 g, 48.8 mmol) of colourless, hexagonal shaped crystals. mp: 51-52 °C. ^{1}H NMR (C$_6$D$_6$, 300 MHz): δ 6.91 (t, 2H), 6.71 (d, 4H), 5.08 (s, ^{1}J(^{1}H-^{29}Si)= 196.5 Hz, 2H), 2.16 (s, 12H, CH$_3$) ppm. ^{13}C NMR (C$_6$D$_6$, 75.5 MHz): *δ* 124.3, 127.5, 130.1, 145.0, 21.3 (CH$_3$) ppm. ^{29}Si NMR (C$_6$D$_6$, 59.64 MHz): *δ* -62.13 ppm. GC-MS: t$_R$= 17.33, m/z = 296.1.

p-tolyl$_2$SiH$_2$ (**34**) was prepared according to literature.[89]

o-tolyl$_2$SiH$_2$ (**35**) was prepared according to literature.[90]

Organo silanes RSiH$_3$

*2,4-xylylSiH$_3$ (**29**)*

4.77g 2,4-xylylSiCl$_3$ (**12**) (20 mmol, 1 equiv.) in 30 mL Et$_2$O, 0.94g LAH pellets (24.8 mmol, 1.2 equiv.) in 100 mL Et$_2$O. 50 mL degassed H$_2$SO$_4$ (10%). Removal of solvent yielded a yellowish oil. Yield 2.02g (74%, 14.8 mmol) ^{1}H NMR (C$_6$D$_6$, 300 MHz): δ 2.09 (s, 3H, CH$_3$), 2.23 (s, 3H, CH$_3$), 4.27 (d, 3H, ^{1}J(^{1}H-^{29}Si) = 197.8 Hz, SiH$_3$), 6.78 (s,1H), 6.81 (d, 1H) 7.39 (d, 1H) ppm. ^{13}C NMR (100 MHz, C$_6$D$_6$): δ 14.30 (CH$_3$), 23.06 (CH$_3$), 126.5, 130.6, 137.5, 140.6, 144.4 ppm.^{29}Si NMR (C$_6$D$_6$, 59.64 MHz): δ −63.93 ppm. GC- MS: t$_R$= 7,757 m/z= 136.1.

*1-naphthylSiH$_3$ (**30**)*

14.06g 1-naphthylSiCl$_3$ (**15**) (53.7 mmol, 1 equiv.) in 20 mL Et$_2$O, 2.92g LAH pellets (76.9, mmol, 1.4 equiv.) in 150 mL Et$_2$O. 70 mL degassed H$_2$SO$_4$ (10%). Removal of solvent yielded a colourless oil. Yield 5.3g (62.4%, 33.5 mmol) ^{1}H NMR (C$_6$D$_6$, 300 MHz): δ 7.86 (d, 1H), 7.54 (m,3H), 7.18 (dd, 2H), 7.08 (dd, 1H), 4.44 (s, ^{1}J(^{1}H-^{29}Si) = 200.708 Hz, 3H).^{13}C NMR (C$_6$D$_6$, 75.5 MHz): δ 137.9, 137.1, 133.5, 131.2, 129.1, 128.1, 127.3, 126.7, 126.1, 125.5 ppm. ^{29}Si NMR (C$_6$D$_6$, 59.64 MHz,): δ -62.819 ppm GC-MS: t$_R$= 11.797; m/z = 158.1.

*p-tolylSiH$_3$ (**31**)*

11.43g *p*-tolylSiCl$_3$ (**13**) (50.7 mmol, 1 equiv.) in 30 mL Et$_2$O, 2.34g LAH pellets (64.0, mmol, 1.2 equiv.) in 150 mL Et$_2$O. 70 mL degassed H$_2$SO$_4$ (10%). Removal of solvent yielded a colourless oil. Yield 1.1g (19%, 8.95 mmol). ^{1}H NMR (C$_6$D$_6$, 300 MHz) δ 7.28 (d, 2H), 6.88 (d, 2H), 4.23 (s, $^1J(^1H-^{29}Si)$ = 199.035 Hz, 3H), 2.04 (s, 3H) ppm. ^{13}C NMR (C$_6$D$_6$, 75.5 MHz): δ 139.82, 136.2, 129.27, 124.34, 21.451 (CH$_3$) ppm. ^{29}Si NMR (C$_6$D$_6$, 59.64 MHz): δ -60,47ppm, GC-MS: t$_R$= 5.63 ; m/z = 122.1 **.**

*benzylSiH$_3$ (**32**)*

6.5 g benzylSiCl$_3$ (**14**) (28.8 mmol, 1 equiv.) in 50 mL Et$_2$O, 1.42g LAH pellets (37.4, mmol, 1.3 equiv.) in 90 mL Et$_2$O. 70 mL degassed H$_2$SO$_4$ (10%). Removal of solvent yielded a colourless oil. Yield 2.49 g (71%, 20.4 mmol). ^{1}H NMR (300.22 MHz, C$_6$D$_6$): *δ* 1.86 (q, 2H), 3,62 (t, $^1J(^1H-^{29}Si)$ = 197.9 Hz, 3H), 6.87-6.95 (m, 3H), 7.03-7.12 (m, 2H) ppm. ^{13}C NMR (75.5 MHz, C$_6$D$_6$): *δ* 140.07, 128.94, 128.23, 125.27, 15.84 ppm . ^{29}Si NMR (59.64 MHz, C$_6$D$_6$): *δ* -55.4 ppm. GC-MS: t$_R$= 6.21 ; m/z = 122.1.

*2,6-xylySiH$_3$ (**37**)*

The compound was obtained as major byproduct in the synthesis of 2,6-xylyl$_2$SiH$_2$ *(**28**).* Spectroscopic data fits to literature.[36]

Triorgano silanes R_3SiH and tetraorgano silanes R_4Si

*1-naphthyl$_3$SiH (**33**)*

1 g 1-naphthyl$_3$SiCl (**16**) (2.25 mmol, 1 equiv.) was solved in 30 mL toluene (due to bad solubility in Et_2O or THF) with slight heating. The solution was added drop wise to a slurry of 0.1 g LAH (2.5 mmol, 1.1 equiv.) in 40 mL Et_2O. The solution was slightly heated for 15 minutes to keep the 1-naphthyl$_3$SiCl dissolved. The solution was stirred vigorously at room temperature for 2h. Excess LAH was quenched carefully with aqueous H_2SO_4 (10%). The organic layer was separated *via* cannula. Evaporation of solvent gives the pure compound as a colourless solid. Yield 0.67 g (73%, 1.6 mmol). ^{1}H NMR (300.22 MHz, C_6D_6): δ 6.99 (t, 3H), 7.14 (s, $^1J(^1H\text{-}^{29}Si)$ = 195.4 Hz, 1H), 7.08-7.23 (m, 6H), 7.62-7.67 (m, 9H), 6.99 (d, 3H) ppm. δ ^{13}C NMR (75 MHz, C_6D_6) δ 138.22, 137.88, 134.00, 131.36, 129.25, 128.89, 126.72, 126.11, 125.84 ppm. ^{29}Si NMR (59.64 MHz, C_6D_6): δ -29.0 ppm. t_R = 24.38 ; m/z = 410.2.

Reaction of 1-naphthyl$_3$SiCl (16) with naphthyl lithium/ phenyl lithium

0.4 g 1-bromonaphthalene 97% (1.87 mmol, 1 equiv.) in 8 mL Et_2O. Cooling to -75 °C. Addition of 1.29 mL *n*-BuLi (2.06 mmol, 1.1 equiv.) *via* syringe. After addition the solution was stirred at -75 °C for 15 min, followed by stirring at 0 °C with an ice bath for 30 min. Stirring at room temperature for 2 hours. 0.83g 1-naphthyl$_3$SiCl (**16**) (1.86 mmol, 1 equiv.) was dissolved in a mixture of 15 mL Et_2O and 15 mL THF and cooled to 0 °C. The naphthyl lithium solution was added drop wise *via* cannula. After complete addition the reaction solution was stirred overnight. A NMR-sample was taken from the solution. No conversion could be detected. The reaction mixture was heated to reflux for 2 days. No conversion was detectable. 0.8 mL phenyl lithium (1.4 mmol, 1.8 M in dibutylether) was added to the solution of 1-naphthyl$_3$SiCl (**16**) (after sampling, approx. 1.4 mmol left) at room temperature. The solution turned from yellow to slightly orange. The solution was refluxed for 5 hours. The solvent was removed and 50 mL toluene added. The precipitate was filtered off and the resulting orange-brown solution was concentrated to half the volume. A colourless solid crystallized at 0 °C.

1-naphthyl$_3$(phenyl)Si: ^{29}Si NMR (59.64 MHz, C_6D_6): δ -29.0 ppm.

4.7 Thermolysis

4.7.1 Equipment and sample preparation

The experiments were performed using a Carbolite single zone horizontal tube furnace GHA 12/600, a Carbolite horizontal tube furnace HZS 12/200/1200 and an Anton Paar Domed Hot Stage DHS 1100.

For the synthesis of the silane precursors see chapter 4.6. Samples were prepared on stainless steel, molybdenum or platinum foil, which were cut in pieces of approximately 0.5 x 0.5 cm. The molybdenum foil was polished with glass wool, rinsed with isopropanol and dried under a nitrogen stream Steel and platinum foil were rinsed with isopropanol and dried in a nitrogen stream prior to use. The foils were only handled with gloves and tweezers to avoid contamination. Molybdenum foil (0.1 x 100 x 200 mm, 99.95%) and platinum foil (0.025 x 25 x 25mm, 99.9%) were purchased from chemPUR and stored under Argon.

Thermolysis procedure:

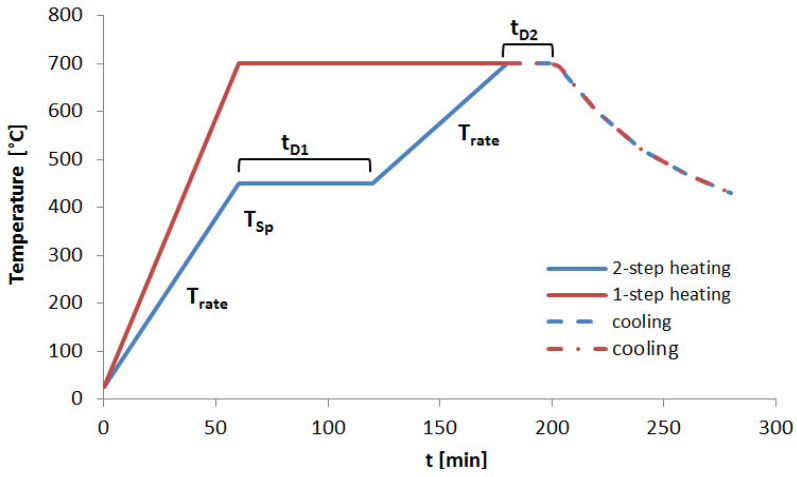

Figure 121: Scheme of heating procedure. T_{Sp}=Setpoint Temperature; t_{D1}/t_{D2}=Dwell Time 1/2; T_{rate}= Heating Rate

Samples were heated (T_{rate}) to a certain setpoint temperature (T_{Sp}) and held there for the dwell time (t_D). In a two-step procedure, samples were afterwards again heated and a second dwell time was applied. In both cases, this process is followed by a non controlled cooling of the samples. Samples were stored under air prior to measurement.

4.7.2 GHA 12/600

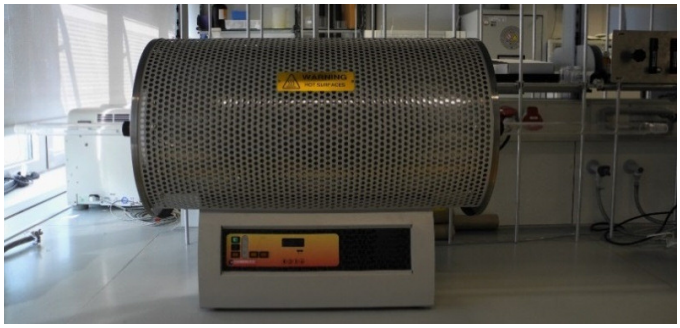

Figure 122: GHA 12/600

The furnace was equipped with a 1.20 m long, quartz schlenk tube (NS 29). The inlet was provided with a three-way stopcock which was connected to a vacuum pump and inert gas (Argon). On the outlet side, a Y-piece was connected to a second stopcock to allow evacuation of the tube (see Figure 123, 5a) and a manometer. A large diameter of the hole of the stopcock is preferred to avoid clogging by reaction products during thermolysis experiments. For single experiments, a condenser and cooling trap with liquid nitrogen after the outlet were used to provide a possibility to capture and further analyze the more volatile reaction products (5b).

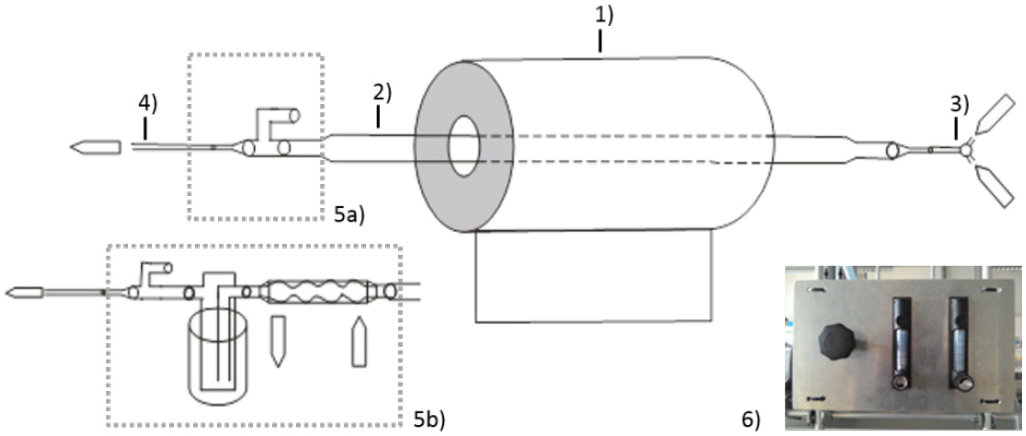

Figure 123: Schematic set up for thermolysis with *GHA 12/600;* 1) furnace, 2) quartz schlenk tube NS 29, 3) three-way stopcock, 4) gas tube, 5a) basic setup, 5b) extended setup, 6) gas flow controller

Gas flow was adjusted by two successive control systems (see Figure 123, 6). Prior to using the quartz tube was washed with acetone (or KOH and isopropanol when more heavily contaminated). It was evacuated to < 0.003 mbar, followed by flushing with argon. This procedure was repeated three times.

Sample preparation:

OE 1–OE 3: The precursor was dissolved and dripped onto the substrate until complete wetting of the surface. The solvent was slowly evaporated in vacuum (100 mbar).

OE 4–OE 5: Approximately 100 mg of the precursor were milled in a mortar to obtain a fine powder, which was put onto the surface and slightly compressed with a spatula.

OE 6: Single crystals were applied onto the surface and warmed until melting on a heating plate. The liquid silane was dispersed on the surface by tilting, until a thin layer was obtained.

Table 24: Experimental details for sample preparation of organo silanes with GHA 12/600; Fe=stainless steel, Mo= molybdenum

Sample No.	Silane	Preparation	c [mol/l]	Surface
OE 1	Si_5Ph_{10} (**36**)	THF solution	0.9	Fe
OE 2	1-naphthyl$_2SiH_2$ (**25**)	Toluene solution	0.028	Mo
OE 3	1-naphthyl$_2SiH_2$ (**25**)	Toluene solution	0.72	Mo
OE 4	1-naphthyl$_2SiH_2$ (**25**)	powder	-	Mo
OE 5	1-naphthyl$_2SiH_2$ (**25**)	powder	-	Mo
OE 6	1-naphthyl$_2SiH_2$ (**25**)	melting	-	Mo

Thermolysis procedure:

OE 1–OE 4: one step process

OE 5–OE 6: two step process

Table 25: Thermolysis details for sample preparation of organo silanes with GHA 12/600, T_{Sp}=setpoint temperature; t_D=dwell time; T_{rate}= heating rate

Sample No.	Silane	T_{Sp} [°C]	T_{rate} [°C/min]	t_D [min]
OE 1	Si_5Ph_{10} (**36**)	750	5	60
OE 2	1-naphthyl$_2SiH_2$ (**25**)	450	5	120
OE 3	1-naphthyl$_2SiH_2$ (**25**)	450	5	120
OE 4	1-naphthyl$_2SiH_2$ (**25**)	450	5	120
OE 5	1-naphthyl$_2SiH_2$ (**25**)	450/700	5	60/60
OE 6	1-naphthyl$_2SiH_2$ (**25**)	450/700	5	60/60

4.7.3 HZS 12/200/1200

Thermolysis experiments were performed in a 3-Zone Furnace with Siemens/Eurotherm control and gas system (see Figure 124). An 1800 mm long quartz work tube (φ 190 mm) with radiation shields and water cooled flanges on both sides was used. On the outlet side a pilot flame with spark ignition (operated with propane) was mounted to burn exhaust gas.

If necessary the quartz tube was cleaned with acetone. Prior to the experiment the tube was purged with nitrogen (10 L/min) for one hour to ensure that all the oxygen had been removed from the tube. The sample was brought into the middle part of the work tube with counter flow of inert gas. The required temperature program was set at the control panel. After finishing the thermolysis the sample was removed from the furnace and stored under air before characterization.

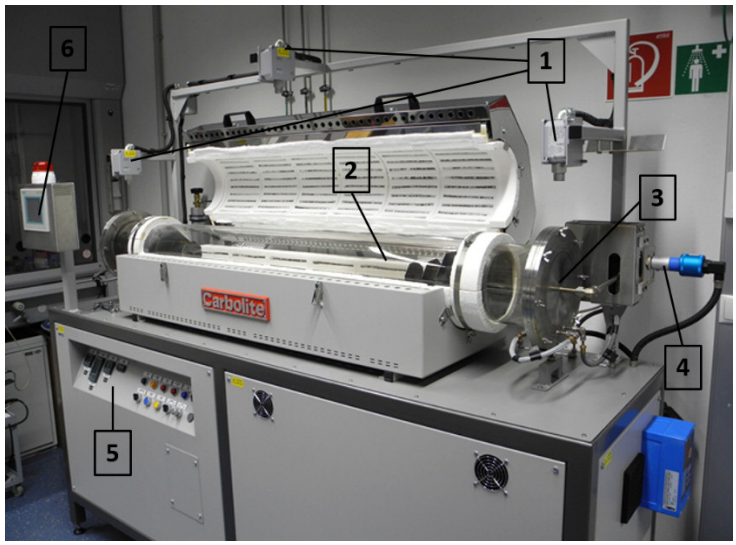

Figure 124: Set up of the HZS 12/200/1200; 1) Hydrogen leak detector, 2) Quartz tube with radiation shields on both sides, 3) water cooled flanges, 4) Pilot safety burner, 5)Temperature/Alarm control, 6) Touchscreen control panel

Sample preparation:

OE 8-OE 10 and OE 13: About 0.1 mL of the pure silane (liquid) was applied to the surface. The liquid silane was dispersed on the surface by tilting, until complete covering of the surface

OE 11: Single crystals were applied onto the surface and warmed until melting on a heating plate. The liquid silane was dispersed on the surface by tilting, until a thin layer was obtained.

OE 12: The precursor was dissolved and dripped onto the substrate until complete wetting of the surface. The solvent was slowly evaporated under vacuum (100 mbar).

Table 26: Experimental details for sample preparation of organo silanes with HZS 12/200/1200; Mo= molybdenum

Sample No.	Silane	Preparation	c [mol/l]	Surface
OE 7	blank	-	-	Mo
OE 8	benzyl$_2$SiH$_2$ (**20**)	pure	-	Mo
OE 9	*p*-tolyl$_2$SiH$_2$ (**34**)	pure	-	Mo
OE 10	1-naphthylSiH$_3$ (**30**)	pure	-	Mo
OE 11	1-naphthyl$_2$SiH$_2$ (**25**)	melting	-	Mo
OE 12	9-anthracenyl$_2$SiH$_2$ (**27**)	toluene solution	0.1	Mo
OE 13	*p*-*n*-butylphenyl$_2$SiH$_2$ (**23**)	pure	-	Mo

Thermolysis procedure:

OE 7–OE 13: two step process

Table 27: Thermolysis details for sample preparation of organo silanes with HZS 12/200/1200; T_{Sp}=setpoint temperature; t_D=dwell time; T_{rate}= heating rate

Sample No.	Silane	T_{Sp} [°C]	T_{rate} [°C/min]	t_D [min]
OE 7 –OE 13	see Table 26	450/700	10	120

4.7.4 DHS 1100 Domed Hot Stage

Figure 125: Anton Paar Domed Hot Stage 1100; 1) Dome, 2) Coupling connection to cooling air supply, 3) Wire to connection device, 4) Fixing ring with clasps, 5) Cooling ring with outlets for cooling air, 6) Sample plate, 7) Springs for fixing the sample, 8) Sample

The sample is fixed on the sample holder with springs to ensure good clamping and maximum temperature homogeneity. For experimental details of thermolysis experiments with the Anton Paar Domed Hot Stage 1100 see Table 28**.** For a second test row of experiments, a modified version of the Heating Stage was used (see Figure 126). In this setup an *in situ* analysis with e.g. SAXS measurements during thermolysis was possible. Additionally, an improved inert gas flow due to a better inlet/outlet system can be obtained. In the unmodified version, only a constant inert gas pressure inside the dome was achievable.

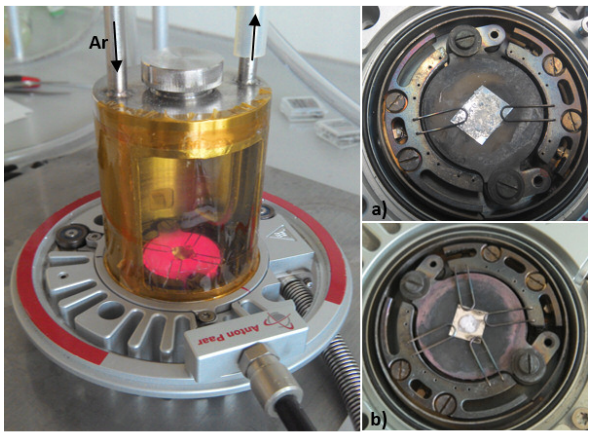

Figure 126: Experimental setup with modified dome a) solving in an appropriate solvent and coating onto the substrate, b) melting onto the foil, followed by spin coating

Sample preparation:

OE 14–OE 15: see OE 4

OE 16-OE 22: see OE 11

Table 28: Experimental details for sample preparation of organo silanes with DHS 1100; Mo= molybdenum, Pt= platinum

Sample No.	Preparation	Surface	T [°C]
OE 14	powder	Mo	700
OE 15	powder	Mo	700
OE 16	melting	Mo	700
OE 17	melting	Mo	700
OE 18	melting	Mo	700
OE 19	melting	Pt	700
OE 20	melting	Pt	700
OE 21	melting	Pt	700
OE 22	melting	Pt	700

Thermolysis procedure:

OE 14–OE 22: one step process

Table 29: Thermolysis details for sample preparation of organo silanes with DHS 1100; T_{Sp}=setpoint temperature; t_D=dwell time; T_{rate}= heating rate

Sample No.	Silane	T_{Sp} [°C]	T_{rate} [°C/min]	t_D [min]
OE 14	1-naphthyl$_2$SiH$_2$ (**25**)	700	50	120
OE 15-OE 22	1-naphthyl$_2$SiH$_2$ (**25**)	700	100	120

4.8 Reactivity experiments

4.8.1 Oligo-/Polymerization

Reaction of phenyl$_2$SiCl$_2$ with lithium - Dekaphenylcyclopentasilane Si$_5$Ph$_{10}$ (36)

A flask was furnished with 4.2g (605 mmol, 2 equiv.) finely cut lithium flakes in 250 ml THF. A dropping funnel was loaded with 76g diphenyldichlorosilane (300 mmol, 1 equiv.) diluted with 100 mL THF. The lithium containing solution was heated to reflux. A small scoop of hexaphenyldisilane was added. The Ph_2SiCl_2 was added drop wise to the refluxing solution during 3 hours. The solution turns from slightly yellow to red. Reflux overnight. Removal of the THF under reduced pressure. 600 ml toluene was added to the solid residue and refluxed for several hours. The solution was kept standing overnight without stirring to allow the salt to precipitate on the flask bottom. The supernatant yellow solution was transferred to a second flask *via* filter-cannula, followed by concentration to a third of the volume under reduced pressure. 500 mL pentane was added. The precipitate was filtered off and dried under vacuum to give a colourless powder. Yield 38 g (70%, 41.7 mmol). mp = 451 °C. ^{13}C NMR (C_6D_6, 75.5 MHz): δ 127.7, 128.7, 134.9, 138.3 ppm. ^{29}Si NMR (C_6D_6, 59.64 MHz): δ -34.2 ppm. IR(<1000 cm^{-1}): 997m ,972 vw,915 w, 855 w, 817 w, 732 vs, 695 vs, 680 sh, 665 sh, 619 vw, 548 vw, 530 w, 480 s, 471 s, 433, 389 w,343 sh, 336 s,325 s, 303 w.[160]

Reaction of 1-naphthyl$_2$SiCl$_2$ (8) with lithium

Lithium flakes (cut under Ar-Athmosphere) : A flask was furnished with 0.75 g lithium flakes (108 mmol, 5 equiv.) in 100 mL THF. 7.13 g 1-naphthyl$_2$SiCl$_2$ (**8**) (20.2 mmol, 1 equiv.) was added in small portions, while the solution was stirred vigorously. The yellow solution turned slightly brown after 5 minutes and a warming could be observed. The reaction solution was cooled temporarily. A colour change to green-black was observed after 60 minutes. The reaction was stirred overnight. THF was removed under reduced pressure and 200 mL of toluene added. The black solution was heated to reflux overnight. The hot solution was transferred to a second flask *via* filter cannula. The solution turned to yellow when in contact with air. The solvent was removed under reduced pressure and a yellow glass-like solid was obtained.

Lithium powder : A flask was furnished with 0.25 g lithium powder (36 mmol, 2.4 equiv.) in 90 mL THF. 5.37 g 1-naphthyl$_2$SiCl$_2$ (**8**) (15.2 mmol, 1 equiv.) solved in 50 ml THF was added in small portions, while the solution was stirred vigorously. The yellow solution turned slightly brown after 60 minutes. No warming could be observed. Stirred overnight and a white precipitate was formed. THF was removed under reduced pressure and 150 mL of toluene added. The solution was heated to reflux overnight. The solution was transferred into a second flask *via* filter cannula. The solvent was removed under reduced pressure and a white-yellow solid was obtained. Attempts to purify the compound by recrystallization, distillation or sublimation failed.

Lithium granules : A flask was furnished with 0.20 g lithium granules (28.8 mmol, 2 equiv.) in 75 mL THF. The solution was heated to reflux and a small scoop of hexaphenyldisilane was added. 5.13 g 1-naphthyl$_2$SiCl$_2$ (**8**) (14.5 mmol, 1 equiv.) solved in 50 ml THF was added in small portions, while the solution was stirred vigorously. The solution turned slightly brown-red after 90 minutes. THF was removed under reduced pressure and 150 mL of toluene added. The solution was heated to reflux overnight. The slightly green solution was transferred into a second flask *via* filter cannula. Removal of the solid yielded a white-yellow solid.

Preparation of metallococene catalyst Cp$_2$TiMe$_2$ (Petasis reagent)

The catalyst was prepared similar to literature.[161] A solution of MeLi (1.6 M in diethylether) was dried under reduced pressure for 2 hours. 30 mL of heptane were added. A slurry of 0.7g Cp_2TiCl_2 (2.8 mmol) in 40 mL heptane was poured onto the MeLi solution and stirred until all red solid (Cp_2TiMe_2) reacted. The yellow solution was transferred

to 3 mL dried MeLi *via* filter cannula and stirred for 3 hours to react remaining $Cp_2TiMeCl$. The solution was transferred into a second flask *via* filter cannula and dried under reduced pressure. The resulting crystalline orange solid was solved in 2 mL dry toluene and was stored in the freezer.

Handling remarks for Cp_2TiMe_2: Decomposition at 97 °C, soluble in aprotic solvents (THF, toluene, Et_2O,..). The solid is unstable at room temperature. Stable in solution (THF/toluene). No significant decomposition when briefly exposed to air and water. Sensitive towards light.[162]

Reaction of 1-naphthylSiH$_3$ (30) with Cp_2TiMe_2

0.9 g 1-naphthylSiH$_3$ (**30**) (5.68 mmol) was dissolved in 2 mL dry toluene. 0.66 mL Cp_2TiMe_2 (0.568 mmol, solution in toluene) was added *via* syringe at room temperature. The orange solution turns to a dark blue after 30 minutes. Stirring overnight, then kept standing at room temperature.

Reaction of 2,6-xylylSiH$_3$ (30) with Cp_2TiMe_2

0.5 g 2,6-xylylSiH$_3$ (3.7 mmol) was dissolved in 2 mL dry toluene. 0.43 mL Cp_2TiMe_2 (0.37 mmol solution in toluene) was added *via* syringe at room temperature. The orange solution turns to a dark blue after 20 minutes. Stirring overnight, then kept standing at room temperature.

Reaction of 1-naphthylSiH$_2$ (30) with Cp_2TiCl_2/n-BuLi

0.82 g 1-naphthyl$_2$SiH$_2$ (**25**) (2.88 mmol) and 22 mg Cp_2TiCl_2 (0.088 mmol) were dissolved in 3 mL dry toluene and cooled to 0 °C. 0.1 mL *n*-BuLi (0.16 mmol, 1.6 M in hexane) was added *via* syringe. A colour change to black was observed after 30 minutes. The solution was heated to 90 °C and kept stirring for 10 hours.

Reaction of 2,6-xylylSiH$_2$ (30) with Cp_2TiCl_2/n-BuLi

0.68 g 2,6-xylyl$_2$SiH$_2$ (**28**) (2.82 mmol) and 19.2 mg Cp_2TiCl_2 (0.077 mmol) were dissolved in 3 mL dry toluene and cooled to 0 °C. 0.096 mL *n*-BuLi (0.154 mmol, 1.6 M in hexane) was added *via* syringe. The solution was heated to 90 °C and kept stirring for 10 hours.

4.8.2 UV- irradiation of organosilanes

The UV irradiation experiments were carried out in a Heraeus laboratory-UV-reactor system equipped with a UV immersion lamp TQ-150, an immersion-/ and cooling tube (see Figure 127). The used immersion lamp is a medium-pressure mercury vapour lamp with a broad emission spectrum in the UV range above 190 nm. The immersion-/ and cooling tube are made of quartz glass with a UV transmission level of 92%. The reaction solution was irradiated in the range of 190 – 600 nm.

For the synthesis of the starting materials see chapter 4.6. UV-VIS experiments of the organosilanes in *n*-hexane were used to determine the most suitable compounds for irradiation. The irradiation experiments were carried out in standard NMR tubes. All reactions were carried out under nitrogen atmosphere. The organosilanes were dissolved in dry C_6D_6 (stored over a potassium mirror) with concentrations of approximately 0.1 mol/L.

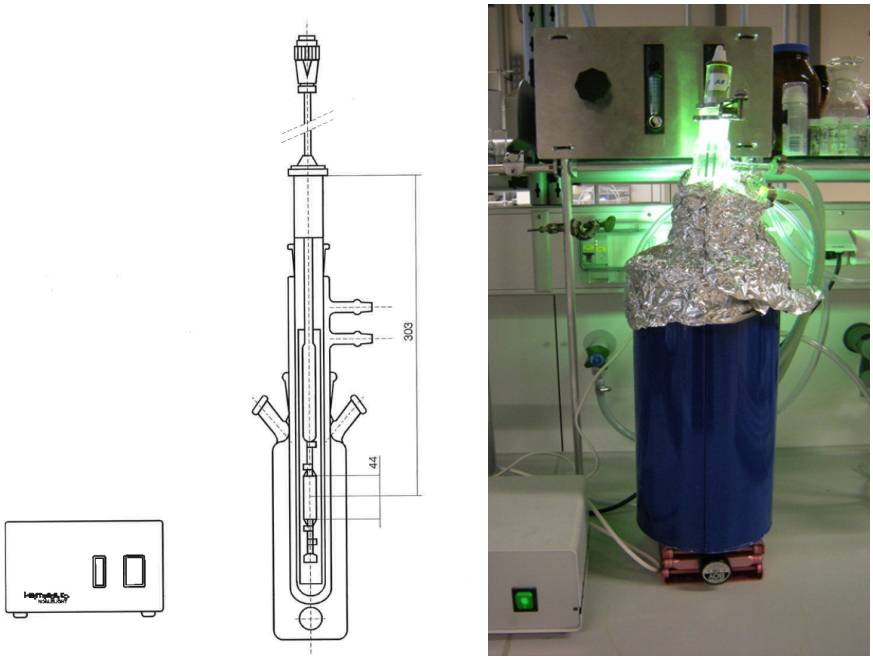

Figure 127: Heraeus laboratory-UV-reactor system, schematic setup

Compound **20, 27** and **30** were selected for the irradiation experiments. The NMR tubes were mounted beside the middle part of the immersion lamp (brightest area) with a constant distance of 2 mm. Irradiation times varied from 5 minutes to 6 hours. For experimental parameters see Table 30.

Table 30: Reaction conditions UV irradiation experiments

Compound	Solvent	Cooling	Reaction temperature
benzyl$_2$SiH$_2$ (**20**)	C_6D_6	water	room temperature (21 °C)
1-naphthylSiH$_3$(**30**)	C_6D_6	water	room temperature (21 °C)
1-naphthylSiH$_3$(**30**)	C_6D_6	MeOH	EtOH/N_2 -78 °C
1-naphtyhlSiH$_3$(**30**)	CH_2Cl_2	MeOH	EtOH/N_2 -78 °C
9-anthracenyl$_2$SiH$_2$(**27**)	C_6D_6	water	room temperature (21 °C)
9-anthracenyl$_2$SiH$_2$(**27**)	pentane	water	room temperature (21 °C)
9-anthracenyl$_2$SiH$_2$(**27**)	C_6D_6	water	room temperature (21 °C)

4.8.3 DXRL (Deep X-Ray Lithography)

The irradiation was performed at the DXRL beamline at ELETTRA using the DEX02 scanner (Jenoptik GmbH). For a more detailed description of the DXRL technique see Perennes *et al.*[163]

Molybdenum foil (0.1 x 100 x 200mm, 99.95%) was purchased from chemPUR and stored under Argon. Standard IR transparent silicon wafers were used. For the synthesis of the starting materials see chapter 4.6. Si_4Ph_{10} and $[SiPh_2]_n$ can be isolated as by-products in the synthesis of Si_5Ph_{10} (see 4.8.1).

Sample preparation: The molybdenum foil was polished and rinsed with isopropanol. The Si-Wafer was washed in boiling acetone, rinsed with isopropanol and dried in a N_2 stream. The silanes were dissolved in dry toluene and slightly heated if necessary. Approximately 10 µl of the solution were dripped on the substrate and spin coated. This process was repeated until complete coating of the surface.

Figure 128: Sample preparation *via* spincoating; a) Coated molybdenium substrate, Sample holder with mask (left) and irradiation chamber of the DXRL (right)

Besides the compounds in Table 31**,** other substances were tried unsuccessfully. Benzyl$_6$SiH$_6$[3] and Si$_6$Ph$_{12}$[3] could not be dissolved in the given solvents (toluene, CH_2Cl_2, EtOH). Benzyl$_2$SiH$_2$ (**20**), *p*-tolyl$_2$SiH$_2$ (**34**) and 1-naphthylSiH$_3$ (**30**) were diluted with an aliquot volume of toluene, but wetting of the surface could not be achieved.

Table 31: Experimental details for DXRL, m=sample mass, V=solvent volume, rpm= rotations per minute, Mo=molybdenum

Compound	m [mg]	V [ml]	Spincoating Wafer t[min]/rpm	Spincoating Mo-foil t[min]/rpm
phenyl$_{10}$Si$_4$	27	0.8	0:45/600	0:30/1000; 0:30/2000
[phenyl$_2$Si]$_n$	111	3	0:30/1000	0:30/1000; 0:30/2000
1-naphthyl$_2$SiH$_2$ (**25**)	46	0.6	0:30/1000	0:30/1000; 0:30/2000
9-anthracenyl$_2$SiH$_2$ (**27**)	7	0.4	0:30/1000	0:30/1000; 0:30/2000
2,6-xylyl$_2$SiH$_2$ (**28**)	60	0.4	no spinning	no spinning
p-*n*-butylphenyl$_2$SiH$_2$ (**23**)	pure	pure	0:30/1000	0:30/1000; 0:30/2000
2,4-xylylSiH$_3$ (**29**)	100	0.11	0:30/1000	0:30/1000; 0:30/2000

The samples were mounted on a mask and irradiated with various doses (see Table 32). For the Mo-foil samples doses from 220 to 7044 J/cm^2 were employed. Samples on Si-Wafers were irradiated only with the highest dose (7044 J/cm^2). Samples were analyzed *via* IR spectroscopy and SEM/EDX.

Table 32: Doses for DXRL irradiation

power on sample [W/cm^2]	time [sec])	Dose [energy/unit surface] [J/cm^2]
2.472	89	220.0
2.472	178.1	440.2
2.472	356.2	880.5
2.472	712.4	1761.1
2.472	1424.8	3522.3
2.472	2849.7	7044.6

[3] compounds were provided by the institute of inorganic chemistry of TU Graz

4.8.3.1 PMMA experiments

0.0208 g 9-anthracenyl$_2$SiH$_2$ (**27**) were mixed with 5.55 g PMMA (AR-P 631-671) and stirred for 30 minutes. The resulting slightly yellow solution was spin coated on a silicon wafer (wafer rinsed with isopropanol and dried prior to use). Spin coating was performed at 2000 rpm for 1 minute followed by soft bake for 2 minutes at 150 °C. The thickness of the resulting film is about 690 nm. The wafer was irradiated *via* DXRL with doses of 2, 50, 125 and 250 kJ/cm^2. A sample with a dose of 0 kJ/cm^2 and 250 kJ/cm^2 was heated to 600 °C and analyzed *via in situ* SAXS analysis. Irradiation and heating were repeated for a pure PMMA sample for comparison.

4.8.4 Selective Chlorination

Reaction was done similar to literature.[141] For the synthesis of the starting materials 1-naphthyl$_2$SiH$_2$ (**25**), 1-naphthylSiH$_3$ (**30**) and 9-anthracenyl$_2$SiH$_2$ (**27**) see chapter 4.6.2. Phenyl$_2$SiH$_2$ (97%), and phenylSiH$_3$ (97%) were purchased from Aldrich, ethyl$_2$SiH$_2$ (98%) and *t*-butyl$_2$SiH$_2$ (97%) from ABCR. TCCA (Trichloroisocyanuric acid, 97%) was purchased from Alfa Aesar. All commercially available products were used without further purification.

General procedure

Approximately 1 mmol of the silane was dissolved in 3-5 mL THF. The flask was cooled to -20 °C with EtOH/N$_2$. TCCA was added in small portions (new addition when last portion completely dissolved). After the addition, the ice bath was removed and the solution allowed to warm to room temperature. The solution was stirred until clouding of the solution was observed. The insoluble parts were filtered off and the solvent removed under reduced pressure. Purification was done *via* bulb to bulb distillation. GC-MS and NMR analysis of the obtained products was performed to determine the product distribution.

For experiment F10, TCCA was dissolved in 10 mL THF in a second flask. The solution was cooled to -20 °C and added drop wise to the silane solution. For experiment F9 powdered TCCA was used and added portion wise in counter N$_2$ flow.

Table 33: Experimental details for the selective chlorination of phenyl$_2$SiH$_2$ (=E) with TCCS in THF; E:TCCA = ratio educt to TCCA.

Exp.	Educt [mmol]	TCCA [mmol]	E:TCCS	Solvent [mL]	Addition time [min]	Reaction time [min]
A	0.9939	0.33	1 : 1	5	10	35
B	0.9939	0.36	1 : 1.1	5	10	35
C	0.9939	0.495	1 : 1.5	5	10	35
D	0.9939	0.5925	1 : 1.78	5	10	45
E	0.9939	0.619	1 : 1.82	5	10	45
F	0.9939	0.66	1 : 2	5	10	45
G	0.9939	0.701	1 : 2.12	5	10	45
H	0.9939	0.742	1 : 2.24	5	13	45

No clouding of the solution could be detected for experiment A7. In all other experiments a formation of a precipitate could be observed after a reaction time of about 60 minutes. All experiments were stirred for about 120 minutes before filtering and analysis. No clouding was observed for experiment P, but the solution turned viscous. In reaction P a complete chlorination was attempted. The slightly higher solvent amount is necessary due to the low solubility of 9-anthracenyl$_2$SiH$_2$ (**27**) in THF.

Table 34: Reaction of phenyl$_2$SiH$_2$ (= educt) with TCCA (E:TCCA=1:1); variation of reaction parameters RT=reaction time, AT= addition time, C= concentration

Exp.	Educt [mmol]	TCCA [mmol]	Solvent [mL]	Addition time [min]	Reaction time [min]	Variation
A1	0.9939	0.33	5	10	60	RT
A2	0.9939	0.33	5	10	120	RT
A3	0.9939	0.33	5	10	1020	RT
A4	0.9939	0.33	5	5	45	AT
A5	0.9939	0.33	2	10	45	C
A6	1.987	0.66	2	10	45	C
A7	0.9939	0.33	10	10	120	C

Table 35: Reaction of phenyl$_2$SiH$_2$ (= educt) with TCCA (E:TCCA=1:2); variation of reaction parameters RT=reaction time, AT= addition time, C= concentration

Exp.	Educt [mmol]	TCCA [mmol]	Solvent [mL]	Addition time [min]	Reaction time [min]	Variation
F1	0.9939	0.66	2	10	45	C
F2	0.9939	0.66	10	10	60	C
F3	4.969	3.3	50	30	60	scale up
F4	4.969	3.3	50	30	60	work-up
F5	0.9939	0.66	5	30	45	AT
F6	9.939	6.6	50	60	45	scale up
F7	9.939	6.6	50	60	45	work-up
F8	0.9939	0.66	10	10	1080	RT
F9	0.9939	0.66	5	10	45	TCCA powder
F10	4.969	3.3	20+10	30	60	TCCA solution

Table 36: Experimental details for the reaction of secondary silane (= educt) with TCCA

Exp.	Silane	Educt [mmol]	TCCS [mmol]	E:TCCS	Solvent [mL]	Reaction time [min]
K	1-naphthyl$_2$SiH$_2$ (**25**)	0.998	0.33	1 : 1	5	40
L	1-naphthyl$_2$SiH$_2$ (**25**)	0.993	0.33	1 : 1	10	60
M	1-naphthyl$_2$SiH$_2$ (**25**)	0.496	0.165	1 : 1	3	60
N	ethyl$_2$SiH$_2$	0.98	0.329	1:1	5	60
O	*t*-butyl$_2$SiH$_2$	1	0.33	1:1	5	60
P	9-anthracenyl$_2$SiH$_2$ (**27**)	0.2	0.13	1 : 2	4	120

Table 37: Experimental details for the reaction of primary silanes (= educt) with TCCA

Exp.	Silane	Educt [mmol]	TCCA [mmol]	E:TCCA	Reaction time [min]	Solvent [mL]	Addition time [min]
I	1-naphthylSiH$_3$ (**30**)	0.993	0.33	1 : 1	30	10	30
I1	1-naphthylSiH$_3$ (**30**)	0.993	0.33	1 : 1	120	10	30
I2	1-naphthylSiH$_3$ (**30**)	0.993	0.33	1 : 1	120	10	30
J	phenylSiH$_3$	1.107	0.369	1 : 1	120	5	30

5 Summary and outlook

In the present work, the synthesis, characterization and reactivity of novel arylsilanes was studied to give a comprehensive overview about the spectroscopic, as well as solid state structures and interactions of various aryl silanes. The obtained organosilanes were investigated regarding their reactivity to reveal novel applications.

Various organo(chloro-)silanes with varying steric bulk were synthesized in which the silicon atom is bonded to either a sp^3 carbon or bonded directly to the sp^2 carbon of an aromatic system. The compounds show *ortho*, *meta* or *para* substitution of the phenyl ring, as well as double substitution in 2,6- and 2,4-position towards the silicon atom. In addition, polyclyclic substituents were as well investigated. The synthesis of organo(chloro)silanes could be achieved by either a lithiation or a Grignard reaction with varying stoichiometry of the active reagent towards $SiCl_4$. The corresponding silanes could be obtained in good yields by reaction of the chlorosilanes with LAH in ethereal solution. Solid state structures of the organo silanes revealed the presence of aromatic secondary interactions, including π–π stacking, edge to face and $CH_3\cdots\pi$ interactions, depending on the nature of the substituent. Additionally, the successful *in situ* crystallization of a liquid silane was achieved via OHCD Laser assisted capillary cryistallization.

The investigations of the ^{29}Si-NMR data showed that the increasing steric demand of the substituent in *ortho* position leads to a ^{29}Si-NMR high-field shift caused by shielding effects towards the silicon atom. In the case of chlorosilanes, the so called “sagging behavior”, which emerges upon successive exchange of substituents on the silicon, could be proven by the position of the ^{29}Si-NMR shifts on a bell shaped curve (which results when shifts are plotted against the sum of electronegativities of the substituents of the silicon). The DFT calculations of ^{29}Si-NMR chemical shifts and coupling constants of organo(chloro)silanes show an exceptionally good agreement between measured and DFT calculated in all cases.

In the thermolysis of organosilanes, 9-anthracenyl$_2$SiH$_2$ (**27**) and 1-naphthyl$_2$SiH$_2$ (**25**) turned out to be the most promising candidate, by generating carbon free particles under certain conditions with a high reproducibility. Even though silanes with other substituents other than naphthyl or anthracenyl produce layers or particles with a higher carbon content, this might lead to the interesting possibility to “tune” the carbon content by intentionally choosing the organic substituent of the organo silane .

Regarding coupling reactions, it could be shown that the reaction of 1-naphthylSiH_3 (**30**) with Cp_2TiMe_2 leads to the desired oligmerization. Polymerization could not be observed, possibly due to the higher steric demand of the naphthyl group as compared to phenyl. For 2,6-xylylSiH_3 (**37**), a reaction takes place but no characterization was possible. Dehydrogenative coupling of secondary silanes with *n*-BuLi/Cp_2TiCl_2 was not sucessful under the used conditions.

Despite our attempts to work under well defined reaction conditions, Wurtz coupling reactions were not successful, leading to unreproducible results.

9-anthracenyl$_2SiH_2$ (**27**) could be successfully irradiated, leading to an intramolecular [4+4] adduct, which was characterized *via* ^{1}H-NMR. Compounds with a smaller π-system (benzyl, naphthyl) did not undergo a reaction under the given conditions. Irradiation of organo silanes by higher energy doses, which was performed with DXRL, led to a presumed breaking of the Si-H bond followed by a oxidation. The irradiation leads to glass like layers which show a much higher homogeneity than the unexposed films. Further analysis and characterization might lead to interesting properties.

The selective chlorination of secondary and primary aryl and alkyl silanes with TCCA could be successfully performed for various organo silanes. For phenyl$_2SiH_2$ 86% product yield could be obtained. Siloxane formation was detected for the chlorination of diethylsilane but not for *t*-butylsilane or the arylsubstituted compounds. All reactions showed the importance of suitable reaction conditions, especially the stoichiometry turned out to be a crucial point and should be performed for all silanes in a future study. Also the influence of a higher temperature on the reaction time should be investigated.

All performed reaction studies revealed interesting characteristics of the starting silanes. More detailed studies might lead to deeper understanding of the reaction mechanism and possible applications.

6 Appendix

6.1 Crystallographic data

Table 38: Crystallographic data and details of measurements for compounds 1, 2 and 5, 8, 9, 11. Mo Kα (λ=0.71073Å). $R_1 = \Sigma/ |F_o| - |F_c|/|\Sigma|F_d$; $wR2 = [\Sigma_w(F_o^2-F_2^2)^2/\Sigma_w(F_o^2)^2]^{1/2}$

Compound	benzyl$_2$SiCl$_2$ (**1**)	fluorenyl$_2$SiCl$_2$ (**2**)	*o*-tolyl$_2$SiCl$_2$ (**5**)	1-naphthyl$_2$SiCl$_2$ (**8**)	2,4-xylyl$_2$SiCl$_2$ (**9**)	2,6-xylyl$_2$SiCl$_2$ (**11**)
Formula	$C_{14}H_{14}Cl_2Si$	$C_{26}H_{18}Cl_2Si$	$C_{14}H_{14}Cl_2Si$	$C_{20}H_{14}Cl_2Si$	$C_{16}H_{18}Cl_2Si$	$C_{16}H_{18}Cl_2Si$
Fw (g mol^{-1})	281.24	429.39	281.24	353.30	309.29	309.29
a (Å)	9.8244(2)	7.4007(2)	6.9270(4)	15.1186(4)	7.9627(3)	8.5365(3)
b (Å)	13.8493(4)	9.6653(3)	15.1723(8)	7.3181(2)	8.1319(3)	8.6184(3)
c (Å)	10.5055(3)	14.8304(5)	13.3144(7)	15.7994(4)	12.6224(4)	10.7234(4)
α (°)	90	96.9000(12)	90	90	105.372(1)	80.4680(18)
β (°)	102.997(1)	103.4840(12)	97.305(2)	110.894(1)	94.096(2)	82.8440(19)
γ (°)	90	104.4250(13)	90	90	96.305(2)	81.8820(19)
V (Å^3)	1392.77(6)	981.00(5)	1387.97(13)	1633.09(7)	779.00(5)	766.09(5)
Z	4	2	4	4	2	2
Crystal size (mm)	0.13×0.12×0.10	0.20×0.19×0.10	0.42×0.18×0.16	0.30×0.10×0.09	0.16×0.09×0.08	0.12×0.11×0.05
Crystal habit	Block, brown	Block, colourless	Block, colourless	Block, colourless	Block, colourless	Block, colourless
Crystal system	Monoclinic	Triclinic	Monoclinic	Monoclinic	Triclinic	Triclinic
Space group	$P2_1/n$	P-1	$P2_1/c$	$P2_1/n$	P-1	P-1
d_{calc} (mg/m^3)	1.341	1.454	1.346	1.437	1.319	1.341
μ (mm^{-1})	0.53	0.40	0.53	0.47	0.48	0.49
T (K)	100(2)	100(2)	100(2)	100(2)	100(2)	100(2)
2ϑ range (°)	2.5–27.1	2.2–27.1	2.0–30.1	2.9–27.1	1.0–25.0	2.9–27.1
F(000)	584	444	584	728	324	324
R_{int}	0.082	0.019	0.033	0.104	0.036	0.029
independent reflns	2428	4329	4070	3556	2723	3373
No. of params	154	262	156	208	176	176
R1, wR2 (all data)	R1 = 0.0458 wR2 = 0.1208	R1 = 0.0264 wR2 = 0.0696	R1 = 0.0618 wR2 = 0.1736	R1 = 0.0582 wR2 = 0.1285	R1 = 0.0439 wR2 = 0.0826	R1 = 0.0409 wR2 = 0.0727
R1, wR2 (>2σ)	R1 = 0.0423 wR2 = 0.1166	R1 = 0.0250 wR2 = 0.0685	R1 = 0.0590 wR2 = 0.1724	R1 = 0.0472 wR2 = 0.1191	R1 = 0.0377 wR2 = 0.0798	R1 = 0.0308 wR2 = 0.0682

Table 39: Crystallographic data and details of measurements for compounds 15, 16 and 2-naphthylSiCl$_3$.[30] Mo Ka (l=0.71073Å). $R_1 = S/ |F_o|- |F_c|/|S|F_d$; $wR2 = [S_w(F_o^2-F_2^2)^2/S_w(F_o^2)^2]^{1/2}$

Compound	1-naphthyl$_3$SiCl (**16**)	1-naphthylSiCl$_3$ (**15**)	2-naphthylSiCl$_3$[30]
Formula	$C_{30}H_{21}ClSi$	$C_{10}H_7Cl_3Si$	$C_{10}H_7Cl_3Si{\cdot}0.5(C_{10}H_8)$
Fw (g mol-1)	445.01	261.60	325.68
a (Å)	9.3870(3)	9.9473(4)	13.5797(8)
b (Å)	11.9962(4)	9.0965(4)	6.0837(4)
c (Å)	12.2797(5)	12.3302(6)	17.6511(10)
α (°)	83.056(2)	90	90
β (°)	70.853(2)	93.312(2)	91.442(2)
γ (°)	83.48 (2)	90	90
V (Å3)	1292.70(8)	1113.84(9)	1457.78(15)
Z	2	4	4
Crystal size (mm)	0.24 × 0.19 × 0.09	0.20 × 0.15 × 0.14	0.10 × 0.05 × 0.03
Crystal habit	Block, colourless	Block, colourless	Block, colourless
Crystal system	Triclinic	Monoclinic	Monoclinic
Space group	P-1	P21/c	P21/n
dcalc (mg/m3)	1.143	1.560	1.484
μ (mm-1)	0.21	0.89	0.69
T (K)	100(2)	100(2)	100(2)
2θ range (°)	2.4–27.1	2.8–27.1	3.0–26.9
F(000)	464	528	664
Rint	0.031	0.120	0.079
independent reflns	5707	2452	3198
No. of params	290	127	172
R1, wR2 (all data)	R1 = 0.0413 wR2 = 0.0907	R1 = 0.0462 wR2 = 0.1066	R1 = 0.0797 wR2 = 0.0907
R1, wR2 (>2σ)	R1 = 0.0335 wR2 = 0.0862	R1 = 0.0390 wR2 = 0.0993	R1 = 0.0404 wR2 = 0.0782

Table 40: Crystallographic data and details of measurements for compounds 21, 25-28 and 34. Mo Kα (λ=0.71073Å). $R_1 = \Sigma / |F_o| - |F_c| / |\Sigma| F_d$; $wR2 = [\Sigma_w(F_o^2 - F_2^2)^2 / \Sigma_w(F_o^2)^2]^{1/2}$

Compound	fluorenyl$_2$SiH$_2$ (**21**)	p-tolyl$_2$SiH$_2$ (**34**)	2,4-xylyl$_2$SiH$_2$ (**26**)	2,6-xylyl$_2$SiH$_2$ (**28**)	1-naphthyl$_2$SiH$_2$ (**25**)	9-anthracenyl$_2$SiH$_2$ (**27**)
Formula	$C_{26}H_{20}Si$	$C_{14}H_{16}Si$	$C_{16}H_{20}Si$	$C_{16}H_{20}Si$	$C_{20}H_{16}Si$	$C_{28}H_{20}Si$
Fw (g mol-1)	360.51	212.36	240.41	240.41	284.42	384.53
a (Å)	9.8085(4)	5.9160(4)	8.1892(5)	12.157(11)	13.9757(4)	17.7258(9)
b (Å)	8.4056(4)	8.0299(6)	12.8961(8)	8.531(9)	8.7811(3)	5.3171(3)
c (Å)	22.3946(11)	25.5211(17)	13.1669(8)	14.448(14)	24.5466(7)	20.6504(10)
α (°)	90	90	90	90	90	90
β (°)	93.1350(19)	90	94.379(3)	110.189(16)	90	95.303(2)
γ (°)	90	90	90	90	90	90
V (Å3)	1843.59(15)	1212.38(14)	1386.48(15)	1406(2)	3012.41(16)	1937.97(17)
Z	4	4	4	4	8	4
Crystal size (mm)	0.20×0.19×0.15	0.29×0.25×0.20	0.29×0.20×0.18	0.48×0.41×0.35	0.24×0.20×0.16	0.27×0.25×0.10
Crystal habit	Block, colourless	Block, colourless	Block, colourless	Block, colourless	Block, colourless	Block, colourless
Crystal system	Monoclinic	Orthorhombic	Monoclinic	Monoclinic	Orthorhombic	Monoclinic
Space group	P21/n	P212121	P21/c	P21/c	Pbca	P21/c
dcalc (mg/m3)	1.299	1.163	1.152	1.135	1.254	1.318
μ (mm-1)	0.14	0.16	0.15	0.14	0.15	0.13
T (K)	100(2)	100(2)	100(2)	100(2)	100(2)	100(2)
2θ range (°)	2.6–27.2	2.7–29.3	3.0–27.2	2.9–27.9	2.2–27.7	2.2–27.1
F(000)	760	456	520	520	1200	808
Rint	0.034	0.054	0.031	0.030	0.032	0.104
independent reflns	4080	3116	3089	3071	3286	3421
No. of params	252	146	234	166	197	270
R1, wR2 (all data)	R1 = 0.0392 wR2 = 0.085	R1 = 0.0490 wR2 = 0.105	R1 = 0.0423 wR2 =0.1147	R1 = 0.0446 wR2 = 0.117	R1 = 0.0407 wR2 = 0.085	R1 = 0.0528 wR2 = 0.115
R1, wR2 (>2σ)	R1 = 0.033 wR2 = 0.0807	R1 = 0.044 wR2 = 0.1021	R1 = 0.0379 wR2 = 0.1105	R1 = 0.036 wR2 = 0.1014	R1 = 0.031 wR2 = 0.0759	R1 = 0.043 wR2 = 0.1047

6.2 TGA/DSC/MS

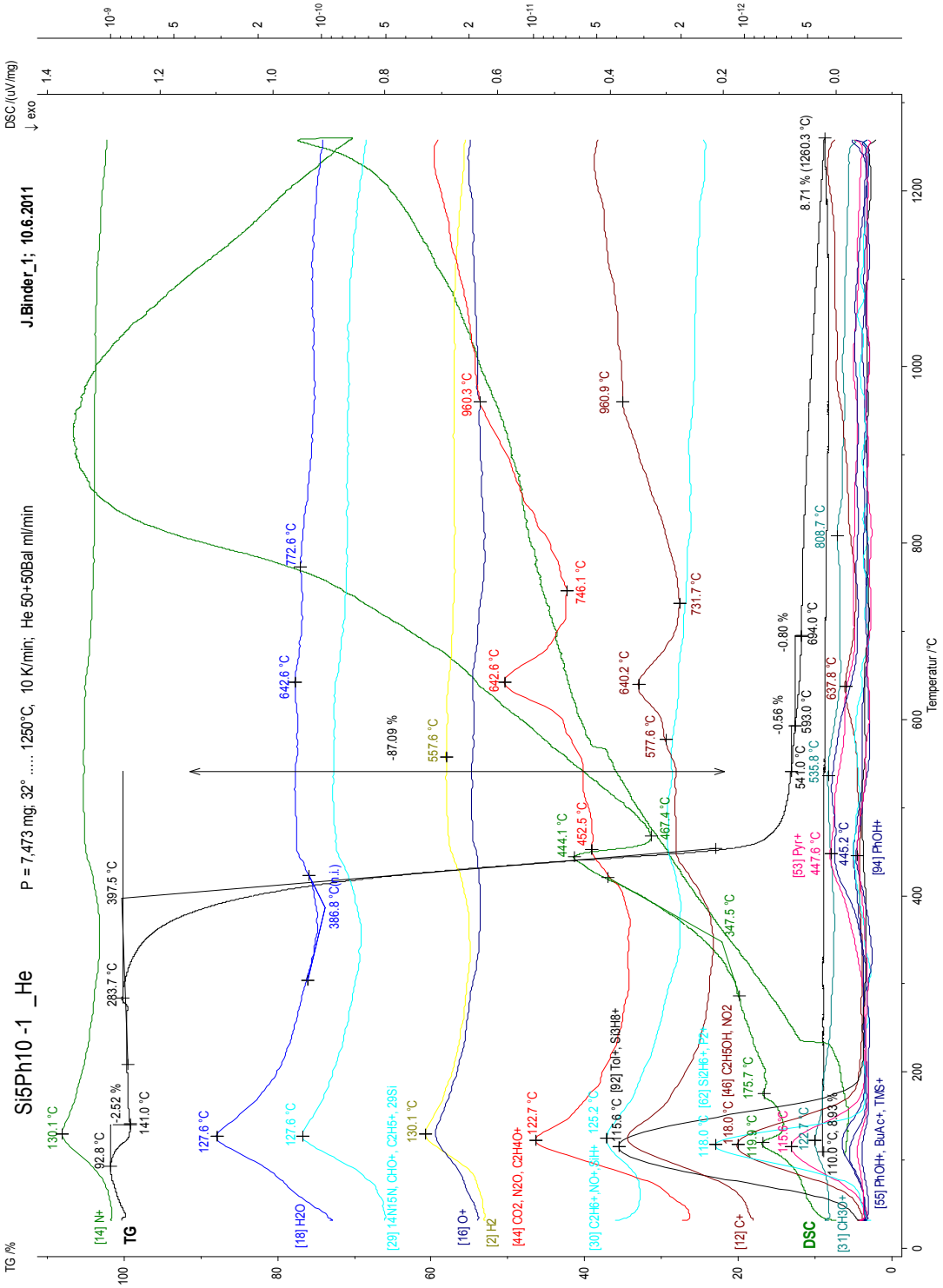

Figure 129: TGA/DSC/MS of Si_5Ph_{10} (36)

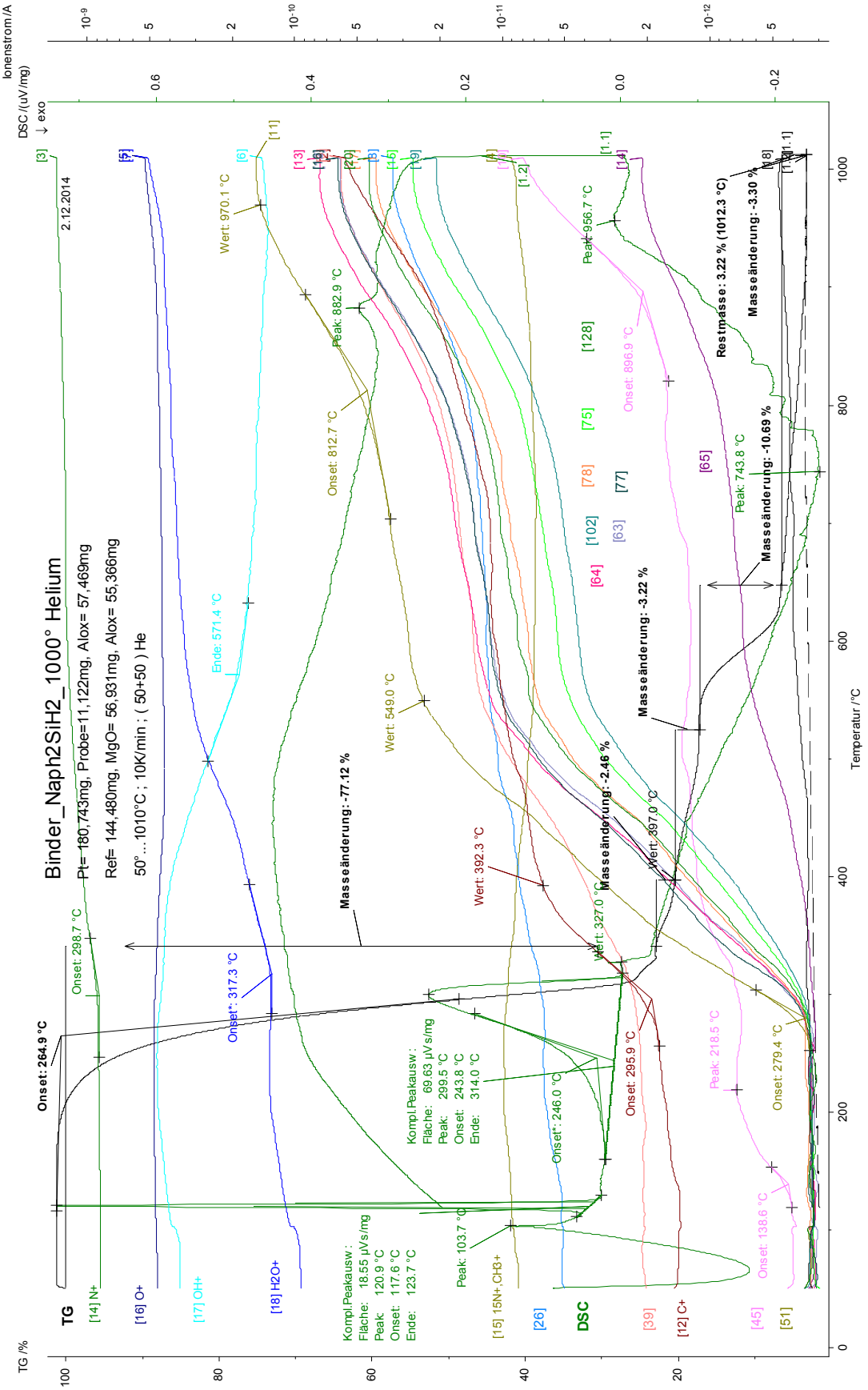

Figure 130: TGA/DSC/MS of 1-naphthyl$_2$SiH$_2$ (25)

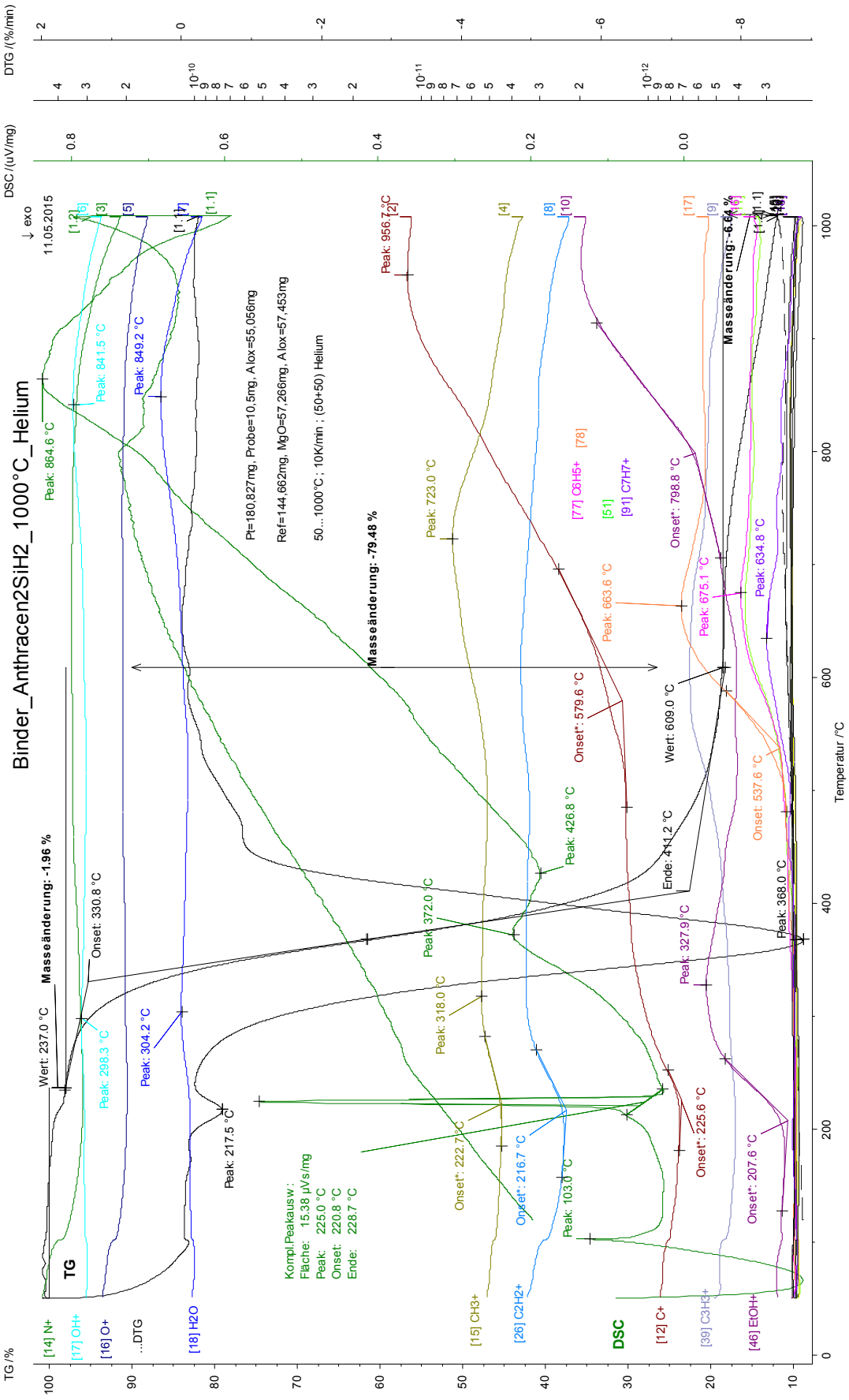

Figure 131: TGA/DSC/MS of 9-anthracenyl$_2$SiH$_2$ (27)

6.3 ATR-IR data

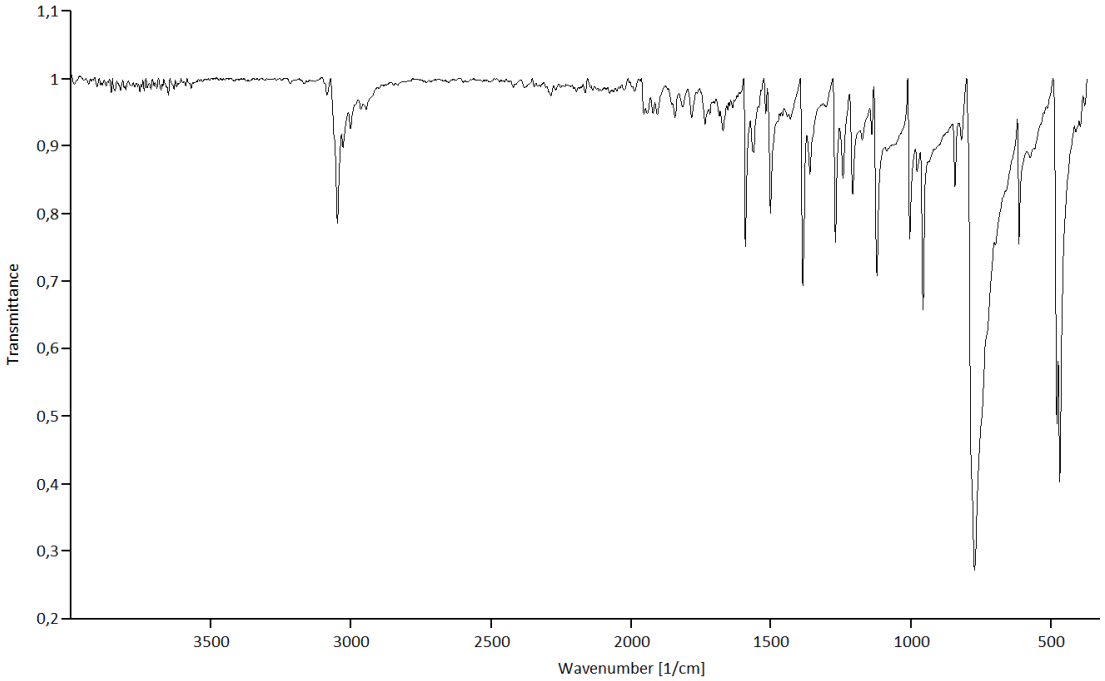

Figure 132: ATR-IR spectra of naphthalene

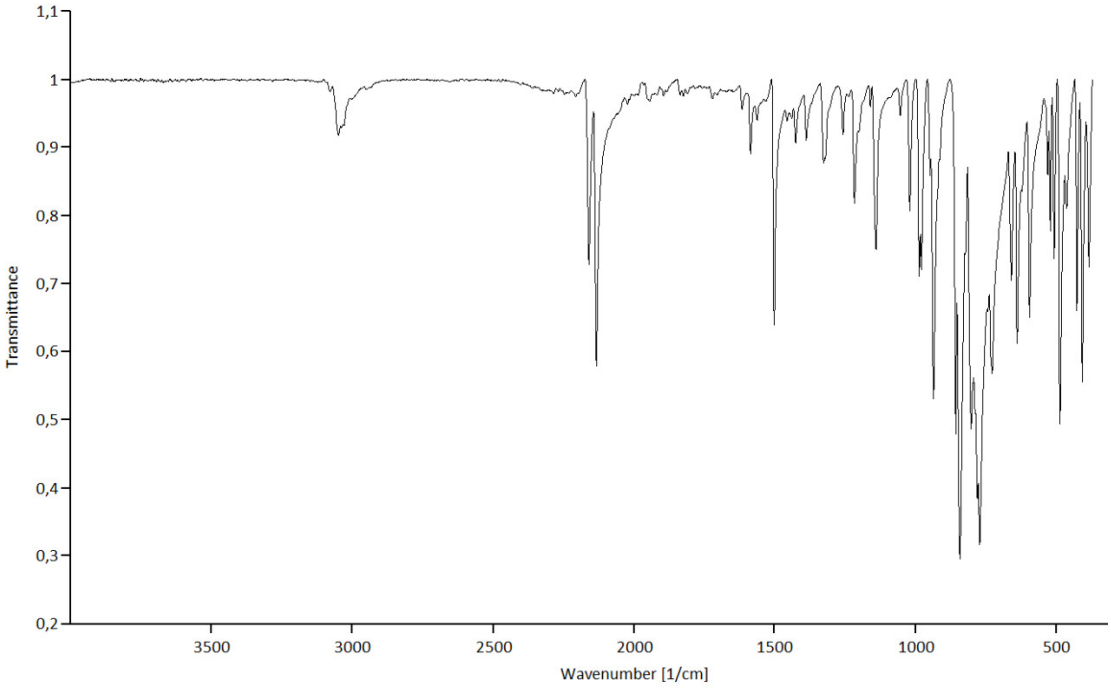

Figure 133: ATR-IR of 1-naphthyl$_2$SiH$_2$ (25)

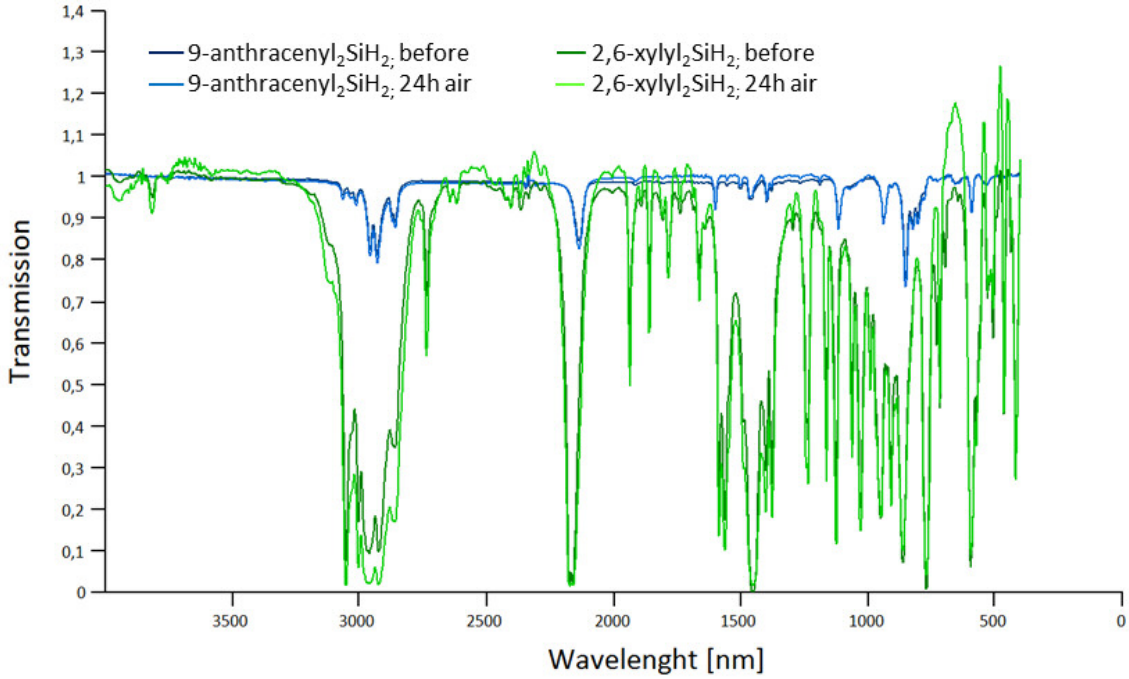

Figure 134: Hydrolysis test of 9-anthracenyl$_2$SiH$_2$ (27) and 2,6-xylyl$_2$SiH$_2$ (28)

6.4 Mass spectroscopy

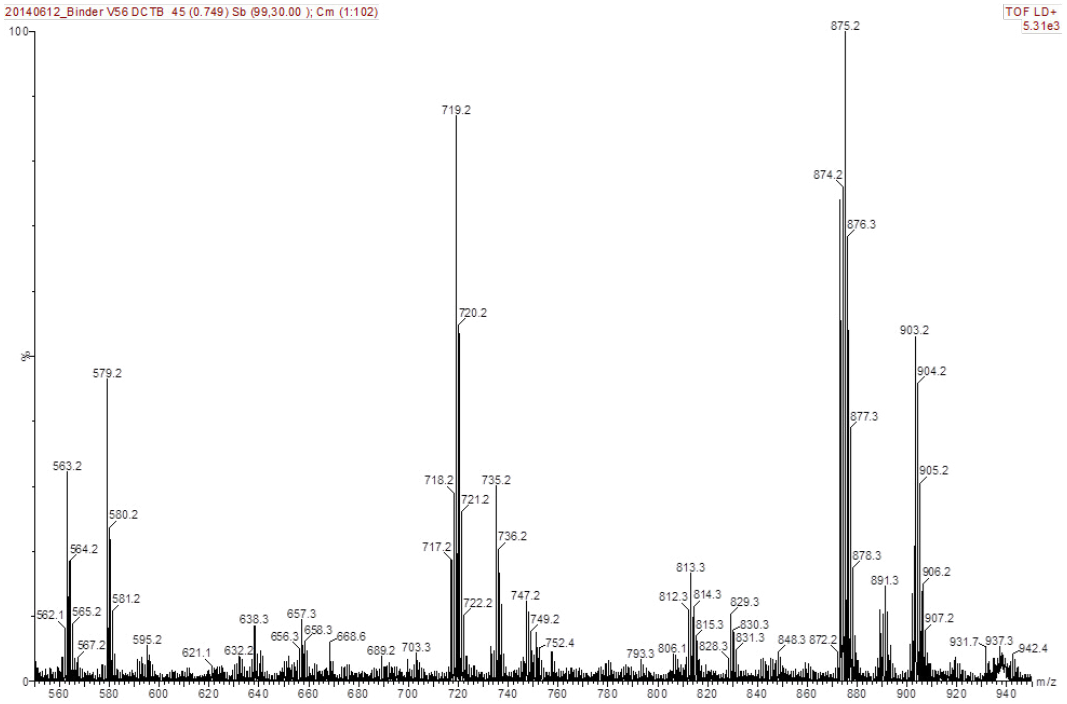

Figure 135: MALDI-TOF of the precipitate [1-naphthyl$_x$SiH$_y$], specific regions

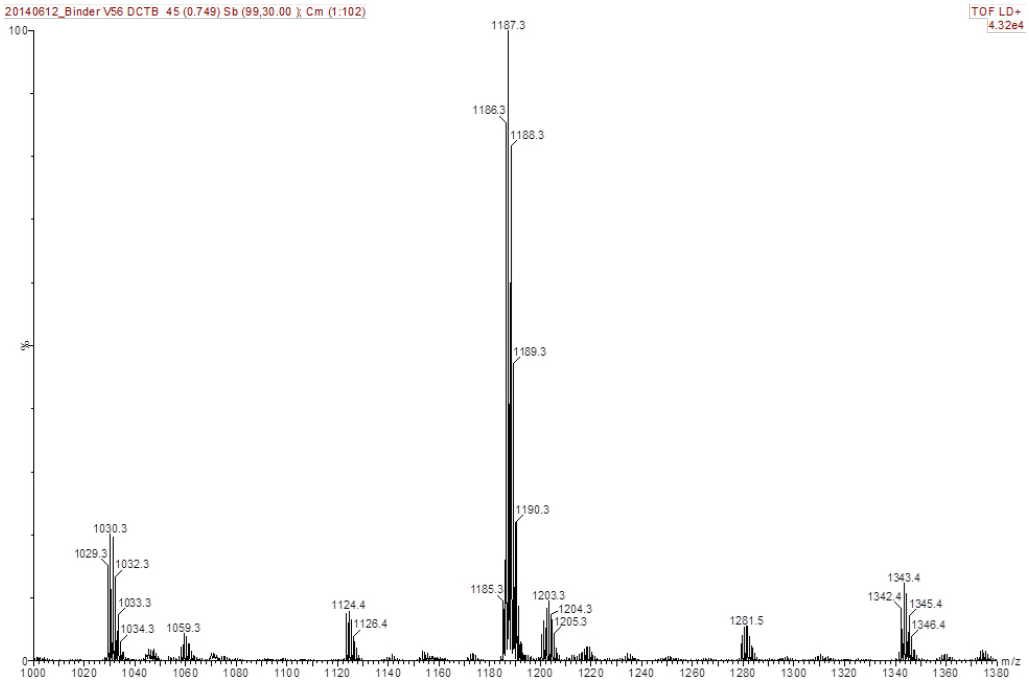

Figure 136: MALDI-TOF of the precipitate [1-naphthyl$_x$SiH$_y$], specific regions

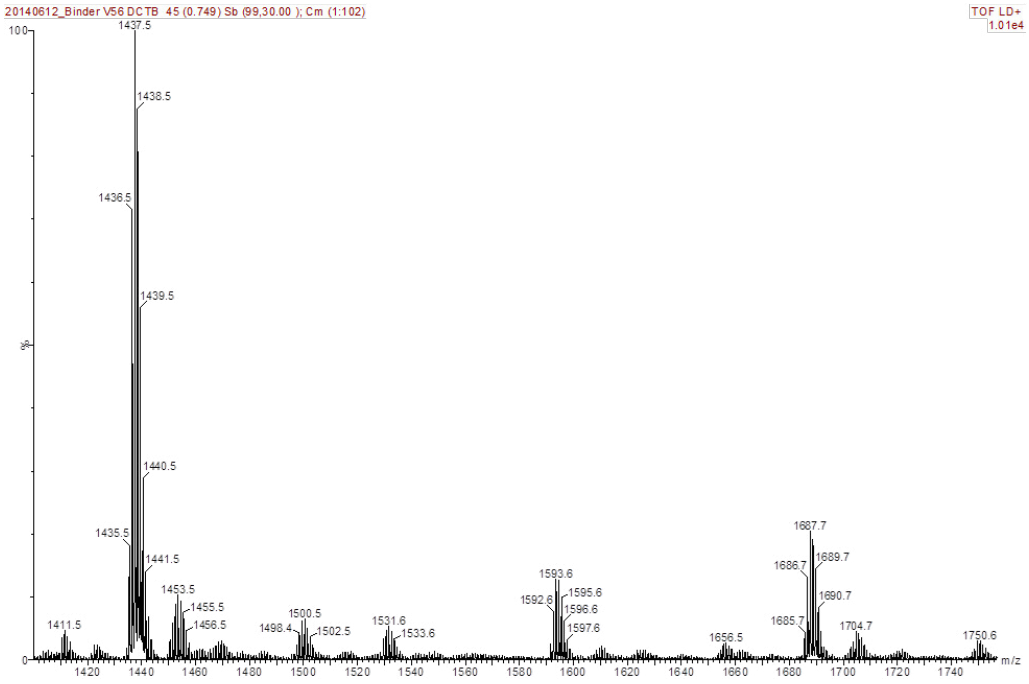

Figure 137: MALDI-TOF of the precipitate [1-naphthyl$_x$SiH$_y$], specific regions

6.5 NMR data

Table 41: DFT calculated ^{29}Si-NMR shifts of cyclic aryl silanes

Compound	Mean value [ppm]	Range [ppm]	Exact shifts [ppm]
1-naphthyl$_{10}$Si$_5$	-80.62	-67 to -95	-67.29, -69.14, -84.37, -87.76, -94.54
1-naphthyl $_8$Si$_4$	-24.22	-10 to -36	-9.57, -22.31, -29.17, -35.83
phenyl$_{10}$Si$_5$	-58.19	-54 to -62	-54.46, -56.50, -58.47, -59.68, -61.86
phenyl$_8$Si$_4$	- 49.31	-45 to -53	-44.98, -46.18, -52.97, -53.13

Table 42: Literature known ^{29}Si-NMR shifts of aryl oligosilanes

Compound	δ [ppm]
phenyl$_{10}$Si$_5$	-34.4
phenyl$_8$Si$_4$	-21.7
ph-*p*-Tol$_{10}$Si$_5$[160]	-35.0
ph-*p*-Tol$_8$Si$_4$[160]	-22.1
p-Tol$_{10}$Si$_5$[160]	-35.2
p-Tol$_8$Si$_4$[160]	-21.9
1-naphthylSiCl$_2$Si*Cl$_3$[143]	1.45, 0.02*
1-naphthylSiCl$_2$SiCl$_2$-1-naphthyl[143]	6.3
1-naphthylSiH$_2$Si*H$_3$[143]	-65.8, -99.35*
1-naphthylSiH$_2$SiH$_2$-1-naphthyl[143]	-63.35

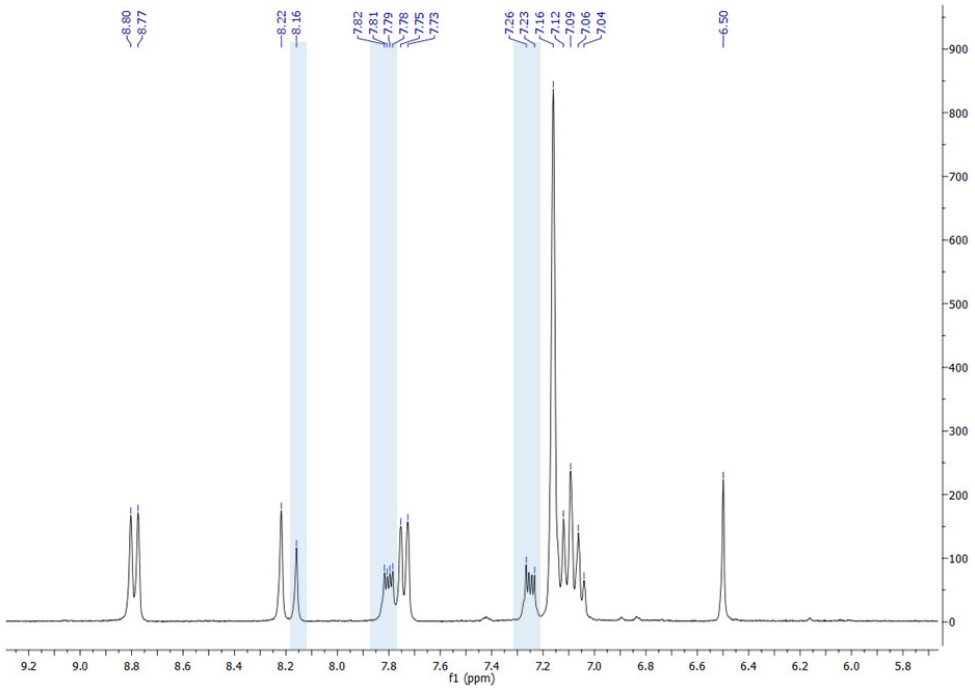

Figure 138: Sample of 9-anthracenyl$_2$SiH$_2$ (27) after 5h vacuum sublimation at 60 °C with residual anthracene (indicated in blue) in C_6D_6

6.6 EDX analysis

Table 43: EDX of 1-naphthyl$_2$SiH$_2$ (25); 7044 J/cm^2, exposed and unexposed

	unexposed		exposed 7044 J/cm^2	
Element	Mass %	Atom %	Mass %	Atom %
C K	68.11	83.02	63.48	75.22
O K	12.16	11.13	21.01	18.69
Si K	7.68	4.01	10.58	5.36
Mo L	12.05	1.84	4.93	0.73

Table 44: EDX of 2,6-xylyl$_2$SiH$_2$ (28); 7044 J/cm^2, exposed and unexposed

	unexposed		exposed 7044 J/cm^2	
Element	Mass %	Atom %	Mass %	Atom %
C K	48.93	82.41	54.55	75.17
O K	1.39	1.76	15.31	15.84
Si K	10.52	7.58	9.07	5.35
Mo L	39.16	8.26	21.06	3.63

Table 45: EDX of 2,4-xylylSiH_3 (26); 7044 J/cm^2, exposed and unexposed

	unexposed		exposed 7044 J/cm^2	
Element	Mass %	Atom %	Mass %	Atom %
C K	54.94	65.48	33.96	65.26
O K	29.97	26.82	15.08	21.75
Si K	0.14	0.08	1.26	1.03
Mo L	14.95	7.62	49.70	11.96

Table 46: EDX of *p*-*n*-butylphenyl$_2SiH_2$ (23); 7044 J/cm^2, exposed and unexposed

	unexposed		exposed 7044 J/cm^2	
Element	Mass %	Atom %	Mass %	Atom %
C K	68.52	81.93	60.14	83.32
O K	14.59	13.10	10.13	10.54
Si K	6.77	3.46	2.35	1.39
Mo L	10.13	1.52	27.38	4.75

Table 47: 9-anthracenyl$_2SiH_2$ (27); 7044 J/cm^2exposed

	exposed 7044 J/cm^2	
Element	Mass %	Atom %
C K	77.66	84.49
O K	14.54	11.88
Si K	7.80	3.63

List of Figures

Bibliography

(1) Herzog, U. In *The Chemistry of Organic Silicon Compounds, Vol. 3*; John Wiley & Sons, Ltd: 2003, p 469.

(2) Riedel, R.; Mera, G.; Hauser, R.; Klonczynski, A. *Journal of the Ceramic Society of Japan* **2006**, *114*, 425.

(3) Greene, T. W.; Wuts, P. G. M. *Protective Groups in Organic Synthesis. 2nd Ed*; John Wiley and Sons, Inc., 1991.

(4) Kocienski, P. J. *Protecting Groups*; 3 ed.; Thieme: Stuttgart, 1994.

(5) Gooding, J. J.; Ciampi, S. *Chemical Society Reviews* **2011**, *40*, 2704.

(6) Denmark, S. E.; Ober, M. H. *Aldrichim. Acta* **2003**, *36*, 75.

(7) Feigl, A.; Bockholt, A.; Weis, J.; Rieger, B. In *Silicon Polymers*; Muzafarov, A. M., Ed.; Springer Berlin Heidelberg: 2011; Vol. 235, p 1.

(8) Malandrino, G. *Angewandte Chemie International Edition* **2009**, *48*, 7478.

(9) Lauterbur, P. C. In *Determination of Organic Substances by Physical Methods*; Nachod, F. C., Phillips, W.D., Ed.; Academic Press: New York, 1962; Vol. 2, p 465.

(10)Constantine, S. P.; Hitchcock, P. B.; Lawless, G. A. *Private Communication* **1995**.

(11)Hurkes, N.; Spirk, S.; Belaj, F.; Pietschnig, R. *Z. Anorg. Allg. Chem.* **2013**, *639*, 2631.

(12)Jones, P. G.; Dix, I. *Private Communication* **2004**.

(13)Jutzi, P.; Kanne, D.; Hursthouse, M.; Howes, A. J. *Chem. Ber.* **1988**, *121*, 1299.

(14)Danilenko, T. N.; Tatevosyan, M. M.; Vlasenko, V. G. *J. Struct. Chem.* **2012**, *53*, 876.

(15)Schaefer, A.; Saak, W.; Haase, D.; Mueller, T. *Angew. Chem., Int. Ed.* **2012**, *51*, 2981.

(16)Lambert, J. B.; Stern, C. L.; Zhao, Y.; Tse, W. C.; Shawl, C. E.; Lentz, K. T.; Kania, L. *J. Organomet. Chem.* **1998**, *568*, 21.

(17)Rofouei, M. K.; Lawless, G. A.; Morsali, A.; Hitchcock, P. B. *Analytical Sciences: X-ray Structure Analysis Online* **2005**, *21*, x103.

(18)Rofouei, M. K.; Lawless, G. A.; Morsali, A.; Hitchcock, P. B. *Inorganica Chimica Acta* **2006**, *359*, 3815.

(19)Schroeck, R.; Angermaier, K.; Sladek, A.; Schmidbaur, H. *J. Organomet. Chem.* **1996**, *509*, 85.

(20)Bolte, M., Private Communication.

(21)Heiserman, D. *Exploring Chemical Elements and Their Compounds*; McGraw-Hill Companies,Incorporated, 1991.

(22)Haynes, W. M. *CRC Handbook of Chemistry and Physics, 93rd Edition*; Taylor & Francis; 2012.

(23)Schmeisser, M.; Schenk, P. W.; Huber, F. *Handbuch der präparativen anorganischen Chemie*; Ferdinand Enke Verlag, 1978.

(24)Moses, A. J. In *IEE Proceedings A (Physical Science, Measurement and Instrumentation, Management and Education)* 1990; Vol. 137, p 233.

(25)Mondolfo, L. F. *Aluminum Alloys: Structure and Properties*; Elsevier Science, 2013.

(26)Grignard, V. *Ann. Chim. Phys.* **1901**, *24*, 433.

(27)Eaborn, C. *Oreganosilicon Compounds*; Butterworths Scientific Publications, 1960.

(28)Clayden, J.; Greeves, N.; Warren, S.; Wothers, P. *Organic Chemistry*; Oxford University Press Inc.: New York, 2001.

(29)Sommer, L. H.; Tyler, L. J. *J. Am. Chem. Soc.* **1954**, *76*, 1030.

(30)Wiesinger, T. Master Thesis, TU Graz, 2013.

(31)Lickiss, P. D. In *The Chemistry of Organic Silicon Compounds, Vol. 4*; John Wiley & Sons, Ltd: 2003, p 695.

(32)Kondo, S.; Bie, Y.; Yamamura, M. *Org. Lett.* **2013**, *15*, 520.

(33)Kondo, S.; Harada, T.; Tanaka, R.; Unno, M. *Org. Lett.* **2006**, *8*, 4621.

(34)Mutahi, M. W.; Nittoli, T.; Guo, L.; Sieburth, S. M. *J. Am. Chem. Soc.* **2002**, *124*, 7363.

(35)Sieburth, S. M.; Nittoli, T.; Mutahi, A. M.; Guo, L. *Angew. Chem., Int. Ed.* **1998**, *37*, 812.

(36)Minge, O.; Nogai, S.; Schmidbaur, H. *Z. Naturforsch., B: Chem. Sci.* **2004**, *59*, 153.

(37)Higo, A.; Kikuchi, T.; Miyake, K.; Sumitomo Chemical Co., Ltd., Japan . 2012, p 30pp.; Chemical Indexing Equivalent to 143:406596 (WO).

(38)Chatgilialoglu, C. *NATO ASI Ser., Ser. C* **1989**, *260*, 115.

(39)Meyer, E. A.; Castellano, R. K.; Diederich, F. *Angewandte Chemie, International Edition in English* **2003**, *42*, 1210.

(40)Janiak, C. *J. Chem. Soc., Dalton Trans.* **2000**, 3885.

(41)Hunter, C. A.; Sanders, J. K. M. *J. Am. Chem. Soc.* **1990**, *112*, 5525.

(42)Nayak, S. K.; Sathishkumar, R.; Row, T. N. G. *CrystEngComm* **2010**, *12*, 3112.

(43)Jennings, W. B.; Farrell, B. M.; Malone, J. F. *Accounts of Chemical Research* **2001**, *34*, 885.

(44)Muller, E.; Martin, H. P. *J. Prakt. Chem./Chem.- Ztg.* **1997**, *339*, 401.

(45)Colombo, P.; Mera, G.; Riedel, R.; Soraru, G. D. *J. Am. Ceram. Soc.* **2010**, *93*, 1805.

(46)Fuchsbichler, B.; Stangl, C.; Kren, H.; Uhlig, F.; Koller, S. *J. Power Sources* **2011**, *196*, 2889.

(47)Lechner, R.; Stegner, A. R.; Pereira, R. N.; Dietmueller, R.; Brandt, M. S.; Ebbers, A.; Trocha, M.; Wiggers, H.; Stutzmann, M. *Journal of Applied Physics* **2008**, *104*, 053701.

(48)Coleman, N. R. B.; O'Sullivan, N.; Ryan, K. M.; Crowley, T. A.; Morris, M. A.; Spalding, T. R.; Steytler, D. C.; Holmes, J. D. *J. Am. Chem. Soc.* **2001**, *123*, 7010.

(49)Kim, S.; Han, T.-H.; Jung, H.-c.; Oh, Y.-S.; Pu, L.; Lee, P.-C.; Nam, J.-D. *Journal of Materials Chemistry* **2011**, *21*, 3025.

(50)Fritzsche, J. *J. Prakt. Chem* **1876**, *44*, 333.

(51)Bouas-Laurent, H.; Castellan, A.; Desvergne, J. P. *Pure Appl. Chem.* **1980**, *52*, 2633.

(52)Breton, G. W.; Vang, X. *J. Chem. Educ.* **1998**, *75*, 81.

(53)Sakurai, H.; Sakamoto, K.; Nakamura, A.; Kira, M. *Chem. Lett.* **1985**, 497.

(54)Takahashi, K.; Takanashi, Y.; Yagai, S.; Kitamura, A.; Karatsu, T. *J. Photopolym. Sci. Technol.* **2010**, *23*, 789.

(55)Noh, T.; Jeong, Y.; Kim, D. *J. Chem. Soc., Perkin Trans. 1* **1998**, 2501.

(56)Seki, S.; Matsui, Y.; Yoshida, Y.; Tagawa, S.; Koe, J. R.; Fujiki, M. *J. Phys. Chem. B* **2002**, *106*, 6849.

(57)West, R. In *The Chemistry of Organic Silicon Compounds*; John Wiley & Sons, Ltd: 2003, p 541.

(58)Sacarescu, L.; Mangalagiu, I.; Simionescu, M.; Sacarescu, G.; Ardeleanu, R. *Macromol. Symp.* **2008**, *267*, 123.

(59)Kipping, F. S.; Sands, J. E. *J. Chem. Soc., Trans.* **1921**, *119*, 830.

(60)Steele, A. R.; Kipping, F. S. *J. Chem. Soc.* **1929**, 2545.

(61)Gilman, H.; Peterson, D. J.; Tomasi, R. A.; Harrell, R. L. *J. Organomet. Chem.* **1965**, *4*, 167.

(62)Pollhammer, G. PhD. thesis, 1986.

(63)Li, H.; Butler, I. S.; Harrod, J. F. *Appl. Spectrosc.* **1993**, *47*, 1571.

(64)Hengge, E.; Bauer, G. *Monatshefte für Chemie* **1975**, *106*, 503.

(65)Shimoda, T.; Matsuki, Y.; Furusawa, M.; Aoki, T.; Yudasaka, I.; Tanaka, H.; Iwasawa, H.; Wang, D.; Miyasaka, M.; Takeuchi, Y. *Nature (London, U. K.)* **2006**, *440*, 783.

(66)Biederman, J. Master Thesis, TU Graz, 2014.

(67)Miller, R. D.; Michl, J. *Chem. Rev.* **1989**, *89*, 1359.

(68)Sacarescu, L.; Kostromin, S.; Bronnikov, S. *Mater. Chem. Phys.* **2015**, *149-150*, 430.

(69)Fukui, H.; Ohsuka, H.; Hino, T.; Kanamura, K. *ACS Appl. Mater. Interfaces* **2010**, *2*, 998.

(70)Acharya, A.; Seki, S.; Koizumi, Y.; Saeki, A.; Tagawa, S. *J. Phys. Chem. B* **2005**, *109*, 20174.

(71)Kim, H. K.; Matyjaszewski, K. *J. Am. Chem. Soc.* **1988**, *110*, 3321.

(72)Matyjaszewski, K.; Chen, Y. L.; Kim, H. K. *ACS Symp. Ser.* **1988**, *360*, 78.

(73)Jones, R. G.; Holder, S. J.; Kluwer Academic Publishers: 2000, p 353.

(74)Aitken, C.; Harrod, J. F.; Samuel, E. *J. Organomet. Chem.* **1985**, *279*, C11.

(75)Woo, H. G.; Tilley, T. D. "Dehydrogenative polymerization of silanes to polysilanes by zirconocene and hafnocene catalysts. A new polymerization mechanism," Univ. California, San Diego, 1989.

(76)Corey, J. Y.; Huhmann, J. L.; Shaltout, R. M.; Kraichely, D. M.; Gordon & Breach: 1995, p 387.

(77)Harrod, J. F. *Coord. Chem. Rev.* **2000**, *206-207*, 493.

(78)Tilley, T. D. *Acc. Chem. Res.* **1993**, *26*, 22.

(79)Corey, J. Y.; Zhu, X. H.; Bedard, T. C.; Lange, L. D. *Organometallics* **1991**, *10*, 924.

(80)Corey, J. Y. *Adv. Organomet. Chem.* **2004**, *51*, 1.

(81)A. Feigl, A. B., J. Weis, B. Rieger In *Advances in Polymer Science*; Muzafarov, A. M., Ed.; Springer-Verlag Berlin Heidelberg: 2011; Vol. 235, p 1.

(82)Pink, H. S.; Kipping, F. S. *Journal of the Chemical Society, Transactions* **1923**, *123*, 2830.

(83)Horvath, R. F.; Chan, T. H. *J. Org. Chem.* **1987**, *52*, 4489.

(84)Chen, Y. X.; Rausch, M. D.; Chien, J. C. W. *Organometallics* **1993**, *12*, 4607.

(85)Yamaguchi, S.; Akiyama, S.; Tamao, K. *Organometallics* **1998**, *17*, 4347.

(86)Gilman, H.; Schwebke, G. L. *Journal of Organic Chemistry* **1962**, *27*, 4259.

(87)Rosenberg, S. D.; Walburn, J. J.; Ramsden, H. E. *J. Org. Chem.* **1957**, *22*, 1606.

(88)Gilman, H.; Brannen, C. G. *J. Am. Chem. Soc.* **1951**, *73*, 4640.

(89)Prince, P. D.; Bearpark, M. J.; McGrady, G. S.; Steed, J. W. *Dalton Trans* **2008**, 271.

(90)Grajewska, A.; Oestreich, M. *Synlett* **2010**, *2010*, 2482.

(91)Cortial, G.; Le Goff, X.-F.; Bousquie, M.; Boisson, C.; Le Floch, P.; Nief, F.; Thuilliez, J. *New Journal of Chemistry* **2010**, *34*, 2290.

(92)Nemes, G. C.; Silaghi-Dumitrescu, L.; Silaghi-Dumitrescu, I.; Escudié, J.; Ranaivonjatovo, H.; Molloy, K. C.; Mahon, M. F.; Zukerman-Schpector, J. *Organometallics* **2005**, *24*, 1134.

(93)Bernal, J. D. *Proc. R. Soc. London, Ser. A* **1924**, *106*, 749.

(94)Zeppek, C.; Fischer, R. C.; Torvisco, A.; Uhlig, F. *Canadian Journal of Chemistry* **2014**, *92*, 556.

(95)Zeppek, C.; Pichler, J.; Torvisco, A.; Flock, M.; Uhlig, F. *Journal of Organometallic Chemistry* **2013**, *740*, 41.

(96)Nakano, T.; Yade, T. *Journal of the American Chemical Society* **2003**, *125*, 15474.

(97)Boese, R.; Nussbaumer, M. *Int. Union Crystallogr., Crystallogr. Symp.* **1994**, *7*, 20.

(98)Boese, R. *Z. Kristallogr. - Cryst. Mater.* **2014**, *229*, 595.

(99)Silaghi-Dumitrescu, L.; Haiduc, I.; Cea-Olivares, R.; Silaghi-Dumitrescu, I.; Escudié, J.; Couret, C. *Journal of Organometallic Chemistry* **1997**, *545–546*, 1.

(100) Cretiu, G.; Silaghi-Dumitrescu, L.; Silaghi-Dumitrescu, I.; Escudié, J.; Toscano, A.; Hernandez, S.; Cea-Olivares, R. *Journal of Organometallic Chemistry* **2002**, *659*, 95.

(101) Meyer, E. A.; Castellano, R. K.; Diederich, F. *Angewandte Chemie International Edition* **2003**, *42*, 1210.

(102) McL Mathieson, A.; Robertson, J. M.; Sinclair, V. C. *Acta Crystallographica* **1950**, *3*, 245.

(103) Binder, J.; Fischer, R. C.; Torvisco, A.; Uhlig, F. *in prep.* **2014**.

(104) Nayak, S. K.; Sathishkumar, R.; Row, T. N. G. *CrystEngComm* **2010**, *12*, 3112.

(105) Boese, R.; 1.0.2.30 ed. 2013.

(106) UK, A. T.; 1.171.36.28.c ed. Oxford, 2014.

(107) Dolomanov, O. V.; Bourhis, L. J.; Gildea, R. J.; Howard, J. A. K.; Puschmann, H. *J. Appl. Crystallogr.* **2009**, *42*, 339.

(108) Blinka, T. A.; Helmer, B. J.; West, R. *Advances in Organometallic Chemistry* **1984**, *23*, 193.

(109) Harloff, J.; Popowski, E.; Reinke, H. *J. Organomet. Chem.* **2007**, *692*, 1421.

(110) Gupta, R. R.; Lechner, D.; Marsmann, H.; Mikhova, B.; Uhlig, F. *Chemical Shifts and Coupling Constants for Silicon-29*; Springer, 2008.

(111) Huheey, J. E. *J. Phys. Chem.* **1965**, *69*, 3284.

(112) Huheey, J. E. *J. Phys. Chem.* **1966**, *70*, 2086.

(113) Ernst, C. R.; Spialter, L.; Buell, G. R.; Wilhite, D. L. *J. Am. Chem. Soc.* **1974**, *96*, 5375.

(114) Blinka, T. A.; Helmer, B. J.; West, R. In *Advances in Organometallic Chemistry*; Stone, F. G. A., Robert, W., Eds.; Academic Press: 1984; Vol. Volume 23, p 193.

(115) Grajewska, A.; Oestreich, M. *Synlett* **2010**, 2482.

(116) Harris, R. K.; Kimber, B. J. *Adv. Mol. Relaxation Processes* **1976**, *8*, 23.

(117) Binder, J. Master, Graz Universtity of Technology, 2011.

(118) *NIST Chemistry WebBook, NIST Standard Reference Database Number 69*; National Institute of Standards and Technology, 2005.

(119) Biedermann, J. Master, Graz University of Technology, 2014.

(120) Li, H.; Butler, I. S.; Harrod, J. F. *Organometallics* **1993**, *12*, 4553.

(121) Hannah, R. W. In *Course Notes on the Interpretation of Infrared and Raman Spectra*; John Wiley & Sons, Inc.: 2004, p 217.

(122) Binder, J. Master Thesis, Technical University of Graz, 2011.

(123) Fujita, T.; Suga, K.; Watanabe, S. *Synthesis* **1972**, *1972*, 630.

(124) Krainer, J. Maser Thesis, Technical University Graz, 2014.

(125) https://www.elettra.trieste.it/elettra-beamlines/dxrl.html Trieste.

(126) Amenitsch, H.; Rappolt, M.; Kriechbaum, M.; Mio, H.; Laggner, P.; Bernstorff, S. *J. Synchrotron Radiat.* **1998**, *5*, 506.

(127) Pedersen, J. S. *Adv. Colloid Interface Sci.* **1997**, *70*, 171.

(128) Kinning, D. J.; Thomas, E. L. *Macromolecules* **1984**, *17*, 1712.

(129) Glatter, O.; Kratky, O. *Small Angle X-ray Scattering*; Academic Press, 1982.

(130) Daudt, W. H.; Hyde, J. F. *J. Am. Chem. Soc.* **1952**, *74*, 386.

(131) Cheng, A. H. B.; Jones, P. R.; Lee, M. E.; Roussi, P. *Organometallics* **1985**, *4*, 581.

(132) Sommer, L. H.; Blankman, H. D.; Miller, P. C. *J. Am. Chem. Soc.* **1954**, *76*, 803.

(133) Tacke, R.; Kornek, T.; Heinrich, T.; Burschka, C.; Penka, M.; Pulm, M.; Keim, C.; Mutschler, E.; Lambrecht, G. *J. Organomet. Chem.* **2001**, *640*, 140.

(134) Fertig, J.; Gerrard, W.; Herbst, H. *J. Chem. Soc.* **1957**, 1488.

(135) Hoffmann, F.; Wagler, J.; Roewer, G. *Eur. J. Inorg. Chem.* **2010**, 1133.

(136) Metz, S.; Naetscher, J. B.; Burschka, C.; Goetz, K.; Kaupp, M.; Kraft, P.; Tacke, R. *Organometallics* **2009**, *28*, 4700.

(137) Nametkin, N. S.; Chernysheva, T. I.; Kuz'min, O. V. *Izv. Akad. Nauk SSSR, Ser. Khim.* **1967**, 2117.

(138) Savela, R.; Zawartka, W.; Leino, R. *Organometallics* **2012**, *31*, 3199.

(139) Kunai, A.; Kawakami, T.; Toyoda, E.; Ishikawa, M. *Organometallics* **1992**, *11*, 2708.

(140) Kunai, A.; Ohshita, J. *J. Organomet. Chem.* **2003**, *686*, 3.

(141) Varaprath, S.; Stutts, D. H. *Journal of Organometallic Chemistry* **2007**, *692*, 1892.

(142) Hafner, T. Master Thesis, Technical University Graz, 2013.

(143) Hassler, K. *Monatshefte für Chemie* **1990**, *121*, 361.

(144) Mitzel, N. W.; Schier, A.; Beruda, H.; Schmidbaur, H. *Chemische Berichte* **1992**, *125*, 1053.

(145) Blessing, R. *Acta Cryst.* **1995**, *51*, 33.

(146) Sheldrick, G. M. *Acta Cryst.* **1990**, *46*, 467.

(147) Sheldrick, G. M. *Acta Cryst.* **2008**, *64*, 112.

(148) Spek, A. L. *Journal of Applied Crystallography* **2003**, *36*, 7.

(149) Spek, A. L. *Acta Cryst.* **2009**, *65*, 148.

(150) Macrae, C. F.; Edgington, P. R.; McCabe, P.; Pidcock, E.; Shields, G. P.; Taylor, R.; Towler, M.; van de Streek, J. *Journal of Applied Crystallography* **2006**, *39*, 453.

(151) Putz, H.; Brandenburg, K. In *Diamond - Crystal and Molecular Structure Visualization*; 3.2i ed.; Crystal Impact: Bonn, Germany.

(152) Frisch, M. J.; Trucks, G. W.; Schlegel, H. B.; Scuseria, G. E.; Robb, M. A.; Cheeseman, J. R.; Scalmani, G.; Barone, V.; Mennucci, B.; Petersson, G. A.; Nakatsuji, H.; Caricato, M.; Li, X.; Hratchian, H. P.; Izmaylov, A. F.; Bloino, J.; Zheng, G.; Sonnenberg, J. L.; Hada, M.; Ehara, M.; Toyota, K.; Fukuda, R.; Hasegawa, J.; Ishida, M.; Nakajima, T.; Honda, Y.; Kitao, O.; Nakai, H.; Vreven, T.; Montgomery Jr., J. A.; Peralta, J. E.; Ogliaro, F.; Bearpark, M. J.; Heyd, J.; Brothers, E. N.; Kudin, K. N.; Staroverov, V. N.; Kobayashi, R.; Normand, J.; Raghavachari, K.; Rendell, A. P.; Burant, J. C.; Iyengar, S. S.; Tomasi, J.; Cossi, M.; Rega, N.; Millam, N. J.; Klene, M.; Knox, J. E.; Cross, J. B.; Bakken, V.; Adamo, C.; Jaramillo, J.; Gomperts, R.; Stratmann, R. E.; Yazyev, O.; Austin, A. J.; Cammi, R.; Pomelli, C.; Ochterski, J. W.; Martin, R. L.; Morokuma, K.; Zakrzewski, V. G.; Voth, G. A.; Salvador, P.; Dannenberg, J. J.; Dapprich, S.; Daniels, A. D.; Farkas, Ö.; Foresman, J. B.; Ortiz, J. V.; Cioslowski, J.; Fox, D. J.; Gaussian, Inc.: Wallingford, CT, USA, 2009.

(153) Adamo, C.; Barone, V. *J. Chem. Phys.* **1998**, *108*, 664.

(154) Kutzelnigg, W.; Fleischer, U.; Schindler, M. In *Deuterium and Shift Calculation*; Springer Berlin Heidelberg: 1991; Vol. 23, p 165.

(155) Zhao, Y.; Truhlar, D. G. *J. Chem. Phys.* **2006**, *125*, 194101/1.

(156) Kuroda, K.; Ishikawa, N. *Nippon Kagaku Zasshi* **1969**, *90*, 322.

(157) Speck, S. B. *J. Org. Chem.* **1953**, *18*, 1689.

(158) Acharya, A.; Seki, S.; Koizumi, Y.; Saeki, A.; Tagawa, S. *J. Phys. Chem. B* **2005**, *109*, 20174.

(159) Ohshita, J.; Kimura, K.; Lee, K.-H.; Kunai, A.; Kwak, Y.-W.; Son, E.-C.; Kunugi, Y. *J. Polym. Sci., Part A: Polym. Chem.* **2007**, *45*, 4588.

(160) Pöschl, U. PhD thesis, Techincal University Graz, 1995.

(161) Pinkas, J.; Cisarova, I.; Conde, A.; Fandos, R.; Horacek, M.; Kubista, J.; Mach, K. *Inorg. Chem. Commun.* **2009**, *12*, 11.

(162) Siebeneicher, H.; Doye, S. *Journal für praktische Chemie* **2000**, *342*, 102.

(163) Perennes, F.; De Bona, F.; Pantenburg, F. J. *Nucl. Instrum. Methods Phys. Res., Sect. A* **2001**, *467-468*, 1274.

AFFIDAVIT

I declare that I have authored this thesis independently, that I have not used other than the declared sources/resources, and that I have explicitly indicated all material which has been quoted either literally or by content from the sources used. The text document uploaded to TUGRAZonline is identical to the present doctoral thesis.

Date

Signature